Modeling the Role of Soil Moisture in North American Summer Climate

by

Jeremy Stephan Pal

A.S., Santa Monica College (1991)
B.S., Loyola Marymount University (1994)
S.M., Massachusetts Institute of Technology (1997)

Submitted to the Department of Civil and Environmental Engineering
in partial fulfillment of the requirements for the degree of

Doctor of Philosophy in Civil and Environmental Engineering

at the

MASSACHUSETTS INSTITUTE OF TECHNOLOGY

June 2001

Author .....
Department of Civil and Environmental Engineering
29 January, 2001

Certified by .....
Elfatih A. B. Eltahir
Associate Professor, Civil and Environmental Engineering
Thesis Supervisor

Accepted by .....
Oral Buyukozturk
Chairman, Department Committee on Graduate Students

Modeling the Role of Soil Moisture in North American Summer Climate

by

Jeremy Stephan Pal

Submitted to the Department of Civil and Environmental Engineering
on 29 January, 2001, in partial fulfillment of the
requirements for the degree of
Doctor of Philosophy in Civil and Environmental Engineering

Abstract

In this thesis, we investigate the physical pathways and mechanisms responsible for shaping the role of soil moisture in North American summer climate using a regional model. To investigate these pathways and mechanisms, we first identify and improve upon some of the deficiencies within the NCAR regional climate model (RegCM), which is used in this study. A new large-scale cloud and precipitation scheme that accounts for the sub-grid variability of clouds is presented and coupled to NCAR RegCM. In addition, a cumulus convective closure that tends to better represent convection in the Great Plains and Midwest is also implemented. Lastly, significant improvements are made to the specification of the initial and boundary conditions of atmospheric and biospheric variables. The combined results show considerable improvements when compared to the old version of the model and display reasonable agreement with observations from satellite and surface station data. Overall, these modifications improve the model's sensitivity, which is critical for both climate change and process studies.

A series of numerical experiments are performed to investigate the local pathways relating initial soil moisture to future precipitation using the 1988 drought and 1993 flood as representative events. These experiments show that increases in initial soil moisture over the Midwest result in an increase in rainfall over the same region. The results suggest that local soil moisture conditions played a significant role in maintaining these extreme events. Soil moisture's impact on both the local energy and water budgets proves to be crucial in determining the strength of the soil moisture-rainfall feedback.

An additional series of experiments are performed to investigate the remote soil moisture-rainfall pathways. The experiments suggest that an accurate representation of the domain-wide spatial variations in soil moisture is critical to accurately reproduce rainfall. The interannual temporal variations of soil moisture are less important. In addition to the local feedbacks, soil moisture perturbations have a pronounced impact on the large-scale dynamics, which tends to induce a storm track shift that enhances the soil moisture-rainfall feedback. Depending on the region, soil moisture perturbations not only impact the local climate, but also remote climates.

Thesis Supervisor: Elfatih A. B. Eltahir
Title: Associate Professor, Civil and Environmental Engineering

Acknowledgments

Research support for this thesis was provided by the Alliance for Global Sustainability.

This work would not have been possible without the help of many others. First, I thank my research advisor, Professor Elfatih Eltahir for his guidance and support through this research. We have grown together; he as professor and I as student. In addition, I thank Professors Dara Entekhabi and Rafael Bras, the other members of my committee, for their guidance and support. Furthermore, I thank all of those of the Eltahir Research Group for their support as friends and colleagues, in particular, Kirsten Findell, Julie Kiang, Eric Small, Guiling Wang, and Xinyu Zheng. Lastly, I thank Frederic Chagnon, Daniel Lüthi, Steve Margulis, and Sonia Seneviratne for their aid in this research.

During this process, I have developed and maintained many friendships that I hope last a lifetime. In particular, Joey Ancrile, Steve Avooski, Peter Israelsson, Jenny Jay, Steve Margulis, Anand Patel, and David Senn have all been great friends and believed in and stood by me during this whole process. Tom Putnam has been like a second father to me. Garbo, my wonderful dog, has been a shoulder to cry on and has listened to me all these years when no one else was there. My parents, David and Marie-Luise Pal, and my grandparents, George (in spirit) and Elisabeth Pal have given me so much love and support. Lastly, Nicole Gasparini has stood by me through the hard times and the good.

Thanks to my friends and family, all of the people of the Parsons Laboratory, and anyone who has helped me in this research.

Contents

1 Introduction **27**

1.1 Importance of Predicting Flood and Drought 27

1.2 Importance of an Accurate Model in Flood and Drought Prediction 31

1.3 Thesis Structure 33

I Model Development **34**

2 Model Description **37**

2.1 Description of Numerical Model 37

2.1.1 General Model Description 37

2.1.2 Description of the Surface Physics 38

2.1.3 Description of the Large-Scale Cloud and Precipitation Schemes 39

2.1.4 Description of the Convective Precipitation Schemes 45

2.2 Model Initialization and Evaluation Datasets 48

2.2.1 Model Simulation Datasets 48

2.2.2 Model Evaluation Datasets 50

3 Role of Large-Scale Clouds and Precipitation **55**

3.1 Introduction 55

3.2 Design of Numerical Experiments 57

3.3 Results: SIMEX versus SUBEX 58

3.3.1 Radiation Budget 59

3.3.2 Water Budget 65

3.3.3 Surface Temperature 67

3.3.4 Simulation of Extreme precipitation Events 73
3.4 Summary and Conclusions 77

4 Role of Convection **81**
4.1 Introduction 81
4.2 Design of Numerical Experiments 83
4.3 Results: FC80 versus AS74 83
4.3.1 Water Budget 83
4.3.2 Radiation Budget 91
4.3.3 Surface Temperature 97
4.3.4 Convection 100
4.4 Simulation of Extreme precipitation Events 103
4.4.1 1988 Drought 103
4.4.2 1993 Flood 105
4.5 Summary and Conclusions 108

II Soil Moisture-Rainfall Feedback Processes **109**

5 Local Soil Moisture-Rainfall Interactions **113**
5.1 Introduction 114
5.2 Theory of the Soil Moisture-Rainfall Feedback Mechanism 117
5.2.1 Radiative Feedbacks 117
5.2.2 Boundary Layer and Moist Static Energy Feedbacks 119
5.2.3 Moist Static Energy and Moist Convection 120
5.3 Description of Numerical Experiments 121
5.4 Results 123
5.4.1 Brief Model Comparison to Precipitation Observations 124
5.4.2 Model Response to Initial Soil Moisture 126
5.5 Summary of Results and Conclusions 136

6 Soil Moisture Distribution and Rainfall **139**
6.1 Introduction 139
6.2 Background 140

6.3 Description of Experiments 143
6.4 Results 146
6.4.1 Role of Soil Moisture in Reproducing Observations of Precipitation 146
6.4.2 Local Effects of Soil Moisture in the Midwest 163
6.4.3 Effects of Soil Moisture in the Western Gulf Coast on the Midwest 170
6.4.4 Effects of Soil Moisture in the Southwest on the Midwest 171
6.5 Discussion of Results 175
6.6 Summary of Results and Conclusions 177

7 Summary of Results and Conclusions and Future Work 179

7.1 Model Development 179
7.1.1 Modifications to the Model Input 179
7.1.2 Modifications to the Large-Scale Clouds and Precipitation 180
7.1.3 Modifications to the Convection Scheme 180
7.2 Soil Moisture-Rainfall Feedback 181
7.2.1 Local Feedbacks 181
7.2.2 Remote Feedbacks 182
7.3 Future Work 183

List of Figures

1-1 May and June 1988 USHCN observations of precipitation expressed as (a) anomalies in mm/day and (b) percentage of normal. Note the USHCN observations only exist over the United States. 28

1-2 June and July 1993 USHCN observations of precipitation expressed as (a) anomalies in mm/day and (b) percentage of normal. Note the USHCN observations only exist over the United States. 30

1-3 Illinois State Water Survey monthly averaged soil saturation from 0 to 10 cm for 1981 to 1993. The lower solid line is the soil saturation for 1988, the upper solid line is for 1993, the dotted lines are the rest of the years, and the dashed line is the average of all of the years. 32

2-1 Plot of the auto-conversion threshold (g/kg) versus temperature (K) for SIMEX (solid line) and SUBEX (dashed for land; dotted for ocean). 40

2-2 Plot of the fractional cloud coverage as a function of relative humidity for the new cloud and precipitation scheme. The dashed curve denotes the values for land and the solid line denotes the values for ocean. 42

3-1 Map of the domain and terrain heights used for the numerical simulations. The outlined Midwest and Gulf Coast boxes are the regions over which spatial averages are taken. 58

3-2 Plot of the simulated top of the atmosphere albedo (y-axis) against the ERBE observations (x-axis). Each data point represents a spatial average over the Midwest box outlined in Figure 3-1. Each digit indicates the month over which the average is taken. The large 5 and 6 refer to May and June of the Drought year (1988). (a) SIMEX; (b) SUBEX. 60

3-3 Plot of the simulated top of the atmosphere outgoing longwave radiation in W/m^2 (y-axis) against the ERBE observations (x-axis). Each data point represents a spatial average over the Midwest box outlined in Figure 3-1. Each digit indicates the month over which the average is taken. The large 5 and 6 refer to May and June of the Drought year (1988). (a) SIMEX; (b) SUBEX. 61

3-4 Plot of simulated simulated incident surface shortwave radiation in W/m^2 (y-axis) against the NASA-SRB data (x-axis). Each data point represents a spatial average over the Midwest box outlined in Figure 3-1. Each digit indicates the month over which the average is taken. The large 5 and 6 refer to May and June of the Drought year (1988). (a) SIMEX; (b) SUBEX. 62

3-5 Plot of the simulated net surface radiation in W/m^2 (y-axis) against the NASA-SRB data (x-axis). Each data point represents a spatial average over the Midwest box outlined in Figure 3-1. Each digit indicates the month over which the average is taken. The large 5 and 6 refer to May and June of the Drought year (1988). (a) SIMEX; (b) SUBEX. 63

3-6 Plot of the overall changes to the net surface radiation results between SIMEX and SUBEX averaged over the entire simulation period. Contours display the RMSE difference between SIMEX and SUBEX in W/m^2. Positive values (solid lines) indicate that the model simulations improved when using SUBEX and negative values (dashed lines) indicate a deterioration. The shading displays direction of the difference between SIMEX and SUBEX. Dark shading indicates that SUBEX simulates more net surface radiation than SIMEX and vice versa. 64

3-7 Plot of the simulated cloud water path in g/m^2 (y-axis) against the ISCCP-D2 observations (x-axis). Each data point represents a spatial average over the Midwest box outlined in Figure 3-1. Each digit indicates the month over which the average is taken. The large 5 and 6 refer to May and June of the Drought year (1988) and the large 6 and 7 refer to June and July of the flood year (1993). The June 1988 value lies in the bottom left corner. (a) SIMEX; (b) SUBEX. 66

3-8 Plot of the simulated precipitation in mm/day (y-axis) against the USHCN observations (x-axis). Each data point represents a spatial average over the Midwest box outlined in Figure 3-1. Each digit indicates the month over which the average is taken. The large 5 and 6 refer to May and June of the Drought year (1988) and the large 6 and 7 refer to June and July of the flood year (1993). The June 1988 value lies in the bottom left corner in both sub-plots. (a) SIMEX; (b) SUBEX. 67

3-9 Plot of the overall changes to the precipitation results between SIMEX and SUBEX averaged over the entire simulation period. Contours (United States only) display the RMSE difference between SIMEX and SUBEX in mm/day; Positive values (solid lines) indicate that the model simulations improved when using SUBEX and negative values (dashed lines) indicate a deterioration. The shading displays direction of the difference between SIMEX and SUBEX. Dark shading indicates that SUBEX simulates more precipitation than SIMEX and vice versa. 68

3-10 Plot of the simulated mean surface temperature in °C (y-axis) against the USHCN observations (x-axis). Each data point represents a spatial average over the Midwest box outlined in Figure 3-1. Each digit indicates the month over which the average is taken. The large 5 and 6 refer to May and June of the Drought year (1988) and the large 6 and 7 refer to June and July of the flood year (1993). The June 1988 value lies in the upper right corner. (a) SIMEX; (b) SUBEX. 69

3-11 Plot of the overall changes to the mean surface temperature results between SIMEX and SUBEX averaged over the entire simulation period. Contours (United States only) display the RMSE difference between SIMEX and SUBEX in °C. Positive values (solid lines) indicate that the model simulations improved when using SUBEX and negative values (dashed lines) indicate a deterioration. The shading displays direction of the difference between SIMEX and SUBEX. Dark shading indicates that SUBEX simulates higher mean surface temperatures than SIMEX and vice versa. . . 71

3-12 Plot of the simulated maximum surface temperature in °C (y-axis) against the USHCN observations (x-axis). Each data point represents a spatial average over the Midwest box outlined in Figure 3-1. Each digit indicates the month over which the average is taken. The large 5 and 6 refer to May and June of the Drought year (1988) and the large 6 and 7 refer to June and July of the flood year (1993). The June 1988 value lies in the top right corner. (a) SIMEX; (b) SUBEX. 72

3-13 Plot of the simulated minimum surface temperature in °C (y-axis) against the USHCN observations (x-axis). Each data point represents a spatial average over the Midwest box outlined in Figure 3-1. Each digit indicates the month over which the average is taken. The large 5 and 6 refer to May and June of the Drought year (1988) and the large 6 and 7 refer to June and July of the flood year (1993). The June 1988 value lies in the top right corner. (a) SIMEX; (b) SUBEX. 73

3-14 USHCN observations of precipitation in mm/day. Contour interval is specified at 1 (mm/day). Shading occurs at values above 2 mm/day and at intervals of 2 mm/day. Note that the USHCN observations only exist over the United States. (a) 1988 May and June average; (b) 1993 June and July average. 74

3-15 1988 May and June simulated United States precipitation (mm/day). Contour interval is specified at 1 (mm/day), and shading occurs at values above 2 mm/day and at intervals of 2 mm/day. (a) SIMEX; (b) SUBEX. 76

3-16 1993 June and July simulated United States precipitation (mm/day). Contour interval is specified at 1 (mm/day), and shading occurs at values above 2 mm/day and at intervals of 2 mm/day. (a) SIMEX; (b) SUBEX. 78

4-1 Plot of the simulated precipitation in mm/day (y-axis) against the USHCN observations (x-axis). Each data point represents a spatial average over the Midwest box outlined in Figure 3-1. Each digit indicates the month over which the average is taken. The large 5 and 6 refer to May and June of the Drought year (1988) and the large 6 and 7 refer to June and July of the flood year (1993). The June 1988 value lies in the bottom left corner in both sub-plots. (a) AS74; (b) FC80. 85

4-2 Plot of the simulated precipitation in mm/day (y-axis) against the USHCN observations (x-axis). Each data point represents a spatial average over the Gulf Coast box outlined in Figure 3-1. Each digit indicates the month over which the average is taken. The large 5 and 6 refer to May and June of the Drought year (1988) and the large 6 and 7 refer to June and July of the flood year (1993). The June 1988 value lies in the bottom left corner in both sub-plots. (a) AS74; (b) FC80. 85

4-3 Plot of the percentage of total precipitation that is convective over the Midwest region outlined in Figure 3-1. Each data point represents the simulated average for the indicated month. The dashed line with stars is for the AS74 simulations, while the dotted line with circles is for the FC80 simulations. 87

4-4 Plot of the percentage of total precipitation that is convective over the Gulf Coast region outlined in Figure 3-1. Each data point represents the simulated average for the indicated month. The dashed line with stars is for the AS74 simulations, while the dotted line with circles is for the FC80 simulations. 87

4-5 Plot of the differences in the percentage of precipitation that is convective between the AS74 and FC80 simulations averaged over June, July, and August. Positive contours (solid lines) indicate that the FC80 runs predict a higher convective fraction while negative contours indicate that the AS74 runs predict a higher convective fraction. Dark and light shading occur at values greater than 10% and less than -10%, respectively. 88

4-6 Plot of the overall changes to the precipitation results between the AS74 and FC80 simulations averaged over June, July, and August. Contours (United States only) display the RMSE difference between the simulations in mm/day; Positive values (solid lines) indicate that the the FC80 simulations perform better than the AS74 simulations; Negative values (dashed lines) indicate that the AS74 simulations perform better. The shading displays direction of the difference between the AS74 and FC80 simulations; Dark shading indicates that FC80 runs simulate more precipitation than the AS74 runs and vice versa. 89

4-7 Plot of the simulated cloud water path in g/m^2 (y-axis) against the ISCCP-D2 observations (x-axis). Each data point represents a spatial average over the Midwest box outlined in Figure 3-1. Each digit indicates the month over which the average is taken. The large 5 and 6 refer to May and June of the Drought year (1988) and the large 6 and 7 refer to June and July of the flood year (1993). The June 1988 value lies in the bottom left corner. (a) AS74; (b) FC80. 90

4-8 Plot of the simulated cloud water path in g/m^2 (y-axis) against the ISCCP-D2 observations (x-axis). Each data point represents a spatial average over the Gulf Coast box outlined in Figure 3-1. Each digit indicates the month over which the average is taken. The large 5 and 6 refer to May and June of the Drought year (1988) and the large 6 and 7 refer to June and July of the flood year (1993). The June 1988 value lies in the bottom left corner. (a) AS74; (b) FC80. 91

4-9 Plot of simulated simulated incident surface shortwave radiation in W/m^2 (y-axis) against the NASA-SRB data (x-axis). Each data point represents a spatial average over the Midwest box outlined in Figure 3-1. Each digit indicates the month over which the average is taken. The large 5 and 6 refer to May and June of the Drought year (1988). (a) AS74; (b) FC80. 92

4-10 Plot of simulated simulated incident surface shortwave radiation in W/m^2 (y-axis) against the NASA-SRB data (x-axis). Each data point represents a spatial average over the Gulf Coast box outlined in Figure 3-1. Each digit indicates the month over which the average is taken. The large 5 and 6 refer to May and June of the Drought year (1988). (a) AS74; (b) FC80. 93

4-11 Plot of the simulated net surface radiation in W/m^2 (y-axis) against the NASA-SRB data (x-axis). Each data point represents a spatial average over the Midwest box outlined in Figure 3-1. Each digit indicates the month over which the average is taken. The large 5 and 6 refer to May and June of the Drought year (1988). (a) AS74; (b) FC80. 94

4-12 Plot of the simulated net surface radiation in W/m^2 (y-axis) against the NASA-SRB data (x-axis). Each data point represents a spatial average over the Gulf Coast box outlined in Figure 3-1. Each digit indicates the month over which the average is taken. The large 5 and 6 refer to May and June of the Drought year (1988). (a) AS74; (b) FC80. 95

4-13 Plot of the overall changes to the net surface radiation results between AS74 and FC80 simulations averaged over June, July, and August. Contours display the RMSE difference between the simulations in W/m^2; Positive values (solid lines) indicate that the Grell scheme utilizing the FC80 closure performs better than the with the AS74 closure assumption; Negative values (dashed lines) indicate that the Grell scheme with the AS74 closure assumption performs better. The shading displays direction of the difference between the AS74 and FC80 simulations; Dark shading indicates that FC80 runs simulate more net surface radiation than the AS74 runs and vice versa. 96

4-14 Plot of the simulated mean surface temperature in °C (y-axis) against the USHCN observations (x-axis). Each data point represents a spatial average over the Midwest box outlined in Figure 3-1. Each digit indicates the month over which the average is taken. The large 5 and 6 refer to May and June of the Drought year (1988) and the large 6 and 7 refer to June and July of the flood year (1993). The June 1988 value lies in the upper right corner. (a) AS74; (b) FC80. 98

4-15 Plot of the simulated mean surface temperature in °C (y-axis) against the USHCN observations (x-axis). Each data point represents a spatial average over the Gulf Coast box outlined in Figure 3-1. Each digit indicates the month over which the average is taken. The large 5 and 6 refer to May and June of the Drought year (1988) and the large 6 and 7 refer to June and July of the flood year (1993). The June 1988 value lies in the upper right corner. (a) AS74; (b) FC80. 98

4-16 Plot of the overall changes to the mean surface temperature results between the AS74 and FC80 simulations averaged over June, July, and August. Contours (United States only) display the RMSE difference between the simulations in W/m^2; Positive values (solid lines) indicate that the FC80 simulations perform better than AS74 simulations; Negative values (dashed lines) indicate that the AS74 simulations assumption perform better. The shading displays direction of the difference between the AS74 and FC80 simulations; Dark shading indicates that FC80 runs are warmer than the AS74 runs and vice versa. 99

4-17 Plot of the differences in the surface moist static energy between the AS74 and FC80 simulations averaged over June, July, and August. Positive contours (solid lines) indicate that the FC80 runs predict a higher amount surface moist static energy while negative contours indicate that the AS74 runs predict a larger amount. Dark and light shading occur at values greater than 1 kJ/kg and less than -1 kJ/kg, respectively. 101

4-18 Plot of the differences in the modified Showalter stability index between the AS74 and FC80 simulations averaged over June, July, and August. Positive contours (solid lines) indicate that the FC80 runs are more unstable while negative contours indicate that the AS74 runs are more unstable. Dark and light shading occur at values greater than 1 K and less than -1 K, respectively. 102

4-19 USHCN observations of precipitation in mm/day. Contour interval is specified at 1 (mm/day). Shading occurs at values above 2 mm/day and at intervals of 2 mm/day. Note that the USHCN observations only exist over the United States. (a) 1988 May and June average; (b) 1993 June and July average. 104

4-20 1988 May and June simulated United States precipitation (mm/day). Contour interval is specified at 1 (mm/day), and shading occurs at values above 2 mm/day and at intervals of 2 mm/day. (a) AS74; (b) FC80. 106

4-21 1993 June and July simulated United States precipitation (mm/day). Contour interval is specified at 1 (mm/day), and shading occurs at values above 2 mm/day and at intervals of 2 mm/day. (a) AS74; (b) FC80. 107

5-1 Illinois State Water Survey soil saturation profile averaged over June, July, and August. The solid line on the left is the profile for 1988; the solid line on the right is for 1993; the dotted lines are the rest of the years; and the dashed line is the average of all of the years. 116

5-2 Diagram relating the pathways through which anomalously wet soil moisture conditions lead to subsequent rainfall. 118

5-3 Map of the domain and terrain heights (m) used for the numerical simulations. The outlined box is the region over which the averages are taken and corresponds to the areas where the drought of 1988 and flood of 1993 were most severe. The contour interval is 100 m. 122

5-4 USHCN observed and RegCM simulated rainfall averaged over June and July of 1988 and 1993: (a) USHCN June and July 1988; (b) RegCM June and July 1988; (c) USHCN June and July 1993; (d) RegCM June and July 1993. The outlined box is the region over which the averages are taken and corresponds to the areas where the drought of 1988 and flood of 1993 were most severe. The units are in mm/day, the contour interval is 1 mm/day, and the shading interval is 2 mm/day. 125

5-5 Simulated monthly rainfall (mm/day) for the 1988 and 1993 simulations as a function of initial soil saturation: (a) total rainfall; (b) convective rainfall; and (c) non-convective rainfall. Each data point represents the average of the May, June, July, August, and September simulations over the Midwest region outlined in Figure 5-3 given the initial soil moisture. The D denotes the drought year (1988) and the F denotes flood year (1993). The boldface D and F denote the control simulations for each year 127

5-6 Plot of relative sensitivity versus soil saturation: (a) 1988; (b) 1993. Each bin on the x-axis represents a range of soil saturations; The end points of each bin are individual simulations where each bar within the bin represents a month. The values on the y-axis represent the percent change in rainfall per percent change in soil moisture. The solid line represents the average of all the months for the given year. 128

5-7 Relative and absolute sensitivities of rainfall to initial soil moisture. Relative sensitivity is a measure of the relative impact of initial soil moisture on future precipitation expressed as a percentage. Absolute sensitivity is defined as the slope of the best fit line of future precipitation to initial soil moisture for each simulation month. The D denotes the drought year (1988) and the F denotes flood year (1993). 131

5-8 Simulated monthly surface radiation fields (W/m^2), for the 1988 and 1993 simulations as a function of initial soil saturation: (a) net radiation; (b) net longwave radiation; and (c) net solar radiation. Each data point represents the average of the May, June, July, August, and September simulations over the Midwest region outlined in Figure 5-3 given the initial soil moisture. The D denotes the drought year (1988) and the F denotes flood year (1993). The boldface D and F denote the control simulations for each year 134

5-9 Simulated monthly surface heat flux fields (W/m^2), for the 1988 and 1993 simulations as a function of initial soil saturation: (a) sensible + latent heat flux; (b) latent heat flux; and (c) sensible heat flux. Each data point represents the average of the May, June, July, August, and September simulations over the Midwest region outlined in Figure 5-3 given the initial soil moisture. The D denotes the drought year (1988) and the F denotes flood year (1993). The boldface D and F denote the control simulations for each year 134

5-10 Simulated monthly moist static energy (KJ/kg), temperature (C), and water vapor mixing ratio (g/kg) for the 1988 and 1993 simulations as a function of initial soil saturation: (a) Moist Static Energy; (b) Temperature; and (c) Mixing Ratio. Each data point represents the average of the May, June, July, August, and September simulations over the Midwest region outlined in Figure 5-3 given the initial soil moisture. The D denotes the drought year (1988) and the F denotes flood year (1993). The boldface D and F denote the control simulations for each year 136

6-1 Climatology of the June, July, and August merged ISWS/HDG root soil saturation (%): (a) Mean; (b) Standard Deviation. 141

6-2 Plot of initial root zone soil saturation (%) for the control simulations: (a) 25 June 1986; (b) 25 June 1987; (c) 25 June 1988; (d) 25 June 1989; (e) 25 June 1990; and (f) 25 June 1993. The contour interval is 10% and shading occurs at values above 20% and at intervals of 20%. 145

6-3 Plot of initial 25 June climatology of the root zone soil saturation (%) for the anomalous fixed patch simulations: (a) 25MWCTL; (b) 25GCCTL; and (c) 75SWCTL. The contour interval is 10% and shading occurs at values above 20% and at intervals of 20%. 147

6-4 July observed USHCN Precipitation Climatology for the years: 1986, 1987, 1988, 1989, 1990, and 1993 (mm/day). Contour interval is specified at 1 (mm/day). Shading occurs at values above 1 mm/day and at intervals of 2 mm/day. Note that the USHCN observations only exist over the United States. 148

6-5 July simulated precipitation climatology for the CTL experiments (mm/day). The soil moisture in each simulation is initialized according to the merged HDG/ISWS dataset and is fully interactive. The FC80 closure assumption is used. Note that only values for the United States are displayed. 149

6-6 July simulated precipitation climatology for the CLM experiments (mm/day). The soil moisture in each simulation is moisture in each simulation is initialized according to the climatology of the merged HDG/ISWS dataset and is fully interactive. The FC80 closure assumption is used. Note that only values for the United States are displayed. 150

6-7 July simulated Precipitation Climatology (mm/day) for the years: 1986, 1987, 1988, 1989, 1990, and 1993. The soil moisture in each simulation is fully interactive and the FC80 closure assumption is used. The initial soil moisture fraction is indicated at the top of each plot. The contour interval is specified at 1 mm/day and shading occurs at values above 1 mm/day and at intervals of 2 mm/day. Note that only values for the United States are displayed. 152

6-8 July simulated precipitation climatology bias and root mean square error (mm/day) computed over the (a) Midwest and (b) Gulf Coast regions outlined in Figure 3-1. The soil moisture in each simulation is fully interactive and the FC80 closure assumption is used. The initial soil saturation is indicated at the top of each bar. Note that values over water are not included in the computations. 153

6-9 July simulated root zone soil saturation climatology (%): (a) CTL; (b) 00%-CTL; (c) 50%-CTL; and (d) 100%-CTL. The soil moisture in each simulation is fully interactive and the FC80 closure assumption is used. 154

6-10 July simulated 500 mb wind vectors (m/s) and geopotential heights (m) climatology: (a) CTL; (b) 00%-CTL; (c) 50%-CTL; and (d) 100%-CTL. The soil moisture in each simulation is fully interactive and the FC80 closure assumption is used. 156

6-11 July differences between control and uniform simulated 500 mb zonal winds (m/s) and sigma 0.895 meridional winds (m/s). The soil moisture in each simulation is fully interactive and the FC80 closure assumption is used. 158

6-12 USHCN observations of precipitation (mm/day): (a) June 1988 and (b) July 1993. Note the USHCN observations only exist over the United States. 159

6-13 June 1988 simulated Precipitation (mm/day) for the following simulations: (a) CTL, (b) CLM (c) 00%, (d) 50%, and (e) 100%. The soil moisture in each simulation is fully interactive and the FC80 closure assumption is used. The initial soil moisture fraction is indicated at the top of each plot. The contour interval is specified at 1 mm/day and shading occurs at values above 1 mm/day and at intervals of 2 mm/day. Note that only values for the United States are displayed. 161

6-14 July 1993 simulated Precipitation (mm/day) for the following simulations: (a) CTL, (b) CLM (c) 25%, (d) 75%, and (e) 100%. The soil moisture in each simulation is fully interactive and the FC80 closure assumption is used. The initial soil moisture fraction is indicated at the top of each plot. The contour interval is specified at 1 mm/day and shading occurs at values above 1 mm/day and at intervals of 2 mm/day. Note that only values for the United States are displayed. 162

6-15 July simulated Precipitation (mm/day) for the following simulations: (a) CTL, (b) CLM (c) 25%, (d) 75%, and (e) 100%. The soil moisture in each simulation is fully interactive and the AS74 closure assumption is used. The initial soil moisture fraction is indicated at the top of each plot. The contour interval is specified at 1 mm/day and shading occurs at values above 1 mm/day and at intervals of 2 mm/day. Note that only values for the United States are displayed. 164

6-16 July differences between control and uniform simulated 500 mb zonal winds (m/s) and sigma 0.895 meridional winds (m/s). The soil moisture in each simulation is fully interactive and the AS74 closure assumption is used. 165

6-17 July simulated Precipitation Climatology (mm/day) for the (a) 25MWCTL simulations and (b) difference between the 25MWCTL and the CTL simulations. The soil moisture in each is initialized according to the merged HDG/ISWS dataset and is fully interactive except in the 25MWCTL simulations over the Midwest region where the soil saturation is held constant at 25%. The FC80 closure assumption is used. Note that only values for the United States are displayed. 166

6-18 July simulated surface climatology difference between the 25MWCTL and CTL simulations: (a) net surface all-wave radiation (W/m^2); (b) surface sensible + latent heat flux longwave (W/m^2); (c) Sigma 0.995 moist static energy (kJ/kg); and (d) convective precipitation (mm/day). The soil moisture in each is initialized according to the merged HDG/ISWS dataset and is fully interactive except in the 25MWCTL simulations over the Midwest region where the soil saturation is held constant at 25%. The FC80 closure assumption is used. Note that only values over land are displayed. 168

6-19 July differences between CTL and 25MWCTL simulated (a) 500 mb geopotential heights (m) and winds (m/s) and (b) sigma 0.895 mixing ratio (g/kg) and winds. The soil moisture in each is initialized according to the merged HDG/ISWS dataset and is fully interactive except in the 25MWCTL simulations over the Midwest region where the soil saturation is held constant at 25%. The FC80 closure assumption is used. 169

6-20 July differences between CTL and 25MWCTL simulated (a) 500 mb zonal winds (m/s) and (b) sigma 0.895 meridional winds (m/s). The soil moisture in each is initialized according to the merged HDG/ISWS dataset and is fully interactive except in the 25MWCTL simulations over the Midwest region where the soil saturation is held constant at 25%. The FC80 closure assumption is used. 169

6-21 July simulated Precipitation Climatology (mm/day) for the (a) 25GCCTL simulations and (b) difference between the 25GCCTL and the CTL simulations. The soil moisture in each is initialized according to the merged HDG/ISWS dataset and is fully interactive except in the 25GCCTL simulations over the western Gulf Coast region where the soil saturation is held constant at 25%. The FC80 closure assumption is used. Note that only values for the United States are displayed. 171

6-22 July simulated surface climatology difference between the 25GCCTL and CTL simulations: (a) net surface all-wave radiation (W/m^2); (b) surface sensible + latent heat flux longwave (W/m^2); (c) Sigma 0.995 moist static energy (kJ/kg); and (d) convective precipitation (mm/day). The soil moisture in each is initialized according to the merged HDG/ISWS dataset and is fully interactive except in the 25GCCTL simulations over the Midwest region where the soil saturation is held constant at 25%. The FC80 closure assumption is used. Note that only values over land are displayed. 172

6-23 July differences between CTL and 25GCCTL simulated (a) 500 mb geopotential heights (m) and winds (m/s) and (b) sigma 0.895 mixing ratio (g/kg) and winds. The soil moisture in each is initialized according to the merged HDG/ISWS dataset and is fully interactive except in the 25GCCTL simulations over the Midwest region where the soil saturation is held constant at 25%. The FC80 closure assumption is used. 173

6-24 July simulated Precipitation Climatology (mm/day) for the (a) 75SWCTL simulations and (b) difference between the 75SWCTL and the CTL simulations. The soil moisture in each is initialized according to the merged HDG/ISWS dataset and is fully interactive except in the 75SWCTL simulations over the western Gulf Coast region where the soil saturation is held constant at 75%. The FC80 closure assumption is used. Note that only values for the United States are displayed. 174

6-25 July differences between CTL and 75SWCTL simulated (a) 500 mb geopotential heights (m) and winds (m/s) and (b) Sigma 0.895 mixing ratio (g/kg) and winds. The soil moisture in each is initialized according to the merged HDG/ISWS dataset and is fully interactive except in the 75SWCTL simulations over the Midwest region where the soil saturation is held constant at 75%. The FC80 closure assumption is used. 175

List of Tables

2.1 List of parameters used in SUBEX and their associated values. 41

2.2 List of verification datasets used in this study. EA denotes equal-area; OLR denotes top of the atmosphere outgoing longwave radiation; ALBEDO denotes top of the atmosphere albedo; SWI denotes incident surface shortwave radiation; RN denotes net surface radiation; CWP denote cloud water path; PPT denotes precipitation; and TMEAN, TMAX, and TMIN denote the mean, maximum, and minimum surface temperatures, respectively. 51

3.1 Summary of the model simulation statistics compared to observations for SUBEX and SIMEX over the Midwest (outlined in Figure 3-1). RMSE denotes root mean square error; ALBEDO denotes top of the atmosphere albedo; OLR denotes top of the atmosphere outgoing longwave radiation; SWI denotes incident surface shortwave radiation; RN denotes net surface radiation; CWP denote cloud water path; PPT denotes precipitation; and TMEAN, TMAX, and TMIN denote the mean, maximum, and minimum surface temperatures, respectively. 59

4.1 Summary of the model simulation statistics compared to observations for both AS74 and FC80 closure assumptions over the Midwest (outlined in Figure 3-1). RMSE denotes root mean square error; ALBEDO denotes top of the atmosphere albedo; OLR denotes top of the atmosphere outgoing longwave radiation; SWI denotes incident surface shortwave radiation; RN denotes net surface radiation; CWP denote cloud water path; PPT denotes precipitation; and TMEAN, TMAX, and TMIN denote the mean, maximum, and minimum surface temperatures, respectively. 84

4.2 Summary of the model simulation statistics compared to observations for both AS74 and FC80 closure assumptions over the Gulf Coast (outlined in Figure 3-1). RMSE denotes root mean square error; ALBEDO denotes top of the atmosphere albedo; OLR denotes top of the atmosphere outgoing longwave radiation; SWI denotes incident surface shortwave radiation; RN denotes net surface radiation; CWP denote cloud water path; PPT denotes precipitation; and TMEAN, TMAX, and TMIN denote the mean, maximum, and minimum surface temperatures, respectively. 86

5.1 Description of each simulation performed in this study. 123

5.2 Average Number of hourly rainfall events within specified intervals occurring between May 1 and September 30 or 1988 and 1993 for the 10%, 50%, and 90% soil saturation simulations. The number in parentheses indicates the percentage of total rainfall. The last row provides the totals over all the intervals with the number in parentheses indicating the total rainfall in mm. The values are computed over the upper Midwest region defined in Figure 5-3. 129

6.1 Description of each simulation performed in this study. 144

Chapter 1

Introduction

1.1 Importance of Predicting Flood and Drought

As the global population continues to grow, the efficient production of food and the supply of water for crops, industry, and domestic use becomes increasingly important. In addition, an increasing number of humans are moving into regions vulnerable to flood and drought. Furthermore, climate change due to increases in atmospheric carbon dioxide concentrations may have a significant impact on the vulnerability of a region to extreme precipitation events. Therefore, the prediction of precipitation, particularly flood and drought, is becoming increasingly important. This study aims to define some of the limits of predictability of late-spring and summer North American precipitation when water supply is in its highest demand.

In 1988, the United States experienced its warmest and driest summer since 1936 (Ropelewski 1988). Figure 1-1 shows maps of observed rainfall expressed as anomalies and percentage of normal averaged over May and June for 1988 over the United States. Strikingly, negative anomalies associated with the widespread drought covered most of the eastern two thirds of the United States. In terms of percentage of normal, much of the West also experienced severe rainfall deficits. Because of these widespread patterns, the 1988 drought is coined the Great North American Drought. Of particular note, the drought was especially pronounced in the Great Plains and Midwest, one of the most agriculturally productive regions in the world, causing severe crop losses. It resulted in approximately 10,000 deaths from heat stress and caused an estimated $30 billion in agricultural damage (Trenberth and Branstator 1992).

Contrary to the drought of 1988, rainfall in the summer of 1993 was anomalously high over most of the upper Midwest (See Figure 1-2). The flooding that occurred was one of the most devastating

(a) May & June 1988 Precipitation Anomalies (mm/day)

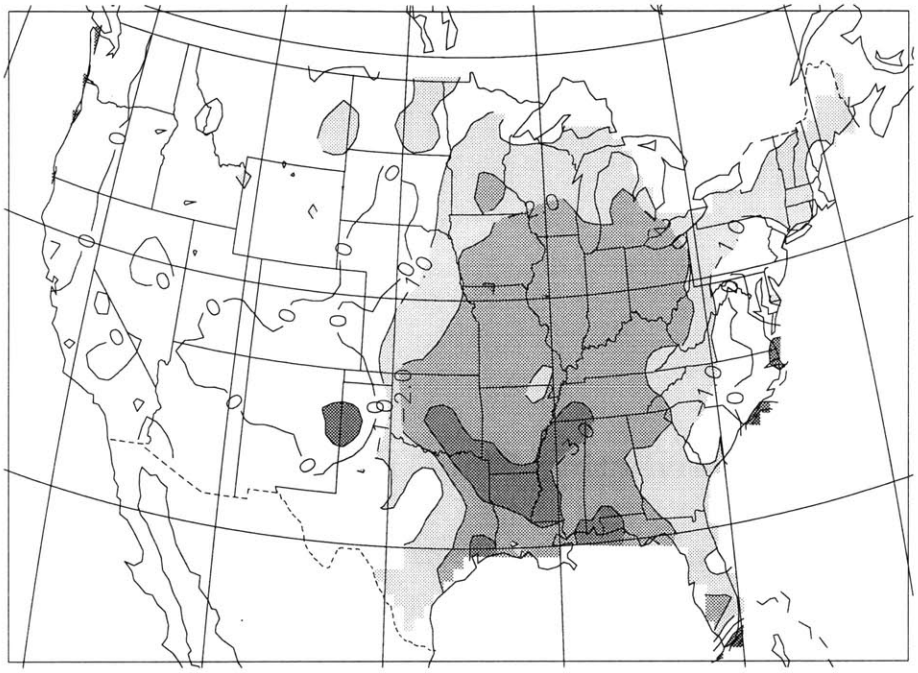

(b) May & June 1988 Percentage of Normal Precipitation

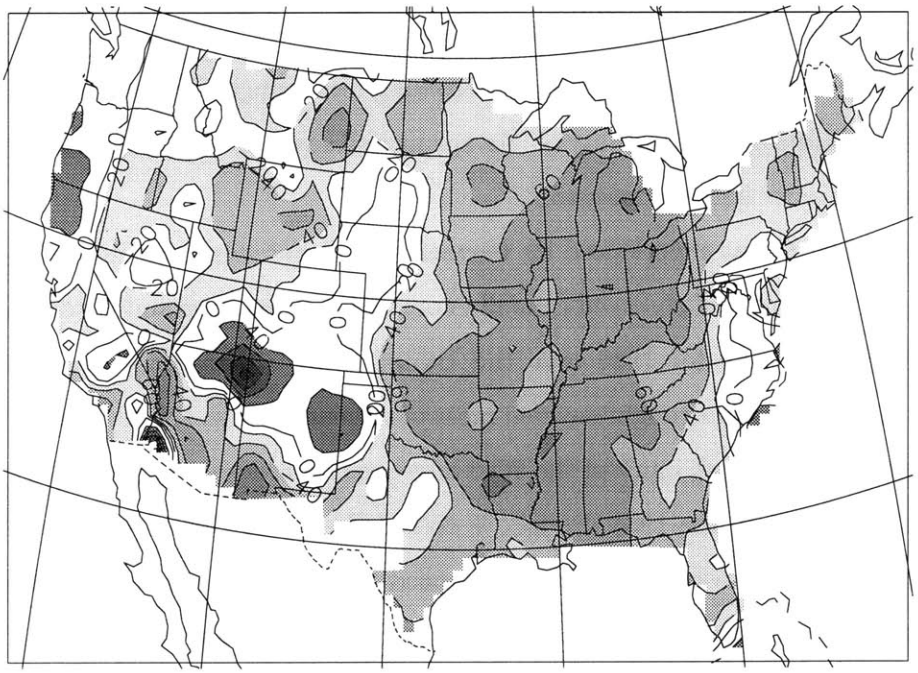

Figure 1-1: May and June 1988 USHCN observations of precipitation expressed as (a) anomalies in mm/day and (b) percentage of normal. Note the USHCN observations only exist over the United States.

in modern history (Kunkel et al. 1994). Record high rainfall and flooding occurred throughout much of the Upper Mississippi River basin and persisted for long periods. The National Oceanic and Atmospheric Administration (NOAA) estimated that the flood caused $15-20 billion in damages (NOAA 1993).

More recently, during late-Spring and early-Summer of 1998, much of the southern United States suffered from its worst drought in recorded history (104 years of record). Associated with these drought-like conditions were extreme crop and livestock losses, increased wildfires, decreased supply of potable water, and increased loss of human lives. By the end of July, Texas and Oklahoma estimated crops losses at $2.0 to $4.0 billion (NOAA 1998b). In Texas alone, over 170 people died from heat related deaths (NOAA 1998b). Wildfires ravaged over 500,000 acres and destroyed 270 homes and businesses in Florida (NOAA 1998a).

The exact causes of extreme summertime flood and drought are relatively unknown. On one hand, Trenberth and Guillemot (1996) conclude that the cause of the drought of 1988 and flood of 1993 were related to La Niña and El Niño, respectively. They suggest that in 1993 the El Niño shifted the inter-tropical convergence zone (ITCZ) south of normal which shifted the storm track southward and created a link to the moisture from the Gulf of Mexico. This link is what they believe to be responsible for the record rainfall observed over the Midwest in 1993. In contrast, for 1988 they suggest that the strong La Niña and the anomalously warm sea-surface temperatures (SSTs) southeast of Hawaii caused a northward shift in the ITCZ, which in turn caused a northward shift in the storm track across North America. They argue that this shift did not allow the Gulf of Mexico moisture link to form and resulted in drought conditions. On the other hand, Bell and Janowiak (1995) argue that anomalous SSTs in the tropical Pacific indirectly contributed to overall magnitude and extent of the 1993 flood. However, they state that no single factor alone caused the flooding. Furthermore, Namias (1991) argues that the La Niña observed in 1988 may have contributed to the drought, but was not the primary cause of the drought. Trenberth and Guillemot (1996) and Namias (1991) both agree that soil moisture may play an important role in the increasing persistence and magnitude of flood and drought. This study aims to isolate the effects of soil moisture on future rainfall by performing a series of numerical experiments where initial soil moisture conditions are varied and the large-scale forcing is kept the same.

Not surprisingly, extreme soil moisture conditions were associated with these extremes in rainfall seen in Figure 1-1 and 1-2. Figure 1-3 shows time series (1981 through 1993) of the Illinois State Water Survey (ISWS) near surface soil saturation data averaged over the state of Illinois (Hollinger

(a) June & July 1993 Precipitation Anomalies (mm/day)

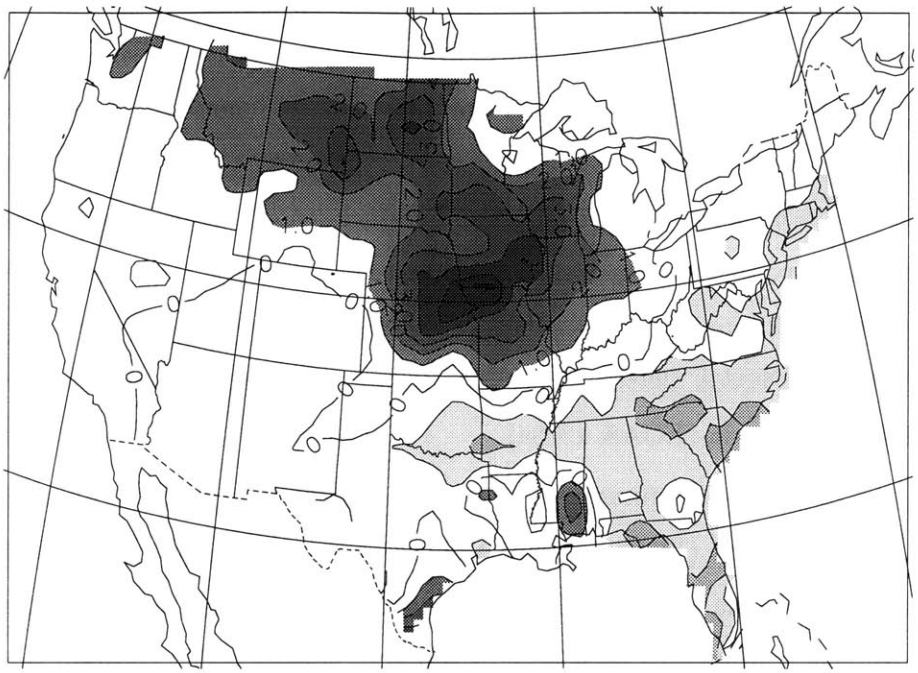

(b) June & July 1993 Percentage of Normal Precipitation

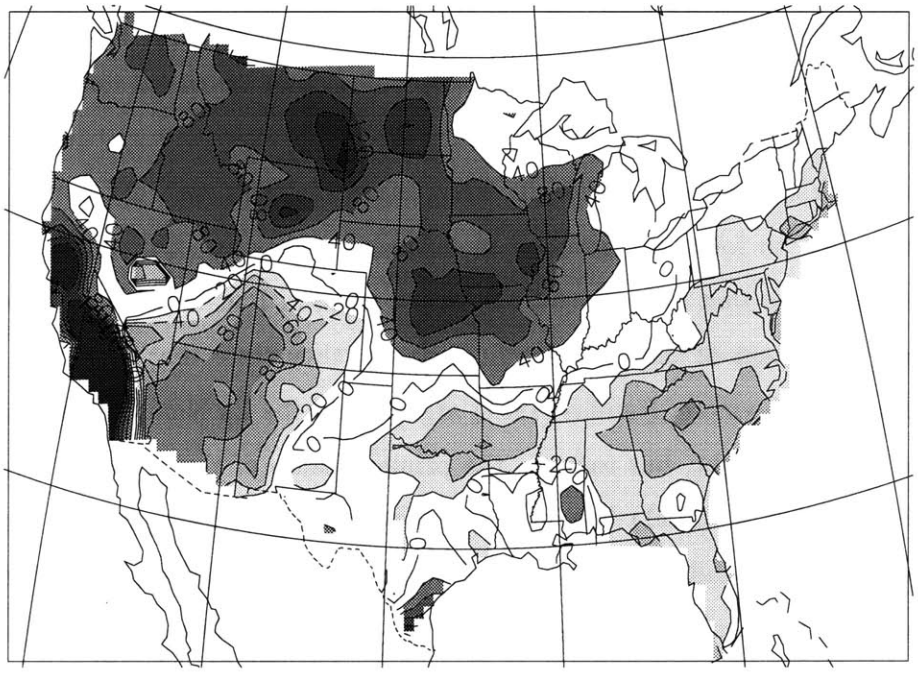

Figure 1-2: June and July 1993 USHCN observations of precipitation expressed as (a) anomalies in mm/day and (b) percentage of normal. Note the USHCN observations only exist over the United States.

and Isard 1994). Clearly, 1988 (lower solid line) was the driest Spring and Summer, in terms of soil saturation, on record, while 1993 (upper solid line) was the wettest. These extremes in soil moisture are likely to be more apparent over Iowa and Missouri where the flood and drought were more extreme than in Illinois (where data are available) during their respective years. This study attempts to determine whether the anomalous soil moisture conditions observed in 1988 and 1993 (and other years) played a role in initiating and/or enhancing the extremes in observed rainfall or whether they were simply a by-product of these extremes. More specifically, it investigates the pathways through which late-spring and summer soil moisture conditions impact extreme North American summertime flood and drought. Understanding these pathways could potentially have significant implications for water resources management and cropping strategies and also help to reduce human and economic losses. If, for example, one can predict that a given summer will receive anomalously high rainfall, then water can be released from reservoirs in advance to reduce damaging floods. Furthermore, farmers can alter their cropping strategies. A major component of this study is investigate the mechanisms and pathways through which soil moisture impacts precipitation over the United States using a numerical model.

1.2 Importance of an Accurate Model in Flood and Drought Prediction

As mentioned above, this study investigates the limits of predictability of extreme summertime flood and drought based on the late-spring and summer soil moisture conditions. Predictions of climate, however, are typically performed using numerical models whose accuracy depends on a variety of factors (e.g. grid resolution, representation of land surface processes, representation of cloud processes, representation of convective processes, etc.). This study aims at clarifying the role that the representation of the clouds and precipitation (both convective and large-scale) play in determining the outcome of the response of a numerical model to changes in initial soil moisture.

As mentioned above, the United States Midwest is one of the most agriculturally productive regions in the world. The crop yield during the growing season depends on a variety of factors including the surface energy and water budgets. Predicting these budgets can be extremely useful for cropping strategies (Mearns et al. 1997). Moreover, these energy and water budgets are also crucial in predicting flood and drought. However, to properly predict these budgets, it is not only mandatory to have a model that accurately represents the land surface, but also a model that

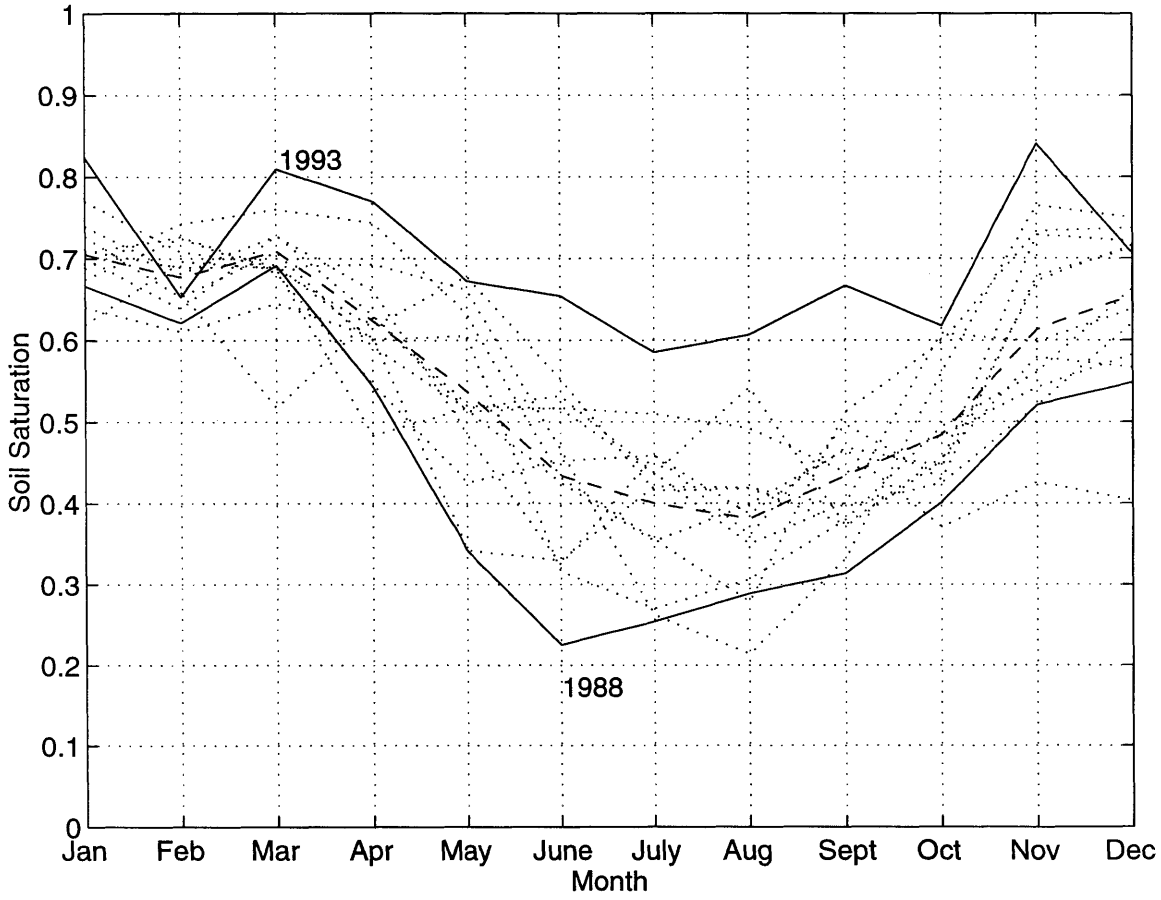

Figure 1-3: Illinois State Water Survey monthly averaged soil saturation from 0 to 10 cm for 1981 to 1993. The lower solid line is the soil saturation for 1988, the upper solid line is for 1993, the dotted lines are the rest of the years, and the dashed line is the average of all of the years.

accurately represents atmospheric properties, such as large-scale dynamics, radiation, clouds, and precipitation. A major component of this thesis is to identify and improve upon deficiencies in the numerical model.

A wealth of data has recently become available from satellites and other standard sources. These data, among other things, provide information about the surface and atmospheric radiation budgets and cloud properties. As a result, these data can be used to improve the physics within a numerical model. In this thesis, we take full advantage of satellite, station, and reanalysis data to identify and improve upon numerical model deficiencies. In doing so, we further improve upon a state of the art tool useful for process studies such as the one presented here.

1.3 Thesis Structure

In addition to the overall introduction and conclusions, the main body this thesis is divided into two parts. In the first part, we provide an overall description the National Center for Atmospheric Research (NCAR) Regional Climate Model (RegCM). This includes a detailed description of some improvements made to RegCM in this thesis. In the second part, the model described and tested in Part I is applied over North America to study soil moisture-rainfall feedback.

Part I is composed of three chapters. In Chapter 2, a description of RegCM is provided. Of particular importance, the old and new large-scale cloud and precipitation scheme and the convection scheme are described in detail along with the structural model improvements. This Chapter also describes the datasets used in this study to verify model performance. Chapter 3 rigorously compares and tests the performance of the old and new large-scale cloud and precipitation schemes. Chapter 4 tests and compares the performance of the Arakawa and Schubert (1974) closure assumption within the Grell convection scheme to the improved Fritsch and Chappell (1980) closure assumption.

Part II is composed of two chapters. The focus of this part is on the numerical modeling of the soil moisture-rainfall feedback using RegCM including the improvements described in Part I. In Chapter 5 the local effects of the soil moisture-rainfall feedback are investigated using a small and hence constrained model domain. In Chapter 6, the domain constraints are lifted and we investigate impacts of soil moisture at both the local- and large-scale climate.

Part I

Model Development

Part I focuses on the development and verification of the NCAR RegCM. These developments include improvements to the representation large-scale clouds and precipitation (Chapter 3). Also, included are modifications to closure assumption within the Grell cumulus convective parameterization. In addition, improvements are made in the representation of the initial and boundary conditions as well as to the specification of the sea surface temperature, vegetation type, and soil moisture. Chapter 2 provides a description of the overall model and modifications as well as a description of the datasets used for running and verifying the model. Chapter 3 compares the old and new representation of large-scale clouds and precipitation and Chapter 4 compares the two convective closure assumptions.

Chapter 2

Model Description

2.1 Description of Numerical Model

In this thesis, we use a modified version of the NCAR RegCM. This section provides a general description this model, in addition to a more detailed description of the large-scale cloud and precipitation, convection, land surface schemes.

2.1.1 General Model Description

The NCAR RegCM was originally developed by Dickinson et al. (1989), Giorgi and Bates (1989), and Giorgi (1990) using the Penn State/NCAR Mesoscale Model version 4 [MM4; (Anthes et al. 1987)] as the dynamical framework. Here we provide only a brief description of RegCM (except for the large-scale cloud and precipitation models); A more detailed description can be found in Giorgi and Mearns (1999) and references therein.

Like MM4, RegCM is a primitive equation, hydrostatic, compressible, sigma-vertical coordinate model. Unlike MM4, RegCM is adept for climate studies. The atmospheric radiative transfer computations are performed using the CCM3 based package (Kiehl et al. 1996), and the planetary boundary layer computations are performed using the non-local formulation of Holtslag et al. (1990). The surface physics calculations are performed using one of two soil-vegetation hydrological process models: (1) Biosphere-Atmosphere Transfer Scheme [BATS; Dickinson et al. (1986)] and (2) Integrated BIosphere Simulator [IBIS; Foley et al. (1996)]. The unresolvable precipitation processes (Cumulus convection) are represented using one of three options: (1) Grell scheme (Grell 1993); (2) Modified-Kuo scheme (Anthes 1977); and (3) Emanuel scheme (Emanuel 1991). The

Grell parameterization is implemented using one of two closure assumptions: (1) Arakawa and Schubert (1974) (denoted hereafter as AS74) closure and (2) Fritsch and Chappell (1980) (denoted hereafter as FC80) closure. RegCM has two options for the representation of resolvable clouds and precipitation: (1) Simplified Explicit Moisture Scheme [Giorgi and Shields (1999); denoted hereafter as SIMEX] and (2) Sub-grid Explicit Moisture Scheme [Pal et al. (2001); denoted hereafter as SUBEX]. The surface physics scheme and both the resolvable (non-convective) and unresolvable (convective) cloud and precipitation schemes are described below.

2.1.2 Description of the Surface Physics

The surface physics computations in RegCM are performed using BATS version 1E (Dickinson et al. 1986). BATS describes the transfer of energy, mass, and momentum between the atmosphere and biosphere. It contains three soil layers (a 10 cm surface layer, a 1 to 2 m root zone, and a 3 m deep soil layer), one vegetation layer (19 land cover/vegetation types), and one snow layer. It has prognostic equations for soil temperature and water content and in the presence of vegetation, canopy air temperature and foliage temperature. In addition to the 19 vegetation types, BATS has twelve soil texture classes ranging from very coarse (sand) to medium (loam) to very fine (heavy clay). In this thesis, the soil texture is a function of the vegetation characterization. For example, desert regions are associated with relatively sandy soils while forests are associated with clayier soils. In BATS, the land-use characterization and soil texture are held constant over the entire simulation at each grid point.

In this thesis, we also coupled Integrated BIosphere Simulator (IBIS) to RegCM (Foley et al. 1996). IBIS integrates a wide range of terrestrial phenomena, including the biophysical, physiological, and ecosystem dynamical processes, into a single physically consistent model. The vegetation cover in IBIS is a combination of different plant functional types (PFTs). PFTs are defined based on physiognomy (trees and grasses), leaf form (broad-leaf and needle-leaf), leaf habit (evergreen and deciduous), and photo-synthetic pathway (C3 and C4). Vegetation canopy is divided into two layers, with woody plants in the upper canopy and herbaceous plants in the lower canopy. Soil texture is represented by the percentage of three different components: sand, silt, and clay. The main difference between BATS and IBIS is that vegetation within IBIS can change with changing climatic conditions. In addition, the transpiration computations are more physically represented within IBIS. For example, IBIS accounts for the differences in stomatal pores sizes associated with carbon dioxide variations. This is particularly important for climate change studies. The results

of the coupling between IBIS and RegCM are preliminary and not presented in this thesis.

2.1.3 Description of the Large-Scale Cloud and Precipitation Schemes

In this subsection, we provide a detailed description of the large-scale cloud and precipitation schemes now implemented in RegCM. By large-scale, we mean non-convective clouds that are resolved by the model. The first scheme described is referred to as the SIMEX (Giorgi and Shields 1999)) and the second scheme is referred to as SUBEX (Pal et al. 2001). Hydrostatic water loading is included in the pressure computations and ice physics are not explicitly represented in either scheme. Both schemes treat only non-convective cloud and precipitation processes; Cumulus convective processes and the other non-convective processes are considered independent of one another during each time step.

Simplified Explicit Moisture Scheme (SIMEX)

SIMEX is a simplified version of the fully explicit moisture scheme presented by Hsie et al. (1984). The Hsie et al. (1984) formulation includes prognostic equations for both cloud water and rainwater. Due to its complexity and hence, heavy computational expense, Giorgi and Shields (1999) simplified the Hsie et al. (1984) scheme into SIMEX. In SIMEX, the prognostic variable for rainwater has been removed and the computations for rainwater accretion, gravitational settling, and evaporation are no longer performed. These simplifications result in a significant reduction in the total model computation time. The following provides a description of SIMEX similar to that presented in Giorgi and Shields (1999).

Cloud water Q_c^{LS} in SIMEX forms when the average grid cell relative humidity exceeds saturation. The water vapor in excess of saturation is converted directly into cloud water. The cloud water can advect, diffuse, and re-evaporate, in addition to form precipitation.

Precipitation P^{LS} in a given model level is formed when the cloud water content exceeds the auto-conversion threshold Q_c^{th} according to the following relation:

$$P^{LS} = C_{ppt}(Q_c^{LS} - Q_c^{th}) \tag{2.1}$$

where $1/C_{ppt}$ can be considered the characteristic time for which cloud droplets are converted into raindrops. Precipitation is assumed to fall instantaneously. The auto-conversion threshold is an increasing function of temperature (see Figure 2-1; solid black line). The steep slope below 265K

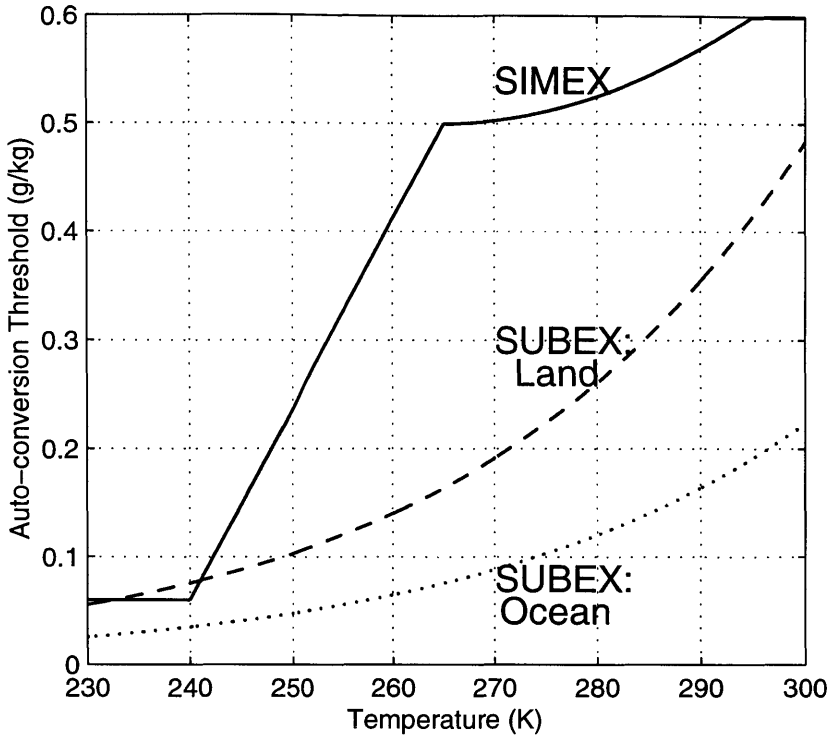

Figure 2-1: Plot of the auto-conversion threshold (g/kg) versus temperature (K) for SIMEX (solid line) and SUBEX (dashed for land; dotted for ocean).

indirectly accounts for the formation of ice which enhances the precipitation formation process.

The fractional cloud cover FC^{LS} at each model level in SIMEX is set to a constant value (75% in the simulations presented here) when super-saturated (cloud) water exists and zero when no cloud water is present. Note FC^{LS} is the fractional coverage in the horizontal direction; The cloud is assumed to fill the grid cell in the vertical direction. Giorgi et al. (1999) suggest that SIMEX's formulation for FC^{LS} is a deficiency in RegCM and should be tied to relative humidity and cloud water content as well as model resolution. SUBEX addresses this issue (among others) and is described in the following subsection.

Sub-grid Explicit Moisture Scheme (SUBEX)

In the atmosphere, variability within regions comparable to the size of a model grid cell often results in saturated areas where clouds exist and sub-saturated areas where clouds are not present. When the saturated fraction of the region is small, so is the cloud fraction and vice versa. Thus, one would expect that there is a direct link between the average grid cell relative humidity (among

other variables) and the cloud fraction as well as the cloud water content. The scheme presented here (SUBEX) accounts for the sub-grid variability observed in nature by linking the average grid cell relative humidity to the cloud fraction and cloud water following the work of Sundqvist et al. (1989). SUBEX, unlike SIMEX, includes simple formulations for raindrop accretion and evaporation. Additional modifications are in the specification of the auto-conversion threshold. These modifications improve the physical manner in which large-scale clouds and precipitation are represented with little computational sacrifice. Table 2.1.3 lists the values of the primary parameters within SUBEX.

Table 2.1: List of parameters used in SUBEX and their associated values.

Parameter	Land	Ocean	Units
Cloud formation threshold rh_{min}	0.8	0.9	
Maximum saturation rh_{max}	1.01	1.01	
Auto-conversion rate C_{ppt}	$5x10^{-4}$	$5x10^{-4}$	s^{-1}
Auto-conversion scale factor C_{acs}	0.65	0.3	
Accretion rate C_{acc}	6	6	$m^3kg^{-1}s^{-1}$
Raindrop evaporation rate C_{evap}	$1x10^{-5}$	$1x10^{-5}$	$(kg\ m^{-2}\ s^{-1})^{-1/2}\ s^{-1}$
Cloud droplet radius R_d	5-10	13	μm

In this approach, each model grid cell is divided into a clear and cloud portion. Any variable, V, is the average of the values in the clear and cloudy portions of the grid cell, V_{nc} and V_c, respectively, weighted by FC^{LS}, by the following relationship:

$$V = FC^{LS}V_c + (1 - FC^{LS})V_{nc}. \tag{2.2}$$

FC^{LS} at a given model level varies based on the average grid cell relative humidity rh according to the following relation:

$$FC^{LS} = \sqrt{\frac{rh - rh_{min}}{rh_{max} - rh_{min}}} \tag{2.3}$$

where rh_{min} is the relative humidity threshold at which clouds begin to form and rh_{max} is the relative humidity where the fractional cloud cover reaches unity. FC^{LS} is assumed to be zero when the rh is less than rh_{min} and unity when rh is greater than rh_{max}. Figure 2-2 displays these curves for ocean and land. Smaller values of rh_{min} are associated with greater sub-grid variability. Typical

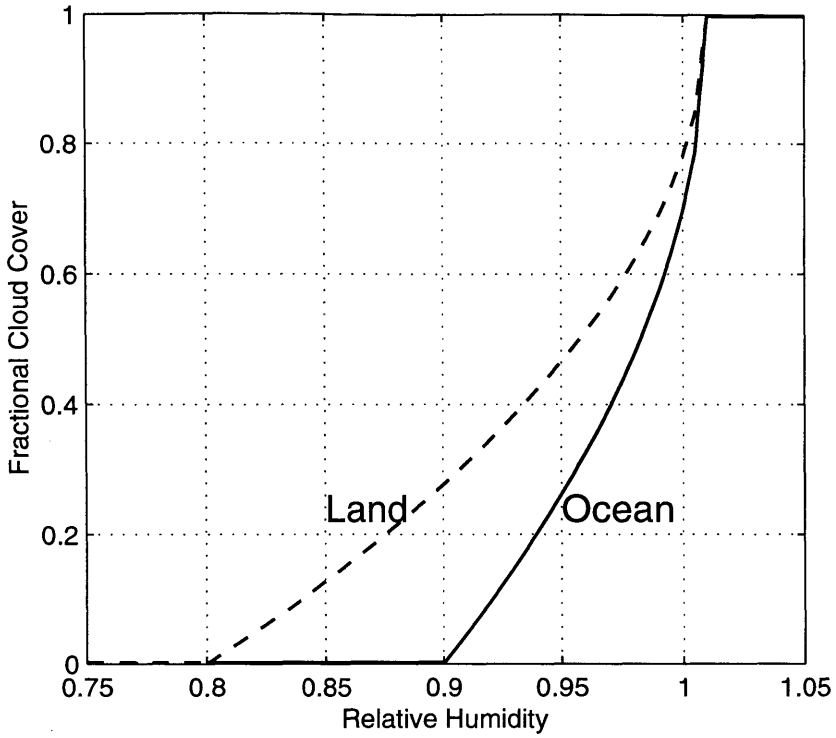

Figure 2-2: Plot of the fractional cloud coverage as a function of relative humidity for the new cloud and precipitation scheme. The dashed curve denotes the values for land and the solid line denotes the values for ocean.

values for rh_{min} range from 60% to 100% depending a variety of factors including the vertical level (Sundqvist 1988), the surface characteristics (Sundqvist et al. 1989), and the model resolution. The threshold over land is often specified lower than the threshold over ocean due sub-grid scale surface heterogeneities that translate upward into the atmosphere (Sundqvist et al. 1989). These heterogeneities can result from variable topography, soil moisture, vegetation, surface friction, etc. The ocean surface is relatively homogeneous in that the surface roughness is small and temperatures do not vary considerably at small scales. Sundqvist et al. (1989) use 75% and 85% for land and ocean, respectively. Within the boundary layer and at lower temperatures (<238K), they let rh_{min} increase linearly to a value near unity. Preliminary experiments varying rh_{min} over the land value by $\pm 5\%$ resulted in negligible changes. Thus, for simplicity, we specify rh_{min} at 80% for land and 90% for ocean and do not allow rh_{min} to vary in the vertical or with temperature. rh_{max} is set to 1.01 allowing water vapor content to exceed the saturation value by one percent.

The formulation for the auto-conversion of cloud water into precipitation in SUBEX is nearly

identical to that in SIMEX. The main difference is in the specification of the auto-conversion threshold and that in-cloud values of Q_c^{LS} are used, as follows:

$$P^{LS} = C_{ppt}(Q_c^{LS}/FC^{LS} - Q_c^{th})FC^{LS} \tag{2.4}$$

Like SIMEX, once precipitation forms, it is assumed to fall instantaneously. The new auto-conversion threshold is based on the analysis of Gultepe and Isaac (1997). They used aircraft observations of cloud liquid water content and related them to temperature. Here the threshold is obtained by scaling the median cloud liquid water content equation according to the following:

$$Q_c^{th} = C_{acs}10^{-0.49+0.013T} \tag{2.5}$$

where T is temperature in degrees Celsius and C_{acs} is the auto-conversion scale factor. By scaling the Q_c^{LS}-T relationship, we assume that the threshold takes the shape of the mean cloud conditions. Over the ocean there are typically less cloud condensation nuclei than over land. As a result, the cloud droplets over the ocean are larger and hence, less buoyant than those over land (Rogers and Yau 1989). Larger cloud droplets tends to result in more collision and coalescence. Thus, continental clouds tend to be thicker than maritime clouds for the same probability of precipitation (Rogers and Yau 1989). Due to these land-ocean contrasts, we specify C_{acs} at 0.65 over land and 0.4 over ocean. These values were selected based on series of preliminary experiments. Figure 2-1 displays the auto-conversion thresholds for SUBEX (dashes for land and dots for ocean). Note that in both SIMEX and SUBEX, the different sizes of cloud droplets over ocean and land are accounted for within the CCM3 radiation package. Also note that the model displays a considerable sensitivity to the specification of Q_c^{th} and C_{acs}. Furthermore, Equation 2.5 does not account for the presence of cloud ice. In light of this, it may be expected that SUBEX under predicts precipitation since cloud ice increase the auto-conversion efficiency [via an increase the amount of CCN; (Rogers and Yau 1989)]. This in turn is likely to result in too much cloud water and will likely adversely impact radiation budget under these conditions. Neglecting ice physics within clouds is a shortcoming in SUBEX and should be addressed in future work.

Raindrop Accretion (SUBEX only)

Raindrop accretion can be an important process under certain climatic conditions (Rogers and Yau 1989). In SIMEX, only the cloud water in excess of the auto-conversion threshold is allowed to

precipitate out (see Equation 2.1). Thus, once clouds form, they often linger at or near the auto-conversion threshold (in the absence of other atmospheric processes such as cloud evaporation). In nature, however, once precipitation initiates (exceeds the auto-conversion threshold), rain droplets falling through clouds collect and remove a portion of the cloud droplets. Thus, neglecting this process can result in an under prediction of precipitation and over prediction of clouds particularly in humid regions; Accounting for it allows the cloud water content to fall below the auto-conversion threshold when precipitation occurs. SUBEX includes a simple formulation for the accretion cloud droplets by falling rain droplets according to the following relation based on Beheng (1994):

$$P_{acc} = C_{acc} Q_c P_{sum} \tag{2.6}$$

where P_{acc} is the amount of accreted cloud water, C_{acc} is the accretion rate coefficient, and P_{sum} is the accumulated large-scale precipitation from above falling through the cloud. Accretion only takes place in the cloudy portions of the grid cell. For simplicity, P_{sum} is assumed to be distributed uniformly across the grid cell. In other words, no knowledge of the cloud fraction in which the precipitation formed is used. In some cases, this may tend to overestimate the effects of accretion.

Raindrop Evaporation (SUBEX only)

As with raindrop accretion, raindrop evaporation can also be an important process under certain conditions (Rogers and Yau 1989). In arid regions, a significant quantity of the precipitation that forms often evaporates before it reaches the surface. Neglecting this process can lead to the simulation of excessive precipitation in arid regions (Small et al. 1999a). SUBEX employs the simple formulation of Sundqvist et al. (1989), as follows:

$$P_{evap} = C_{evap}(1 - rh) P_{sum}^{1/2} \tag{2.7}$$

where P_{evap} is the amount of evaporated precipitation and C_{evap} is the rate coefficient. More raindrop evaporation occurs where the air is dry relative to saturation. As with the formulation for accretion, P_{sum} is assumed to to be distributed uniformly across the grid cell. Only raindrops falling through the cloud-free portion of the grid box are allowed to evaporate. Inclusion of this process may also result in an decrease in the number of numerical grid point storms (Molinari and Dudek 1986).

2.1.4 Description of the Convective Precipitation Schemes

Convective precipitation is computed using one of three schemes: (1) Grell scheme (Grell 1993); (2) Modified-Kuo scheme (Anthes 1977); and (3) Emanuel scheme (Emanuel 1991). In addition, the Grell parameterization is implemented using one of two closure assumptions: (1) AS74 closure and (2) FC80 closure.

Grell Scheme

The Grell scheme (Grell 1993), similar to the AS74 parameterization, considers clouds as two steady-state circulations: an updraft and a downdraft. No direct mixing occurs between the cloudy air and the environmental air except at the top and bottom of the circulations. The mass flux is constant with height and no entrainment or detrainment occurs along the cloud edges. The originating levels of the updraft and downdraft are given by the levels of maximum and minimum moist static energy, respectively. The Grell scheme is activated when a lifted parcel attains moist convection. Condensation in the updraft is calculated by lifting a saturated parcel. The downdraft mass flux (m_0) depends on the updraft mass flux (m_b) according to the following relation:

$$m_0 = \frac{\beta I_1}{I_2} m_b, \tag{2.8}$$

where I_1 is the normalized updraft condensation, I_2 is the normalized downdraft evaporation, and β is the fraction of updraft condensation that re-evaporates in the downdraft. β depends on the wind shear and typically varies between 0.3 and 0.5. Rainfall is given by

$$P^{CU} = I_1 m_b (1 - \beta). \tag{2.9}$$

Heating and moistening in the Grell scheme are determined both by the mass fluxes and the detrainment at the cloud top and bottom. In addition, the cooling effect of moist downdrafts is included.

Due to the simplistic nature of the Grell scheme, several closure assumptions can be adopted. RegCM2's default version directly implements the quasi-equilibrium assumption of AS74. It assumes that convective clouds stabilize the environment as fast as non-convective processes

destabilize it as follows:

$$m_b = \frac{ABE'' - ABE}{NA\Delta t}, \tag{2.10}$$

where ABE is the buoyant energy available for convection, ABE'' is the amount of buoyant energy available for convection in addition to the buoyant energy generated by some of the non-convective processes during the time interval Δt, and NA is the rate of change of ABE per unit m_b. The difference $ABE'' - ABE$ can be thought of as the rate of destabilization over time Δt. ABE'' is computed from the current fields plus the future tendencies resulting from the advection of heat and moisture and the dry adiabatic adjustment.

Another stability based closure assumption that is commonly implemented in GCMs and RCMs is the FC80 type closure assumption. In this closure, it is assumed that convection removes the ABE over a given time scale as follows:

$$m_b = \frac{ABE}{NA\tau}, \tag{2.11}$$

where τ is the ABE removal time scale.

The fundamental difference between the two assumptions is that the AS74 closure assumption relates the convective fluxes and rainfall to the tendencies in the state of the atmosphere, while the FC80 closure assumption relates the convective fluxes to the degree of instability in the atmosphere. Both schemes achieve a statistical equilibrium between convection and the large-scale processes. However, this subtle distinction in the implementation of the closure will prove to be an important difference.

Kuo Scheme

Convective activity in the Kuo scheme is initiated when the moisture convergence M in a column exceeds a given threshold and the vertical sounding is convectively unstable. A fraction of the moisture convergence β moistens the column and the rest is converted into rainfall P^{CU} according to the following relation:

$$P^{CU} = M(1-\beta). \tag{2.12}$$

β is a function of the average relative humidity $\overline{RH}$ of the sounding as follows:

$$\beta = \begin{cases} 2(1-\overline{RH}) & \overline{RH} \geq 0.5 \\ 1.0 & \text{otherwise} \end{cases} \tag{2.13}$$

Note that the moisture convergence term includes only the advective tendencies for water vapor. However, evapotranspiration from the previous time step is indirectly included in M since it tends to moisten the lower atmosphere. Hence, as the evapotranspiration increases, more and more of it is converted into rainfall assuming the column is unstable. The latent heating resulting from condensation is distributed between the cloud top and bottom by a function that allocates the maximum heating to the upper portion of the cloud layer. To eliminate numerical point storms, a horizontal diffusion term and a time release constant are included so that the redistributions of moisture and the latent heat release are not performed instantaneously (Giorgi and Bates (1989) and Giorgi (1991)).

Convective Clouds

For each moist convectively active layer, RegCM2 simulates the convective fractional cloud coverage by the following relation:

$$FC^{CU} = \begin{cases} 1-(1-FC^{MAX})^{1/N} & \text{if moist convection} \\ 0.0 & \text{otherwise} \end{cases} \tag{2.14}$$

where N is the number of model levels within the convectively active column and FC^{MAX} is the maximum fractional convective cloud coverage (0.8 in the simulations presented here). If a given layer is not convectively active, the convective cloud fraction is set to zero. This equation accounts for the tall narrow nature of convective clouds. Lastly, the convective cloud water content (Q_C^{CU}) is assumed to be constant (0.6 g/m^3 in the simulations presented here). The convective cloud fraction water are used only in the atmospheric radiation computations. Admittedly, this formulation over simplifies the complex nature of convective cloud cover and liquid water content which may pose some problems in the simulation of radiative fields and it should be addressed in future work.

2.2 Model Initialization and Evaluation Datasets

As mentioned in Subsection 1.2, a wealth of data which can be useful for modeling purposes has recently become available. These data include observations from satellites, surface stations, and rawinsondes among other sources. In this thesis we take advantage of several satellite datasets, one surface station datasets, and a reanalysis dataset. This section describes some of these datasets in addition to some of the statistical analyses performed on them.

2.2.1 Model Simulation Datasets

Because RegCM is a limited area model, it requires initial conditions and time-dependent lateral boundary conditions for wind components, temperature, surface pressure, and water vapor. An accurate representation of these boundary conditions is often essential for many regional climate model applications. Here, we force each simulation at the lateral boundaries using the National Centers for Environmental Prediction (NCEP) Reanalysis data (Kalnay et al. 1996). The NCEP data have a spatial resolution of 2.5° X 2.5°, are distributed at 17 pressure levels (8 for humidity), and are available at time intervals of 6 hours. Traditionally, RegCM has been forced by 12-hour European Center for Medium-Range Weather Forecasts (ECMWF) original IIIb global non-analysis data [Bengtsson et al. (1982); Mayer (1988); Trenberth and Olson (1992)]. The ECMWF data have occasional model improvements which lead to inconsistencies within the product between years. This can cause significant problems in studies investigating interannual variability. In addition, the temporal resolution (twice daily) may not fully resolve the diurnal cycle of many processes such as the Great Plains low-level jet (Higgins et al. 1997b). The consistent model and high temporal resolution of the NCEP reanalysis product should provide significant improvements to the ECMWF non-reanalysis used in many RegCM applications. In addition, we made improvements to the interpolation procedure to better represent the data on the model grid. These improvements include a correction for the Gibbs phenomenon that occurs as a result of the spectral to latitude-longitude transformation and results in noisy surface fields (e.g. ±50 m over the ocean surface). The correction is applied over ocean surfaces by adjusting the surface heights and surface pressure to sea level. It is particularly important when the domain boundaries lie over ocean regions (as is often the case here).

The SSTs are prescribed using data provided by the United Kingdom Meteorological Office [UKMO; Rayner et al. (1996); one degree grid]. The atmospheric fields are initialized using the

NCEP Reanalysis data. Similar to Pal and Eltahir (2001), soil moisture is initialized using a dataset that merges soil moisture data from the Illinois State Water Survey [ISWS; Hollinger and Isard (1994)], Huang et al. (1996) (denoted hereafter as HDG), and a climatology based on the vegetation type (see Section 2.2 below). The vegetation is specified using the Global Land Cover Characterization (GLCC) data provided by the United States Geological Survey's (USGS's) Earth Resources Observation System Data Center (Loveland et al. 1999). This is a state of the art vegetation dataset that is derived from 1-km Advanced Very High Resolution Radiometer (AVHRR) satellite data. These data should provide for a more accurate representation of land surface processes than those of the original 13 RegCM/MM4 vegetation data types (Haagenson et al. 1989). The soil texture class is prescribed according to the vegetation characterization.

Soil Moisture Datasets

The initialization of soil moisture in models is important for an accurate representation of the land surface energy balance. To initialize soil moisture in the control simulations, this study takes advantage of a merged dataset created in this thesis that combines three datasets: ISWS; HDG; and a vegetation based climatology (denoted hereafter as HDG/ISWS).

The ISWS is responsible for a network of direct soil moisture measurement stations across the state of Illinois [see Hollinger and Isard (1994)]. Since 1981, biweekly measurements have been taken at 11 depths from the surface to two meters over 17 grass-covered sites across Illinois. To date, it provides the most accurate and the most spatially and temporally extensive soil moisture dataset of its kind in North America. Although this is the best dataset available in North America, it does not cover a large enough spatial range to initialize the entire domain of typical three-dimensional modeling experiments.

The HDG soil moisture data used in this study comes from a simulated dataset created over the continental United States generated from the 344 climate divisions data (Huang et al. 1996). It spans the period from 1931 through 1993. The model used to generate these data is based on the water budget of the soil and uses monthly station rainfall and temperature as inputs. Its four parameters are calibrated using observed rainfall, temperature, and runoff from an area in Oklahoma. The soil moisture model performs remarkably well when compared to the ISWS soil moisture data (correlation coefficient = 0.84). Therefore, this dataset should be adequate in initializing the domain of the regional climate model.

As mentioned in Subsection 2.1.2, BATS requires soil moisture data at 3 soil levels, however,

the HDG data is given as one volumetric value. A relation between the ISWS and HDG data is developed to generate a more realistic vertical soil moisture profile over the entire domain. The soil saturation at a given layer k and location i, j ($S_{i,j,k}$) is the ratio of the average ISWS value at the given layer ($ISWS_k^{avg}$) to the HDG value over Illinois (HDG_{ILL}^{avg}) multiplied by the HDG value ($HDG_{i,j}$) according to the following relation:

$$S_{i,j,k} = \frac{ISWS_k^{avg}}{HDG_{ILL}^{avg}} * HDG_{i,j}. \tag{2.15}$$

This approximation translates the vertical profile structure from the Illinois data to the rest of the domain. Although, vertical soil water profile structures are regionally dependent, this method provides a more reasonable way to initialize soil moisture that accounts for the vertical variability.

The land portions of the domain that do not include the United States in this thesis (i.e. Canada and Mexico) are initialized with a soil moisture climatology based on the vegetation type. Moister values are associated with trees and drier values are associated with deserts and grasslands according to Giorgi and Bates (1989).

2.2.2 Model Evaluation Datasets

Four datasets are used are used to evaluate the model performance: (1) National Aeronautics and Space Administration (NASA) Earth Radiation Budget Experiment [ERBE; Barkstrom (1984)], (2) NASA-Langley Surface Radiation Budget data [NASA-SRB; Darnell et al. (1996) and Gupta et al. (1999)], (3) International Satellite Cloud Climatology Project D2 data [ISCCP-D2; Rossow and Schiffer (1999)], and (4) United States Historical Climatology Network [USHCN; Karl et al. (1990)]. Each of these datasets are independent of the NCEP Reanalysis data used to force the model. Table 2.2 provides a summary of the spatial and temporal coverage of the observational fields used to evaluate the model's performance.

ERBE Data

The ERBE data are derived from satellite observations of the top of the atmosphere fluxes (Barkstrom 1984). They represent the balance between incoming energy from the sun and outgoing longwave and shortwave energy from the Earth. The data span the period February 1985 through April of 1989 and are provided on a 2.5° equal-area grid. For convenience, we project the data onto a 2.5° latitude-longitude grid.

Table 2.2: List of verification datasets used in this study. EA denotes equal-area; OLR denotes top of the atmosphere outgoing longwave radiation; ALBEDO denotes top of the atmosphere albedo; SWI denotes incident surface shortwave radiation; RN denotes net surface radiation; CWP denote cloud water path; PPT denotes precipitation; and TMEAN, TMAX, and TMIN denote the mean, maximum, and minimum surface temperatures, respectively.

	ERBE	NASA-SRB	ISCCP-D2	USHCN
Grid	2.5° EA	2.5° EA	2.5° EA	344 Stations
Time span	8502-8904	8307-9106	8601-8701; 8707-9312	Full coverage
Fields	OLR	SWI	CWP	PPT
	ALBEDO	RN		TMEAN
				TMAX
				TMIN

In this thesis, we use the top of the atmosphere outgoing longwave radiation and albedo to evaluate the model. Kiehl and Ramanathan (1990) report that the time-averaged accuracy of the fluxes is within 10 W/m^2. It is likely, however, that the biases vary by region and season. In addition, the uncertainty is likely to be higher when comparing individual months of a particular year.

ISCCP-D2 Data

The ISCCP-D2 data provide comprehensive cloud property information based on satellite measurements [Rossow et al. (1996) and Rossow and Schiffer (1999)]. These data span January 1986 through December 1993 (missing February 1987 through June 1987) and are provided on a 2.5° equal-area grid. For convenience, we project the data onto a 2.5° latitude-longitude grid. In this study, we use the cloud water path measurements to evaluate the model. The D2 product is significantly more accurate than the original C2 product, however, precise numbers on the accuracy of these data are unclear. To our knowledge, these are the best measurements of cloud water content available for our purposes.

NASA-SRB Data

The NASA-SRB data are derived from a variety of data sources, including the ISCCP-C1 and ERBE data products [Darnell et al. (1996) and Gupta et al. (1999)]. To generate the shortwave product, the ISCCP-C1 and ERBE data are used as input into two different algorithms: the Pinker

algorithm (Pinker and Laszlo 1992) and the Staylor algorithm (Darnell et al. 1992). The longwave data are generated using the Gupta algorithm (Gupta et al. 1992). The data span from July 1983 through June 1991, and like the ISCCP-D2 and ERBE data, the NASA-SRB data are provided on a 2.5° equal-area grid. Again for convenience, we project the data onto a 2.5° latitude-longitude grid.

Gupta et al. (1999) indicate that there are significant biases over coastal regions, snow/ice covered regions, regions with high aerosol concentrations, and regions with extensive river and mountain valleys. For model comparison, we use the incident surface shortwave radiation and net surface radiation (net shortwave plus net longwave). Gupta et al. (1999) report a time-averaged bias of 5 W/m^2 and root mean square error of between 11 and 24 W/m^2 for incident surface shortwave. However, when comparing monthly averaged point measurements at individual locations, the biases can be larger than 100 W/m^2. For our region of interest, we should not expect errors larger than 50 W/m^2 except potentially near the coasts and over the Rocky Mountains. In addition, Gupta et al. (1999) suggest that errors ISCCP-C1 input data may pose problems with the SRB longwave data. This may be problematic for the longwave component of net radiation data used to evaluate the model.

USHCN Data

The USHCN data include monthly averaged mean, maximum, and minimum temperature and total monthly precipitation (Karl et al. 1990). The dataset consists of 1221 high-quality stations from the United States Cooperative Observing Network within the 48 contiguous United States and was developed to assist in the detection of regional climate change. The period of record varies for each station but generally includes the period from 1900 through 1996.

The precipitation and temperature data are interpolated onto the RegCM grid. The interpolation is performed by exponentially weighting the station data according to the distance of the station from the center of the RegCM grid cell, with a length-scale of 50 km. In addition, the temperature data are corrected for elevation differences between the model and the USHCN data.

Statistics

Monthly averages from the data described above and model output are computed over regions such as the Midwest and Gulf Coast. The following provides a summary of the statistics used to test and verify the model in Chapters 3 and 4.

The bias between the model simulations and the observational data represents the model's ability to reproduce observed mean conditions. The root mean square error (RMSE) provides an indication of the overall error of the model simulations compared to the observational data. It should be noted that the RMSE contains the bias within the statistic. Therefore, an improvement to the bias typically results in an improvement to the RMSE. The slope and RMSE provide a measure of the model's ability to simulate the seasonal and interannual variability; A slope greater than unity indicates that the model over predicts the seasonal and/or interannual variability and a slope less than unity indicates an under prediction. The scatter of the model output around their best fit line to observations describes the accuracy of the model in simulating the processes that represent the interannual variability. Combined improvements to the bias, RMSE, and slope imply improvements to the model's ability to accurately represent observations of both the mean conditions as well as variability at daily to interannual scales.

Chapter 3

Role of Large-Scale Clouds and Precipitation

In many applications of the NCAR RegCM, an accurate simulation of the energy and water cycles is crucial (Giorgi and Mearns 1999). The presence of clouds and resulting precipitation is the primary control on these budgets. It is therefore important to accurately represent cloud processes in many modeling applications. Clouds, however, are often poorly represented in both regional and global climate models (RCMs and GCMs, respectively) partly because some of the key cloud processes occur at spatial and temporal scales not resolved by current models. This chapter presents a simple, yet physical, resolvable-scale (non-convective) moist physics and cloud scheme for the NCAR RegCM that accounts for the sub-grid variability of clouds, the accretion of cloud water, and the evaporation of raindrops.

Section 3.1 briefly introduces this chapter. Section 3.2 describes the setup of the numerical experiments that compare the old and new large-scale cloud and precipitation schemes (SIMEX and SUBEX, respectively). The results and conclusions are provided in Sections 3.3 and 3.4, respectively. Note a description of each of these schemes is provided in Chapter 2.

3.1 Introduction

The response of the climate system to changes in soil moisture, as well as, greenhouse gases, sulfate aerosols, and vegetation is strongly influenced by cloud processes. For example, the IPCC (1995) Report on climate change indicates that the representation of cloud characteristics accounts for a large portion of the uncertainty in climate change predictions. They further indicate that inclusion

of different cloud representations could result in dramatic effects as much as to double the expected 2.5^{o}C warming or to reduce it by half. As another example, Pal and Eltahir (2001) suggest that cloud processes play an important role in determining the strength of the soil moisture-rainfall feedback. They show that under certain conditions, a strong response of clouds to changes in soil moisture can nearly negate the soil moisture-rainfall feedback. The representation of clouds is also important for simulations of other land surface changes, including deforestation (e.g. Eltahir and Bras (1994)), desertification (e.g. Xue (1996)), and desiccation of inland water bodies (e.g. Small et al. (1999b)).

In the old version of RegCM [SIMEX moist physics; Giorgi et al. (1999)], the representation of land surface, radiation, and boundary layer processes (among others) is quite elaborate (Giorgi and Mearns 1999). However, the representation of cloud processes is not nearly as sophisticated. It is shown in this chapter that over North America, the old version of RegCM tends to be too cloudy at times when clouds exist and not cloudy enough in low-cloud conditions. As a result, the seasonal variability of clouds tends to be overestimated. RegCM with SIMEX seems to neglect key processes required to accurately predict the observed variability of clouds.

To accurately simulate precipitation one needs to account for various processes including those that occur at scales finer than the model resolution. In the atmosphere, clouds often form over part of an area comparable to the size of a model grid cell when the area-average humidity is below 100%. Thus, fractional cloud coverage varies between zero and 100% over the same area. Molinari and Dudek (1986) investigate a rainfall event that occurred over the northeastern portion of the United States using a RCM. They indicate that neglecting the sub-grid variability delays the onset of precipitation. The collection of cloud droplets from raindrops falling through clouds and the evaporation of falling raindrops can be very important processes (Rogers and Yau 1989). Not including the former can lead to an underestimation of precipitation intensity and volume particularly over cloudy regions. Not including the latter, can lead to an overestimation of precipitation particularly over arid regions (Small et al. 1999a) and can result in unrealistic model instabilities (Molinari and Dudek 1986). SIMEX neglects the above sub-grid processes, while our new scheme, SUBEX, accounts for these processes based on the work of Sundqvist et al. (1989) and others.

3.2 Design of Numerical Experiments

In this section, we provide a description of the numerical experiments performed in this study. Each run is initialized on the 15th of March for each of the following years: 1986, 1987, 1988, 1989, 1990, and 1993. The runs are integrated for one year and 17 days (18 days for the simulations initialized in 1987 due to the 1988 leap year). The first 17 (or 18) days are ignored for model spin-up considerations. The simulation for each year is performed twice; one run using SIMEX to represent the large-scale cloud and precipitation processes and another using SUBEX. The pair of simulations for each year is identical except for the choice of large-scale cloud and precipitation scheme. Note that the Grell scheme with the AS74 closure assumption is utilized in these simulations.

The simulations are initialized on the 15th of March so that snow cover can somewhat reasonably be initialized at zero. (Future efforts should be directed towards including a snow cover dataset to initialize the model.) In addition, this gives soil moisture within BATS time to spin-up before the summer when biosphere-atmosphere interactions are most pronounced. Lastly, the simulations are divided into year long runs to minimize drift in soil moisture.

The years 1986, 1987, 1988, 1989, 1990, and 1993 are selected because observational based data exist for model evaluation from the NASA ERBE [except for 1989, 1990, and 1993; Barkstrom (1984)], NASA-SRB [except for 1993; Darnell et al. (1996) and Gupta et al. (1999)] and the ISCCP-D2 (Rossow and Schiffer 1999). Details on each of these datasets are provided in Section 2.2. In 1988 and 1993, the United States Midwest experienced severe summertime drought and flood, respectively. These years are also selected to determine how SIMEX and SUBEX compare in their response to extreme forcings.

Figure 3-1 depicts the domain and associated topography for the simulations presented in this chapter (and Chapters 4 and 6). Close attention has been paid to the selection of the model domain so that the boundary conditions do not fully constrain the model. In addition, the number of boundary points occurring over complex topography have been minimized. The grid is defined on a modified version of RegCM's Mercator map projection in that the origin of the projection is no longer constrained to the equator. The added generality minimizes the deviation of the map-scale factors from unity even when compared to the commonly used Lambert Conformal map projection. This results in less distortion, especially as domain edges are approached. The domain center is located at 37.581°N and 95°W and the origin is rotated to 40°N and 95°W. In the horizontal, the grid is 129 points in east-west direction and 80 in the north-south with a resolution of 55.6 km

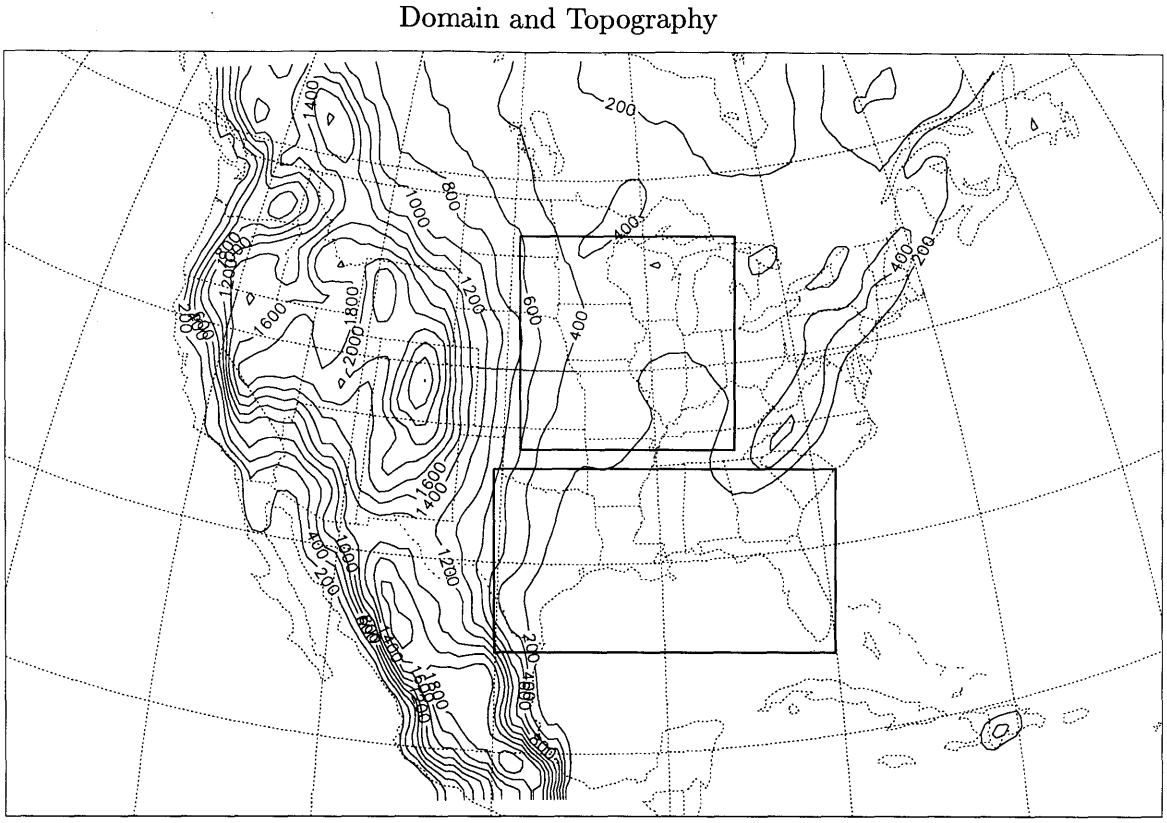

Figure 3-1: Map of the domain and terrain heights used for the numerical simulations. The outlined Midwest and Gulf Coast boxes are the regions over which spatial averages are taken.

(approximately half a degree). There are 14 vertical sigma levels with highest concentration of levels near the surface (0.02, 0.07, 0.135, 0.21, 0.3, 0.405, 0.51, 0.615, 0.72, 0.815, 0.895, 0.95, 0.98, and 0.995). The model top is at 50 mb.

3.3 Results: SIMEX versus SUBEX

In this section, the simulations utilizing SIMEX to represent the large-scale cloud and precipitation physics are compared to those utilizing SUBEX. Monthly averages from the data are computed over the Upper Midwest defined in Figure 3-1 and then compared to observations. We focus on the Midwest because it is one of the most agriculturally productive regions in the world. In addition, it is a region that is vulnerable to extreme summer flood and drought. As a result, it is particularly important to accurately simulate the energy and water budgets of this region. Furthermore, the observational data used to evaluate the model performance are less likely to have errors due to the relatively flat and homogeneous land surface. Table 3.1 provides a summary of the statistics

computed over the Midwest. A description of the of statistics and the meaning is provided in Subsection 2.2.2.

Table 3.1: Summary of the model simulation statistics compared to observations for SUBEX and SIMEX over the Midwest (outlined in Figure 3-1). RMSE denotes root mean square error; ALBEDO denotes top of the atmosphere albedo; OLR denotes top of the atmosphere outgoing longwave radiation; SWI denotes incident surface shortwave radiation; RN denotes net surface radiation; CWP denote cloud water path; PPT denotes precipitation; and TMEAN, TMAX, and TMIN denote the mean, maximum, and minimum surface temperatures, respectively.

	SIMEX			SUBEX		
	Bias	RMSE	Slope	Bias	RMSE	Slope
Albedo	0.097	0.108	1.41	0.024	0.037	0.91
OLR	-19.3	22.6	1.42	0.5	8.2	1.24
SWI	-26.2	30.9	1.03	-3.9	13.2	1.01
RN	-20.3	22.9	0.96	-9.9	13.4	1.03
CWP	64.6	74.3	1.22	-17.3	31.2	0.14
PPT	-0.37	0.72	0.62	-0.06	0.65	0.73
TMEAN	-1.10	2.00	0.98	-0.25	1.15	1.00
TMAX	-2.12	2.96	1.05	-0.81	1.65	1.04
TMIN	1.24	1.99	0.92	1.68	1.98	0.97

3.3.1 Radiation Budget

In many modeling applications, it is crucial to accurately simulate the surface energy budget. To do so, however, it is essential that the atmospheric components of the water and energy budgets are adequately predicted. In this subsection, we evaluate the model's performance in simulating the top of the atmosphere albedo and outgoing longwave radiation and the surface incident shortwave radiation and net radiation.

Top of the atmosphere albedo determines the amount of incoming solar radiation that is reflected back into space and can be used as a surrogate for cloud amount. Figure 3-2 displays the model predictions of top of the atmosphere albedo compared to the ERBE observations. In the simulations with RegCM using SIMEX, almost every data point lies above the one-to-one line corresponding to a large bias (0.097) which is nearly equal to the RMSE (0.108). This is a clear indication that SIMEX tends to overestimate cloud amount. The slope of the best fit data is 1.41 indicating that SIMEX also overestimates the seasonal variability of albedo and hence, cloud coverage. Most of this overestimation occurs during the warmer months of the year (April through September) where the

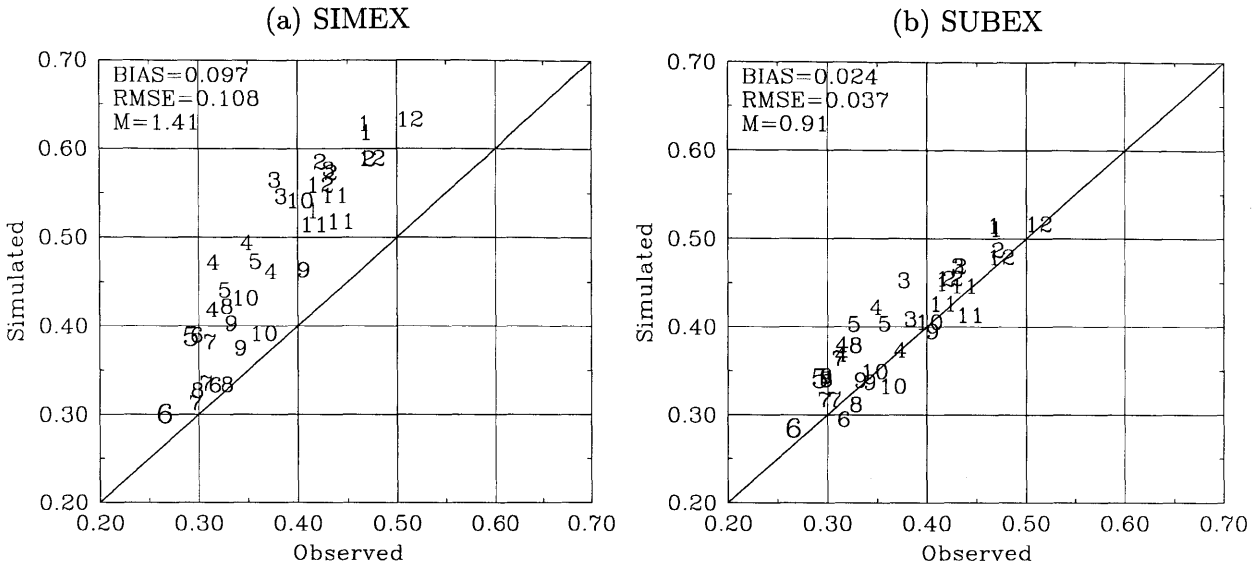

Figure 3-2: Plot of the simulated top of the atmosphere albedo (y-axis) against the ERBE observations (x-axis). Each data point represents a spatial average over the Midwest box outlined in Figure 3-1. Each digit indicates the month over which the average is taken. The large 5 and 6 refer to May and June of the Drought year (1988). (a) SIMEX; (b) SUBEX.

slope of the data is steeper than 1.41. With this in mind, a correction of the bias alone will not be adequate; improvements in the the seasonal and interannual variability are also required. RegCM using SUBEX to represent the moist physics performs significantly better in reproducing the mean observations of top of the atmosphere albedo (bias=0.024). SUBEX also performs considerably better in representing the seasonal and interannual variability of albedo (slope=0.91). In addition, there is reduced scatter about best fit and one-to-one lines of the model data against observations (RMSE=0.037). Although there are improvements to this scatter, a significant amount still remains.

Top of the atmosphere outgoing longwave radiation is also a key component of the atmospheric energy balance and can be used as a measure of cloud height (i.e. cloud top temperature). Figure 3-3 displays the top of the atmosphere outgoing longwave radiation for both SIMEX and SUBEX against the ERBE observations. RegCM with SIMEX substantially underestimates the outgoing longwave radiation indicating that there are too many high clouds. This is reflected in the low bias of 19.3 W/m^2 which nearly equals the RMSE (22.6 W/m^2) and is consistent with SIMEX's overestimation of albedo seen above. Also consistent with above, there tends to be an overestimation of the seasonal and interannual variability of clouds (especially during the spring and summer months) reflected in the large slope of the best fit line (1.42). RegCM with SUBEX performs significantly better than SIMEX in simulating the top of the atmosphere outgoing longwave

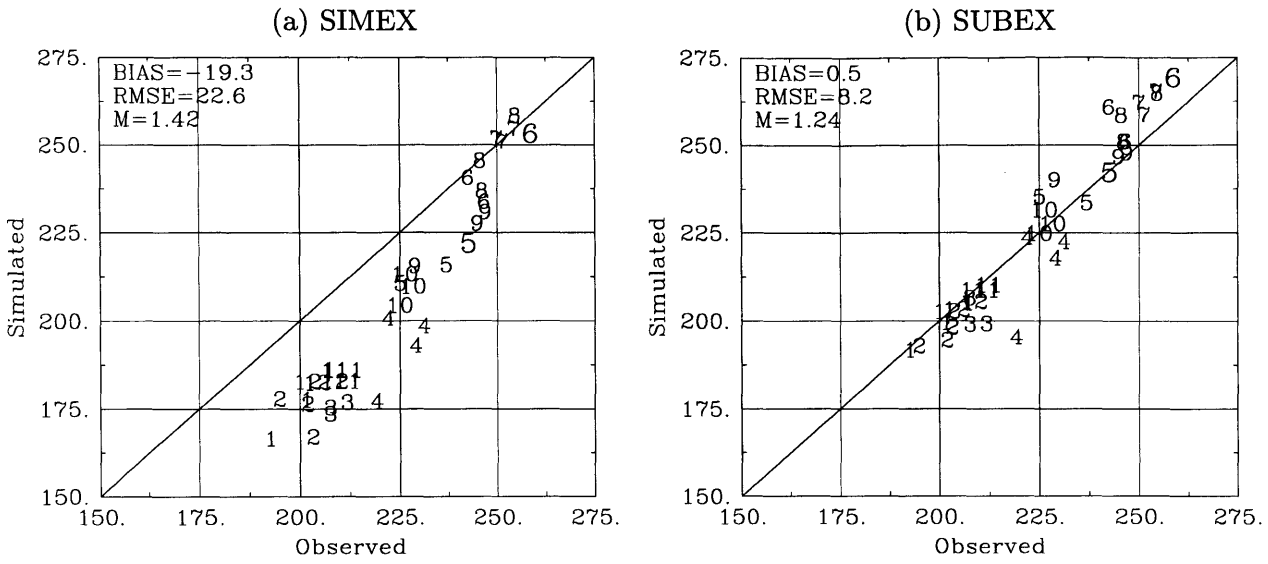

Figure 3-3: Plot of the simulated top of the atmosphere outgoing longwave radiation in W/m^2 (y-axis) against the ERBE observations (x-axis). Each data point represents a spatial average over the Midwest box outlined in Figure 3-1. Each digit indicates the month over which the average is taken. The large 5 and 6 refer to May and June of the Drought year (1988). (a) SIMEX; (b) SUBEX.

radiation. The bias and RMSE are reduced to 0.5 W/m^2 and 8.2 W/m^2, respectively. Furthermore, both the slope of the best fit line (1.24) and scatter of the simulation data about the best fit line to observations are considerably reduced suggesting that SUBEX performs better in representing the seasonal and interannual variability. Much of this improvement in the seasonal variability is a result of improvements during the spring and summer months, however, an overestimation of the variability still remains during these months. The above improvements indicate that SUBEX outperforms SIMEX over the Midwestern United States in reproducing the atmospheric radiation budget, as well as the vertical distribution of clouds.

Incident surface shortwave radiation is the main energy input to the hydrologic cycle of the surface. It reflects the integrated effect of the clouds that lie above the biosphere. Figure 3-4 shows that the improvements in the prediction of the atmospheric radiation budget (top of the atmosphere albedo and outgoing longwave radiation) also translate into improvements in the prediction of incident surface shortwave radiation. In the SIMEX simulations, the model tends to underestimate incident shortwave radiation at the surface over the Midwest region in nearly every month. This is reflected in the overall low bias of 26 W/m^2 and the RMSE of 31 W/m^2. These results are also consistent with SIMEX's over prediction of top of the atmosphere albedo and under prediction of top of the atmosphere outgoing longwave radiation. Although the slope is near unity (1.03), SIMEX

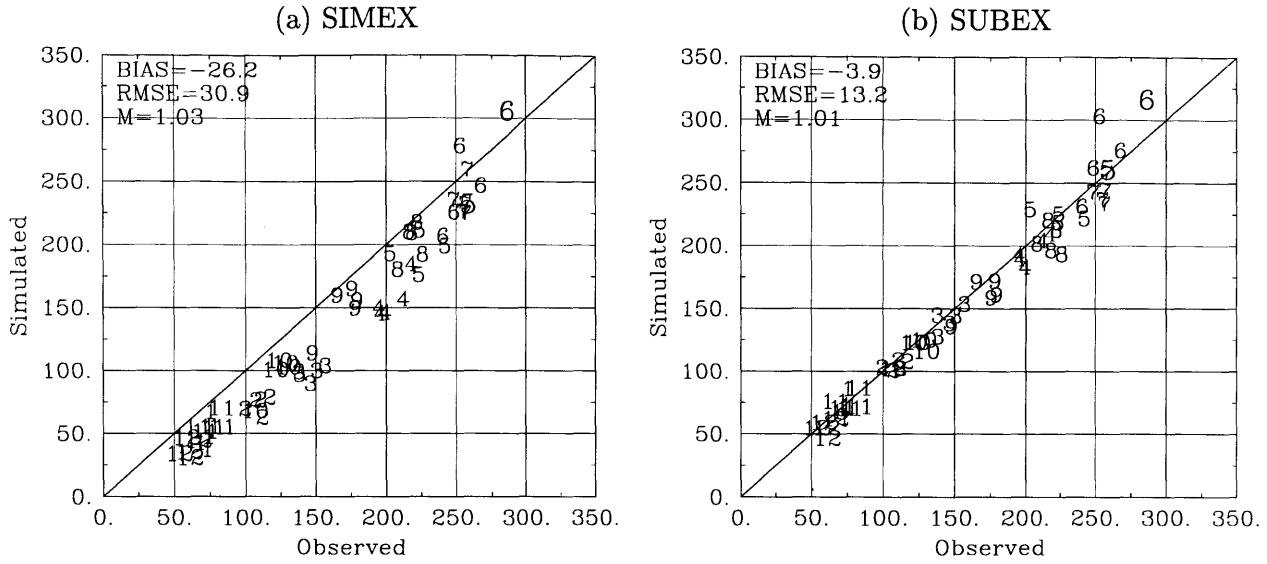

Figure 3-4: Plot of simulated simulated incident surface shortwave radiation in W/m^2 (y-axis) against the NASA-SRB data (x-axis). Each data point represents a spatial average over the Midwest box outlined in Figure 3-1. Each digit indicates the month over which the average is taken. The large 5 and 6 refer to May and June of the Drought year (1988). (a) SIMEX; (b) SUBEX.

tends to overestimate the seasonal variability during months of high incident shortwave radiation (as with the above findings). The simulations using SUBEX do much better job in reproducing the NASA-SRB data over the Midwest. The bias and RMSE are substantially reduced to -4 W/m^2 and 13 W/m^2, respectively. Furthermore, the slope of the data (1.01) is near unity and the scatter of the data about the best fit line (and one-to-one line) is considerably reduced indicating that SUBEX is able to better reproduce the seasonal and interannual variability of the incoming solar radiation. In addition, the tendency for the model to overestimate the seasonal variability during spring and summer months has been reduced, but not completely removed.

Net surface radiation is a key component of the surface energy budget. It determines the turbulent fluxes into the atmospheric boundary layer. Figure 3-5 displays the simulation results against the NASA-SRB data. Consistent with above, SUBEX outperforms SIMEX. The bias is reduced from -20 W/m^2 to -10 W/m^2 and the RMSE is reduced from 23 W/m^2 to 13 W/m^2 between SUBEX and SIMEX, respectively. The scatter about the best fit line also improves in the SUBEX simulations. Again, both models tend to overestimate the seasonal variability during the spring and summer months. This overestimation is somewhat smaller in the SUBEX simulations.

Figure 3-6 displays the improvement (or deterioration) seen in the simulated net surface radiation between SUBEX and SIMEX averaged over the entire simulation period. On the whole,

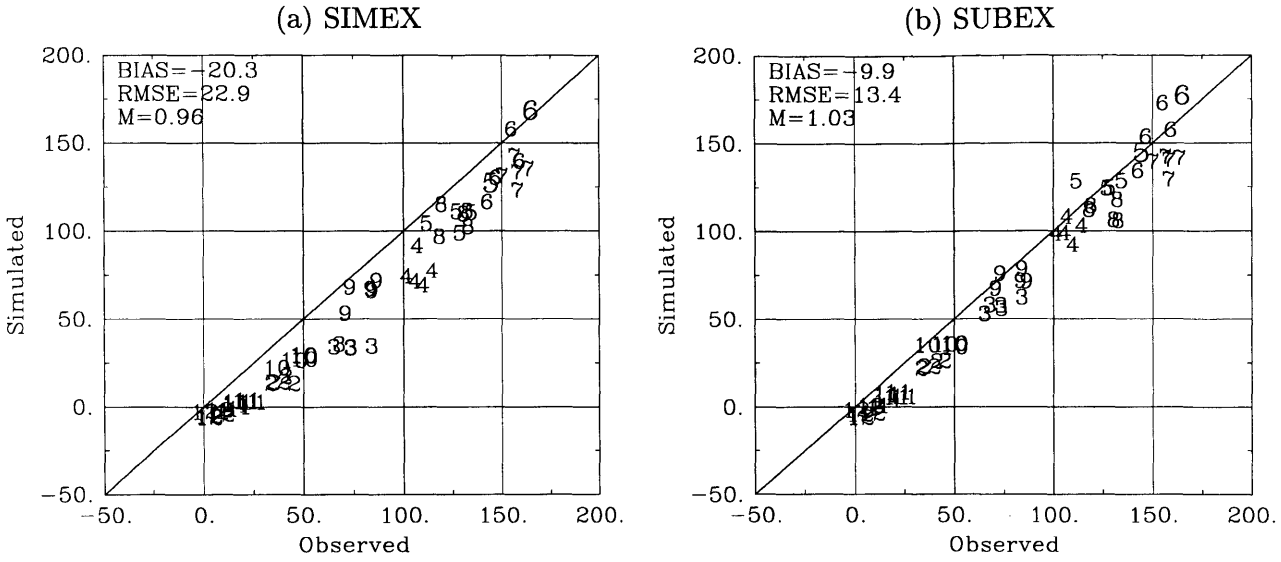

Figure 3-5: Plot of the simulated net surface radiation in W/m^2 (y-axis) against the NASA-SRB data (x-axis). Each data point represents a spatial average over the Midwest box outlined in Figure 3-1. Each digit indicates the month over which the average is taken. The large 5 and 6 refer to May and June of the Drought year (1988). (a) SIMEX; (b) SUBEX.

improvements result over entire domain when using SUBEX to represent the large-scale cloud and precipitation processes. Two exceptions lie in coastal regions off Southern California and Sinaloa, Mexico. This deterioration may be partly explainable by significant biases over coastal regions in the NASA-SRB data (See Subsection 2.2.2 or Gupta et al. (1999)). The largest improvements are observed over the Pacific Northwest and the Atlantic Ocean. These are both regions where SIMEX tends to overestimate cloud amounts. Over the majority of North America, there is a 6 to 10 W/m^2 improvement. There is some seasonal dependence in that the improvements tend to be largest in the spring and smallest in the summer (not shown). Lastly, over no portion of the domain do the simulations using SIMEX simulate more net surface radiation than those using SUBEX. (This is why no light shading exists.) Thus, all the improvements result from an increase in the simulation of net surface radiation (dark shading).

Overall, RegCM using SUBEX results in substantially better performance in representing the atmospheric and surface energy budgets. The biases in all components of the of the radiation budget were reduced to values near zero. In addition, the representation of seasonal variability is improved. However, an overestimation (but reduction when compared to SIMEX) in the variability remains during the spring and summer months. This may point to deficiencies in the representation of convective cloud cover and water, since this problem occurs primarily in convectively active

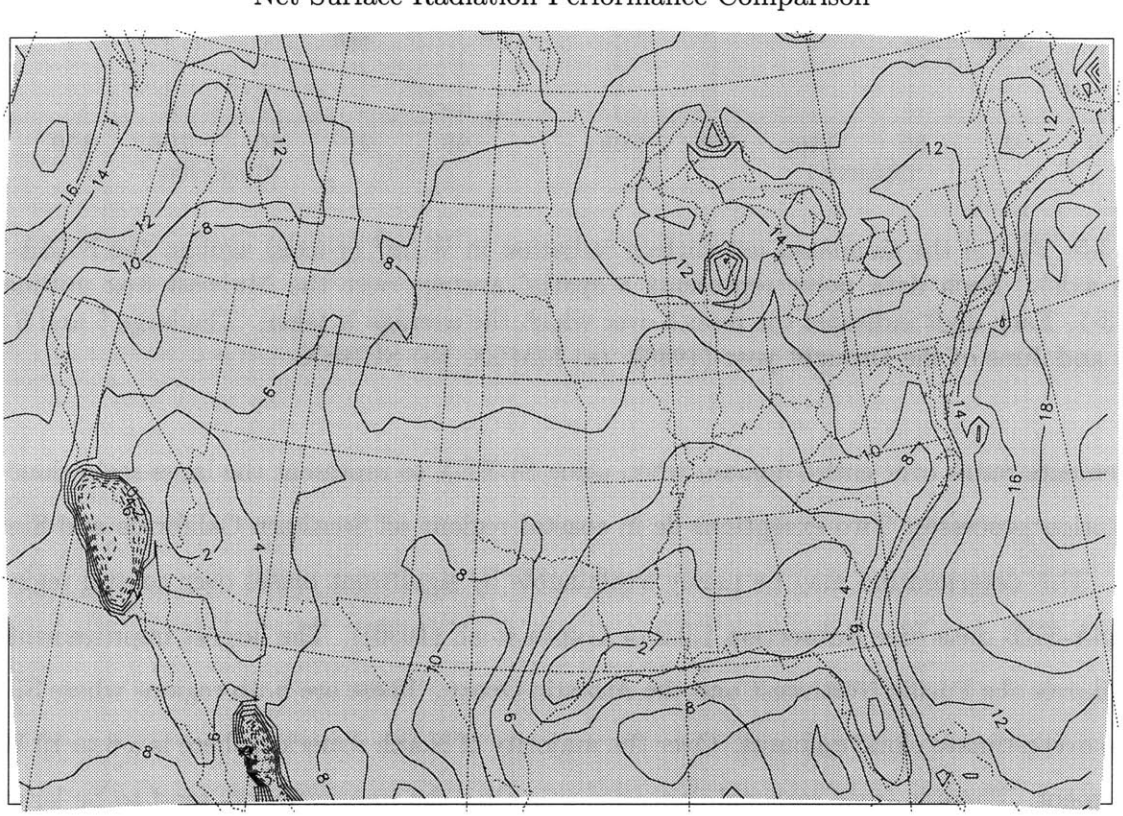

Figure 3-6: Plot of the overall changes to the net surface radiation results between SIMEX and SUBEX averaged over the entire simulation period. Contours display the RMSE difference between SIMEX and SUBEX in W/m^2. Positive values (solid lines) indicate that the model simulations improved when using SUBEX and negative values (dashed lines) indicate a deterioration. The shading displays direction of the difference between SIMEX and SUBEX. Dark shading indicates that SUBEX simulates more net surface radiation than SIMEX and vice versa.

months. The following subsection investigates whether the improvements in the energy budget result in improvements to the water budget.

3.3.2 Water Budget

In this subsection, we compare the model simulations to observations of cloud water path and precipitation.

Figure 3-7 compares the model results to the ISCCP-D2 observations of cloud water path for both SIMEX and SUBEX. As alluded to above, SIMEX tends to significantly overestimate cloud water path over the Midwestern United States. The bias is 65 g/m^2 and the RMSE is 74 g/m^2. These values are comparable to size of the observed cloud water contents in this region. This overestimation is consistent with the results of the energy budget in that too little shortwave radiation reaches the surface, too little longwave radiation leaves the top of the atmosphere, and the top of the atmosphere albedo is too high. In addition, SIMEX overestimates the seasonal and interannual variability reflected in the slope (1.22) and scatter of the data about the best fit line. SUBEX performs better in representing observed mean cloud water path conditions. The bias and RMSE have been reduced to -17 g/m^2 and 31 g/m^2, respectively. Although this is a significant improvement, SUBEX over corrects the seasonal and interannual variability problem observed in SIMEX (slope=0.14). More specifically, it tends not to accurately represent the high cloud amounts observed in November, December, and January. The reason for this may have to do with an artificial cap placed on the cloud water path of 400 g/m^2. Without this cap, RegCM using SIMEX often overestimates cloud water path by an order of magnitude. SUBEX retains this cap which may be a large portion of the reason why it underestimates cloud water path in the cloudier months. In addition, the lack of ice phase within SUBEX's cloud physics may contribute to the deficiencies.

Precipitation is the most important variable of the surface water budget and is probably the most difficult to simulate. Figure 3-8 shows that improvements in the prediction of the radiation budget result in improvements in the prediction of precipitation over the Midwest. SIMEX underestimates precipitation by 0.37 mm/day and contains significant variability in the error (RMSE=0.72 mm/day). In addition, it significantly underestimates the seasonal variability (slope=0.62). Of particular importance, extreme wet precipitation events (greater than 3 mm/day) which typically occur in the spring and summer in the Midwest tend to be underrepresented. In the simulations using SUBEX, the precipitation bias is significantly reduced (-0.06 mm/day), while

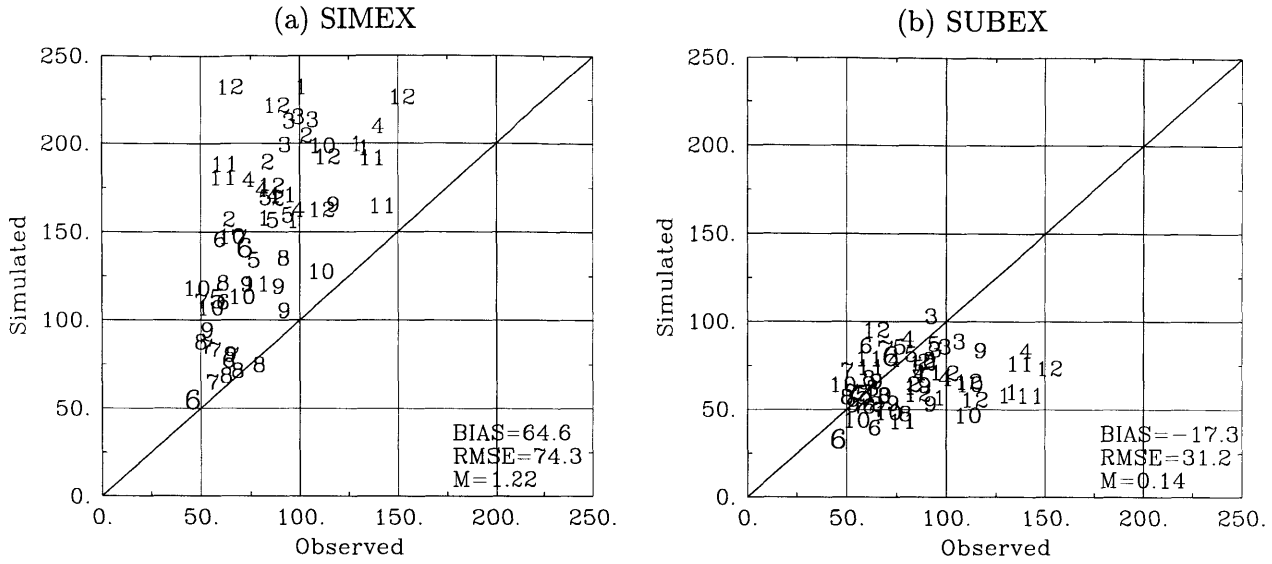

Figure 3-7: Plot of the simulated cloud water path in g/m^2 (y-axis) against the ISCCP-D2 observations (x-axis). Each data point represents a spatial average over the Midwest box outlined in Figure 3-1. Each digit indicates the month over which the average is taken. The large 5 and 6 refer to May and June of the Drought year (1988) and the large 6 and 7 refer to June and July of the flood year (1993). The June 1988 value lies in the bottom left corner. (a) SIMEX; (b) SUBEX.

the RMSE still remains high (0.65 mm/day). In addition, there is a significant improvement in the simulation of the seasonal and interannual variability (slope=0.73); SUBEX does a considerably better job in representing the high extremes in precipitation. Note that June and July of the flood year (1993, denoted by the large six and seven in the top right portion of the plot) now fall close to the observed values. In addition, both schemes do a particularly poor job in simulating September of 1986 and 1993. It is determined that the large- and meso-scale dynamics were poorly simulated during these months (too much northerly flow; too little southerly flow; not shown). Neglecting these months, would provide some correction to the low slopes. The mechanisms resulting in the improved simulation of extreme wet precipitation events are described in Subsection 3.3.4.

Figure 3-9 displays the improvement (or deterioration) seen in the simulated precipitation between SUBEX and SIMEX over the United States averaged over the entire simulation period. (Note that contours only exist over the United States since the USHCN data does not exist elsewhere.) On the whole, improvements result over the majority of the United States when using SUBEX over SIMEX to represent the large-scale cloud and precipitation processes. Exceptions tend to lie along Pacific and Atlantic coastlines and the Southwest United States. East of the ~103°W (Rocky Mountains), most of the improvements result due to an increase in precipitation (dark shading); There is degradation in performance where the precipitation decreases (light shading). In

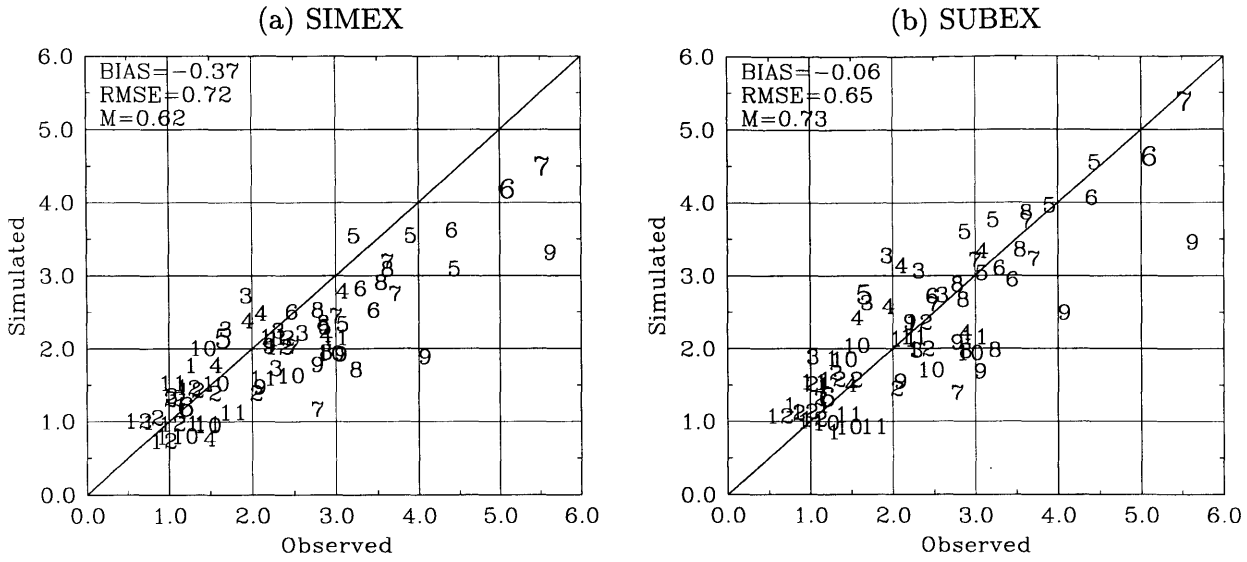

Figure 3-8: Plot of the simulated precipitation in mm/day (y-axis) against the USHCN observations (x-axis). Each data point represents a spatial average over the Midwest box outlined in Figure 3-1. Each digit indicates the month over which the average is taken. The large 5 and 6 refer to May and June of the Drought year (1988) and the large 6 and 7 refer to June and July of the flood year (1993). The June 1988 value lies in the bottom left corner in both sub-plots. (a) SIMEX; (b) SUBEX.

contrast, to the west ~103°W most of the improvements occur due to a decrease in precipitation; The performance decreases when precipitation increases. In general, SUBEX is able to better represent the processes responsible for precipitation in the different regimes of the United States.

Overall, SUBEX significantly improves the representation of the water budget over the Midwestern United States. These improvements, however, are not as large as those seen with the energy budget (see Subsection 3.3.1). The benefits to the mean conditions of energy budget are primarily due to improvements in the overall cloud amount (see Figure 3-7). The reason for the improvements to the seasonal and interannual variabilities are more difficult to identify. It is likely that the variable fractional cloud coverage (see Equation 2.3 and Figure 2-2) plays an important role in these improvements.

3.3.3 Surface Temperature

Like precipitation, surface temperature is also one of the most difficult fields to accurately predict due to its dependence on a variety of factors. This subsection compares the SIMEX and SUBEX simulations to the USHCN observations of mean, minimum, and maximum temperature. Note that model temperatures have been adjusted to reconcile differences between station and model

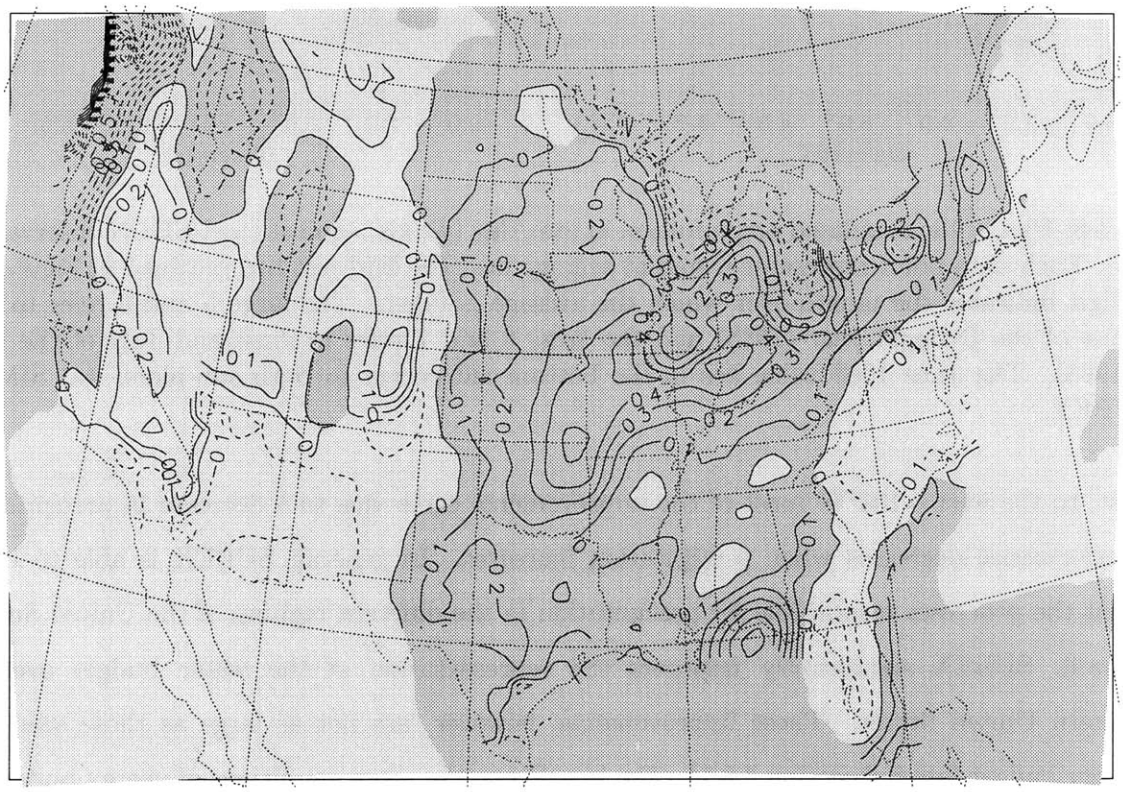

Figure 3-9: Plot of the overall changes to the precipitation results between SIMEX and SUBEX averaged over the entire simulation period. Contours (United States only) display the RMSE difference between SIMEX and SUBEX in mm/day; Positive values (solid lines) indicate that the model simulations improved when using SUBEX and negative values (dashed lines) indicate a deterioration. The shading displays direction of the difference between SIMEX and SUBEX. Dark shading indicates that SUBEX simulates more precipitation than SIMEX and vice versa.

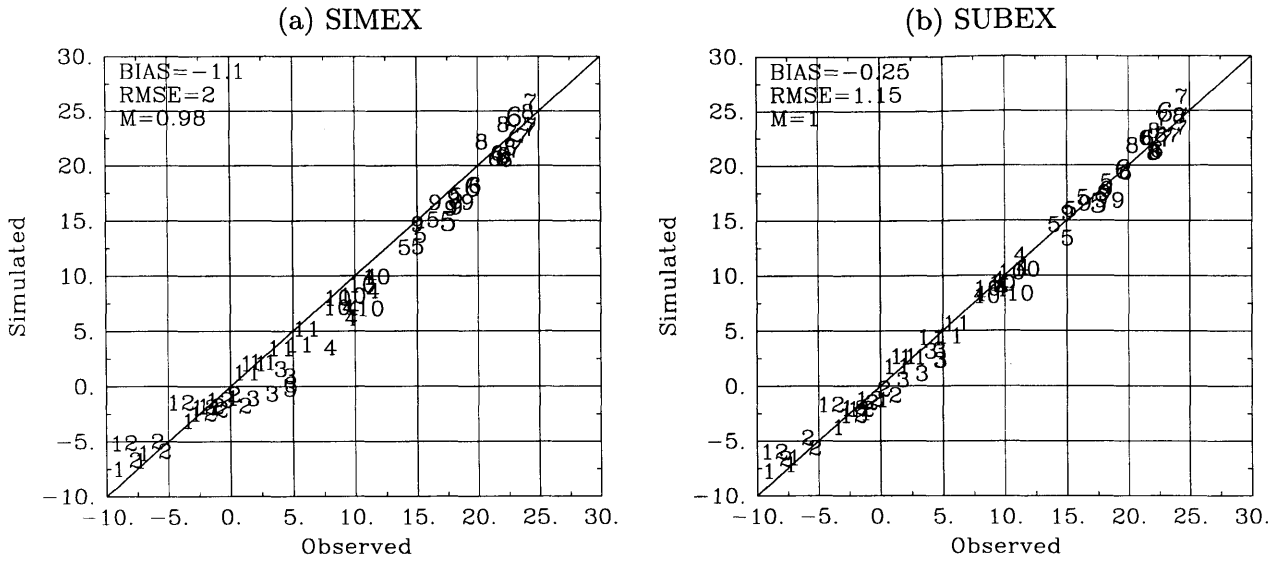

Figure 3-10: Plot of the simulated mean surface temperature in °C (y-axis) against the USHCN observations (x-axis). Each data point represents a spatial average over the Midwest box outlined in Figure 3-1. Each digit indicates the month over which the average is taken. The large 5 and 6 refer to May and June of the Drought year (1988) and the large 6 and 7 refer to June and July of the flood year (1993). The June 1988 value lies in the upper right corner. (a) SIMEX; (b) SUBEX.

elevation.

Figure 3-10 compares the predictions of mean surface temperature from each cloud model to observations. SIMEX tends to significantly underestimate the mean surface temperature (bias=-1.10°C) and contains a fair amount of variability (RMSE=2.00°C). The overall seasonal variability is well represented (slope=0.98), although significant biases occur during the transition seasons (spring and autumn). The best performance occurs during the consistent regimes (summer and winter). These two factors imply that simply removing the bias within the parameters of the SIMEX is unlikely to be satisfactory. When using SUBEX, the simulation of mean surface temperature significantly improves. The bias and RMSE are reduced to -0.25°C and 1.15°C, respectively. Although the slopes of both schemes are similar (slope=1.00 in SUBEX), SUBEX performs better in simulating the seasonal variability of mean surface temperature; A significant portion of the low bias that exists in the SIMEX simulations during the transition seasons is removed. This improvement does not occur at the expense of the summer and winter months. These overall results suggest that RegCM using SUBEX is better able to represent the processes that determine the interannual variability than RegCM using SIMEX.

Figure 3-11 displays the improvement (or deterioration) seen in the simulated mean surface

temperature between SUBEX and SIMEX over the United States averaged over the entire simulation period. Note that contours only exist over the United States since the USHCN data does not exist elsewhere. On the whole, improvements result over the majority of the United States when using SUBEX over SIMEX to represent the large-scale cloud and precipitation processes. However, large degradations in the performance occur over a significant portion of the United States. This region is strikingly correlated areas where the model elevation exceeds the USHCN data by more than 200 m. It is plausible that the applied elevation correction is not reasonable when the model terrain and USHCN terrain differ significantly. Like net surface radiation, the simulations using SUBEX predict a greater mean surface temperature over the all of the land. (This is why no light shading exists.) Thus, all the improvements result from an increase in the simulation of mean surface temperature (dark shading).

Maximum temperature (Figure 3-12) displays properties to those for mean surface temperature. In SIMEX, there is a low bias of 2.12°C, a RMSE of 2.96°C, and a slope of 1.05. The low bias is consistent with the under prediction of incident surface shortwave radiation. As with mean surface temperature, the SIMEX simulations tend towards a cold bias during the transition seasons and have little bias during the consistent regimes. SUBEX is able to correct a significant portion of the biases observed during the spring and autumn months, however, there is still room for improvement. The overall bias, RMSE, and slope of the simulations using SUBEX are -0.81°C, 1.65°C, and 1.04, respectively. These results suggest improvements in the ability of SUBEX to simulate the interannual variability of maximum surface temperature.

The results for minimum surface temperature are presented in Figure 3-13. The simulations using SIMEX have a significant warm bias of 1.24°C and a RMSE of 1.99°C. In addition, the overall seasonal variability is somewhat underrepresented (slope=0.92); Most of the underrepresentation occurs during colder months (December through March). SUBEX tends to overestimate minimum surface temperature even more so than SIMEX (bias=1.68 °C). The RMSE (1.98 °C), however, remains nearly the same as with SIMEX. Since the bias is part of the RMSE, the variability of the simulation data about the one-to-one line decreases in SUBEX. This suggests that processes representing the variability in minimum surface temperature are better represented in SUBEX. However, the processes that represent the mean conditions are not as well represented as they are in SIMEX. With the decrease in cloud amount seen in Figure 3-7, one may expect a decrease in the longwave radiation emitted towards the land surface and hence, a decrease in nighttime (minimum) surface temperatures. Upon further inspection, however, it is evident that the increase in net surface

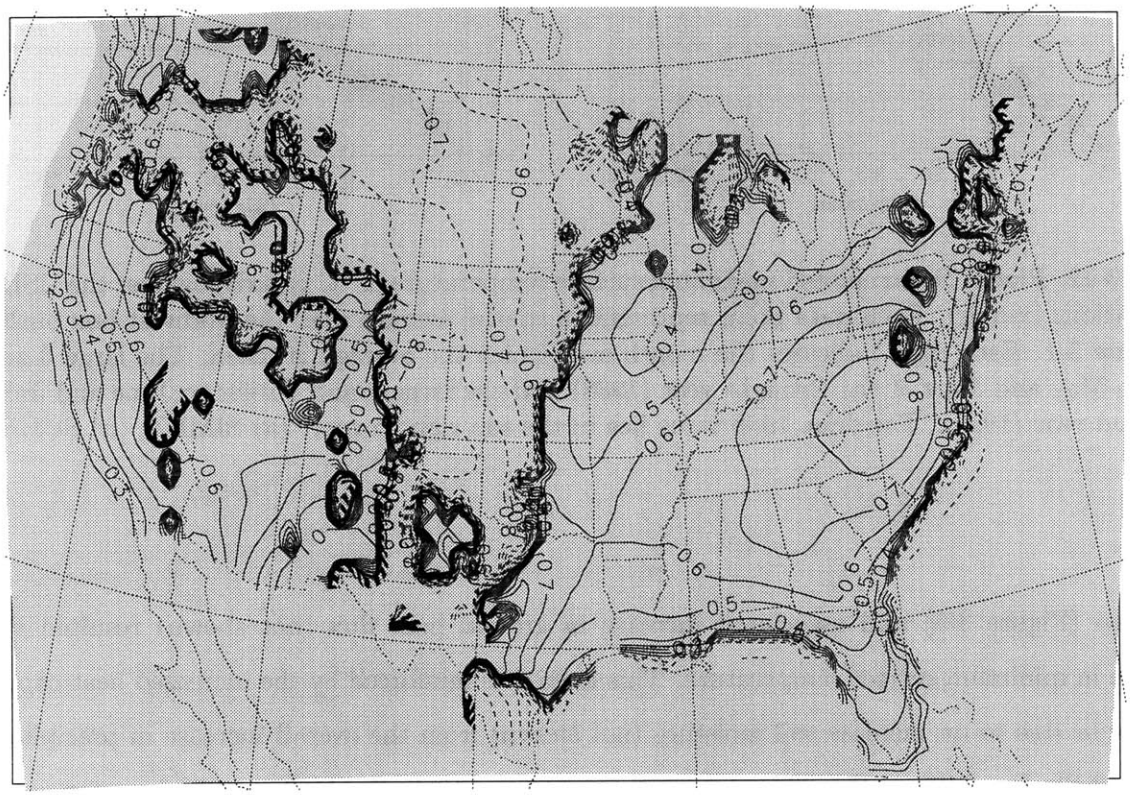

Figure 3-11: Plot of the overall changes to the mean surface temperature results between SIMEX and SUBEX averaged over the entire simulation period. Contours (United States only) display the RMSE difference between SIMEX and SUBEX in °C. Positive values (solid lines) indicate that the model simulations improved when using SUBEX and negative values (dashed lines) indicate a deterioration. The shading displays direction of the difference between SIMEX and SUBEX. Dark shading indicates that SUBEX simulates higher mean surface temperatures than SIMEX and vice versa.

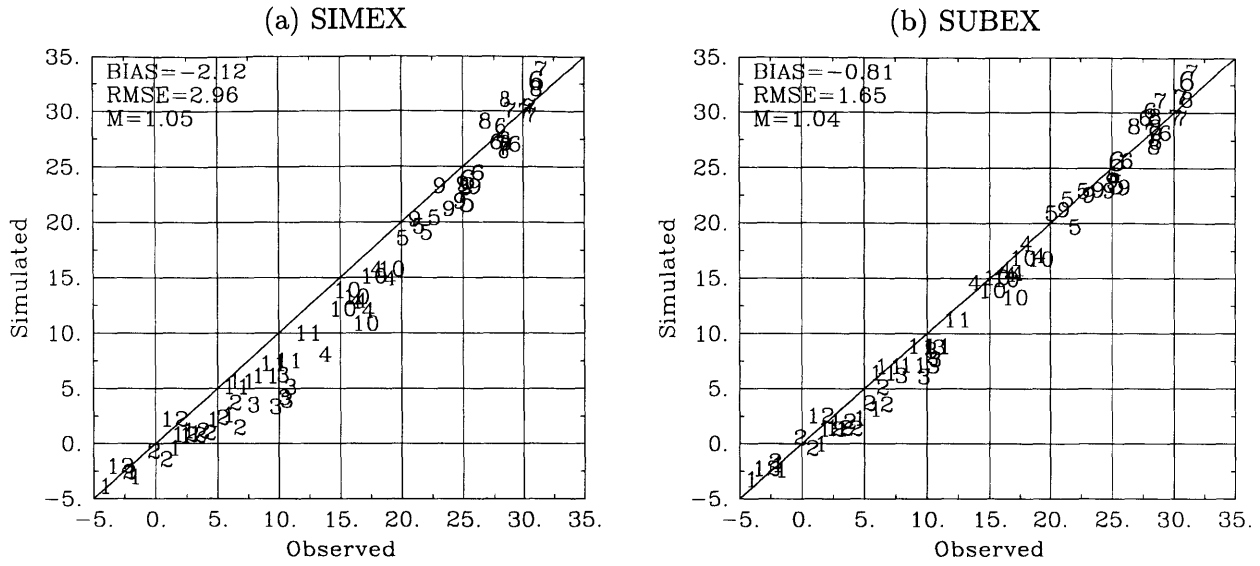

Figure 3-12: Plot of the simulated maximum surface temperature in °C (y-axis) against the USHCN observations (x-axis). Each data point represents a spatial average over the Midwest box outlined in Figure 3-1. Each digit indicates the month over which the average is taken. The large 5 and 6 refer to May and June of the Drought year (1988) and the large 6 and 7 refer to June and July of the flood year (1993). The June 1988 value lies in the top right corner. (a) SIMEX; (b) SUBEX.

radiation (Figure 3-5) and associated increase in ground heat flux (not shown) resulted in an increase in minimum surface temperature. This is further reinforced by the increased heat capacity of the soils due to an increase soil moisture (not shown) from the overall increase in precipitation (Figure 3-8). In addition, the water vapor content of the air in the lower atmosphere tends to be larger in the SUBEX simulations (not shown) resulting in an enhanced greenhouse effect for water vapor also increasing the nighttime temperatures. These factors suggest an inconsistency between the biosphere model (BATS) and the overlying atmospheric processes. It should be expected that if the atmospheric water and energy budgets are improved, the land surface water and energy budgets should also improve. This is not the case with mean conditions (bias) of minimum surface temperature. Lastly, SUBEX performs slightly better in representing the seasonal variability of minimum surface temperature (slope=0.97).

Despite the increase in the bias in minimum surface temperature, RegCM using SUBEX to represent the large-scale cloud and precipitation processes results in significant improvements to the simulation of the surface temperature fields.

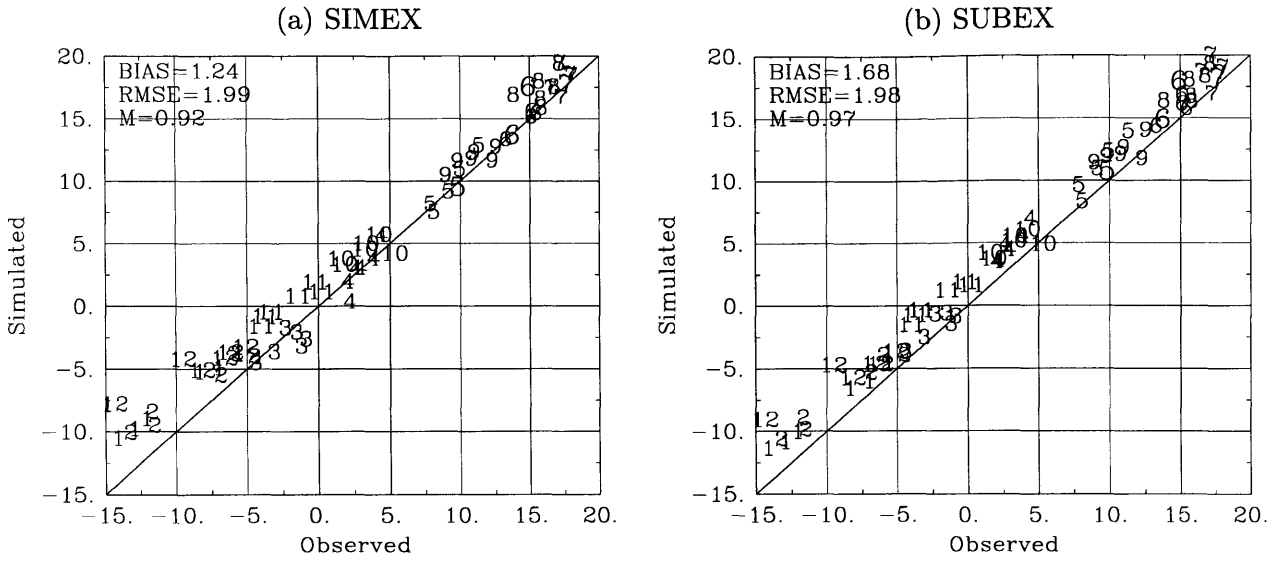

Figure 3-13: Plot of the simulated minimum surface temperature in °C (y-axis) against the USHCN observations (x-axis). Each data point represents a spatial average over the Midwest box outlined in Figure 3-1. Each digit indicates the month over which the average is taken. The large 5 and 6 refer to May and June of the Drought year (1988) and the large 6 and 7 refer to June and July of the flood year (1993). The June 1988 value lies in the top right corner. (a) SIMEX; (b) SUBEX.

3.3.4 Simulation of Extreme precipitation Events

In the summer of 1988, the United States Midwest experienced its warmest and driest summer since the dust-bowl era of the 1930s (Figure 3-14a; Ropelewski (1988)). In contrast, record high rainfall and flooding occurred and persisted throughout much of the summer during 1993 (Figure 3-14b; Kunkel et al. (1994)). This subsection investigates how the choice of the large-scale cloud and precipitation scheme impacts the simulation of the above extreme events.

1988 Drought

Figure 3-14a displays the USHCN observed precipitation over the United States averaged over May and June of 1988, the most extreme drought months. With a few regional exceptions, most of the continental United States received less than 2 mm/day of rainfall during May and June of 1988.

Figure 3-15 displays the precipitation for both the SIMEX and SUBEX simulations averaged over the same period (May and June of 1988). Both schemes do an excellent job in simulating the observed lack of precipitation over the United States. However, the individual features of the precipitation are not perfectly simulated in either scheme. This may in part be due to the somewhat unpredictable nature of precipitation (especially convective) and also may be in part be due to the

(a) May and June 1988 USHCN Precipitation

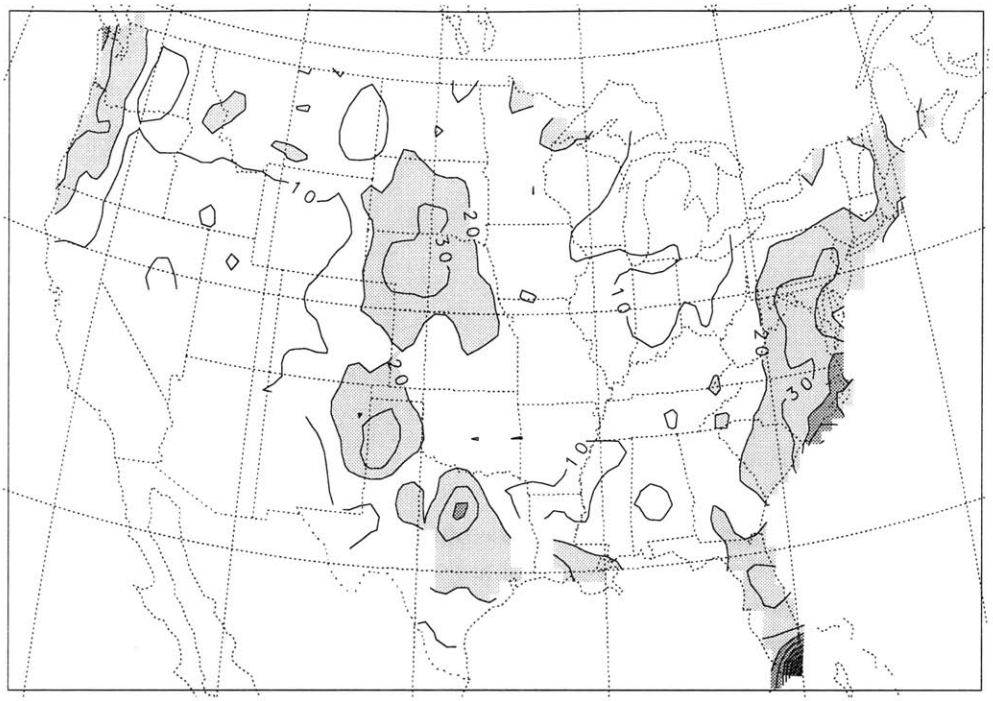

(b) June and July 1993 USHCN Precipitation

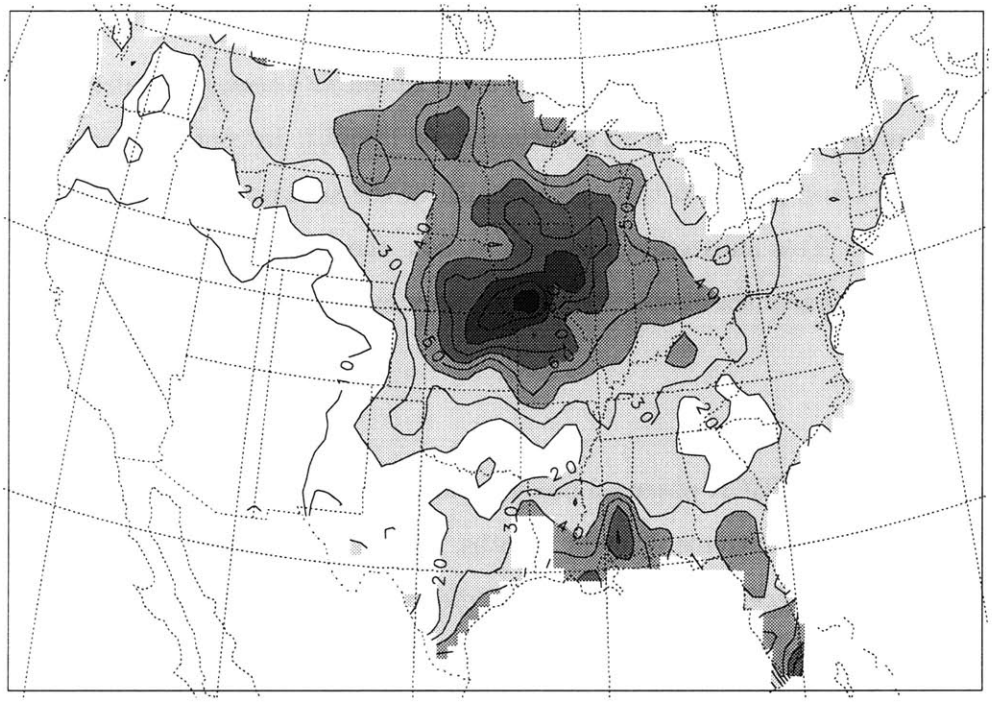

Figure 3-14: USHCN observations of precipitation in mm/day. Contour interval is specified at 1 (mm/day). Shading occurs at values above 2 mm/day and at intervals of 2 mm/day. Note that the USHCN observations only exist over the United States. (a) 1988 May and June average; (b) 1993 June and July average.

representation of the boundary conditions and model physics. SIMEX predicts the precipitation distribution over the Gulf Coast states slightly better than SUBEX, while SUBEX better represents the distribution along the eastern seaboard states. The precipitation amounts over the Midwest in May and June of 1988 seem to be slightly over predicted in SUBEX due to increases in both convective and non-convective precipitation (especially in May). In SUBEX, clouds form earlier than in SIMEX due to the lower relative humidity threshold (0.8 in SUBEX; 1.0 in SIMEX) which increases the likelihood of clouds. In addition, SUBEX has a lower auto-conversion threshold (See Figure 2-1) reducing the average cloud water path (See the large 5 and 6 in Figure 3-7). Under such conditions, these two effects result in an increase in non-convective precipitation (not shown). Furthermore, the increase in incident surface shortwave radiation (See the large 5 and 6 Figure 3-4) from the decrease in cloud water path outweighs the decrease in net surface longwave radiation resulting from the warmer surface temperatures and lower cloud amount. This tends to result in an increase in net surface radiation (See the large 5 and 6 Figure 3-5) yielding in an increase in convective precipitation (not shown). This mechanism appears to responsible for the increase in May and June 1988 precipitation seen in the SUBEX simulations. Overall, it is difficult to argue that one scheme performs better than the other for the drought of 1988. Most importantly, both models are able to simulate the overall lack of observed precipitation. Overall, in both SUBEX and SIMEX simulate the general lack of precipitation is captured though the details are simulated less accurately. These results are similar to the regional climate model simulations of the 1988 drought displayed by the Project to Intercompare Regional Climate Simulations (Takle et al. 1999).

1993 Flood

Much of the upper Midwest received greater than 4 mm of precipitation per day during June and July of 1993 (Figure 3-14b). Peak values above 8 mm/day occurred over much Iowa, Nebraska, Missouri, and Kansas. The largest peak (~10-11 mm/day) occurred along the Iowa-Missouri border. A smaller peak occurred along the coast of Mississippi and Louisiana (~6-7 mm/day).

Figure 3-16 displays the simulated rainfall for both large-scale cloud and precipitation schemes averaged over June and July of 1993. SIMEX is able to simulate the region over the upper Midwest in which rainfall exceeds 4 mm/day. However, it is not able to simulate the precipitation in excess of 8 mm/day that occurred over much of Iowa, Nebraska, Missouri, and Kansas. SUBEX not only simulates the flood region, it also simulates the region in excess of 8 mm/day more accurately. The general location of the flood region, however, is simulated too far to the north and east of

(a) May and June 1988 SIMEX Precipitation

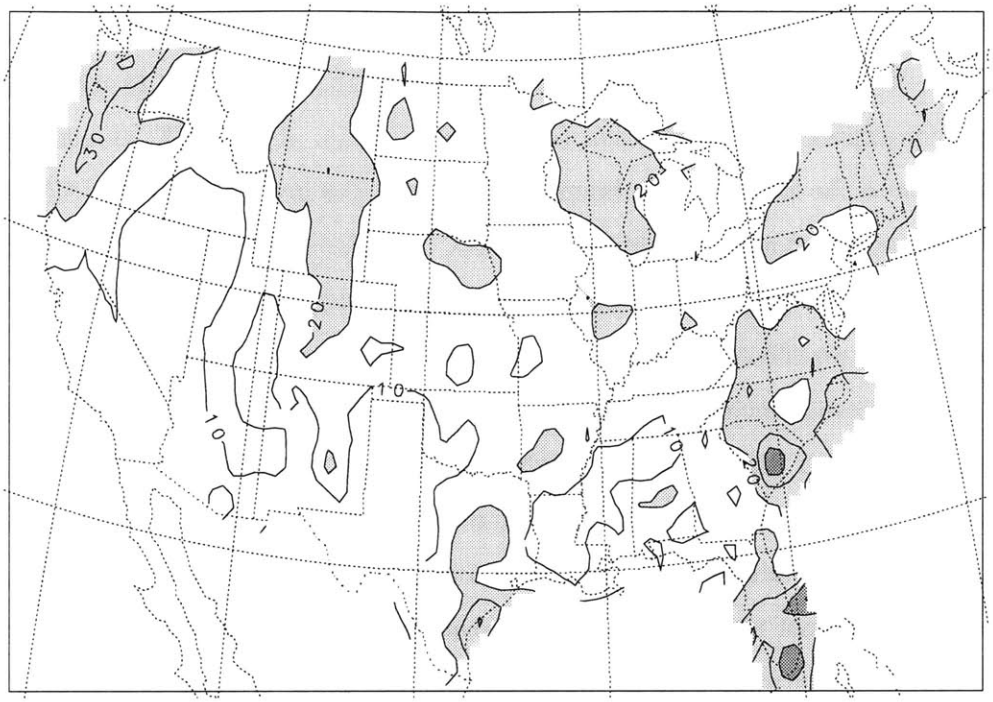

(b) May and June 1988 SUBEX Precipitation

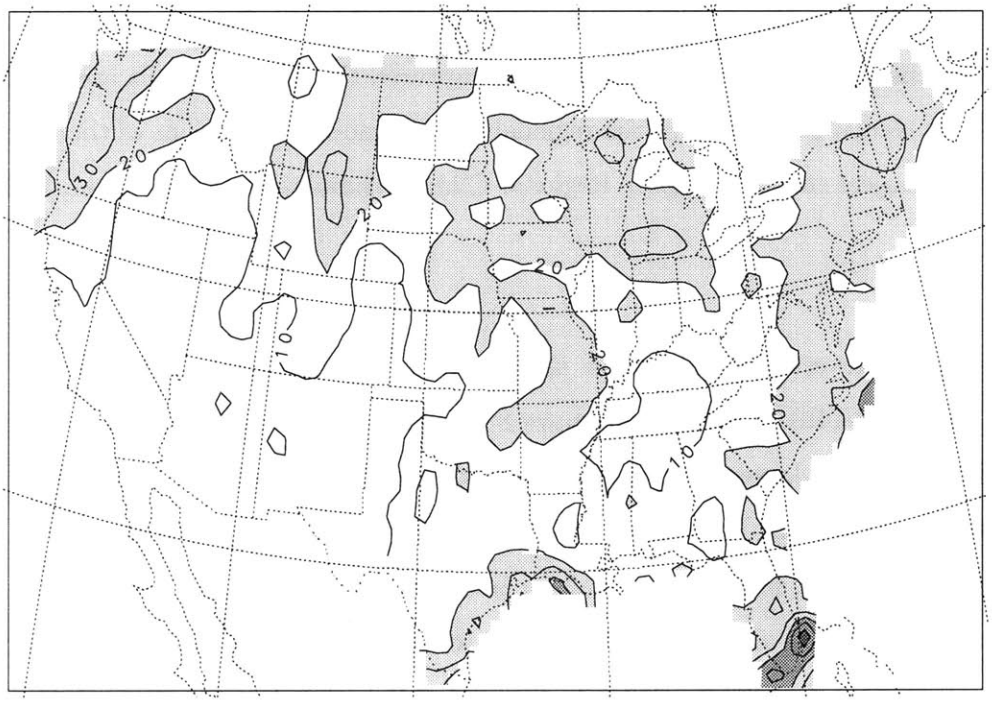

Figure 3-15: 1988 May and June simulated United States precipitation (mm/day). Contour interval is specified at 1 (mm/day), and shading occurs at values above 2 mm/day and at intervals of 2 mm/day. (a) SIMEX; (b) SUBEX.

observed. In addition, the peak maximum is underestimated by approximately 2 mm/day. Lastly, both models more or less perform adequately in representing the distribution of precipitation in the rest of the United States. For example, they capture the precipitation peak observed along the coast of Mississippi and Louisiana and the surrounding dry Gulf Coast region. Overall, both models perform well in capturing the spatial distribution of precipitation observed in June and July of 1993, however, SUBEX better simulates the magnitude of the flood peak.

The reasons that SUBEX more accurately represents the 1993 summer flooding over the upper Midwest are both directly and indirectly related to the simulation of cloud water path. First, the lower auto-conversion threshold specification (see Figure 2-1) results in an increase in the amount of cloud water that is converted to non-convective precipitation. Second, the reduction in cloud water results in an increase in incident surface shortwave radiation. This yields an increase in the energy available for convection and results in an increase convective precipitation (not shown). Lastly, the increase in soil moisture resulting from the increase in precipitation is also likely to have enhanced the precipitation during the summer of 1993.

3.4 Summary and Conclusions

A simple, yet physically based, large-scale cloud and precipitation scheme which accounts for the sub-grid variability of clouds is presented (SUBEX). Also highlighted are significant modifications made to the specification of the initial and boundary conditions of atmospheric and biospheric variables. Two sets of simulations each consisting of six one-year runs are performed over North America using RegCM with the moist physics from two different schemes: SIMEX and SUBEX. The only difference between the sets of simulations is the representation of large-scale cloud and precipitation processes. The sets of the simulations are compared to observations of various radiation and cloud fields from satellite based datasets and precipitation and surface temperature from surface station based datasets.

Overall, SUBEX significantly improves the model's simulation of the energy and water budgets. The most significant improvements occur in the prediction of the radiation fields (incident surface shortwave radiation, net surface radiation, outgoing longwave radiation, and albedo) and in the prediction of extreme wet precipitation events (namely the summer of 1993). Not only does SUBEX reduce the biases between the simulation and observations (except minimum surface temperature), it also significantly improves the simulation of the seasonal and interannual variability.

(a) June and July 1993 SIMEX Precipitation

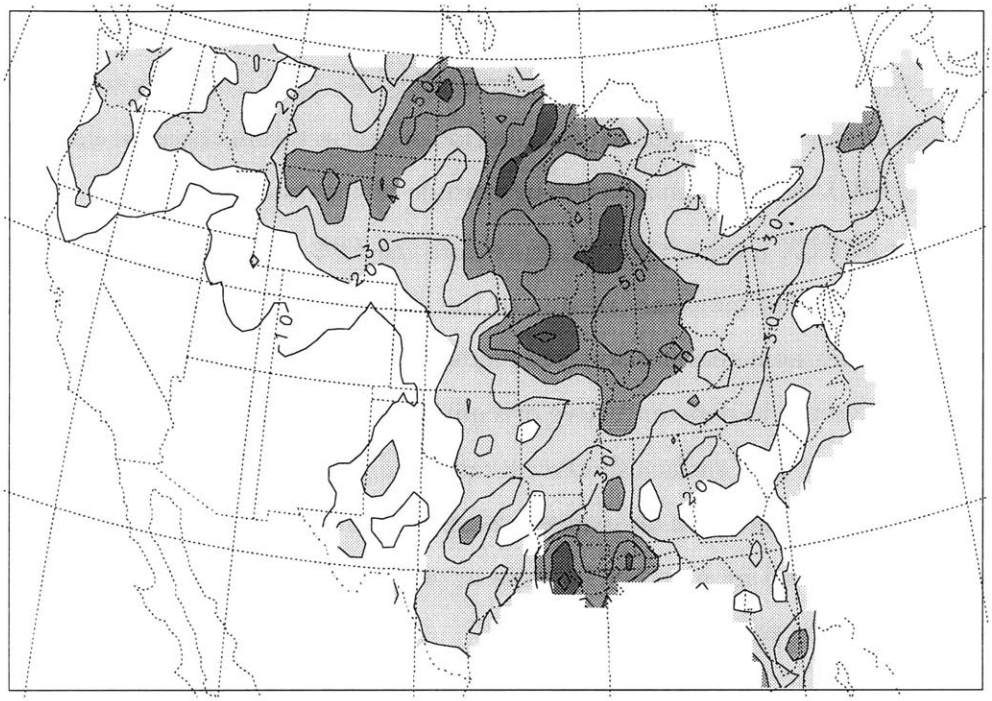

(b) June and July 1993 SUBEX Precipitation

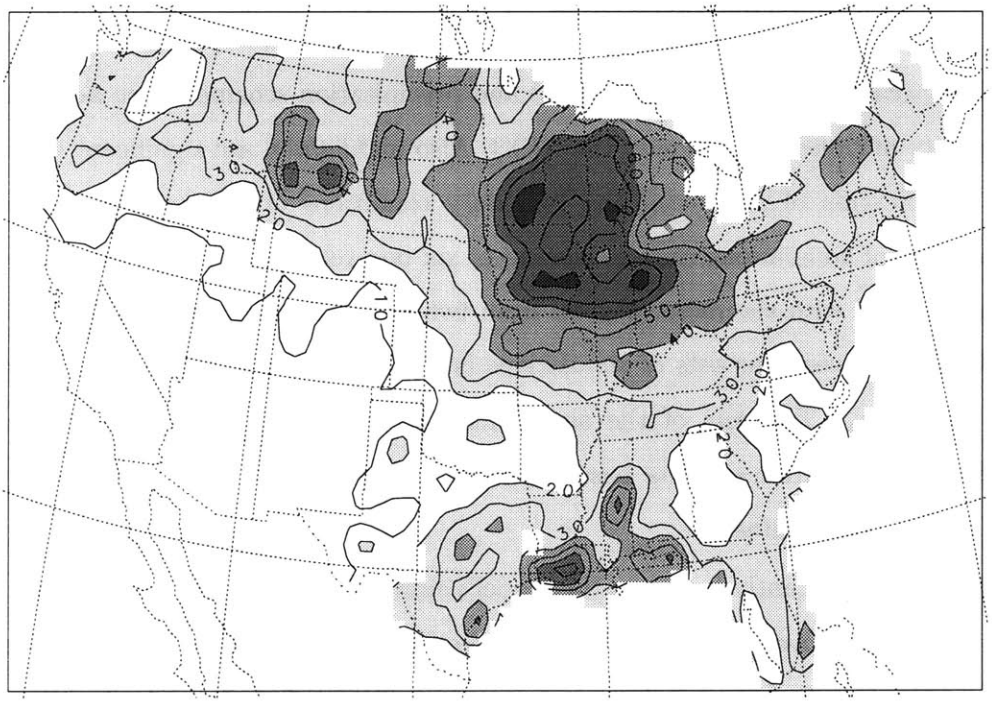

Figure 3-16: 1993 June and July simulated United States precipitation (mm/day). Contour interval is specified at 1 (mm/day), and shading occurs at values above 2 mm/day and at intervals of 2 mm/day. (a) SIMEX; (b) SUBEX.

SUBEX proves to be crucial in the simulation of the flooding that occurred in the summer of 1993. Without SUBEX, the rainfall over the flood region is simulated as only slightly above normal. On the other hand, few major differences are observed between the schemes in the simulation of the spring/summer drought of 1988. Both models, however, adequately represent the low amounts of observed precipitation.

Overall, SUBEX provides a more accurate representation of the fields that are important to the energy and water budgets. These improvements are seen in both the mean conditions as well as variability at daily to interannual scales. The latter suggests that the new scheme improves the model's sensitivity which is critical for both climate change and process studies.

Chapter 4

Role of Convection

In this chapter we investigate the differences between the AS74 and FC80 closure assumptions within the Grell convective parameterization by performing a series of numerical experiments over North America using the modified version of RegCM presented in Chapter 2. This chapter is briefly introduced in Section 4.1. Section 4.2 provides a description the numerical experiments performed in this study. The results of the experiments are described in Section 4.3. And Section 4.5 describes the conclusions of the study.

4.1 Introduction

Moist convective processes typically occur at a spatial scale that is considerably smaller than the resolution of most GCM and RCM simulations. In most GCMs and RCMs the vertical and temporal scales are adequately resolved, but the horizontal scales are not. To resolve convection, horizontal scales on the order of 1 km are required. Most GCMs and RCMs run at resolutions of 100s of km and 10s of km, respectively. As a result, convective processes need to be parameterized and, hence representation of these processes is difficult and often inadequate. Implied in convection schemes is the assumption that statistical properties of convection can be deduced with knowledge of the large-scale (resolved) variables. Thus, convection in each model grid cell represents an ensemble of convective clouds.

Because of these assumptions, convective precipitation is often difficult to adequately predict. Convection also depends on a variety of physical processes such as the temperature and moisture profiles of the atmosphere, topography, surface fluxes, and wind-shear (Giorgi 1991). Because of these complexities, climate models tend to perform better in regimes where resolvable-scale (large-

scale) precipitation dominates [Pal et al. (2001); see Chapter 3]. Thus, considerable efforts have gone into the representation of convection and a wide variety of parameterizations exist. Giorgi and Shields (1999) show that model performance varies considerably depending on the choice of convective parameterization. Sun et al. (1999) show that not only does the model performance depend on the choice of convection scheme, they also show that it varies depending on the closure assumption within the convection scheme. This study investigates how the choice of closure assumption impacts the model performance within the modified version of RegCM (described in Chapter 2).

Over eastern Africa, Sun et al. (1999) find more favorable results with the FC80 closure assumption within the Grell (1993) convection scheme when compared to the AS74 closure assumption. However, they disregard the FC80 closure because it does not directly include the interactions between cumulus clouds and the large-scale circulation (quasi-equilibrium assumption). However, Emanuel (1994) indicates that all schemes that simulate convection according to the stability of a vertical column will establish a statistical equilibrium over a period of time. Thus, although the quasi-equilibrium assumption is not explicitly enforced in the FC80 closure, under most conditions it satisfies the assumption over several time steps. Exceptions are under circumstances of large conditional instability (such as capping inversions).

Moist convection tends to occur in two forms (Emanuel 1994). In the first form, convective clouds tend to reach an equilibrium with the large-scale forcing. This type of convection is particularly appropriate in maritime and tropical settings and is best represented by the quasi-equilibrium closure assumption such the AS74. Under these conditions, using the FC80 closure assumption may tend to result in a unrealistically noisy precipitation field. The second type of convection tends to result from stored energy which is released by a triggering mechanism. This type of convection tends to be more explosive and associated with mid-latitude land regions and is better represented by a closure assumption that consumes the energy according to a specified time-scale such as the FC80. Using the AS74 closure assumption under these conditions may tend to result in a dampening of these events (lower intensity, longer duration). Over the typical domain of a climate model, quite often both types of convection occur.

4.2 Design of Numerical Experiments

In this section, we provide a brief description of the numerical experiments performed in this chapter. Each run is initialized on the 15th of March for each of the following years: 1986, 1987, 1988, 1989, 1990, and 1993. The runs are integrated for six months and 17 days; The first 17 days are discarded for model spin-up considerations. The details on the reasons for selecting the initialization dates are described in Section 3.2. The simulation for each year is performed twice; one run using the Grell scheme with the AS74 closure assumption to represent the convective processes and another using the FC80 closure assumption. The pair of simulations for each year is identical except for the choice of closure assumption within the Grell scheme. Note that some of the parameters in the FC80 simulations have been modified to optimize performance. Figure 3-1 depicts the domain and associated topography for the simulations presented in this study. More details regarding the domain configuration can be found in Section 3.2.

4.3 Results: FC80 versus AS74

In this section, we compare the simulations utilizing the AS74 closure assumption within the Grell convection scheme to those using the FC80 closure assumption. Note that SUBEX represents the large-scale cloud and precipitation processes. Monthly averages from the data are computed over the Upper Midwest and Gulf Coast states defined in Figure 3-1 and then compared to observations. A summary of statistics for the Midwest and Gulf Coast are provided in Tables 4.1 and 4.2.

4.3.1 Water Budget

To demonstrate the water budget, we compare the model to observations of cloud water path and precipitation.

Precipitation is the most important variable of the surface water budget and tends to be the most difficult to simulate. Figure 4-1 shows that RegCM performs similarly in reproducing observed precipitation over the Midwest independent of the choice of convective closure assumption (AS74 or FC80). Both sets of simulations tend to underestimate the mean conditions by 0.19 mm/day. However, the average absolute error in the AS74 simulations (RMSE=0.75 mm/day) is less than that in the FC80 simulations (RMSE=0.88 mm/day). On the other hand, the FC80 simulations reproduce the extreme conditions (slope=0.74) better than the AS74 simulations (slope=0.67). Much of the bias, RMSE, and low slope are a result poor model performance during September

Table 4.1: Summary of the model simulation statistics compared to observations for both AS74 and FC80 closure assumptions over the Midwest (outlined in Figure 3-1). RMSE denotes root mean square error; ALBEDO denotes top of the atmosphere albedo; OLR denotes top of the atmosphere outgoing longwave radiation; SWI denotes incident surface shortwave radiation; RN denotes net surface radiation; CWP denote cloud water path; PPT denotes precipitation; and TMEAN, TMAX, and TMIN denote the mean, maximum, and minimum surface temperatures, respectively.

	AS74			FC80		
	Bias	RMSE	Slope	Bias	RMSE	Slope
PPT	-0.19	0.75	0.67	-0.19	0.88	0.74
CWP	-7.9	19.6	0.37	-10.2	20.9	0.76
Albedo	0.029	0.042	0.76	0.005	0.038	1.07
OLR	3.5	10.5	1.49	2.1	13.8	1.89
SWI	-4.3	17.1	1.13	11.7	22.8	1.35
RN	-7.2	13.4	0.96	3.2	11.2	1.09
TMEAN	-0.06	0.99	1.03	-0.05	1.13	1.06
TMAX	-0.21	1.37	1.08	0.18	1.61	1.18
TMIN	1.50	1.73	0.96	1.07	1.52	0.92

for four of the six years; Neglecting all of the Septembers from the statistical computations, results in significant improvements (not shown). It is determined that during September the large- and meso-scale dynamics are poorly represented compared to the NCEP Reanalysis data (too much northerly flow; too little southerly flow; not shown).

Over the Gulf Coast region, the model performance with both closure assumptions degrades when compared to the Midwest region (see Figures 4-1 and 4-2). In nearly every month, the AS74 simulations tend to underestimate the USHCN observations (bias=-0.69 mm/day). The scatter of the data, however, about the best fit line to observations remains relatively low. The FC80 simulations perform considerably better in representing the mean precipitation conditions (bias=-0.3 mm/day), however, the scatter of the data about the best fit line is considerably higher.

Figure 4-3 displays the percentage of total monthly precipitation that is convective averaged for both the AS74 and FC80 simulations over the Midwest region. As expected, the summer months (June, July, and August) are the most convectively active months. During these months, the AS74 runs simulate more than 50% of the precipitation as convective while the FC80 runs simulate nearly 65%. Strikingly, the FC80 simulations tend to simulate a 10 to 15% higher convective fraction during all of the months. The largest differences occur during the summer months. The increase in convective fraction comes from both an increase in convective precipitation and a decrease in

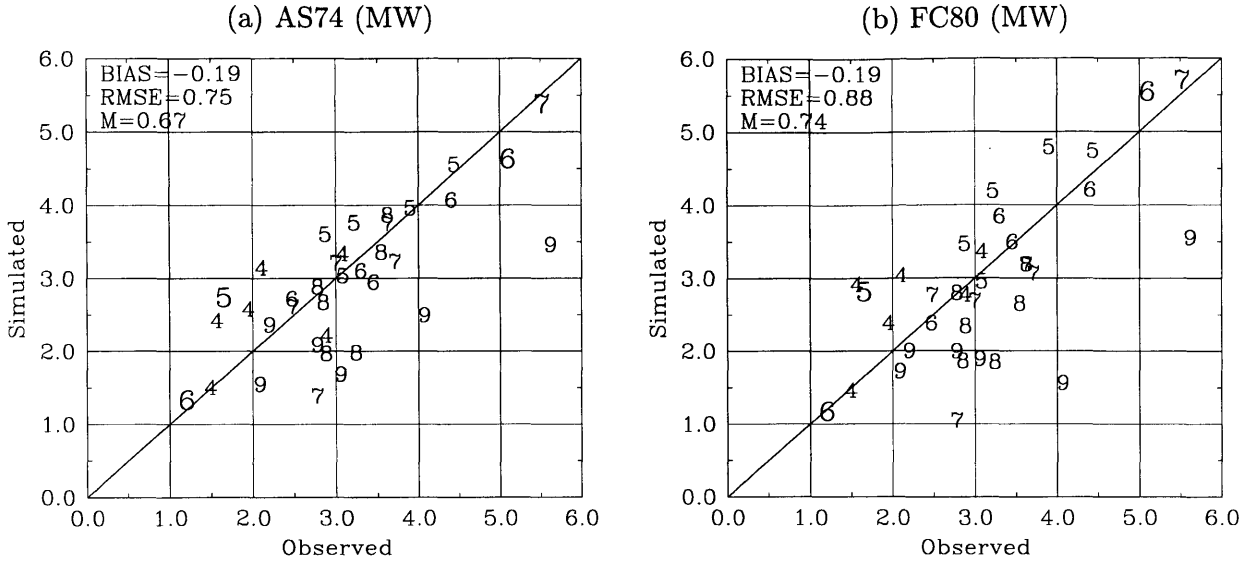

Figure 4-1: Plot of the simulated precipitation in mm/day (y-axis) against the USHCN observations (x-axis). Each data point represents a spatial average over the Midwest box outlined in Figure 3-1. Each digit indicates the month over which the average is taken. The large 5 and 6 refer to May and June of the Drought year (1988) and the large 6 and 7 refer to June and July of the flood year (1993). The June 1988 value lies in the bottom left corner in both sub-plots. (a) AS74; (b) FC80.

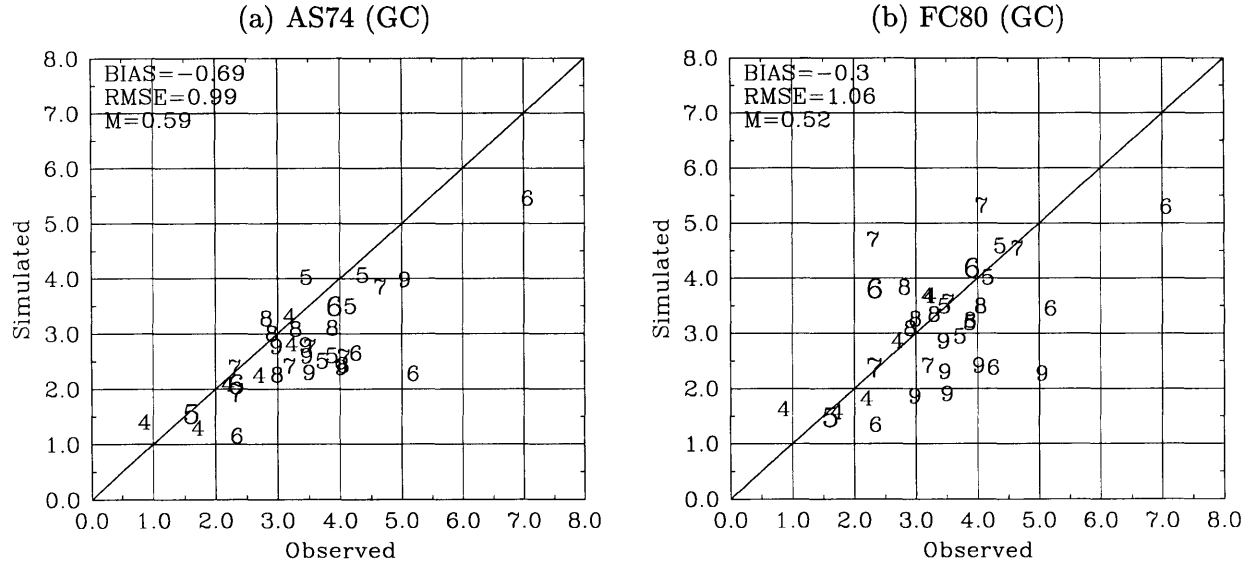

Figure 4-2: Plot of the simulated precipitation in mm/day (y-axis) against the USHCN observations (x-axis). Each data point represents a spatial average over the Gulf Coast box outlined in Figure 3-1. Each digit indicates the month over which the average is taken. The large 5 and 6 refer to May and June of the Drought year (1988) and the large 6 and 7 refer to June and July of the flood year (1993). The June 1988 value lies in the bottom left corner in both sub-plots. (a) AS74; (b) FC80.

Table 4.2: Summary of the model simulation statistics compared to observations for both AS74 and FC80 closure assumptions over the Gulf Coast (outlined in Figure 3-1). RMSE denotes root mean square error; ALBEDO denotes top of the atmosphere albedo; OLR denotes top of the atmosphere outgoing longwave radiation; SWI denotes incident surface shortwave radiation; RN denotes net surface radiation; CWP denote cloud water path; PPT denotes precipitation; and TMEAN, TMAX, and TMIN denote the mean, maximum, and minimum surface temperatures, respectively.

	AS74			FC80		
	Bias	RMSE	Slope	Bias	RMSE	Slope
PPT	-0.69	0.99	0.59	-0.30	1.06	0.52
CWP	13.2	29.0	-0.06	-4.90	19.0	0.41
Albedo	0.074	0.088	0.23	0.039	0.059	0.03
OLR	7.0	10.7	0.50	-3.6	18.0	0.18
SWI	-29.0	41.9	0.93	-1.20	22.8	1.15
RN	-28.9	35.0	0.61	-11.4	18.0	0.86
TMEAN	-1.56	1.82	0.93	-1.19	1.48	1.03
TMAX	-1.21	1.89	0.87	-0.52	1.68	1.09
TMIN	0.42	0.84	0.94	0.31	0.86	0.97

non-convective (not shown).

The significant differences in convective fraction between the two closure assumptions is even more pronounced over the Gulf Coast region (Figure 4-4). The AS74 simulations predict values ranging from 30% in April to 60% in June and July down to 50% in September. On the other hand, the FC80 simulations range from 50% April to 80% in June, July, and August, down to 70% in September. During the summer months, the differences are in excess of 20%.

Figure 4-5 displays the difference in convective fraction averaged over June, July, and August between the two sets of simulations (FC80-AS74). Other than over few isolated regions such as a portion of the Rocky mountains, a higher convective fraction of precipitation occurs when utilizing the FC80 closure assumption. The regional differences in the fraction of precipitation that is convective sheds light upon the reasons for the performance differences between the closure assumptions. The effects of these differences will be discussed in greater detail in Subsection 4.3.4.

Figure 4-6 displays the improvement (or deterioration) seen in the simulated precipitation between AS74 and FC80 simulations over the United States averaged over June, July, and August. (Note that contours only exist over the United States since the USHCN data do not exist elsewhere.) The performance of each closure assumption exhibits a strong regional dependence. In general, the AS74 simulations tend to perform better (negative contours) over most of the Rocky Mountains

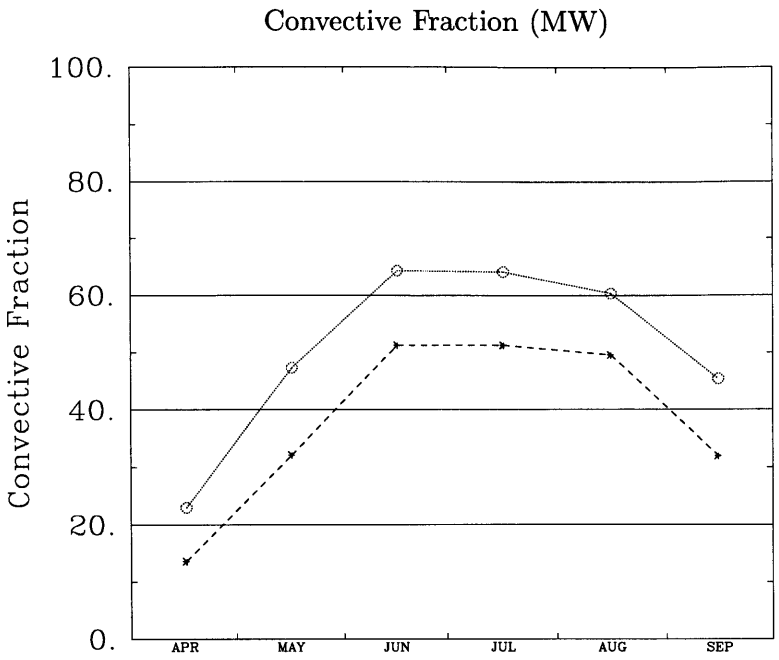

Figure 4-3: Plot of the percentage of total precipitation that is convective over the Midwest region outlined in Figure 3-1. Each data point represents the simulated average for the indicated month. The dashed line with stars is for the AS74 simulations, while the dotted line with circles is for the FC80 simulations.

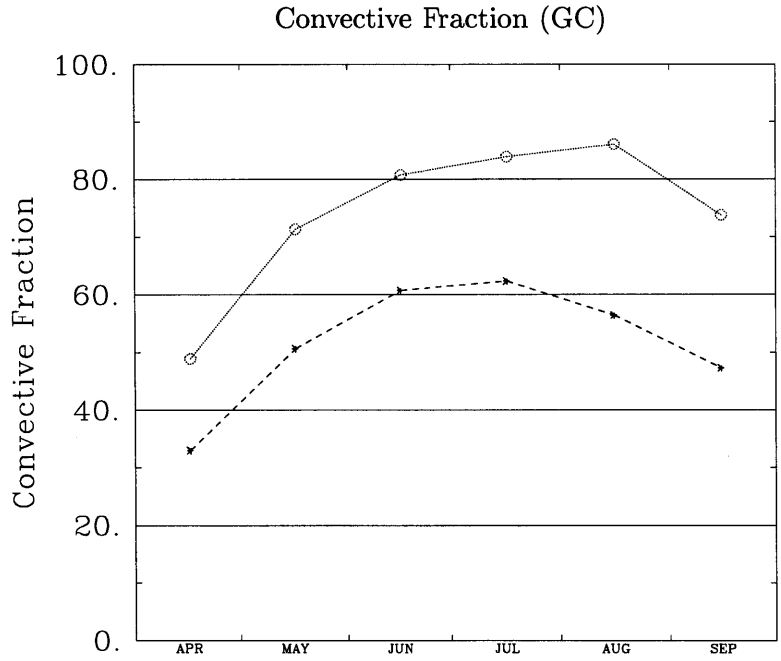

Figure 4-4: Plot of the percentage of total precipitation that is convective over the Gulf Coast region outlined in Figure 3-1. Each data point represents the simulated average for the indicated month. The dashed line with stars is for the AS74 simulations, while the dotted line with circles is for the FC80 simulations.

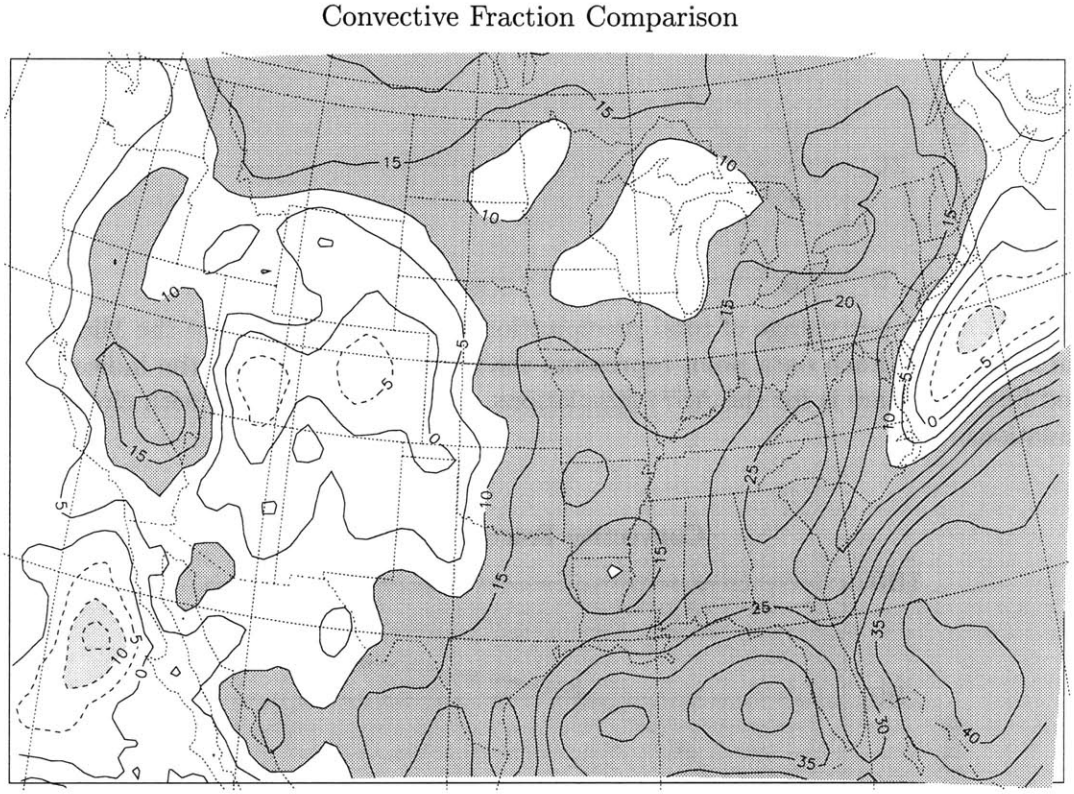

Figure 4-5: Plot of the differences in the percentage of precipitation that is convective between the AS74 and FC80 simulations averaged over June, July, and August. Positive contours (solid lines) indicate that the FC80 runs predict a higher convective fraction while negative contours indicate that the AS74 runs predict a higher convective fraction. Dark and light shading occur at values greater than 10% and less than -10%, respectively.

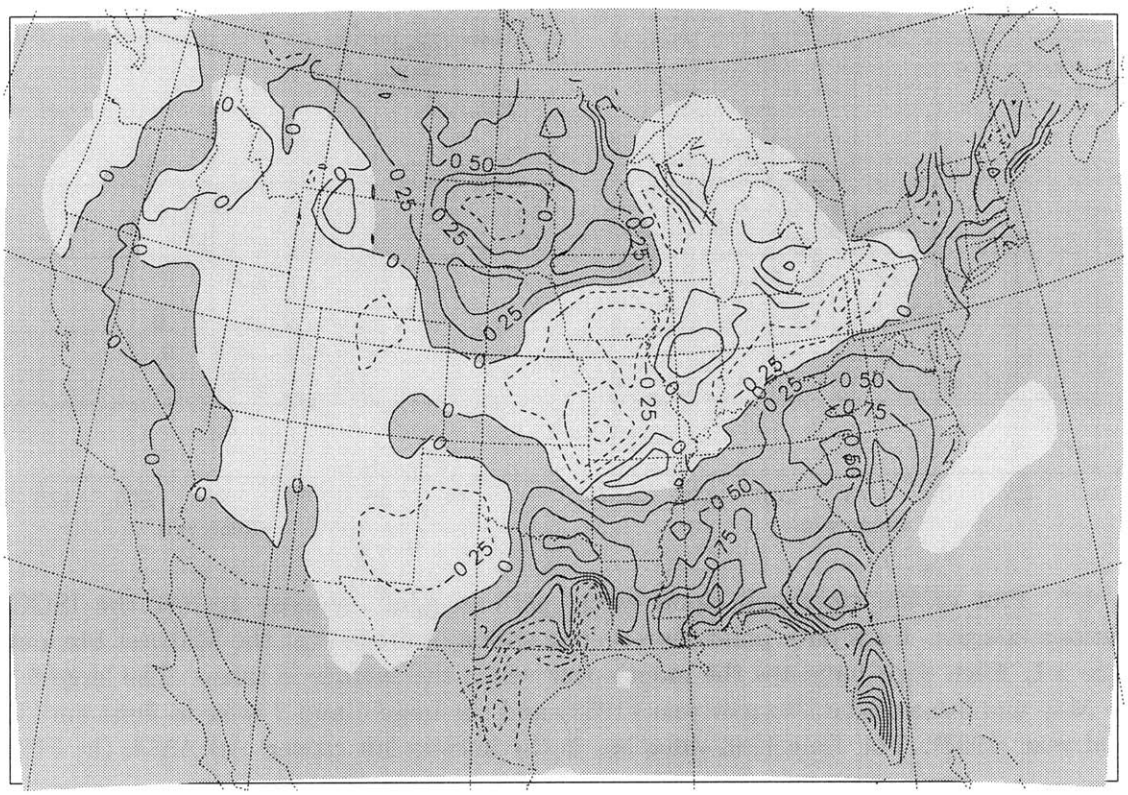

Figure 4-6: Plot of the overall changes to the precipitation results between the AS74 and FC80 simulations averaged over June, July, and August. Contours (United States only) display the RMSE difference between the simulations in mm/day; Positive values (solid lines) indicate that the the FC80 simulations perform better than the AS74 simulations; Negative values (dashed lines) indicate that the AS74 simulations perform better. The shading displays direction of the difference between the AS74 and FC80 simulations; Dark shading indicates that FC80 runs simulate more precipitation than the AS74 runs and vice versa.

and central Midwest. The FC80 simulations tend to perform better over the Gulf Coast and Atlantic Seaboard states, the upper Midwest, and the South. Most of the regions where the FC80 simulations perform better the AS74 simulations are associated with a substantial increase in the convective fraction of precipitation (see Figure 4-5; dark shading). The AS74 simulations tend to be superior when the AS74 precipitation exceeds the FC80 precipitation, and vice versa. On the whole, the FC80 simulations tend outperform the AS74 simulations over the United States during the summer. However, the differences in overall performance are small.

Figure 4-7 compares the model results to the ISCCP-D2 observations of cloud water path for both the AS74 and FC80 simulations over the Midwest region. Both sets of simulations perform adequately in reproducing the mean conditions of cloud water; The bias is -8 g/m^2 in

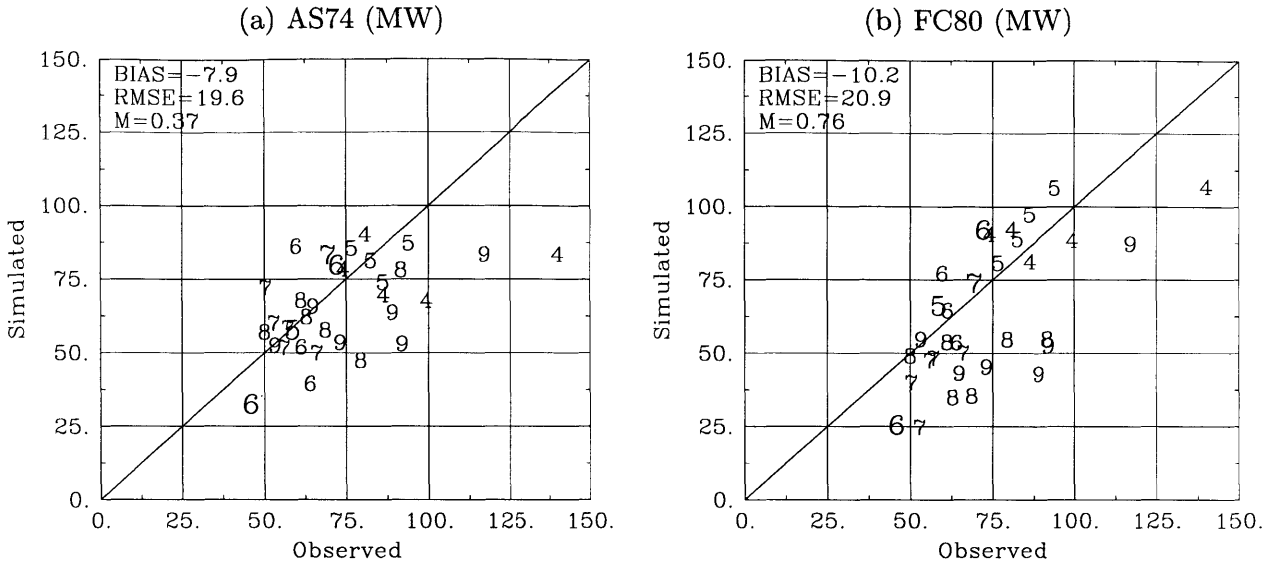

Figure 4-7: Plot of the simulated cloud water path in g/m^2 (y-axis) against the ISCCP-D2 observations (x-axis). Each data point represents a spatial average over the Midwest box outlined in Figure 3-1. Each digit indicates the month over which the average is taken. The large 5 and 6 refer to May and June of the Drought year (1988) and the large 6 and 7 refer to June and July of the flood year (1993). The June 1988 value lies in the bottom left corner. (a) AS74; (b) FC80.

the AS74 simulations and -10 g/m^2 in the FC80 simulations. There is, however, considerable scatter of the data about the one-to-one line in both sets of simulations; The RMSE is 20 g/m^2 in the AS74 simulations and 21 g/m^2 in the FC80 simulations. However, the FC80 simulations perform significantly better in reproducing the seasonal and interannual variability reflected in the lower deviation of the slope from unity (0.76 versus 0.37); The AS74 simulations show little skill in representing these variabilities. This better performance of FC80 simulations tends to result from improvements in the prediction of spring cloud water path. Although this performance is significantly better than the AS74 simulations, there is still considerable room for improvement especially during the summer months. The difficulties in simulating the summer cloud water path with both closure assumptions may be in part due to the crude representation of convective cloud fraction and water (see Subsection 2.1.4).

Similar to precipitation, over the Gulf Coast region, the performance significantly degrades when compared to the Midwest region (Figure 4-8). The AS74 simulations perform adequately in representing the mean cloud conditions (bias=13 g/m^2). However, they show little skill in predicting the seasonal and interannual variability (RMSE=29 g/m^2 and Slope=-0.06). The FC80 simulations perform significantly better than the AS74 simulations in predicting the mean conditions (bias=-

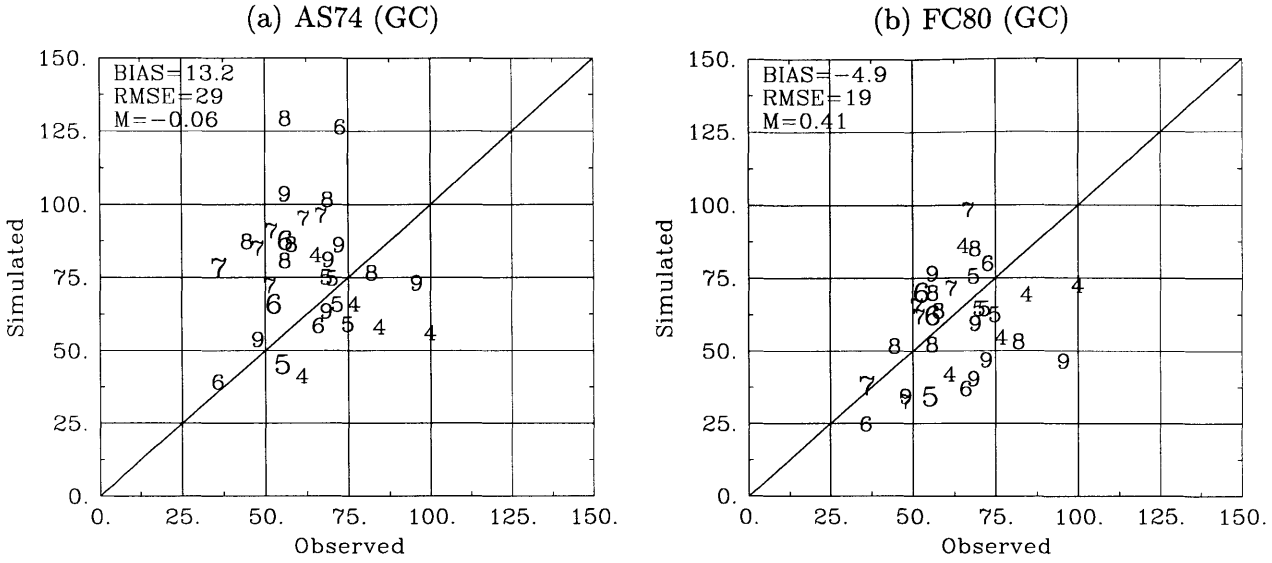

Figure 4-8: Plot of the simulated cloud water path in g/m^2 (y-axis) against the ISCCP-D2 observations (x-axis). Each data point represents a spatial average over the Gulf Coast box outlined in Figure 3-1. Each digit indicates the month over which the average is taken. The large 5 and 6 refer to May and June of the Drought year (1988) and the large 6 and 7 refer to June and July of the flood year (1993). The June 1988 value lies in the bottom left corner. (a) AS74; (b) FC80.

5 g/m^2) and the seasonal and interannual variabilities (RMSE=19 g/m^2 and slope=0.41). However, there is considerable room for improvements. As seen in Figure 4-4, a significant percentage of the precipitation that occurs over the Gulf Coast region is convective. Thus, deficiencies in the representation of convective cloud fraction and cloud water are likely to have played a role in the poor representation of cloud water path. Although the AS74 simulations predict a lower convective fraction, clouds are better represented in the FC80 simulations.

Overall, both closures assumptions adequately represent mean conditions of the water budget (precipitation and cloud water path) over the United States. The simulations implementing the FC80 closure assumption, however, perform considerably better in simulating the seasonal and interannual variabilities (especially with cloud water path). Regionally, both sets of simulations tend to perform better over the Midwest region compared to the Gulf Coast region.

4.3.2 Radiation Budget

In many modeling applications, it is crucial to accurately simulate the surface energy budget. To do so, however, it is essential that the atmospheric components of the water and energy budgets are adequately predicted. In this subsection, we evaluate the model's performance in simulating the

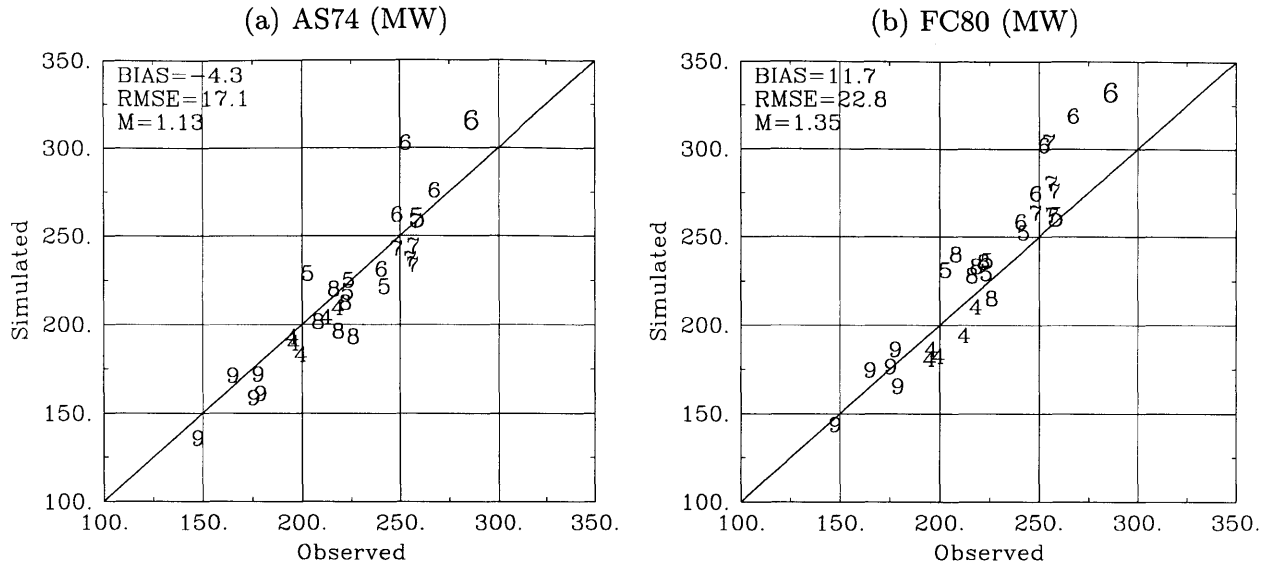

Figure 4-9: Plot of simulated simulated incident surface shortwave radiation in W/m^2 (y-axis) against the NASA-SRB data (x-axis). Each data point represents a spatial average over the Midwest box outlined in Figure 3-1. Each digit indicates the month over which the average is taken. The large 5 and 6 refer to May and June of the Drought year (1988). (a) AS74; (b) FC80.

top of the atmosphere albedo and outgoing longwave radiation and the surface incident shortwave radiation and net radiation.

Incident surface shortwave radiation is the main energy input to the hydrologic cycle of the surface. It reflects the integrated effect of the clouds that lie above the biosphere. Figure 4-9 displays how well each of the sets of simulations perform in reproducing the NASA-SRB incident surface shortwave radiation over the Midwest region. The AS74 simulations perform well in simulating the mean incident surface shortwave radiation conditions (bias=-4 W/m^2). Given that the AS74 simulations tend to underpredict cloud water (Figure 4-7), one would expect an overprediction of incident surface shortwave radiation. This inconsistency may be a result of the oversimplified representation of cloud water and cloud fraction (see Subsection 2.1.4). The seasonal and interannual variabilities are reasonably well represented (RMSE=17 W/m^2 and m=1.13). Similar to above, deficiencies in the FC80 simulations are largest during the convectively active months (especially June) which are responsible for most of the 11.7 W/m^2 bias and the over prediction of the seasonal variability (m=1.35). In general, the AS74 scheme does a superior job in reproducing the NASA-SRB incident surface shortwave radiation.

Consistent with the water budget results, over the Gulf Coast the AS74 simulations ability to simulate the incident surface shortwave radiation significantly degrades (Figure 4-10a) when

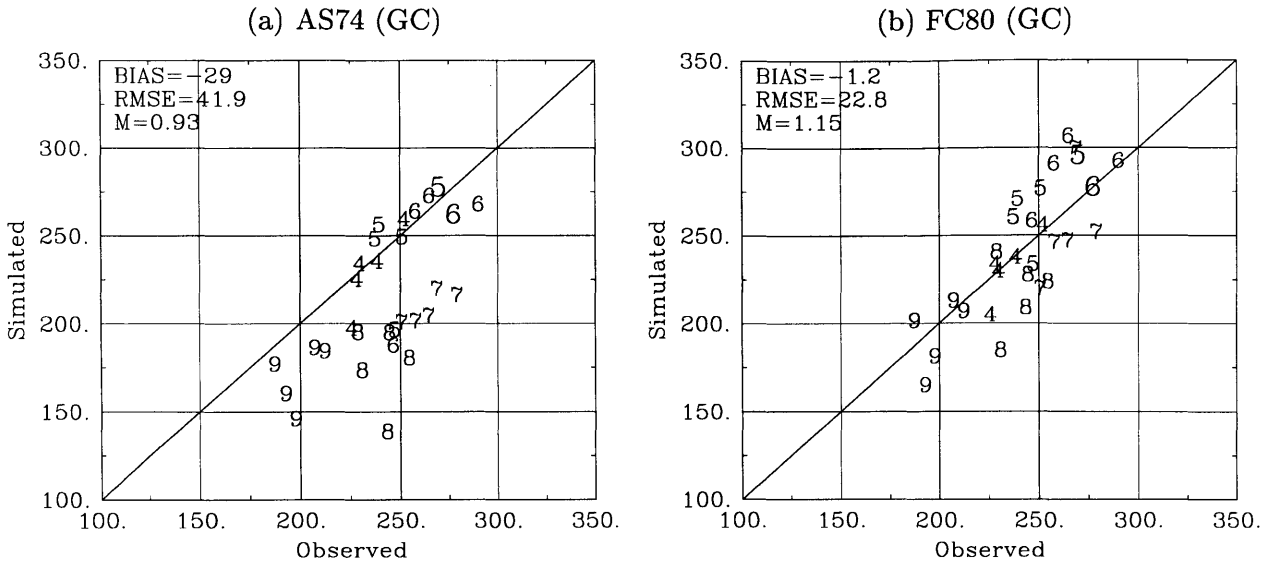

Figure 4-10: Plot of simulated simulated incident surface shortwave radiation in W/m^2 (y-axis) against the NASA-SRB data (x-axis). Each data point represents a spatial average over the Gulf Coast box outlined in Figure 3-1. Each digit indicates the month over which the average is taken. The large 5 and 6 refer to May and June of the Drought year (1988). (a) AS74; (b) FC80.

compared to the Midwest. The bias and RMSE increase to -29 W/m^2 and 42 W/m^2, respectively. As with the Midwest region, this is somewhat inconsistent with the prediction of cloud water path. Given the large bias in incident surface shortwave radiation, one would expect the cloud water path bias to be greater than shown Figure 4-8. The FC80 simulations, on the other hand, perform reasonably well in simulating the incident surface shortwave radiation (Figure 4-10b). The bias is -1 W/m^2 and RMSE is 23 W/m^2. Considering that the bias is negligible, the RMSE is quite high indicating that there is considerable scatter about the one-to-one line.

Net surface radiation is a key component of the surface energy budget. It determines the turbulent fluxes into the atmospheric boundary layer. Figure 4-11 displays the simulation results against the NASA-SRB data. The AS74 closure tends to under predict net surface radiation (bias=7.2 W/m^2). In addition, the scatter about the best fit line to the NASA-SRB data and the one to one line is higher in the AS74 simulations than the FC80 simulations. This suggests that the FC80 closure assumption better represents the processes that determine the seasonal and interannual variability. The FC80 closure tends to over predict net surface radiation during the June. Note, however, that some of these statistical improvements result due to the cancelling of errors. That is, some of the over prediction of summer incident surface shortwave radiation (Figure 4-9b) is cancelled due to a reduction in the amount of longwave radiation remitted towards

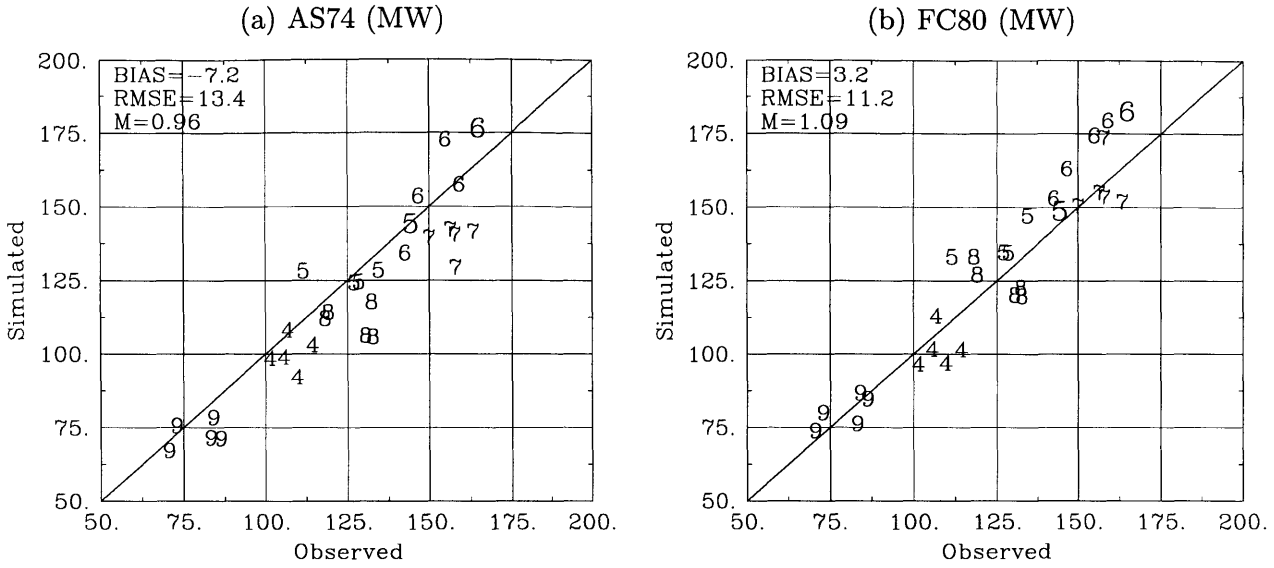

Figure 4-11: Plot of the simulated net surface radiation in W/m^2 (y-axis) against the NASA-SRB data (x-axis). Each data point represents a spatial average over the Midwest box outlined in Figure 3-1. Each digit indicates the month over which the average is taken. The large 5 and 6 refer to May and June of the Drought year (1988). (a) AS74; (b) FC80.

the surface due to a lack of clouds. Nevertheless, the net radiation still tends to remain too high during the convectively active months. This cancellation effect is not as pronounced in the AS74 simulations.

Over the Gulf Coast, the AS74 simulations severely underestimate net surface radiation (bias=-29 W/m^2; Figure 4-12b). In addition, there is a significant underestimate of the seasonal and interannual variabilities (RMSE=35 W/m^2 and slope=0.61). The overall bias is nearly identical to the bias in incident surface shortwave radiation. Given that the positive bias in cloud water path is relatively small, the longwave radiation re-emitted by the clouds towards the surface is not large enough to cancel the error. The FC80 simulations perform considerably better than the AS74 simulations in predicting net surface radiation. The bias, RMSE, and slope are -11 W/m^2, 18 W/m^2, and 0.86, respectively. There is, however, a considerable bias in July and August.

Figure 4-13 compares the performance of the predicted net surface radiation between the AS74 and FC80 simulations averaged over the entire simulation period. On the whole, the simulations using the FC80 closure assumption display better performance than those using the AS74 closure assumption. The superior performance tends to result primarily from an increase in net surface radiation (dark shading). Over North America, two exceptions lie over the Great Lakes and a small region at the borders of Iowa, Nebraska, Kansas, and Missouri. Significant exceptions also

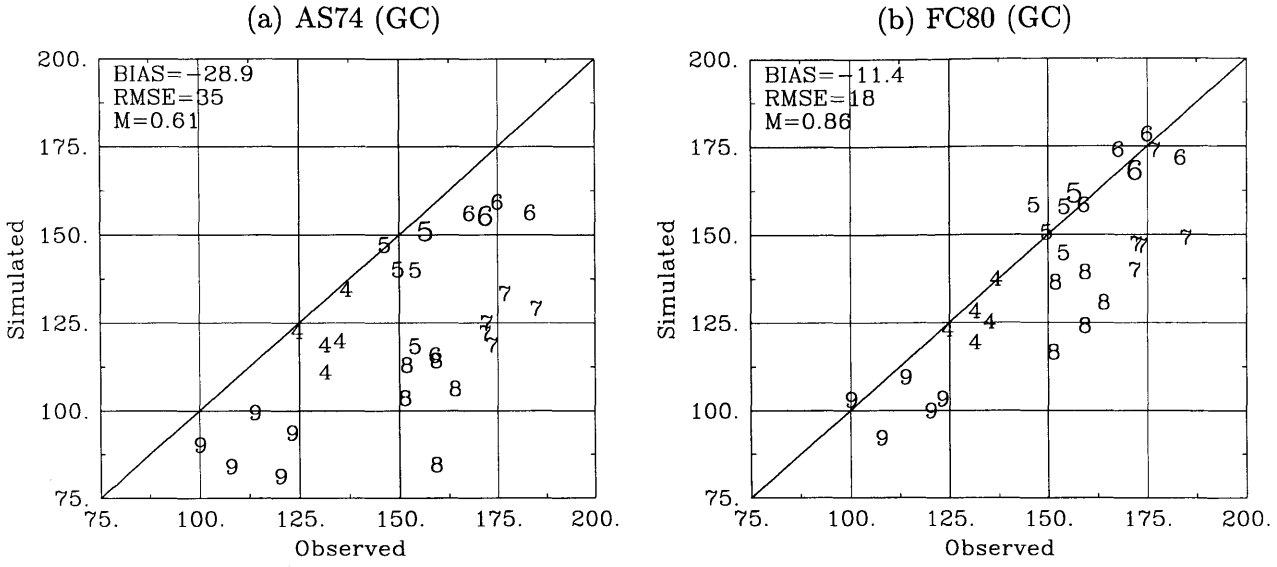

Figure 4-12: Plot of the simulated net surface radiation in W/m^2 (y-axis) against the NASA-SRB data (x-axis). Each data point represents a spatial average over the Gulf Coast box outlined in Figure 3-1. Each digit indicates the month over which the average is taken. The large 5 and 6 refer to May and June of the Drought year (1988). (a) AS74; (b) FC80.

occur over the oceans. The most notable improvements occur along the Atlantic Seaboard and Gulf Coast states and the states surrounding these regions (10 to 40 W/m^2) when compared to the AS74 simulations. These regions also correspond to significant improvements in the prediction of precipitation resulting from an increase in convective precipitation (see Figures 4-5 and 4-6). Over these regions, the AS74 simulations produce too many clouds resulting in too little incident surface shortwave radiation (not shown) and too little precipitation (see Figure 4-6). It is likely that these simulations do not accurately partition the total precipitation into the convective and non-convective forms (i.e. too little convective and too much non-convective). Convective clouds tend to be less radiatively active than non-convective (see Subsections 2.1.3 and 2.1.4). Not only does an increase in convective fraction of precipitation tend to result in an increase in incident shortwave radiation, it is also likely to result in an increase in net radiation and hence a further increase in convective precipitation. The FC80 simulations seem to more accurately represent the partition between convective and non-convective precipitation in addition to the energy budget over the United States (especially the Atlantic Seaboard and Gulf Coast states).

Overall, the differences in performance of the AS74 and FC80 simulations exhibit mixed results. Cloud fields in the FC80 simulations display less skill due to the combination of a higher convective precipitation fraction and an oversimplified convective cloud fraction and water parameterization.

Net Surface Radiation Performance Comparison

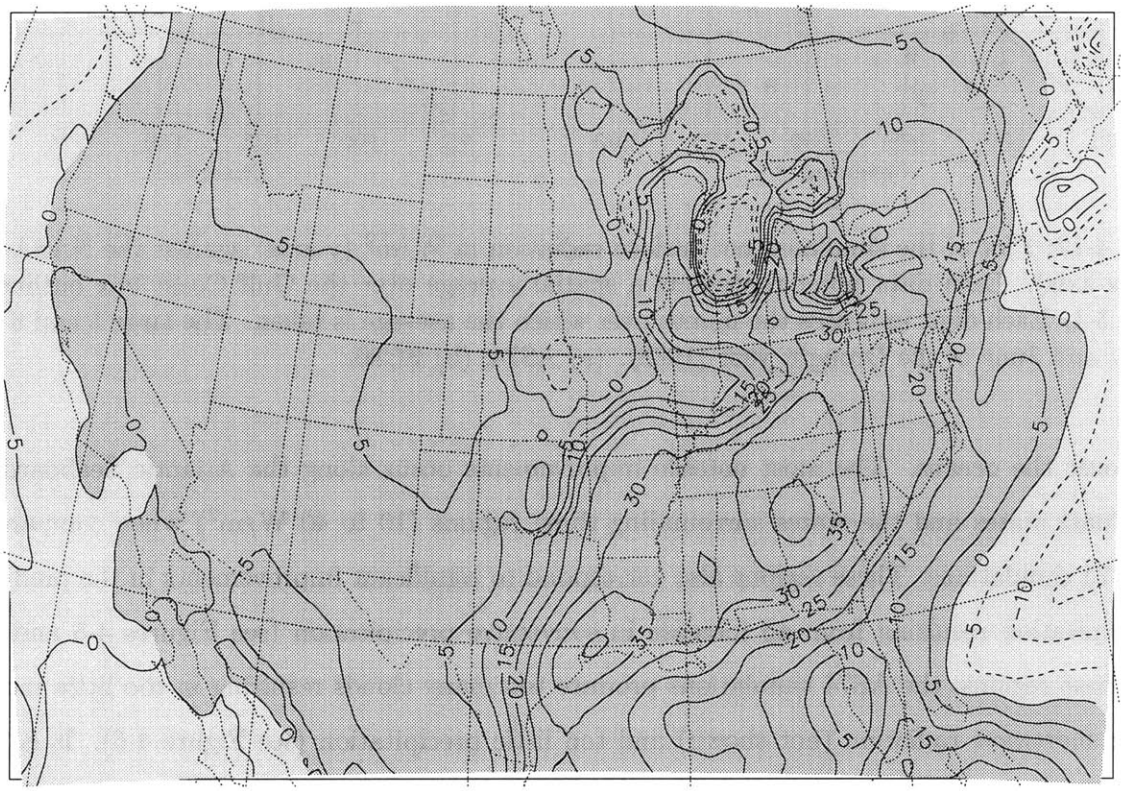

Figure 4-13: Plot of the overall changes to the net surface radiation results between AS74 and FC80 simulations averaged over June, July, and August. Contours display the RMSE difference between the simulations in W/m^2; Positive values (solid lines) indicate that the Grell scheme utilizing the FC80 closure performs better than the with the AS74 closure assumption; Negative values (dashed lines) indicate that the Grell scheme with the AS74 closure assumption performs better. The shading displays direction of the difference between the AS74 and FC80 simulations; Dark shading indicates that FC80 runs simulate more net surface radiation than the AS74 runs and vice versa.

However, the higher convective fraction results an enhanced performance over the Gulf Coast and Atlantic Seaboard states. In addition, the FC80 simulations tend to result in superior performance in the prediction of net surface radiation. However, in some cases the improvements result from a cancellation of biases. Over the Gulf Coast region, the biases are not completely consistent between the water budget and energy budget.

4.3.3 Surface Temperature

Like precipitation, surface temperature is also one of the most difficult fields to accurately predict due to its dependence on a variety of factors. This subsection compares the AS74 and FC80 simulations to the USHCN observations of mean, minimum, and maximum temperature. Note that model temperatures have been adjusted to reconcile differences between station and model elevation.

Figure 4-14 compares the predictions of mean surface temperature from each cloud model to observations over the Midwest. Both the AS74 and FC80 simulations perform well in reproducing observations of mean surface temperature over the Midwest. In both sets of simulations, the bias is nearly zero, the RMSE is approximately one degree, and the slope is near unity. All of the above suggests that both closure assumptions perform well in representing the mean conditions, as well as, the seasonal and interannual variabilities of mean surface temperature over the Midwest during the spring and summer.

Figure 4-15 shows that the results over the Gulf Coast region are not nearly as positive; both the AS74 and FC80 simulations significantly underestimate mean surface temperature. Although the errors are relatively large in both sets of simulations, the FC80 runs perform better than the AS74. This is consistent with the underestimation of net surface radiation seen in both sets of simulations which is greater in the AS74 case than the FC80.

Figure 4-16 displays the improvement (or deterioration) seen in the simulated mean surface temperature between AS74 and FC80 simulations averaged over June, July, and August. Note that contours only exist over the United States since the USHCN data does not exist elsewhere. In general, performance of each closure assumption is regionally dependent. The AS74 simulations perform better over the central and northern Atlantic Seaboard states, in addition to the Great Plains and Rocky Mountains. Note that Great Plains and Rocky Mountains region exhibiting improvements in the AS74 runs are associated with regions where the model elevation exceeds the USHCN elevation by more 200 m. Thus, the results over this region may be somewhat unreliable.

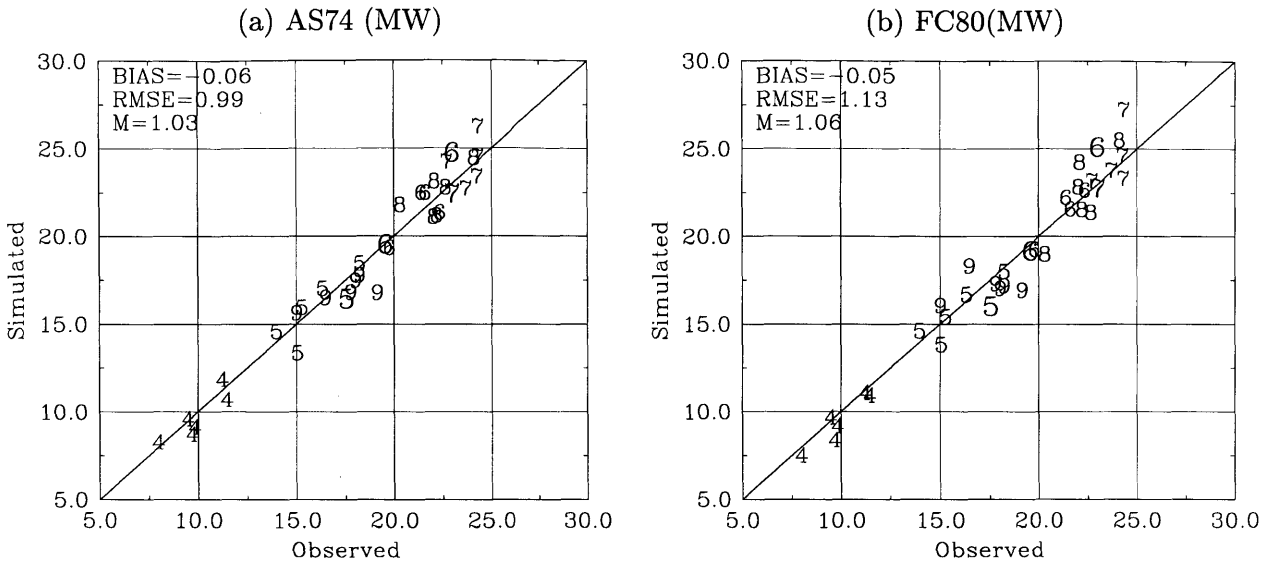

Figure 4-14: Plot of the simulated mean surface temperature in °C (y-axis) against the USHCN observations (x-axis). Each data point represents a spatial average over the Midwest box outlined in Figure 3-1. Each digit indicates the month over which the average is taken. The large 5 and 6 refer to May and June of the Drought year (1988) and the large 6 and 7 refer to June and July of the flood year (1993). The June 1988 value lies in the upper right corner. (a) AS74; (b) FC80.

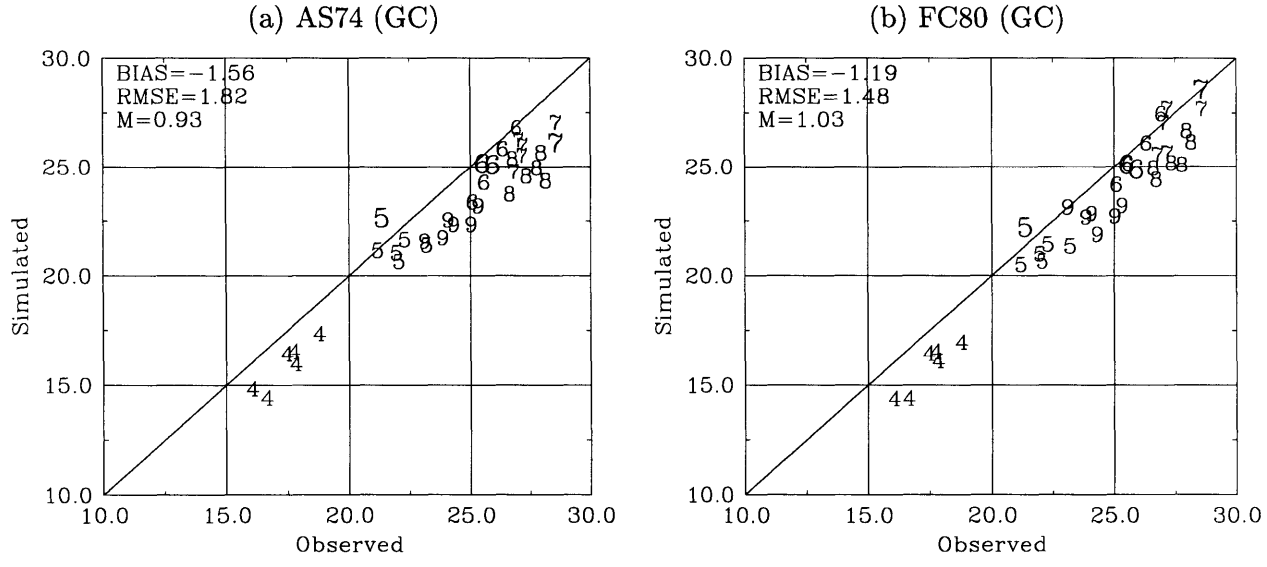

Figure 4-15: Plot of the simulated mean surface temperature in °C (y-axis) against the USHCN observations (x-axis). Each data point represents a spatial average over the Gulf Coast box outlined in Figure 3-1. Each digit indicates the month over which the average is taken. The large 5 and 6 refer to May and June of the Drought year (1988) and the large 6 and 7 refer to June and July of the flood year (1993). The June 1988 value lies in the upper right corner. (a) AS74; (b) FC80.

Mean Surface Temperature Performance Comparison

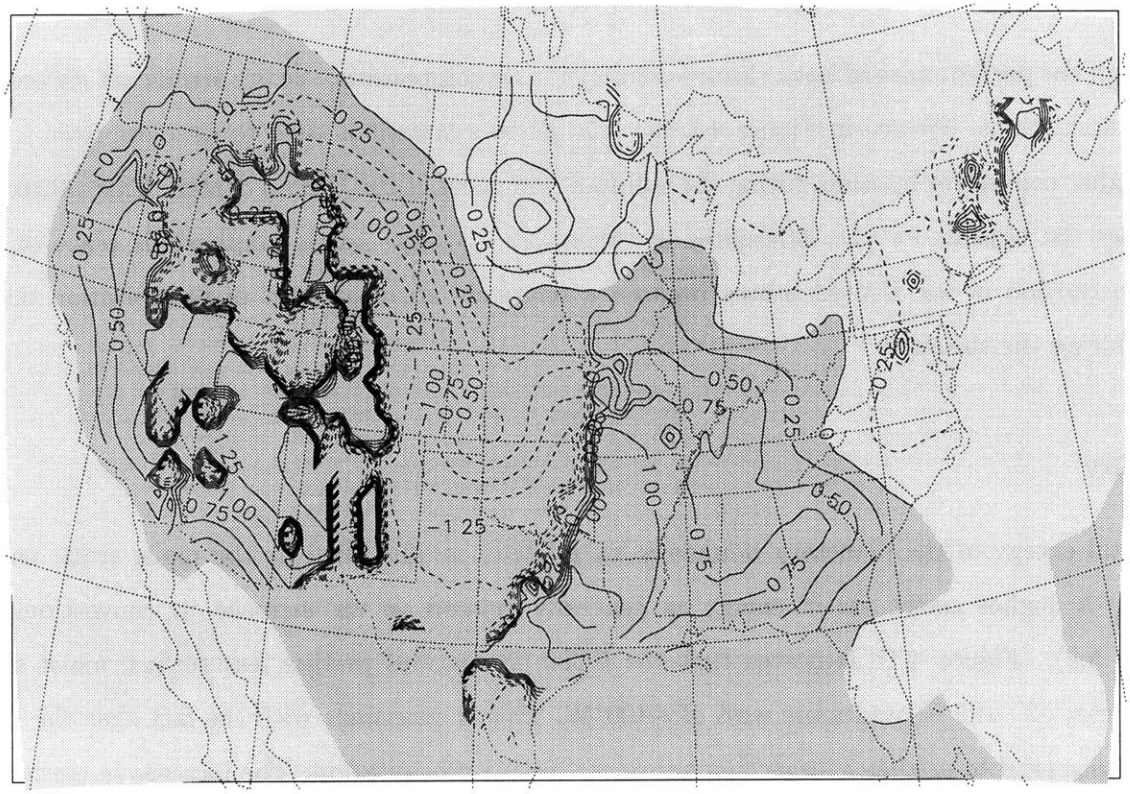

Figure 4-16: Plot of the overall changes to the mean surface temperature results between the AS74 and FC80 simulations averaged over June, July, and August. Contours (United States only) display the RMSE difference between the simulations in W/m^2; Positive values (solid lines) indicate that the FC80 simulations perform better than AS74 simulations; Negative values (dashed lines) indicate that the AS74 simulations assumption perform better. The shading displays direction of the difference between the AS74 and FC80 simulations; Dark shading indicates that FC80 runs are warmer than the AS74 runs and vice versa.

The FC80 simulations better represent the mean surface temperature conditions of the Gulf Coast, Midwest, and states along the Pacific Ocean. Over the Gulf Coast and Midwest states, much of the superior performance is a result of an increase in mean surface temperature resulting from an increase in incident surface shortwave radiation. This region is also associated with improvements in the simulation of precipitation and net radiation.

Overall, RegCM utilizing the FC80 closure assumption tends to perform better than RegCM utilizing the AS74 closure assumption in representing the mean conditions of surface temperature over the Midwest and Gulf Coast. The FC80 runs tend to perform better because of the better radiation budget performance.

4.3.4 Convection

Although the performance of both closure assumptions is comparable, the are significant differences in the simulations. We see in Figure 4-5 that the FC80 simulations tend to simulate from a 5 to 30% higher convective fraction during the summer over most of the United States. This subsection identifies the reasons for the differences in convective activity. Little emphasis is place on the western portion of the United States because a relatively small amount of precipitation occurs there during the summers.

Stability

The total energy of the planetary boundary layer (PBL) is quantified by the moist static energy (MSE). A higher moist static energy is generally related to an increase in convection (see Section 5.2). Figure 4-17 indicates that the FC80 simulations predict less surface moist static energy east of ~100°W and more west of ~100°W. This is consistent with the fact that the FC80 simulations tend to predict a larger amount of convective precipitation. The increase in convection reduces the amount of instability by redistributing the near-surface high-MSE air aloft (increase in updraft mass flux). This suggests that a lower MSE is required to initiate convection with the FC80 closure. It also suggests that more of the instability is removed with the FC80 closure. Since the AS74 simulations require a larger amount of MSE to initiate and maintain convection, the MSE remains higher near the surface. To the east of ~100°W, there tends to be an increase in near-surface MSE with the largest differences over the Four Corners States (New Mexico, Arizona, Colorado, and Utah). The Four Corners States is one of the few regions where there is a decrease in convective precipitation with the FC80 simulations.

Figure 4-18 displays the difference in the Showalter (1953) stability index (modified) between the two sets of simulations averaged over June, July, and August. The Showalter index is computed by lifting an 850 mb parcel dry adiabatically to saturation and then pseudo-adiabatically to 500 mb. The lifted 500 mb temperature is then subtracted from the 500 mb temperature. A positive value indicates stability while a negative values indicates an instability. Here, we use a modified Showalter Index that accounts for topography by using sigma levels. Instead of using the 850 mb and 500 mb pressure levels, we use the 0.895 and 0.51 sigma levels. This accounts for the lower pressures associated with higher elevations such as the Rocky Mountains where the surface pressure reaches 700 mb. Overall, the FC80 simulations tend to be more stable than the AS74 simulations. In fact,

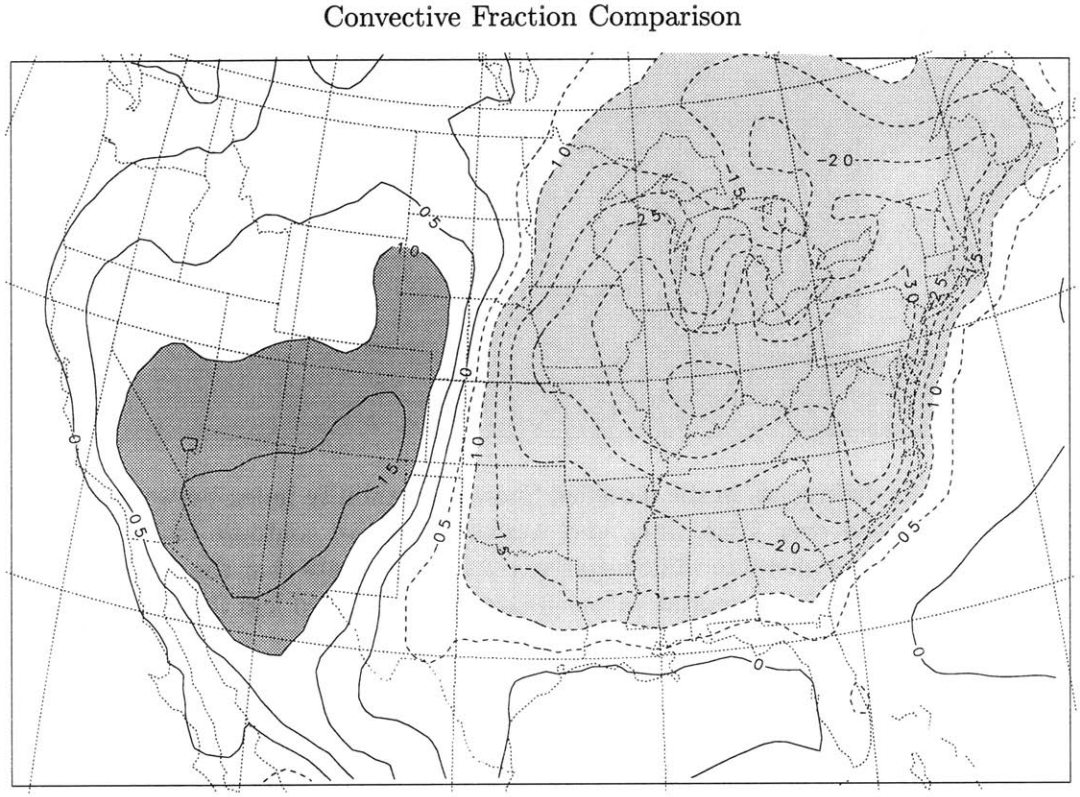

Figure 4-17: Plot of the differences in the surface moist static energy between the AS74 and FC80 simulations averaged over June, July, and August. Positive contours (solid lines) indicate that the FC80 runs predict a higher amount surface moist static energy while negative contours indicate that the AS74 runs predict a larger amount. Dark and light shading occur at values greater than 1 kJ/kg and less than -1 kJ/kg, respectively.

Showalter Stability Index Comparison

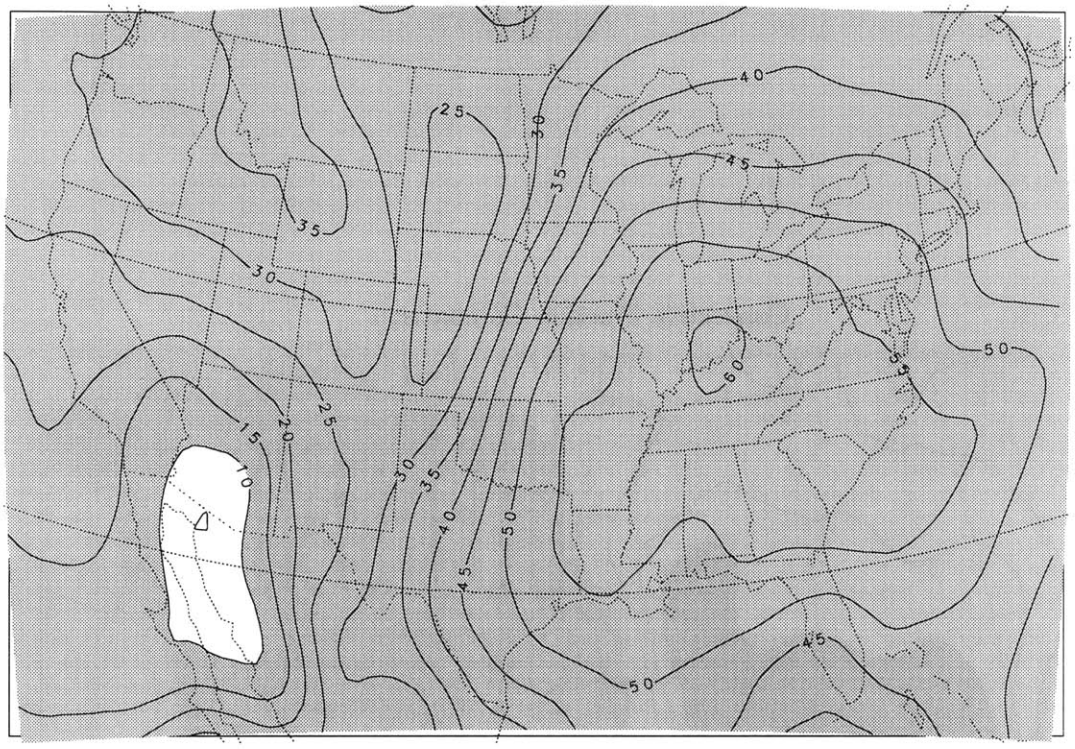

Figure 4-18: Plot of the differences in the modified Showalter stability index between the AS74 and FC80 simulations averaged over June, July, and August. Positive contours (solid lines) indicate that the FC80 runs are more unstable while negative contours indicate that the AS74 runs are more unstable. Dark and light shading occur at values greater than 1 K and less than -1 K, respectively.

there is an increase in stability over the entire domain when using the FC80 closure over the AS74. The largest increase occurs over the eastern United States which is consistent with the differences in near-surface MSE. However, inconsistent with the near-surface MSE differences, the stability also increases over the western United States. Generally speaking, since the western United States tends to be dry during the summer, changes in stability may not result in significant changes in convection. This, however, does not explain the reduction in convection over the Four Corners region.

The reason convection tends to trigger later in the AS74 simulations has to do with the direct coupling of the cumulus-scale and large-scale in the closure assumption (see Equation 2.10). Under certain conditions, the large-scale component can inhibit convection from forming. In the AS74 closure, convection is a function of the destabilization rate, not directly a function of the stability. Thus, if the atmosphere is very unstable, but the change in stability is small (or tending towards stability), convection will be small. However, with the FC80 closure assumption, convection

is directly a function of the stability; a large amount of CAPE yields intense convection (see Equation 2.11). Because of the differences in the closures, the atmosphere can often take longer to stabilize in the AS74 closure. This can cause downwind shifts in the location of the convective precipitation peaks compared to the FC80 closure. In addition, it can lead to less intense, longer duration events as well as a broadening of the convective region. The broadening and downwind shift of the convective precipitation peak occurs because it tends to take longer to stabilize the atmosphere (assuming the FC80 convective removal time scale τ is set to a reasonable value). The differences in the amount of convection are also a function of the model parameters. For example, if the convective FC80 removal time scale is increased, there will be a tendency for an decrease in convection and hence, more similar results to the AS74 closure.

4.4 Simulation of Extreme precipitation Events

As mentioned in Chapter 1, in the summer of 1988, the United States Midwest experienced its warmest and driest summer since the dust-bowl era of the 1930s (Figure 4-19a; Ropelewski (1988)). In contrast, record high rainfall and flooding occurred and persisted throughout much of the summer during 1993 (Figure 4-19b; Kunkel et al. (1994)). This subsection investigates how the choice of closure assumption within the Grell convection scheme impacts the simulation of the above extreme events.

4.4.1 1988 Drought

Figure 4-19a displays the USHCN observed precipitation over the United States averaged over May and June of 1988, the most extreme drought months. With a few regional exceptions, most of the continental United States received less than 2 mm/day of rainfall during May and June of 1988.

Figure 4-20 displays the precipitation for both the AS74 and FC80 simulations averaged over the same period (May and June of 1988). Both set of simulations do an excellent job in simulating the observed lack of precipitation over the United States. However, the individual features of the precipitation are not perfectly simulated in either scheme. This may in part be due to the somewhat unpredictable nature of precipitation (especially convective) and also may be in part be due to the representation of the boundary conditions and model physics. Both the AS74 and FC80 simulations predict too much precipitation over the upper Midwest and too little over the Great Plains. In addition, there is a tendency for the FC80 simulations to predict too much precipitation along the

(a) May and June 1988 USHCN Precipitation

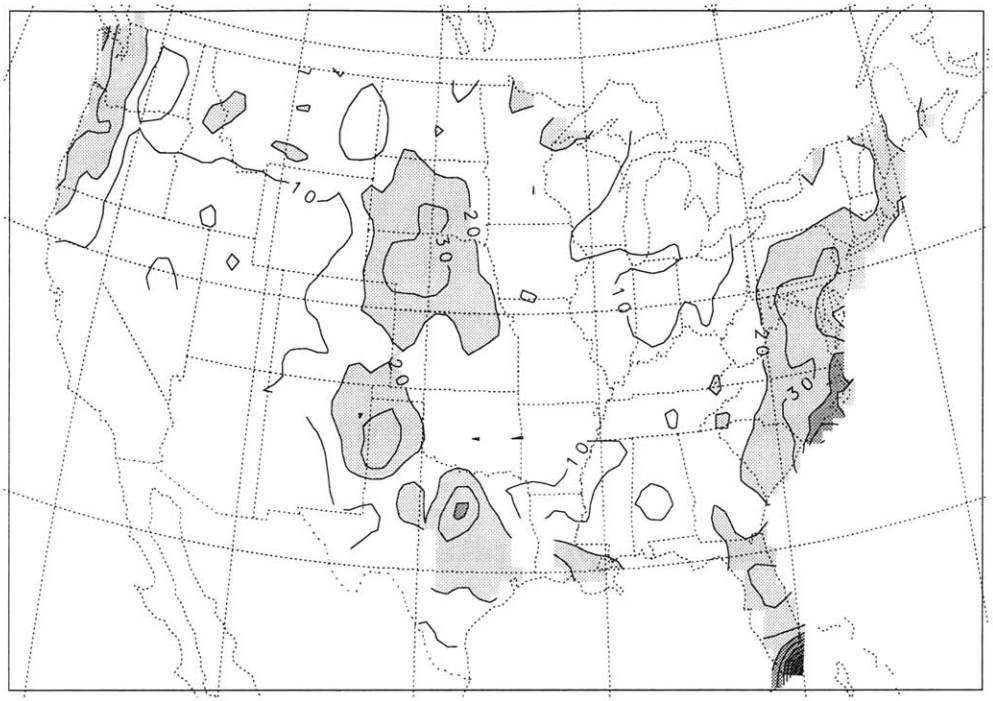

(b) June and July 1993 USHCN Precipitation

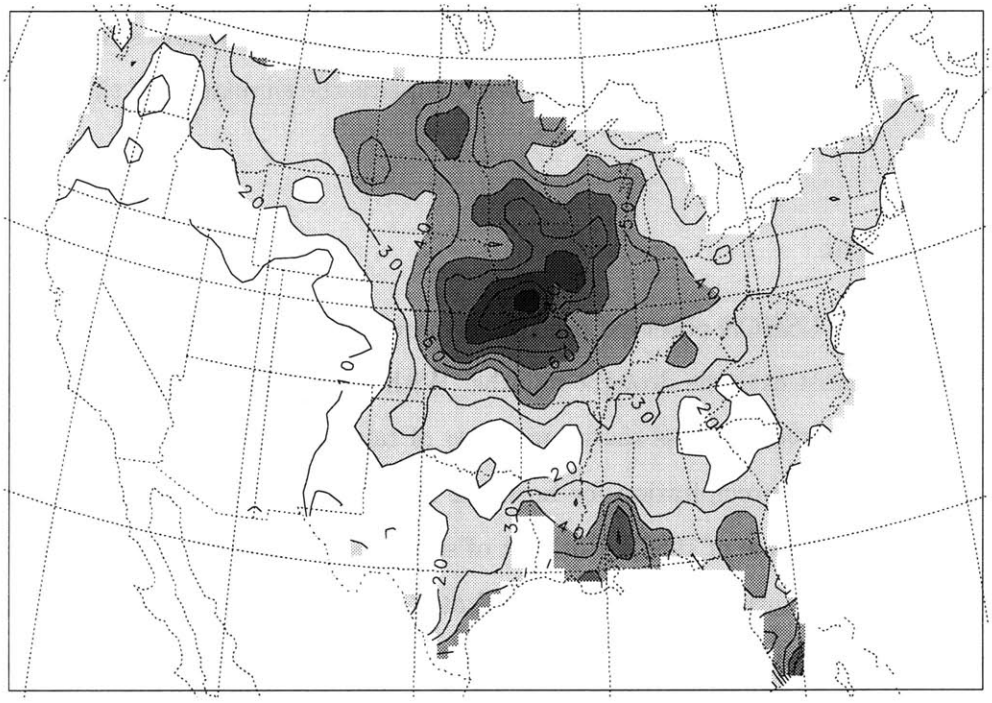

Figure 4-19: USHCN observations of precipitation in mm/day. Contour interval is specified at 1 (mm/day). Shading occurs at values above 2 mm/day and at intervals of 2 mm/day. Note that the USHCN observations only exist over the United States. (a) 1988 May and June average; (b) 1993 June and July average.

Gulf Coast and Atlantic Seaboard states. This is consistent with the higher amounts of convective activity and lower cloud cover in the FC80 simulations.

Overall, it is difficult to argue that one scheme performs better than the other for the drought of 1988. Most importantly, both models are able to simulate the overall lack of observed precipitation. Furthermore, it should be noted that these results for the 1988 drought are similar to those shown in the Project to Intercompare Regional Climate Simulations in that the general lack of precipitation was captured though the details were simulated less well (Takle et al. 1999).

4.4.2 1993 Flood

During June and July of 1993, much of the upper Midwest received greater than 4 mm of precipitation per day (Figure 4-19b). Peak values above 8 mm/day occurred over much Iowa, Nebraska, Missouri, and Kansas. The largest peak (~10-11 mm/day) occurred along the Iowa-Missouri border. A smaller peak occurred along the coast of Mississippi and Louisiana (~6-7 mm/day).

Figure 4-21 displays the simulated rainfall for both the AS74 and FC80 simulations averaged over June and July of 1993. Both sets of simulations are not only able to simulate the region over the upper Midwest in which rainfall exceeds 4 mm/day, but also the region in excess of 8 mm/day that occurred over much of Iowa, Nebraska, Missouri, and Kansas. The general location of the flood region, however, is simulated too far to the north and east of observed. This shift is more pronounced in the AS74 simulations. In addition, the peak maximum is under predicted by approximately 2 mm/day AS74 simulations while it is predicted fairly well in the FC80 simulations. Lastly, both models more or less perform adequately in representing the distribution of precipitation in the rest of the United States. For example, they capture the precipitation peak observed along the coast of Mississippi and Louisiana and the surrounding dry Gulf Coast region. Overall, RegCM regardless of the choice of closure assumption performs well in capturing the spatial distribution of precipitation observed in June and July of 1993. However, the FC80 simulations slightly better simulate the location and magnitude of the flood peak.

The FC80 simulations more accurately predict the location and magnitude of the flood peak because the FC80 closure assumption tends to trigger at lower levels of instability (see Subsection 4.3.4). In addition, since convection with the FC80 closure assumption is related to the degree of instability, as opposed to the rate of instability as it is with the AS74 closure assumption, the instability tends to be consumed sooner and thus upwind of the AS74 simulations.

(a) May and June 1988 AS74 Precipitation (mm/day)

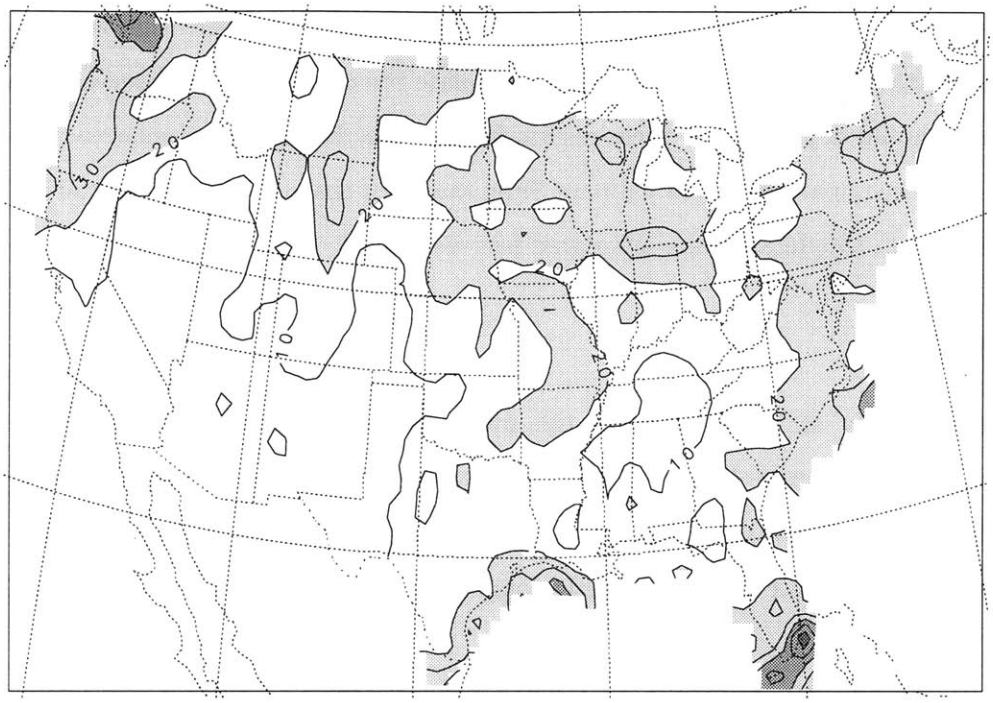

(b) May and June 1988 FC80 Precipitation (mm/day)

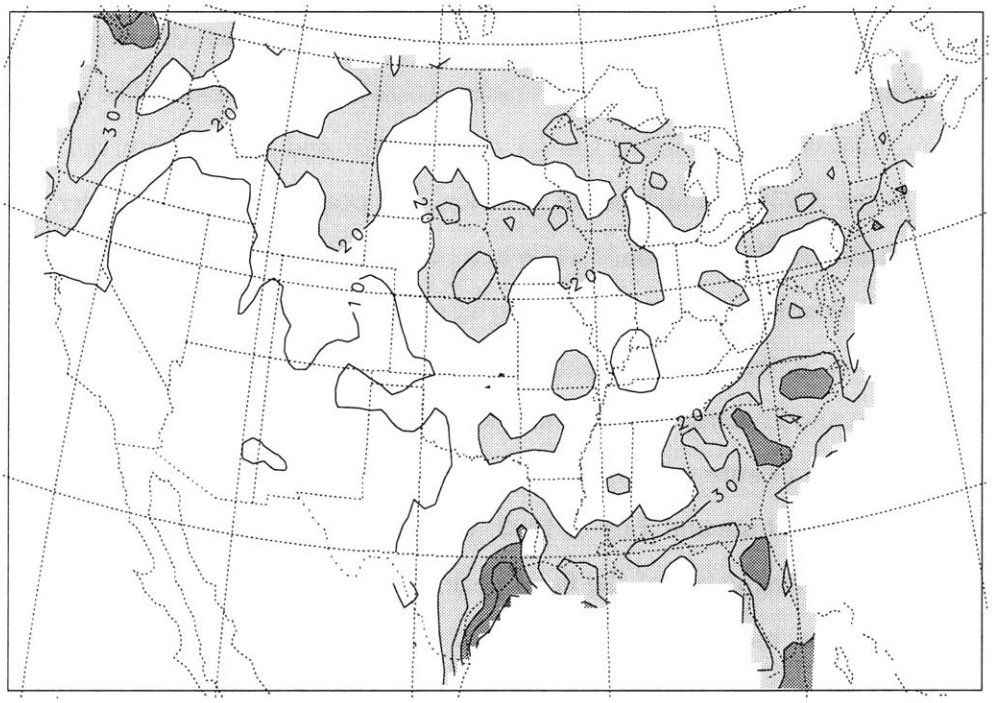

Figure 4-20: 1988 May and June simulated United States precipitation (mm/day). Contour interval is specified at 1 (mm/day), and shading occurs at values above 2 mm/day and at intervals of 2 mm/day. (a) AS74; (b) FC80.

(a) June and July 1993 AS74 Precipitation (mm/day)

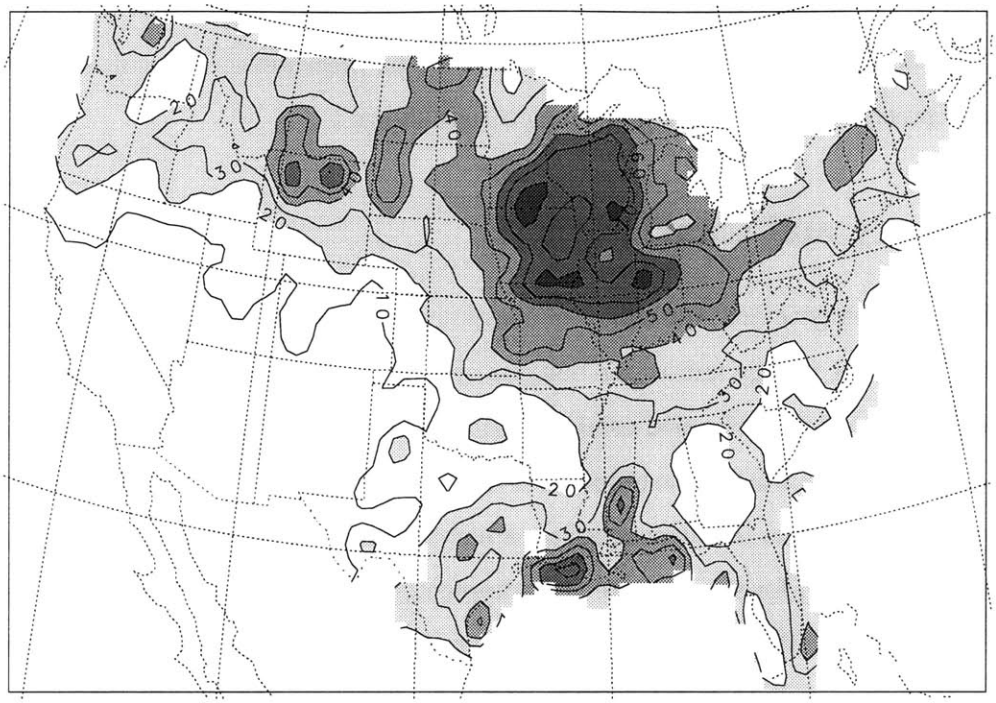

(b) June and July 1993 FC80 Precipitation (mm/day)

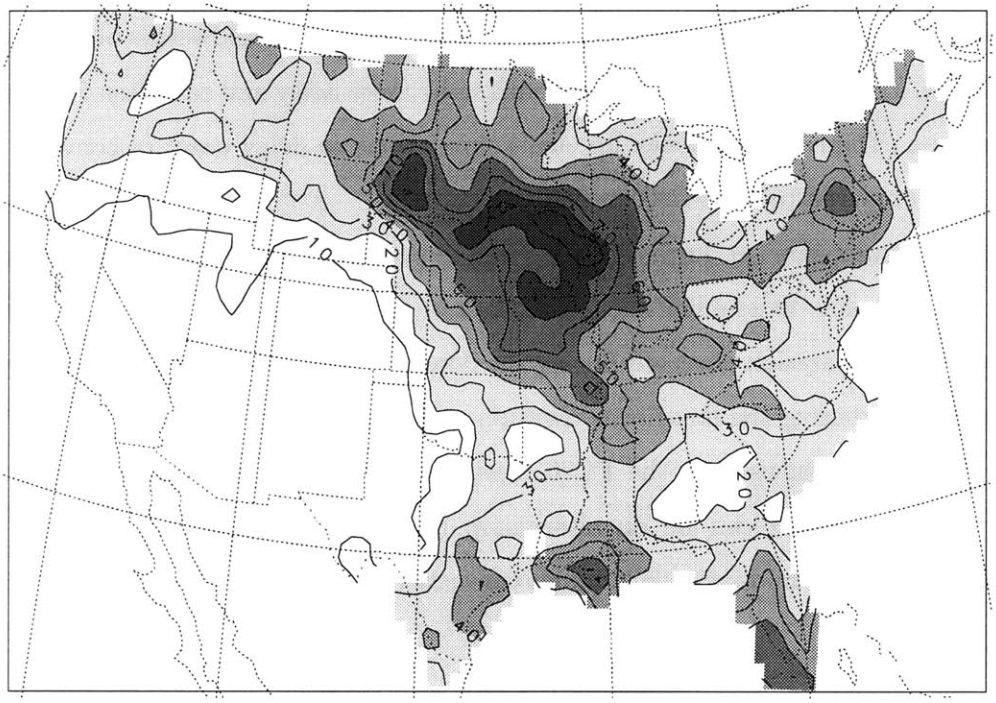

Figure 4-21: 1993 June and July simulated United States precipitation (mm/day). Contour interval is specified at 1 (mm/day), and shading occurs at values above 2 mm/day and at intervals of 2 mm/day. (a) AS74; (b) FC80.

Furthermore, the increase in soil moisture resulting from the increase in precipitation is also likely to have enhanced the precipitation in the FC80 simulations. Note that a set of FC80 simulations with a slightly different parameter set than the simulations presented here result in an even better distribution of precipitation over the flood region (not shown).

4.5 Summary and Conclusions

In this study, we investigate how the choice of convective closure assumption impacts simulation of atmosphere and surface energy and water budgets over North America using a modified version of RegCM. Each simulation is performed using the Grell scheme to represent convection. In one set of simulations, the quasi-equilibrium assumption is used as the dynamic control. In the other set, the dynamic control is related to the atmospheric stability. A series of six month (spring and summer) simulations are performed for six separate years implementing each convective closure assumption.

RegCM regardless of the convective closure assumption performs adequately in reproducing observations of various radiative and hydrologic fields. However, significant differences exist. In addition, some of the errors seen in the water budget are not consistent with the energy budget.

The explosive nature of convective storms in the Great Plains and Midwest is better described by the FC80 closure. However, the FC80 closure tends to be more noisy and can often form unobserved grid point storms. There is a tendency for AS74 simulations to delay onset of convection causing downwind shift compared to the FC80 predictions.

Both closure assumptions perform relatively well in predicting the drought of 1988 and flood of 1993. They are both able to simulate the overall lack of precipitation observed during the drought and the excessive precipitation observed during the flood. The FC80 simulations, however, perform slightly better in predicting the flood peak location and magnitude.

Overall, this study shows that the FC80 closure assumption implemented within the Grell convective parameterization can be an alternative to the more commonly used AS74 closure especially when modeling mid-latitude summer convection.

Part II

Soil Moisture-Rainfall Feedback Processes

In this part of the study, the modified NCAR RegCM described in Part I is used to investigate the role that soil moisture plays in the predictability of spring and summer precipitation over North America, in particular the Great Plains and Midwest. Chapter 5 explores the soil moisture-atmosphere interactions on a local scale where a series of small domain experiments are performed. Chapter 6 describes the impact of how the large-scale distribution of soil moisture impacts future precipitation by performing a series of large domain experiments.

Chapter 5

Local Soil Moisture-Rainfall Interactions

This chapter investigates the local impacts of soil moisture on the climate system over the United States Midwest. We first consider the the theory of the local soil moisture-rainfall feedback mechanism (Section 5.2). We then test the theory by performing a series of numerical experiments over the eastern two thirds of the United States using the modified RegCM introduced in Part I. The domain size is relatively small so that the local impact of the soil moisture-rainfall feedback can be isolated from changes in the large-scale circulation.

The following questions are addressed in this chapter: Are the persistent patterns in extreme hydrologic events such as the drought of 1988 and flood of 1993 maintained by external forcings or are they maintained by internal mechanisms involving the soil moisture-rainfall feedback? What role does the magnitude and direction of the prior soil moisture anomaly play in the soil moisture-rainfall feedback? How does the timing of this anomaly impact the strength of the feedback? And what are the pathways responsible for it? An extensive series of numerical experiments are performed to investigate these issues. Section 5.1 introduces this chapter. Section 5.2 provides background on the theory of the soil moisture-rainfall feedback. Section 5.3 gives a description the experiments performed. The results and conclusions of the numerical experiments are described in Section 5.4 and Section 5.5, respectively.

5.1 Introduction

The soil moisture-rainfall feedback depends on a variety of factors. These factors include the time of year, local soil moisture conditions, remote soil moisture conditions, vegetation characteristics, direction of the soil moisture anomaly, remote forcings, etc. In this chapter, we attempt to address the impact that local soil moisture conditions over the Midwest have on the local climate.

Over the Midwest, summer soil moisture anomalies are generally initiated by remote springtime large-scale circulation anomalies. For example, Trenberth and Guillemot (1996) conclude that the 1988 drought and 1993 flood were initiated by storm track shifts generated by the anomalous SSTs in the El Niño region (see Chapter 1). In this study, we investigate the soil moisture-rainfall feedback, given the existing large-scale circulation anomaly. By using a small domain, we are able to constrain the large-scale circulation anomaly. Thus, changes in soil moisture are unable to generate significant changes to the large-scale circulation. Therefore, we are able to isolate the impacts of soil moisture in local sense. The impacts of soil moisture anomalies on the large-scale circulation are investigated in Chapter 6.

A study by Eltahir (1998) describes the physical mechanisms and processes resulting in the positive feedback between initial soil moisture and future rainfall. He suggests that anomalously high soil moisture conditions yield an increase in moist static energy per unit mass of boundary layer air and hence more rainfall in convective regimes. The mechanisms responsible for the feedback are directly linked to the surface energy budget and will be discussed in further detail in Section 5.2. Zheng and Eltahir (1998) confirm these hypotheses using a two-dimensional model over West Africa. In this study, we further investigate the soil moisture-rainfall feedback mechanism by examining how late-spring and summer soil moisture anomalies affect subsequent rainfall using a three-dimensional regional climate model over the Midwestern United States. The hypotheses of Eltahir (1998) are tested using the Drought of 1988 and Flood of 1993 as examples.

The persistence of a flood or drought event can often depend on the direction of the soil moisture anomaly. For example, Brubaker and Entekhabi (1996) find using a conceptual land-atmosphere model that rainfall is more responsive to negative soil moisture perturbations than positive. Longer recovery times are found for dry anomalies due to evaporation falling in the soil control regime. In this chapter, we investigate how the direction of the soil moisture anomaly impacts the persistence of the soil moisture-rainfall feedback.

Observations of soil moisture are extremely limited both on the spatial and temporal scale. As

a result, conclusions regarding the initiation and persistence of flood and drought are difficult to make using observations alone. Recently, however, using observed soil moisture and rainfall data over the state of Illinois, Findell and Eltahir (1997) found that the feedback between soil moisture and future rainfall is a function of the time of year. More specifically, they found that soil moisture and subsequent rainfall in the following three weeks to show a significant correlation in the summer and little or no correlation for the rest of the year. This summertime correlation is stronger than the serial correlation of rainfall, indicating that there is a positive feedback between soil moisture and rainfall over the state of Illinois during summer months. A study by Huang et al. (1996) somewhat contradicts the results of Findell and Eltahir (1997). They show using a soil moisture product simulated from United States meteorological station observations of precipitation and temperature that evaporation anomalies are smaller in magnitude than those for precipitation. In addition, they find that evaporation displays a strong correlation to soil moisture. Thus, they argue that anomalous evaporation resulting from anomalous soil moisture conditions has little impact on future precipitation. They further indicate that soil moisture is a better predictor of summer temperature than precipitation. One aspect of this study is to investigate how future precipitation responds to initial soil moisture using a numerical model. Another aspect of this study is to investigate how the timing of the soil moisture anomaly impacts the strength of flood and drought conditions.

Many numerical modeling studies, with a few exceptions, conclude that a positive feedback exists between soil moisture and rainfall (e.g. Atlas et al. (1993), Beljaars et al. (1996), Mintz (1984), Oglesby (1991), Rind (1982), Rowntree and Bolton (1983), and Yeh et al. (1984)). In general, these studies indicate that rainfall in the United States and other regions is sensitive to soil moisture conditions during months with pronounced convective activity, such as summers in mid-latitudes. Most of these studies, however, prescribe unrealistic scenarios for soil moisture. In many instances, evapotranspiration is considered to be a surrogate for soil moisture and is maintained with no dynamic feedback at values close to zero for the dry simulations and close to the potential evaporation for the wet runs. In less extreme cases, soil moisture is prescribed uniformly both vertically and horizontally at the wilting point ($\sim$30% or less of soil saturation) for the dry runs and at the field capacity ($\sim$90% of soil saturation) for the wet runs where two-way interaction is allowed.

Figure 5-1 presents the ISWS soil saturation profiles averaged over June, July and August for Illinois. Although there are extreme interannual variations at or near the surface soil layer, the lower layers (below $\sim$1m) display considerably less variability. Thus, over Illinois and surrounding

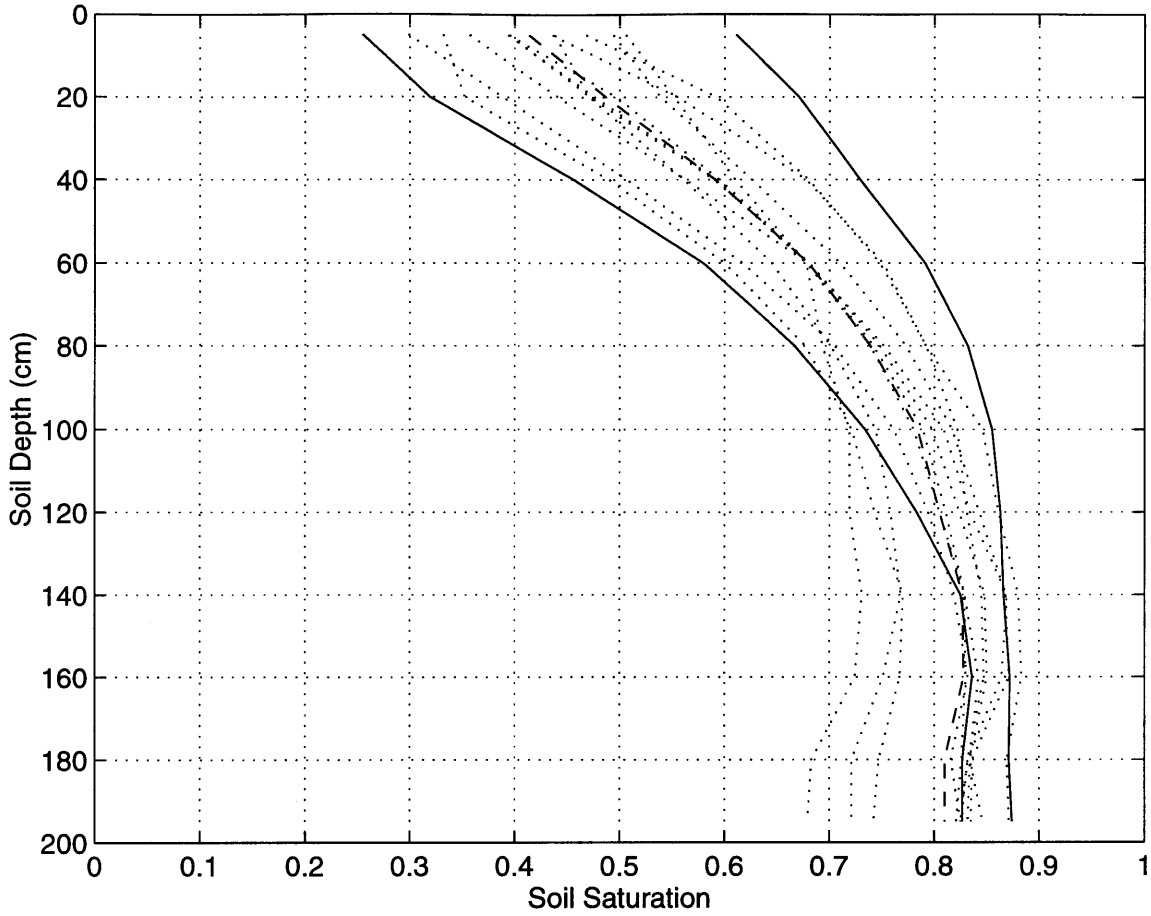

Figure 5-1: Illinois State Water Survey soil saturation profile averaged over June, July, and August. The solid line on the left is the profile for 1988; the solid line on the right is for 1993; the dotted lines are the rest of the years; and the dashed line is the average of all of the years.

regions, it may be unreasonable to initialize soil moisture below the surface layer at values much less than 70%. Similarly, in arid regions, it is probably unreasonable to initialize soil moisture below the surface layer at values greater than 40% or so. Conceivably more realistic anomalies in soil moisture have a relatively minor impact on rainfall. In this study, we investigate how the magnitude of the soil moisture anomaly affects the soil moisture-rainfall feedback. In doing so, we utilize a soil moisture dataset that combines information from the ISWS data and the pseudo-observed soil moisture dataset of Huang et al. (1996). In addition, this study differs from most of the above studies in that we focus on the mechanisms and pathways of the soil moisture-rainfall feedback.

5.2 Theory of the Soil Moisture-Rainfall Feedback Mechanism

Soil moisture plays an important role in the climate system. In the scope of this study, soil moisture is defined as water that is available for evapotranspiration from bare soil and vegetated areas. It provides a long-term memory mechanism for the rainfall that occurs throughout the year. The soil moisture storage is depleted during warmer portions of the year when evapotranspiration tends to exceed rainfall (typically Spring and Summer) and replenished during the colder portions of the year (Autumn and Winter). The evapotranspiration from the land surface is used to moisten and cool the planetary boundary layer (PBL). The amount of moistening and cooling that occurs affects the energetics of the PBL.

Classically, researchers have focused on the soil moisture-rainfall feedback as a water recycling process, neglecting the radiative processes. Recently, however, Betts and Ball (1994), Entekhabi et al. (1996), Eltahir (1998), and Schär et al. (1999) have suggested that soil moisture not only impacts the water budget of the surface and the PBL, but it also impacts the energy budget. This section describes the mechanisms and pathways through which soil moisture impacts the near surface variables that affect boundary layer processes and rainfall based on Eltahir (1998). Figure 5-2 provides a schematic diagram of these processes.

5.2.1 Radiative Feedbacks

Anomalously wet soils are often associated with greener denser vegetation and darker soils. Both greener denser vegetation and darker soils yield a lower surface albedo. A lower surface albedo implies that more of the incoming solar radiation is absorbed at the surface. In other words, neglecting any cloudiness feedback, more incoming solar radiation (on average) is likely to be absorbed by the surface during periods of anomalously wet soils than during periods of anomalously dry soils. It is important to note that any feedback that results in an increase in cloudiness with increasing soil moisture tends to balance or in some cases outweigh the surface albedo effect, as will be discussed later.

Anomalously high soil moisture also tends to lower the Bowen ratio (ratio of sensible heat flux to latent heat flux) by increasing the surface latent heat flux and decreasing the surface sensible heat flux. The increase in latent heat flux moistens the lower atmosphere and hence, increases downward longwave radiation due to the greenhouse effect of atmospheric water vapor. The same process cools the surface and hence, reduces the outgoing surface longwave radiation due to the

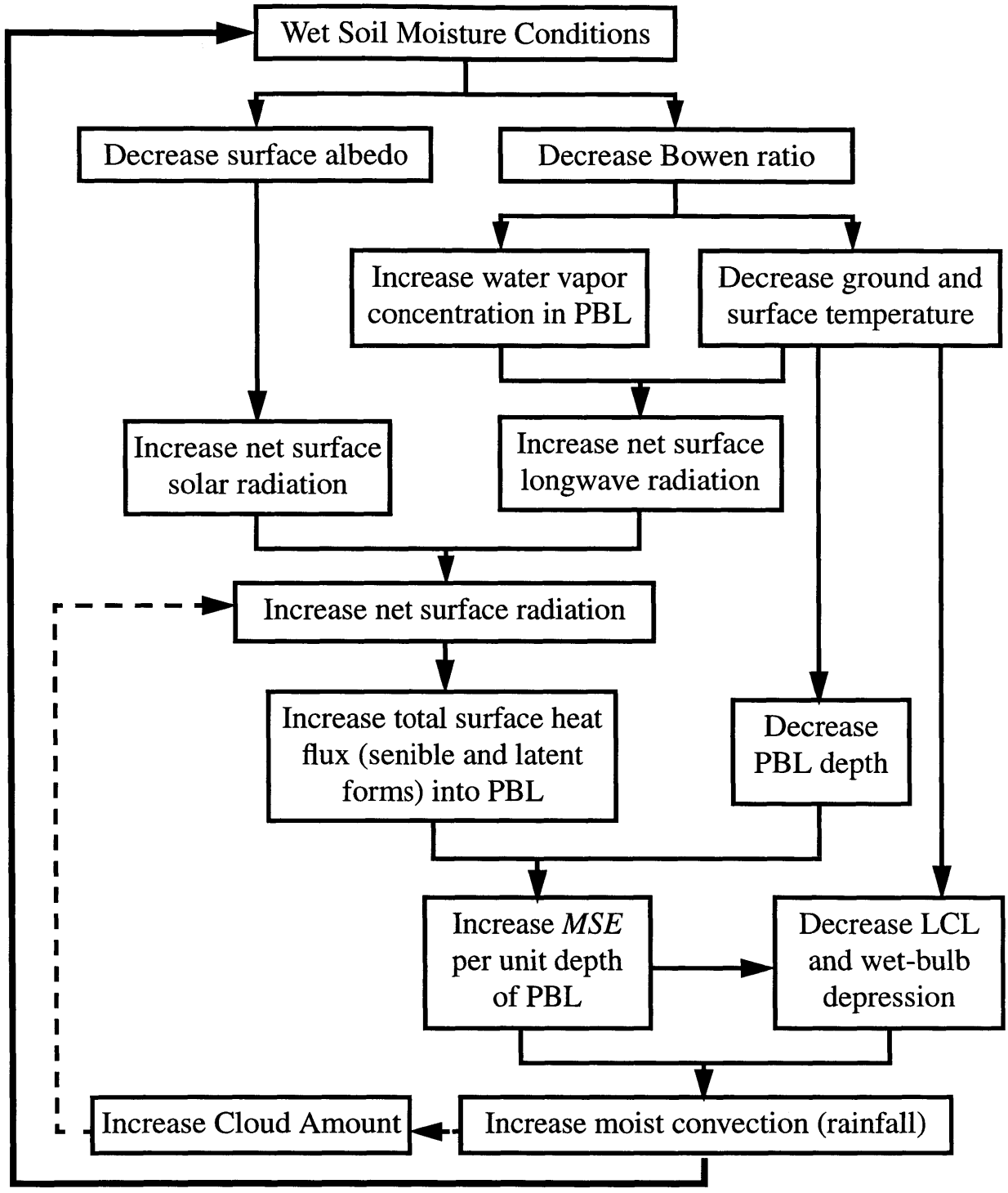

Figure 5-2: Diagram relating the pathways through which anomalously wet soil moisture conditions lead to subsequent rainfall.

Stefan-Boltzmann Law. Overall, the decrease in the Bowen ratio with increasing soil moisture results in an increase in net longwave radiation at the surface.

As mentioned above, the cloud feedback may play an important role in the response of the surface radiation budget to changes in soil moisture. If more clouds result due to an increase in soil moisture, more of the outgoing longwave radiation is re-emitted towards the surface. This further increases the net surface longwave radiation and tends to balance a significant portion of the reduction in incoming surface solar radiation resulting from the increase in clouds. The strength of the cloud feedback is an important factor in determining the strength of the response of net surface radiation to changes in soil moisture.

In summary, anomalously wet soils tend to increase both the net surface solar radiation (via the albedo feedback) and the net surface longwave radiation (via the Bowen ratio feedback). This yields an increase in net all-wave radiation. The sensitivity of clouds to changes in soil moisture may alter this response.

5.2.2 Boundary Layer and Moist Static Energy Feedbacks

The above subsection suggests that anomalously wet soils are associated with an increase in net surface radiation. Net surface radiation is balanced by the sum of the latent, sensible, and soil heat fluxes. On the long time-scale, the soil heat flux can be considered negligible. Thus, the net radiation (or total surface heat flux) is equivalent to total fluxes of latent and sensible heat.

The total energy of the PBL can be described by the moist static energy (MSE). ($MSE = gZ + C_pT + LQ$, where g is the acceleration due to gravity, Z is elevation, C_p is the specific heat capacity at constant pressure, T is temperature, L is the latent heat of vaporization, and Q is the water vapor mixing ratio.) At large spatial scales (i.e. neglecting advection), the MSE of the PBL is supplied by the total flux of heat from the surface and depleted by the entrainment of low MSE air existing above the PBL, radiative cooling, and negative heat fluxes associated with convective downdrafts. Thus, with all else being equal, anomalously wet soil moisture conditions tend to increase the MSE of the PBL via an increase in total heat flux supplied from the surface.

Soil moisture also has a pronounced impact on the depth the PBL. As implied above, drier soils are associated with higher fluxes of sensible heat. A high sensible heat flux is associated with greater turbulent energy. This tends to increase turbulent mixing which increases the PBL growth rate and hence the depth of the PBL. Thus, even neglecting the increase in MSE supplied by the surface, anomalously wet soil moisture conditions tend to result in an increase in the MSE per unit

depth (mass) of PBL.

MSE within the PBL tends to be well mixed (height invariant). However, above the PBL in the troposphere, the vertical distribution of MSE tends to decrease with elevation. As the PBL grows, low MSE air from above the PBL is entrained. This tends to lower the overall MSE of the PBL (Betts and Ball 1994). In addition, as the PBL grows in height, it entrains air of increasingly lower MSE from above (since the MSE above the PBL decreases with elevation). This results in an enhanced reduction of the MSE of the PBL. It is suggested in the above paragraph that anomalously wet soils result in a decrease in the growth rate of the PBL. This tends to reduce the amount of low MSE air entrained from above PBL and hence increase the overall MSE of the PBL.

In summary, changes in soil moisture conditions contribute to the overall MSE of the PBL in three ways: (1) surface fluxes from below the PBL; (2) PBL depth; and (3) entrainment from above the PBL. Anomalously wet soils tend to increase the flux of high MSE air into the PBL from below, reduce the PBL height increasing the MSE per unit mass of air, and reduce the amount of entrained air of low MSE from above the PBL. Each of these effects are additive and contribute to a relative increase of MSE per unit mass of air in the PBL.

5.2.3 Moist Static Energy and Moist Convection

As stated above, soil moisture plays an important role in determining the total MSE in the PBL. The impacts of soil moisture above the PBL are relatively minor. This implies that the changes in soil moisture alter the stability profile of the atmosphere. Since an increase in soil moisture tends to increase the overall MSE of the PBL and has little impact on the MSE above the PBL, the MSE vertical profile tends towards instability. As a result, moist convection occurs to redistribute the MSE towards neutral conditions. Furthermore, the increase in PBL MSE should result in an increase in the convective available potential energy (CAPE) (Williams and Renno 1993). CAPE can be directly related to storm size. Thus, anomalously wet soil moisture conditions tend to increase the frequency (via an increase in instability) and magnitude (via an increase in CAPE) of convective rainfall events. A recent study by Eltahir and Pal (1996) confirms these ideas using data from the Amazon Forest. They indicate that an increase in wet-bulb temperature (a quantity proportional to MSE) increases the convective instability and hence, the frequency and magnitude of rainfall events in the tropics and the summer hemisphere.

Soil moisture is also likely to have an impact on the cloud base. Since soil moisture exhibits a positive relationship with low-level water vapor and a negative relationship with low-level

temperature, the wet-bulb depression (dry bulb temperature minus wet-bulb temperature) should display a higher sensitivity to soil moisture than water vapor and temperature taken separately (Findell and Eltahir 1999). Wet-bulb depression is related to the lifting condensation level which is an approximate measure of the cloud base. An increase in soil moisture tends to result in a decrease in the height of the cloud base via a decrease in wet-bulb depression. On average, this should increase the likelihood of occurrence of convective rainfall. In addition, a lower cloud base should result in a deeper cloud (assuming the cloud top height remains constant). This should result in an increase in the magnitude of convective rainfall events.

In summary, two additive factors contribute to soil moisture's impact on the frequency and magnitude of convective rainfall events: (1) MSE of the PBL and (2) cloud base height. Soil moisture exhibits a positive relationship with PBL MSE and a negative relationship with the cloud base height. The response of both these effects on the occurrence and size of convective rainfall events operates in the same direction. If the arguments presented in this section hold true, anomalously wet soil moisture conditions should lead to an increase in the frequency and volume of convective rainfall. This increase in rainfall wets the soil and therefore, results in a positive feedback between soil moisture and rainfall.

5.3 Description of Numerical Experiments

The purpose of this study is to investigate the pathways and mechanisms through which initial soil moisture conditions impact subsequent rainfall. A series of numerical experiments using the modified version of the NCAR RegCM presented in Part I are performed to investigate the impact of soil moisture on the energy and water balances of the PBL over the Midwest using the drought of 1988 and flood of 1993 as representative events. This section provides a description of these experiments.

The model domain is centered around the state of Illinois at 40.5°N and 90°W and projected on a Lambert conformal grid. The domain size is 2050-km X 2500-km with horizontal grid point spacing of 50 km. At this resolution, the main topographic features of the domain are captured. The model domain and topography are shown in Figure 5-3. This region captures the primary area of drought of 1988 and flood of 1993 (see Figures 1-1 and 1-2, respectively). The western boundary lies along the eastern slopes of the Rocky mountains. The boundaries were not moved further west to avoid the impacts of complex topography and lack of adequate data in mountainous regions to

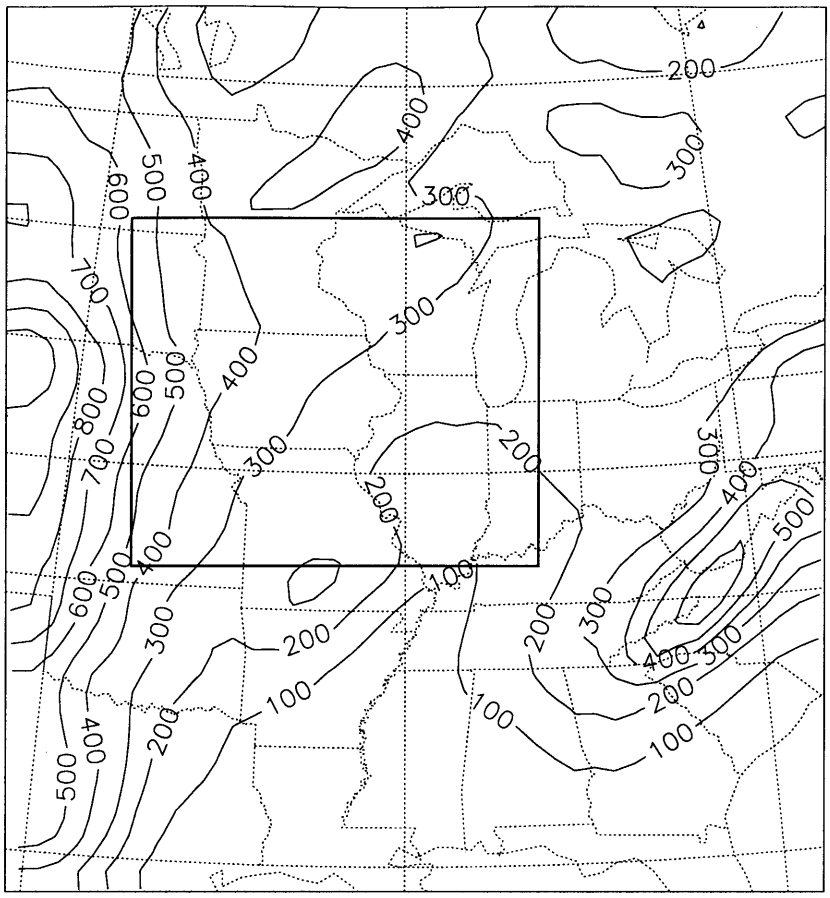

Figure 5-3: Map of the domain and terrain heights (m) used for the numerical simulations. The outlined box is the region over which the averages are taken and corresponds to the areas where the drought of 1988 and flood of 1993 were most severe. The contour interval is 100 m.

force the model. As a result, the western boundary lies close to the drought and flood regions. There are 14 vertical sigma levels with highest concentration of levels near the surface (0.02, 0.07, 0.135, 0.21, 0.3, 0.405, 0.51, 0.615, 0.72, 0.815, 0.895, 0.95, 0.98, and 0.995). The model top is at 50 mb. Lastly, the Anthes-Kuo scheme is used to represent convection.

The vegetation is characterized using the Global Land Cover Characterization (GLCC) data (Loveland et al. 1999). The predominant vegetation type of the domain is crops which are characterized by a shallow root zone depth (1.0 m). Hence, the majority of the water for evapotranspiration is extracted from the upper portions of the soil which is consistent with Figure 5-1 in that there is little variability in the soil column below 1 m. During the peak growing season (Summer), crops achieve a relatively high maximum fractional vegetation coverage (85%) and leaf area index (6) and a relatively low minimum stomatal resistance (40 s/m). All of these

parameters suggest that crops transpire more than the remaining vegetation types. The other dominant vegetation types within the model domain are: short and tall grass, disturbed forest, evergreen needleleaf trees and deciduous broadleaf trees, and mixed woodland. The soil texture class is prescribed according to the vegetation characterization. The primary soil texture over the domain is comparable to a loam soil. The values for porosity, wilting point, and saturated hydraulic conductivity associated with this texture class are 48%, 33%, and $6.3\text{x}10^{-3}$ mm/s, respectively. Although the soil properties vary in the horizontal, they do not vary in the vertical.

To develop an understanding of the physical mechanisms involved in the soil moisture-rainfall feedback, a series of numerical experiments for several different months are performed each of which differ in the initial soil saturation. Month long simulations are performed for May, June, July, August, and September of 1988 and 1993. The control runs for each month and year are initialized using the merged HDG/ISWS dataset described in Subsection 2.2.1. In addition, a set of integrations are performed with the soil moisture initialized uniformly in the vertical and horizontal at values of 10%, 25%, 50%, 75%, and 90% of saturation. In total, there are 6 different soil moisture initializations for each month and year. Table 5.1 provides a description of the experiments performed in this study.

Table 5.1: Description of each simulation performed in this study.

Simulation Months:
• May, June, July, August, and September 1988
• May, June, July, August, and September 1993
Simulation Duration: 1 month
Soil saturation (initialized on the 1st of each month):
• Observed HDG/ISWS.
• 10% uniformly over entire domain and depth
• 25% uniformly over entire domain and depth
• 50% uniformly over entire domain and depth
• 75% uniformly over entire domain and depth
• 90% uniformly over entire domain and depth

5.4 Results

This section describes the results of the simulations performed in this chapter. In the first subsection, we briefly compare the modeled rainfall to the observations, and in the second

subsection, we investigate the sensitivity of the model to initial soil moisture.

5.4.1 Brief Model Comparison to Precipitation Observations

This subsection compares the control simulations to the United States Historical Climatology Network (USHCN) data [Karl et al. (1990); see Subsection 2.2.2].

Figure 5-4 compares the observed gridded USHCN rainfall averaged over June and July for both 1988 and 1993 to the model simulated rainfall for the same months. June and July of 1988 and 1993 are selected for comparison because they represent the severest months of the drought and flood. When making the comparisons, it should be noted that USHCN observations do not exist over Canada.

For June and July of 1988, the model performs well in capturing the lack of observed rainfall in the northern portion of the domain. In addition, the model captures the general region of rainfall greater than 2 mm/day in the southern portion of the domain. There are, however, small isolated regions of rainfall in excess of the observations. Furthermore, there is a considerable underestimation of precipitation along the southern and southwestern boundaries. It is believed that this is a result of the proximity of the boundaries to these regions. In addition, it is likely that the suppression of rainfall at the southern boundary may have resulted in the unobserved isolated rainfall peaks which formed downwind.

For June and July of 1993, the model performs well in reproducing the anomalously high rainfall in the upper Midwest. However, the model underestimates the overall magnitude of the flood peak by approximately 2 mm/day. In addition, the location of the peak is simulated too far to the north and east of the observed peak. This shift may be a consequence of the proximity of the flood peak to the western boundary. Similar to the 1988 simulations, the model does not perform well in reproducing the observed rainfall distribution in the southern boundary of the domain. Again, this may be due to the location of the boundaries.

In summary, the model performs well in reproducing the drought and flood events over the upper Midwest observed in 1988 and 1993, respectively. Some deficiencies do exist in simulating the precise location and overall magnitude of the flood peak in 1993. Although only June and July of 1988 and 1993 are compared to observations, the model exhibits a similar performance in the other months simulated. Of significant note, the model can clearly distinguish between the two extreme years. This is important because it indicates that the model is able to capture the interannual variability. With this in mind, it is reasonable to proceed with the sensitivity experiments.

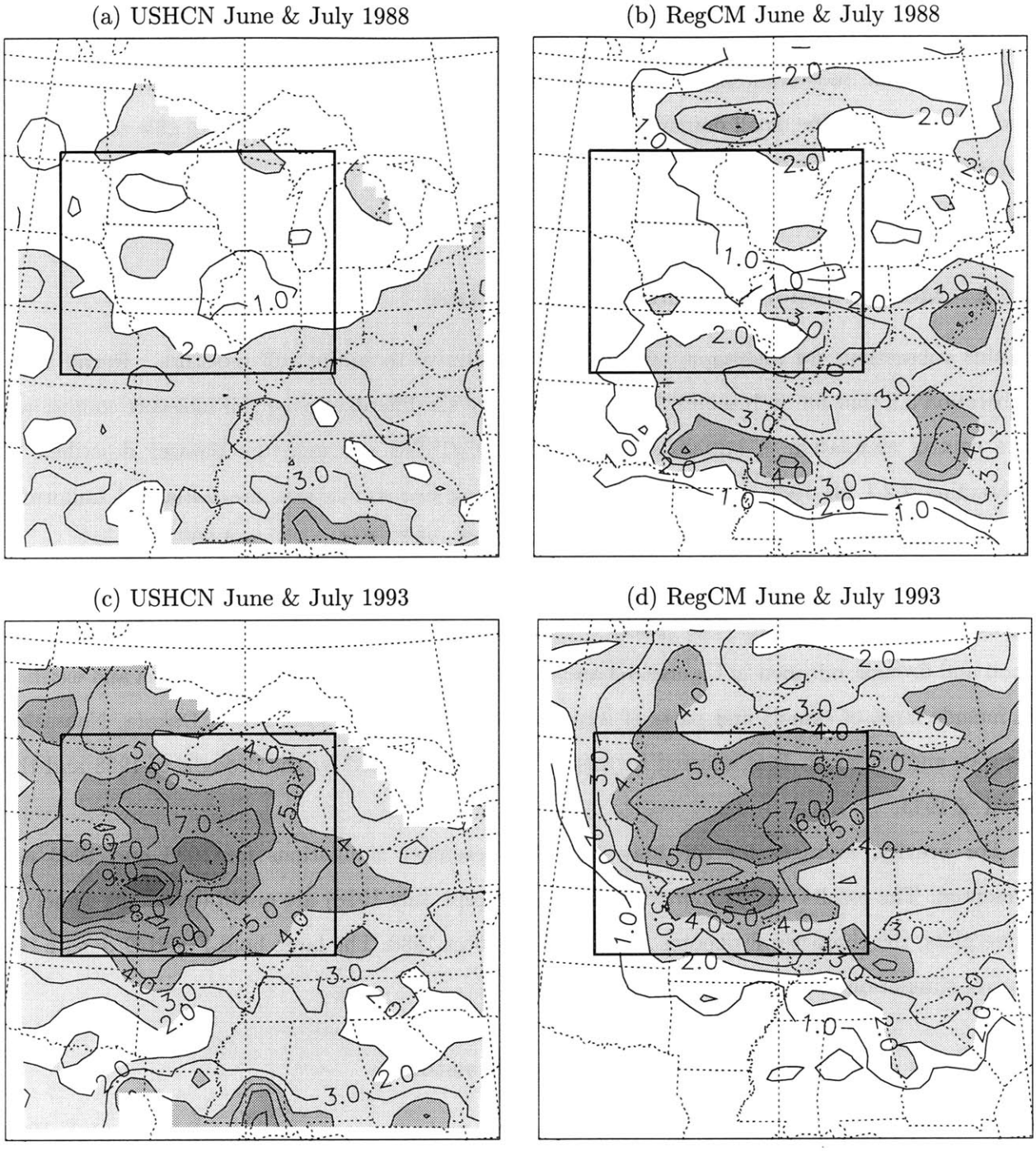

Figure 5-4: USHCN observed and RegCM simulated rainfall averaged over June and July of 1988 and 1993: (a) USHCN June and July 1988; (b) RegCM June and July 1988; (c) USHCN June and July 1993; (d) RegCM June and July 1993. The outlined box is the region over which the averages are taken and corresponds to the areas where the drought of 1988 and flood of 1993 were most severe. The units are in mm/day, the contour interval is 1 mm/day, and the shading interval is 2 mm/day.

On a final note, Seth and Giorgi (1998) found that the strength of the soil moisture-rainfall feedback can be dependent on the location of the domain boundaries. The point of this study is to develop an understanding of the key processes and mechanisms in the soil moisture-rainfall feedback. By using the small domain, in addition to computation savings, we are able to constrain the spatial location of the drought and flood in their respective years. This allows us to better identify the key mechanisms and processes the responsible for the soil moisture-rainfall feedback.

5.4.2 Model Response to Initial Soil Moisture

In this subsection, we investigate the model's sensitivity to initial soil moisture. Recall from Subsection 5.3 that for each month and year, there are six different initial soil moisture conditions. The control simulation is initialized using the HDG/ISWS soil moisture dataset described in Subsection 2.2.1 for 1988 and 1993 and the remaining five simulations are initialized uniformly in the horizontal and vertical at soil saturations of 10%, 25%, 50%, 75%, and 90%.

The comparisons are made using monthly and spatial averages of a set of hydrologic fields against initial soil moisture. The spatial average is made over the region severely affected by the flood and drought outlined in Figures 5-3 and 5-4. This region is centered around Iowa and extends to include most of Illinois and parts of Indiana, Wisconsin, Minnesota, South Dakota, Nebraska, Kansas, and Missouri. It is selected because it was most affected by the drought of 1988 and the flood of 1993.

For brevity, averages for the May through September simulations for 1988 and 1993 are presented. The results for the individual months (except July 1988) are qualitatively the same. In these plots, the character F denotes 1993 and D denotes 1988; The large bold F and D denote the control simulation for their respective years.

Sensitivity of Future Rainfall to Initial Soil Moisture

Figure 5-5 depicts a summary of the total, convective, and non-convective rainfall for the July 1988 and 1993 simulations as a function of initial soil moisture. On the whole, a considerable sensitivity of total rainfall to changes in initial soil moisture is displayed in both years; There is a 50% to 60% increase when increasing soil saturation from the low to high extremes [10% to 90% of saturation; Figure 5-5a]. This sensitivity is primarily a result of an increase in convective rainfall where there is nearly a 250% increase between the extremes in soil moisture (Figure 5-5b); Non-convective rainfall tends to remain virtually constant with soil moisture for both years (Figure 5-5c). It should be noted

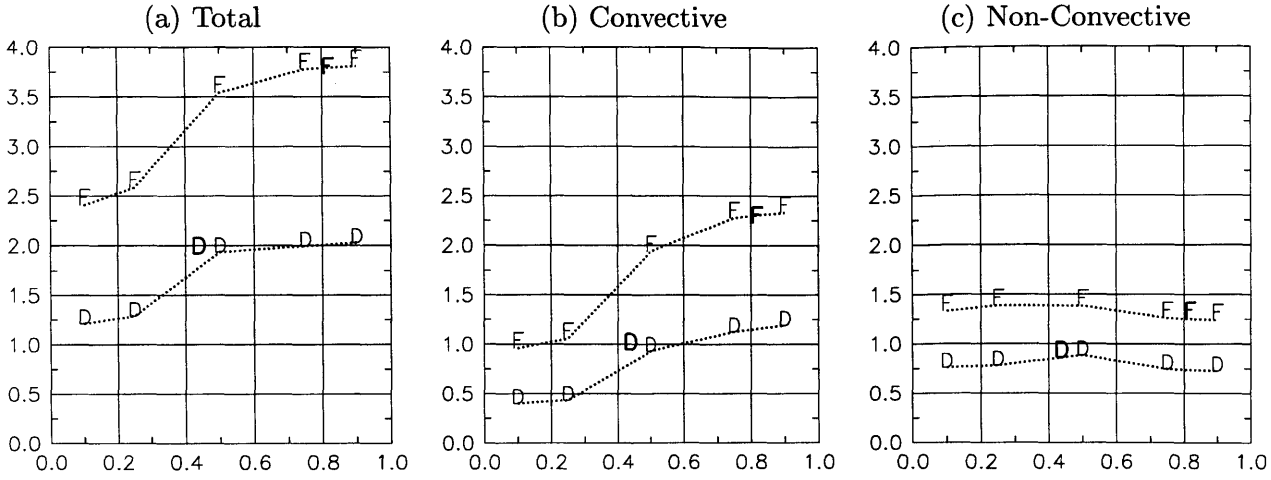

Figure 5-5: Simulated monthly rainfall (mm/day) for the 1988 and 1993 simulations as a function of initial soil saturation: (a) total rainfall; (b) convective rainfall; and (c) non-convective rainfall. Each data point represents the average of the May, June, July, August, and September simulations over the Midwest region outlined in Figure 5-3 given the initial soil moisture. The D denotes the drought year (1988) and the F denotes flood year (1993). The boldface D and F denote the control simulations for each year

that Pan et al. (1996) and Pal and Eltahir (1997) suggest that the choice of cumulus convective parameterization can impact the strength of the soil moisture-rainfall feedback.

The response of future rainfall to initial soil moisture is non-linear. Figure 5-6 is a plot of the relative sensitivity of total rainfall to initial soil saturation expressed as the percent change in rainfall per percent change in soil moisture. Each individual bar is computed from two simulations. For example, the July of 1988 bar in the 25% to 50% soil saturation range is computed using the 25% and 50% soil saturation simulations. In nearly every case, rainfall in the 25% to 50% soil moisture range is most sensitive. The 50% to 75% range also exhibits considerable sensitivity (except July 1988), however, it is significantly weaker than the 25% to 50% range. The weakest sensitivities are displayed in the highest and lowest soil saturations. Note that the relative sensitivity of convective rainfall to initial soil saturation (not shown) is considerably larger than that of total rainfall since non-convective rainfall is unresponsive to changes in soil moisture (except for July 1988 in the 50% to 75% soil saturation range) [see Figure 5-5(c)]. The July 1988 simulations in the 50% to 75% soil saturation range behave differently than the rest of the simulations in that a significant negative feedback to soil saturation is displayed. In this particular case, this explained by the fact that non-convective rainfall significantly decreases when soil saturation is increased from 50% to 75% and convective rainfall remains virtual constant; thus the significant negative sensitivity displayed in Figures 5-6(a) and (c) in this range.

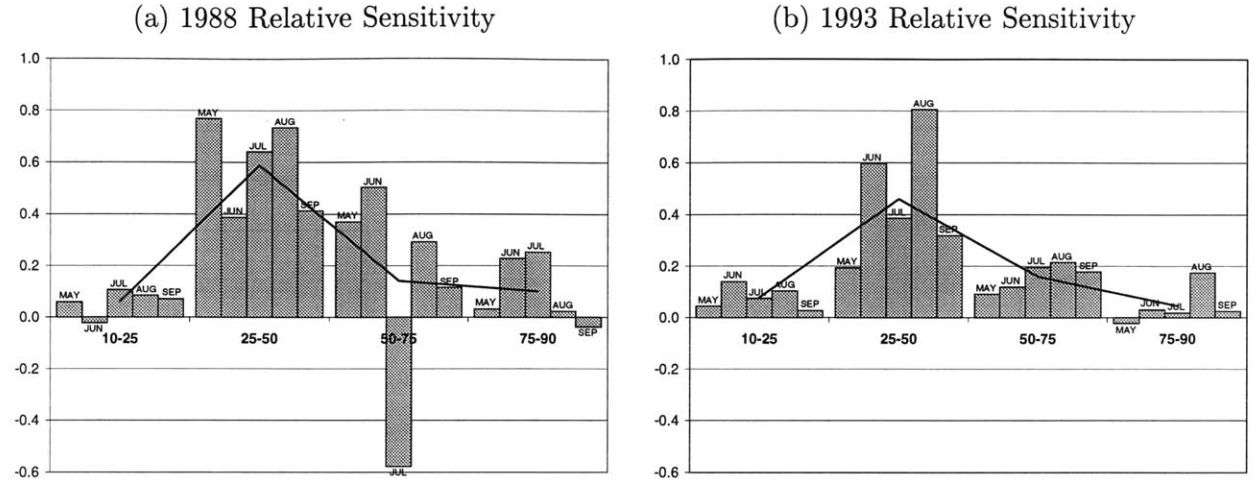

Figure 5-6: Plot of relative sensitivity versus soil saturation: (a) 1988; (b) 1993. Each bin on the x-axis represents a range of soil saturations; The end points of each bin are individual simulations where each bar within the bin represents a month. The values on the y-axis represent the percent change in rainfall per percent change in soil moisture. The solid line represents the average of all the months for the given year.

The low sensitivity of future rainfall to initial soil saturation in the 10% to 25% soil saturation range is due to transpiration ceasing when the soil saturation falls below its wilting point (approximately 33% of saturation in these simulations). In this regime, the response of rainfall to changes in soil moisture is largely due to changes in bare soil evaporation, some interception loss, and some transpiration from the upper soil layer when the wilting point is exceeded shortly after rainfall events (not shown). Little sensitivity of rainfall to soil moisture is also exhibited at the higher values of soil moisture (>75%). This is a result of the evapotranspiration reaching the potential evaporation rate when the soils are unlimiting (atmosphere controlled).

Summertime soil saturation values over Illinois typically range from 40% near the surface to 80% at depth (see Figures 1-3 and 5-1). With this in mind, it would be expected that the depth averaged (surface to 1 m) soil saturation values over the upper Midwest would lie around 60% during normal years. (One might expect this value to be slightly lower since more of the water for evapotranspiration is extracted near the surface.) The distinct asymmetry displayed in Figure 5-6 suggests that a perturbation (say 20%) to this value would lead to different responses depending on the direction of the perturbation. On one hand, a perturbation to drier conditions would place the soil saturation in the most sensitive (soil controlled) regime displayed in Figure 5-6. This would likely cause the rainfall to display significant response to the drier surface conditions. On the other hand, a perturbation to wetter conditions would result in a significant, but less dramatic response.

Table 5.2: Average Number of hourly rainfall events within specified intervals occurring between May 1 and September 30 or 1988 and 1993 for the 10%, 50%, and 90% soil saturation simulations. The number in parentheses indicates the percentage of total rainfall. The last row provides the totals over all the intervals with the number in parentheses indicating the total rainfall in mm. The values are computed over the upper Midwest region defined in Figure 5-3.

Interval		1988			1993	
(mm/day)	10%	50%	90%	10%	50%	90%
0.1-0.5	1185 (4.1)	1192 (2.7)	1127 (2.7)	1003 (1.9)	787 (1.3)	678 (1.1)
0.5-1.0	384 (5.8)	385 (3.7)	496 (4.5)	407 (3.3)	337 (1.9)	371 (2.0)
1.0-2.0	446 (13.6)	482 (9.3)	498 (9.0)	446 (7.0)	455 (5.3)	481 (5.2)
2.0-4.0	428 (24.8)	501 (19.4)	585 (21.7)	552 (17.4)	652 (14.6)	684 (14.3)
4.0-8.0	230 (25.9)	456 (34.1)	458 (32.7)	564 (35.2)	849 (37.7)	801 (33.9)
8.0-16.0	98 (21.4)	170 (23.5)	164 (21.6)	282 (32.2)	435 (34.8)	516 (38.4)
$\geq$16.0	10 (4.4)	28 (7.3)	31 (7.8)	16 (3.0)	32 (4.4)	37 (5.1)
Totals:	2781 (199)	3214 (313)	3359 (332)	3270 (382)	3547 (539)	3568 (577)

A similar assymetric response is also exhibited in Brubaker and Entekhabi (1996) using a conceptual land-atmosphere model. Overall, the results presented here and in Brubaker and Entekhabi (1996) indicate that rainfall over the Midwest is more responsive to negative soil moisture anomalies than positive. This also suggests in the context of these experiments that the soil moisture-rainfall feedback would tend to favor more persistent drought conditions in comparison to flood conditions.

Table 5.2 presents the number of rainfall events occurring between May 1 and October 1 of both 1988 and 1993 within the specified interval for the 10%, 50% and 90% soil saturation simulations over the upper Midwest region shown in Figures 5-3 and 5-4. The numbers in parentheses indicate the percentage of the total rainfall occurring within the indicated interval (except the bottom row). The bottom row provides the totals over all the intervals with the number in parentheses indicating the total volume of rainfall (in mm).

Moving from dry to wet conditions results in both an increase in the number of rainfall events and the total volume of rainfall (bottom row of Table 5.2); In 1988, there is a 21% increase in the number of events and a 67% increase in the volume, and in 1993 the increases are 9 % and 51%, respectively. The majority of the increased frequency and intensity occurs when increasing soil moisture from 10% to 50% of saturation. This is consistent with the above findings which favor a stronger soil moisture-rainfall feedback under dry conditions as opposed to wet.

In 1988, other than a small decrease in the 0.1 to 0.5 mm/day range, an increase in the number of rainfall events with increasing soil moisture occurs in all of the intervals. Furthermore, there

is tendency for the percentage of total rainfall to decrease in the lower intervals (< 4 mm/day) and to increase in the moderate and high intervals (> 4 mm/day). Hence, the majority of the increase in volume can be explained by an increase in the number of large events where most of the total rainfall occurs. The 1993 simulations display a somewhat different pattern than 1988 in that there is a significant decrease in the number of small rainfall events (< 1 mm/day). However, similar to 1988, there is a tendency for an increase in the number of rainfall events in the remaining intervals. Also somewhat similar to 1988, the percentage of rainfall occurring in the low to low-moderate rainfall intervals (< 4 mm/day) tends to decrease with increasing soil saturation and the percentage tends to increase in the higher intervals (> 8 mm/day) with little change in the moderate range. This shift in distribution of rainfall to larger events from increasing soil moisture results in the significant increase in overall rainfall.

Overall, increasing soil moisture over the upper Midwest tends to result in a moderate increase in the number of rainfall events and a substantial increase in the magnitude of the rainfall events. In both 1988 and 1993, there tends to be a decrease or little change in the number of small rainfall events and an increase in the number of moderate to large events when increasing soil saturation. The overall volume of rainfall increases because of a shift in the frequency distribution towards larger events much like what is shown in Eltahir and Pal (1996). There they suggest that an increase (decrease) in wet bulb temperature over the Amazon results an increase (decrease) in the frequency and magnitude of rainfall.

Model Response to the Timing of the Soil Moisture Anomaly

As mentioned in Section 5.1, Findell and Eltahir (1997) found, using the ISWS soil moisture data, that the feedback between soil moisture and subsequent rainfall is strongest in June and July and weakest in winter months. Hence, we should expect the June and July simulations to show a greater sensitivity to soil moisture than the May, August, and September simulations. Figure 5-7 displays the relative and absolute sensitivities of future rainfall to initial soil saturation as a function of month. The relative sensitivity is a measure of the relative impact of initial soil moisture on future rainfall. It expresses the percent change in rainfall per percent change in soil saturation. The absolute sensitivity is defined as the slope of the best fit line to the soil moisture-rainfall data shown in Figure 5-5(a) (not including the control integration). It is a measure of the change in rainfall between bone dry initial conditions and fully saturated.

The relative sensitivity of future rainfall to initial soil moisture [Figure 5-7(a)] varies from

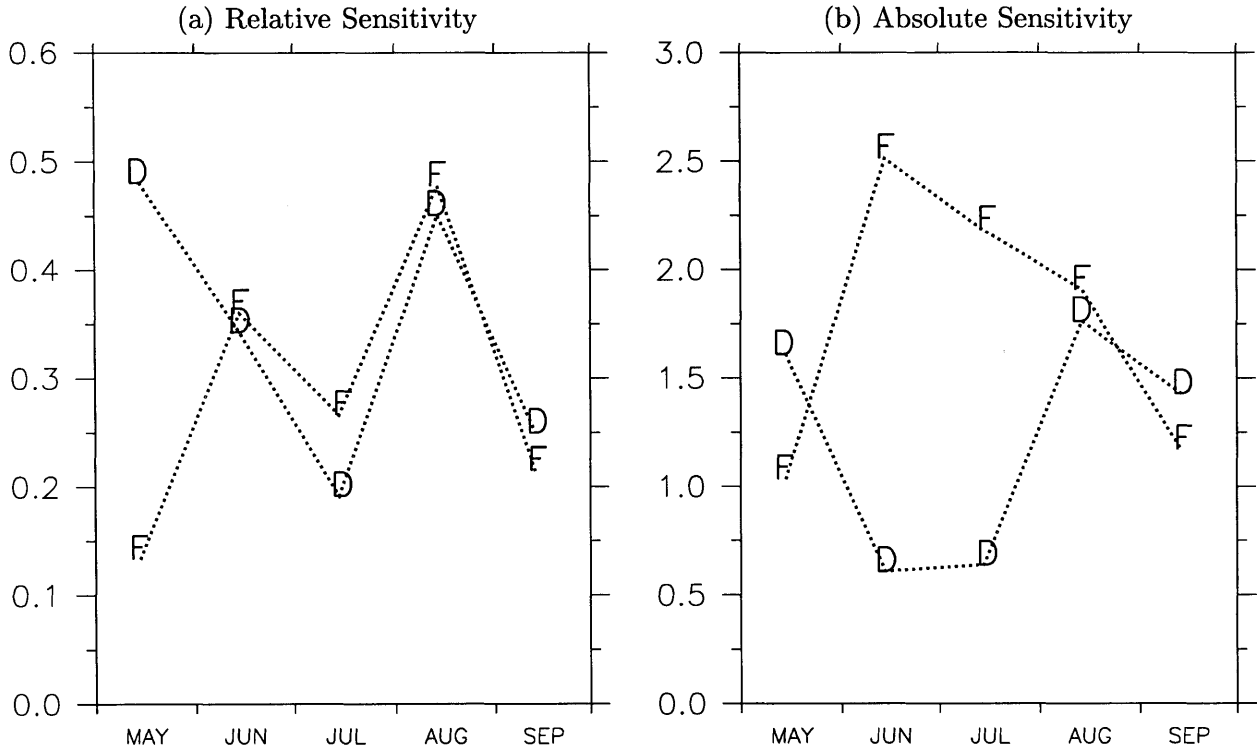

Figure 5-7: Relative and absolute sensitivities of rainfall to initial soil moisture. Relative sensitivity is a measure of the relative impact of initial soil moisture on future precipitation expressed as a percentage. Absolute sensitivity is defined as the slope of the best fit line of future precipitation to initial soil moisture for each simulation month. The D denotes the drought year (1988) and the F denotes flood year (1993).

approximately 0.1 to 0.5 percent change in rainfall per percent change in soil saturation. It does not show a clear pattern with the time of year. This suggests that the timing of the soil moisture anomaly had little impact on the relative change of rainfall during May, June, July, August, and September during 1988 and 1993.

The absolute sensitivities [Figure 5-7(b)] lie between 0.6 and 2.5 mm/day per unit change in soil saturation. On average, the absolute sensitivity is 1.2 mm/day for 1988 and 1.8 mm/day for 1993. The difference in rainfall between the control simulations for 1988 and 1993 is approximately 1.8 mm/day (see Figure 5-5). Although this difference is similar to the absolute sensitivity, it is unrealistic for soil moisture in the Midwest to vary from bone dry conditions to fully saturated. Thus, in the context of these simulations, soil moisture alone could not have caused the extremes observed in 1988 and 1993. However, Figure 5-6 indicates that the majority of the soil moisture-rainfall sensitivity is exhibited in the 25% to 75% soil saturation regime. Soil moisture over the Midwest typically falls within these bounds. This suggests that soil moisture played an important role in the persistence and maintenance of the extreme events.

Consistent with the findings of Findell and Eltahir (1997), the 1993 simulations exhibit the greatest soil moisture-rainfall sensitivity in absolute terms during June and July; The 1988 simulations do not exhibit this consistency. In terms of relative sensitivity, neither year displays an obvious pattern with the time of year. Note that the the summers of 1988 and 1993 are extreme years. The large-scale conditions may have had an enhanced importance in these events. Additional simulations of years with more normal rainfall conditions are likely to be required to gain a better sense of how the timing of the soil moisture anomaly impacts future rainfall.

Soil Moisture-Rainfall Pathways

This subsection focuses on the pathways through which soil moisture affects future rainfall described in Section 5.2 and Figure 5-2. Figures 5-5, 5-8, 5.4.2, and 5-10 summarize these results. Again, for brevity, only the averages of the May through September of 1988 and 1993 simulations will be investigated.

It is suggested in Section 5.2 that soil moisture is likely to have a pronounced impact on rainfall in convective regimes as opposed to non-convective regimes. Figure 5-5 indicates that convective rainfall for the control simulations tends to be greater than non-convective rainfall both in July of 1988 and 1993 (bold D and F, respectively). This implies that it is useful to investigate the processes described in Section 5.2.

In Subsection 5.2.1, it is suggested that anomalously high soil moisture should result in an increase in net surface radiation due to an increase in net longwave and shortwave radiation (barring any cloud feedback). Figure 5-8 displays the surface radiation summary for the July 1988 and July 1993 simulations over the affected flood and drought region. Consistent with the sensitivities of convective and total rainfall to soil moisture (See Figure 5-5), the simulations display a positive feedback between net surface radiation and soil moisture. This feedback is considerably stronger in 1988 than 1993. Like the rainfall sensitivity, the net surface radiation sensitivity is strongest in the 25% to 50% initial soil moisture range. However, when the initial soil saturations exceeds 50%, the net surface radiation remains nearly constant. Upon further inspection, it is evident that the net surface longwave radiation sensitivity is the dominant factor responsible for the net radiation-soil moisture feedback. This suggests that the surface cooling and/or the greenhouse effect for water vapor play an important role in the soil moisture-rainfall feedback. On the other hand, the net surface shortwave radiation displays a strong negative feedback to initial soil moisture. This suggests that the decrease in net solar radiation associated with the increase in cloudiness dominates the increase associated with the decrease in albedo from the wetter soils and greener denser vegetation (not shown). BATS does not account for the relationship between vegetation albedo and soil moisture. Although we do not expect this vegetation feedback to be nearly as strong as the cloud feedback shown in these simulations, its inclusion should result in an increased sensitivity between net surface radiation and soil moisture.

In Subsection 5.2.2, we indicate that the sum of the surface latent and sensible heat fluxes should balance the net surface radiation at long time-scales. Figure 5.4.2 displays a summary of the surface heat fluxes versus initial soil moisture for the affected flood and drought region. This figure indicates that the sum of the latent and sensible heat fluxes display a significant sensitivity to initial soil moisture and nearly balance the net surface radiation (within 5 W/m^2). (Note that the range on the y-axis of Figure 5.4.2 is considerably larger than that of Figure 5-8.) There is a small tendency for the ground heat flux to decrease with increasing soil moisture. This decrease is responsible for the slightly higher latent plus sensible heat flux sensitivity than net radiation. This mechanism, which is not discussed in Section 5.2, results in an additional positive feedback between soil moisture and rainfall

The response of the sum of the latent and sensible heat fluxes to soil moisture is determined by competing factors; The latent heat flux tends to increase with increasing soil moisture while the sensible heat flux tends to decrease. The simulations presented here indicate that the change in

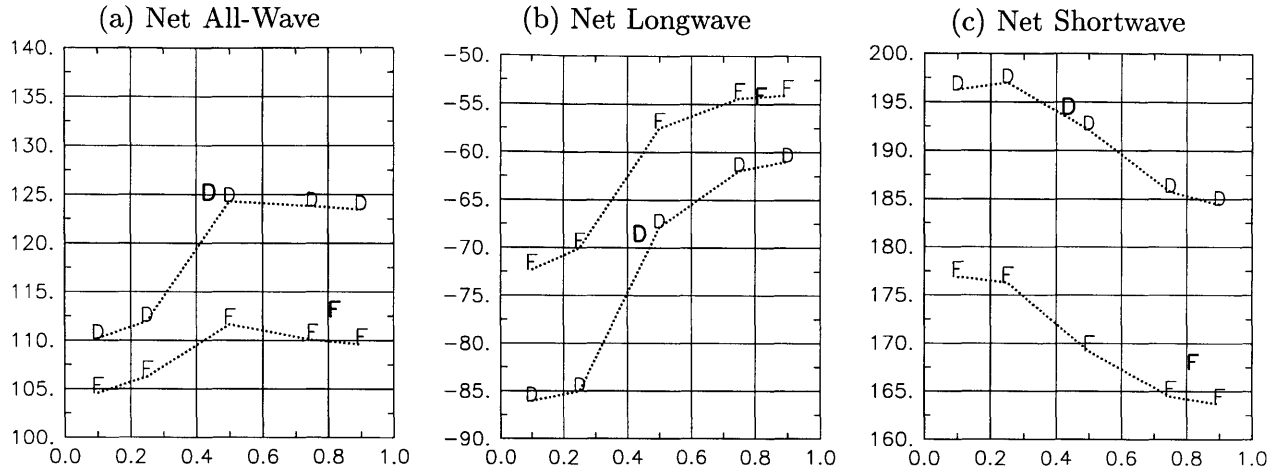

Figure 5-8: Simulated monthly surface radiation fields (W/m^2), for the 1988 and 1993 simulations as a function of initial soil saturation: (a) net radiation; (b) net longwave radiation; and (c) net solar radiation. Each data point represents the average of the May, June, July, August, and September simulations over the Midwest region outlined in Figure 5-3 given the initial soil moisture. The D denotes the drought year (1988) and the F denotes flood year (1993). The boldface D and F denote the control simulations for each year

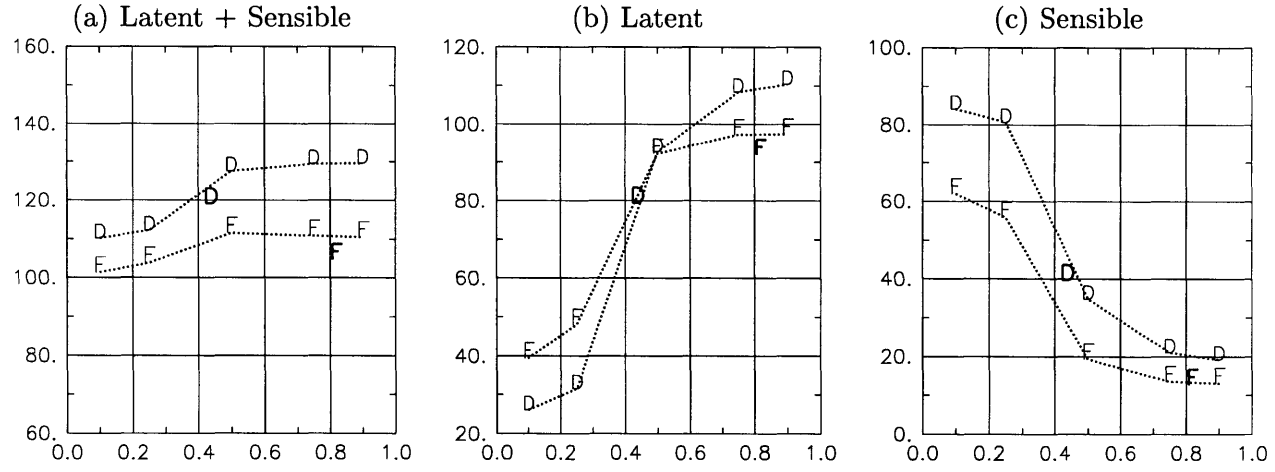

Figure 5-9: Simulated monthly surface heat flux fields (W/m^2), for the 1988 and 1993 simulations as a function of initial soil saturation: (a) sensible + latent heat flux; (b) latent heat flux; and (c) sensible heat flux. Each data point represents the average of the May, June, July, August, and September simulations over the Midwest region outlined in Figure 5-3 given the initial soil moisture. The D denotes the drought year (1988) and the F denotes flood year (1993). The boldface D and F denote the control simulations for each year

latent heat flux with changes in initial soil moisture tends to outweigh the corresponding change in sensible heat flux. In addition, associated with the decrease in sensible heat flux with increasing soil moisture is a decrease in PBL height (not shown). Thus, not only does the heat flux into the PBL increase, the heat flux added per unit depth of PBL increases even more significantly.

As alluded to in Subsection 5.4.2, the response of the latent heat flux to increases in soil moisture is non-linear. The highest sensitivity occurs in between 25% and 50% of saturation, and the lowest sensitivities occur at the lower and higher soil saturations. The lack of sensitivity at the lower soil moisture values is primarily a result of transpiration ceasing due to the soil saturation falling below the wilting point. The lack of sensitivity at the higher soil moisture values is likely to be a result of evapotranspiration reaching the potential evaporation rate. Consequently, the highest sensitivities are seen in between these extremes. This feature is carried over to the other surface fields presented in this paper.

Figure 5-10 displays soil moisture's impact on the surface moist static energy, temperature, and water vapor mixing ratio. As is the case with the sum of the latent and sensible heat fluxes, the magnitude of the surface MSE is determined by competing factors of temperature and humidity; anomalously high soil moistures are typically associated with lower near surface temperatures and higher near surface humidities. It is evident from Figure 5-10 that soil moisture has a pronounced impact on both the low-level mixing ratio and temperature. Again like the sum of the latent and sensible heat fluxes, the moisture component outweighs the temperature component. In other words, the increase in mixing ratio with increasing soil moisture outweighs the decrease in temperature yielding an overall increase in MSE. Note that the MSE tends to be more sensitive to soil moisture than the sum of the sensible and latent heat fluxes. The increased sensitivity is likely to be a result of changes in the PBL height and in the amount of entrainment of low MSE air from above the PBL. Thus, increases in soil moisture tend to increase the flux of high MSE air into the PBL from below (increase in the sum of the latent and sensible heat fluxes), increase the MSE per unit mass of air (shallower PBL depth), and reduce the amount of entrained air of low MSE from above the PBL (decrease in the PBL growth rate). The combination of these additive processes is largely responsible for the increase in convective activity.

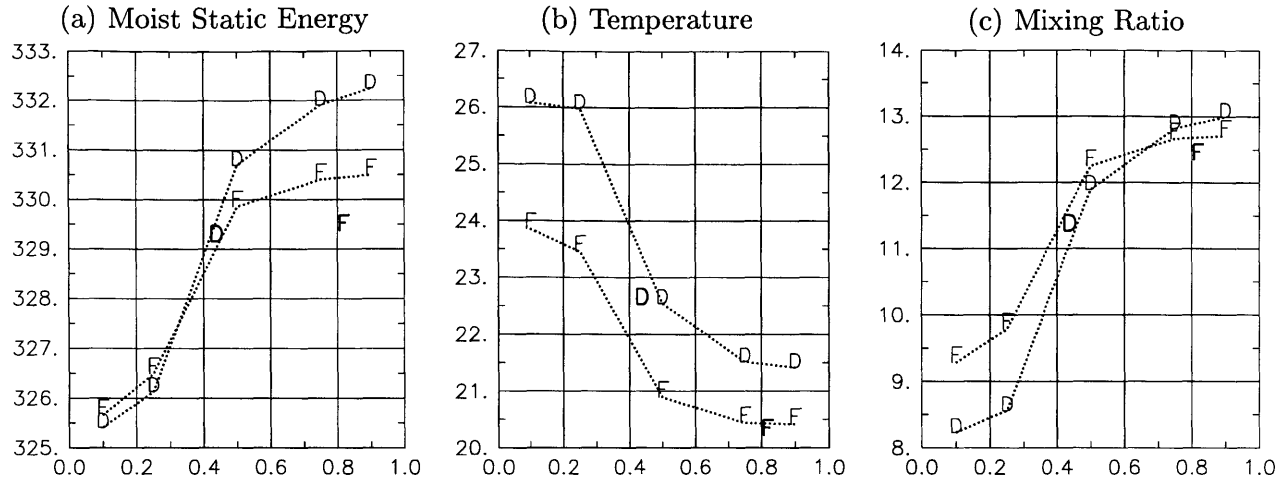

Figure 5-10: Simulated monthly moist static energy (KJ/kg), temperature (C), and water vapor mixing ratio (g/kg) for the 1988 and 1993 simulations as a function of initial soil saturation: (a) Moist Static Energy; (b) Temperature; and (c) Mixing Ratio. Each data point represents the average of the May, June, July, August, and September simulations over the Midwest region outlined in Figure 5-3 given the initial soil moisture. The D denotes the drought year (1988) and the F denotes flood year (1993). The boldface D and F denote the control simulations for each year

5.5 Summary of Results and Conclusions

In this chapter, we investigate the physical pathways and mechanisms responsible for the soil moisture-rainfall feedback using a modified version of NCAR's RegCM. The extreme drought of 1988 and the extreme flood of 1993 are used as representative events. Several questions are addressed: Are the persistence patterns in extreme hydrologic events maintained by external forcings or were they maintained by internal mechanisms involving soil moisture? What role does the magnitude and direction of the soil moisture anomaly play? How does the timing of the soil moisture anomaly impact the strength of the feedback? And what are the pathways responsible for the soil moisture-rainfall feedback?

To address these questions, we perform several numerical experiments. The soil saturation in each simulation is initialized with one of six different distributions of soil saturation ranging from 10% to 90% including an observed (control) distribution. Month long simulations are performed during May, June, July, August, and September for 1988 and 1993. The following are the four main conclusions of this study:

1. Increases in initial soil moisture are shown to result in an increase in future rainfall over the Midwest. Soil moisture's impact on both the energy and water budgets proves to be crucial in determining the strength of the soil moisture-rainfall feedback.

2. The simulations indicate that there is an assymetric response in the soil moisture-rainfall feedback due to the existence of multiple evapotranspiration regimes. The asymmetry is weighted such that the soil moisture rainfall-feedback is stronger during drought conditions than flood conditions. This suggests that the soil moisture-rainfall feedback favors droughts compared to floods over the Midwest.

3. The simulations indicate that the soil moisture-rainfall feedback remains strong when the model is initialized at observed extremes in soil saturation. Based on these model results, one would conclude that soil moisture did play a significant role in maintaining the persistence patterns of the drought of 1988 and the flood of 1993. However, the simulations suggest that the initiation of the events are likely to be a result of large-scale circulation anomalies.

4. During the late spring and summer, the strength of the soil moisture- rainfall feedback displays little dependence on the timing of the soil moisture anomaly. This suggests that knowledge of the soil moisture conditions during any of these months can improve the predictability of rainfall.

The choice of domain and convective parameterization is likely to have played a small but significant role in the outcome of the above conclusions. The following chapter investigates these issues.

Chapter 6

Role of the Distribution of Soil Moisture in Determining Rainfall

6.1 Introduction

In Chapter 5, we investigated the soil moisture-rainfall feedback using a small domain. We used a small domain so that the effects of changes in soil moisture on the large-scale dynamics could be constrained. Seth and Giorgi (1998) found that for RCMs the strength of the soil moisture-rainfall feedback can be dependent on the location of the domain boundaries. They determined that small domains can produce spurious dynamical effects when the sensitivity to internal model processes are tested. Thus, they conclude that for internal process studies that the boundaries must be placed well outside the region of influence. In this chapter, we use a large model domain to develop an understanding of the soil moisture-rainfall feedback at large-scales. By using the large domain, the dynamical impacts resulting from changes in soil moisture can be considered.

The following questions are addressed in this chapter: Are the interannual variations of soil moisture useful for predicting precipitation? Are the spatial variations of soil moisture useful for predicting precipitation? Are there remote regions in which anomalous soil moisture conditions impact precipitation over the Midwest? An extensive series of numerical experiments are performed to investigate these issues. Section 6.2 provides a background for this study. Section 6.3 gives a description the experiments performed. The results are described in Section 6.4. The discussion of the results and the conclusions are provided in Sections 6.5 and 6.6, respectively.

6.2 Background

During the spring and summer, low-level flow traveling westward across the Gulf of Mexico turns northward into the United States when it reaches Mexico. It then travels across the Great Plains and into the Midwest. This phenomena is commonly referred to as the Great Plains Low-Level Jet (referred to hereafter as LLJ). It often transports moisture from the Gulf of Mexico to the Great Plains and Midwest and is thus often associated with severe precipitation events (e.g. flood of 1993). When the LLJ is weak, drought conditions over the Great Plains and Midwest are likely to occur (e.g. drought of 1988). The goal of this chapter is to determine how the distribution of soil moisture, both local and remote, impacts the LLJ and other rainfall producing mechanisms over the Midwestern United States.

As mentioned in Section 5.1, most numerical modeling studies of the soil moisture-rainfall feedback prescribe unrealistic scenarios for soil moisture. In many instances, evapotranspiration is considered to be a surrogate for soil moisture and is maintained with no dynamic feedback at values close to zero for the dry simulations and close to the potential evaporation for the wet runs. In less extreme cases, soil moisture is prescribed uniformly both vertically and horizontally at the wilting point (~30% or less of soil saturation) for the dry runs and at the field capacity (~90% of soil saturation) for the wet runs where two-way interaction is allowed. Figure 6-1a, shows that averaged June, July, and August soil moisture exhibits a great deal of spatial variability that these studies do not account for. Furthermore, Figure 6-1b shows that the variability of soil moisture does not exist to the degree that these studies suggest. For example, initializing the soil saturation at 90% the Southwest is unreasonable given that the average soil saturation is around 25±12%. In Chapter 5 we investigated the soil moisture-rainfall feedback in a local sense. The small domain was configured over the eastern two thirds of the United States. Over this region, the summertime climatological soil moisture is relatively uniform (Figure 6-1a). However, in this study, we use a domain that spans much of North America. Thus, the assumption of soil moisture uniformity may be unreasonable. One aspect of this study is to investigate the impact of initializing soil moisture uniformly across the domain versus accounting for the spatial and temporal variabilities.

Figure 6-1a shows that the largest spatial variability in June, July, August soil saturation occurs in a 10° band along the 100°W meridian (other than the Pacific Northwest). McCorcle (1988), using a regional forecasting model, analyzes a spring precipitation event over the Great Plains and indicates that contrasting soil moistures between the Rocky Mountains and Great Plains

(a) JJA Root Zone Soil Saturation

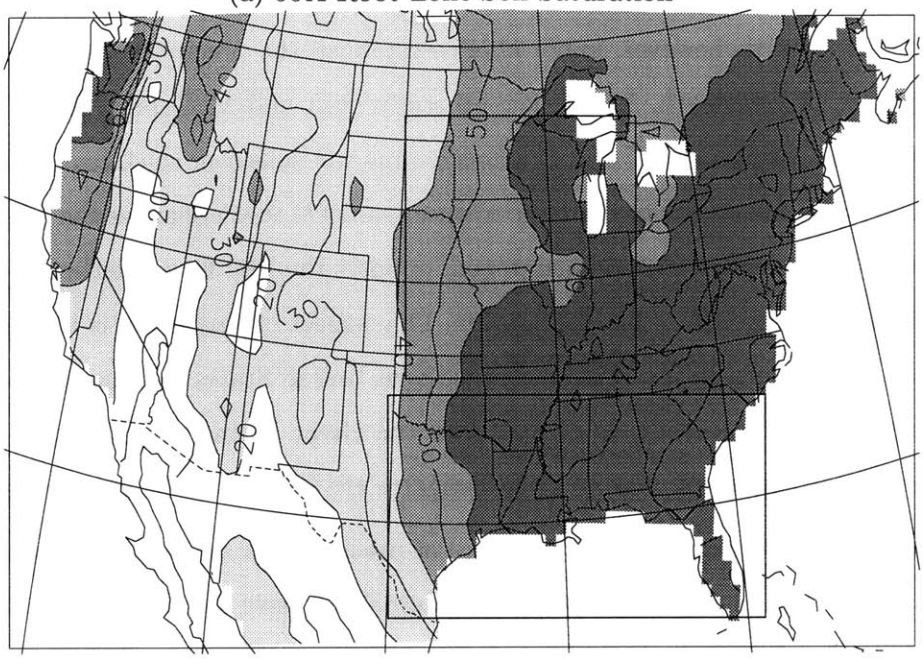

(b) JJA Standard Deviation

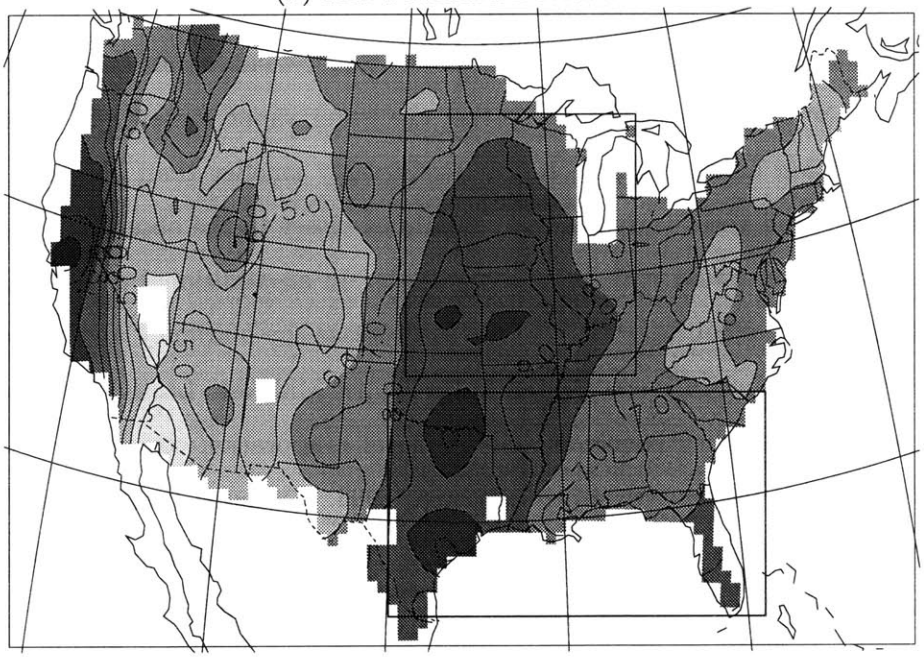

Figure 6-1: Climatology of the June, July, and August merged ISWS/HDG root soil saturation (%): (a) Mean; (b) Standard Deviation.

play a significant role in determining the strength of the LLJ. More specifically, a simulation with saturated soils over the Rocky Mountains and bone dry soils over the rest of the domain results in a weaker LLJ than a simulation with saturated soils over the Great Plains and bone dry soils elsewhere. McCorcle (1988), however, is not able to establish the precise mechanisms responsible for the differences in LLJ strength. In a follow-up study, Fast and McCorcle (1990), using a two-dimensional model, show that dry soil over the Rockies and wet soils over the Great Plains induce an ageostrophic wind component (due to the temperature gradient) that enhances the LLJ at night. In the converse case, the ageostrophic wind component opposes the LLJ flow. Neither of these studies investigates the resulting precipitation distribution. One aspect of this study is to investigate how the soil moisture distribution in the eastern and western United States impacts not only the LLJ, but also the magnitude and location of rainfall over the Great Plains and Midwest. In addition, rather than focusing on one event, this study investigates the impact on the climatology of rainfall.

Paegle et al. (1996) investigate the dependence of precipitation on surface evaporation during the Midwest flood of 1993 using a regional climate model. In their simulations, evaporation rates are held fixed and the domain is comparable in size and location to the domain we use in the Chapter 5 experiments. They indicate that the net moisture flux from the LLJ is significantly larger than the rainfall rate over the flood region. Thus, they conclude that changes to the surface evaporation impact the buoyancy of the LLJ rather the water vapor content. In their simulation, however, the evaporation and precipitation are considerably smaller than observed, which may impact their findings. Had these variables been simulated closer to the observed, the rainfall rate and net LLJ moisture flux would have been comparable. In an additional experiment, they find that wet conditions over the Southern Plains tend to decrease the buoyancy and hence strength of the LLJ resulting in a tendency for less rainfall in the Upper Midwest. Lastly, from an experiment with a wet upper Midwest, they conclude that the local evaporation conditions over the upper Midwest had little impact on the strength of the flood 1993. Although Paegle et al. (1996) found changes to the strength of the LLJ with changes in soil moisture, their domain is too small to investigate how changes in soil moisture impact larger features such as the storm track. In this study, we perform a similar set of experiments using a larger, relatively unconstrained domain. In addition, the HDG/ISWS soil moisture dataset allows us to perform these experiments with reasonable surface evaporation conditions.

None of the above studies investigate the role of soil moisture in determining the position of the storm track. Observational studies of Namias (1955), Namias (1982), and Namias (1991) indicate

that droughts over the United States are often associated with anomalous upper-level anticyclones resulting in a northward shift in the storm track location. Furthermore, Namias (1982) and Namias (1991) speculate that the anomalously dry soil moisture conditions associated with drought are likely to have played a role in the persistence of drought by strengthening and anchoring the anticyclones. His studies argue that the increase in sensible heating encourages the growth of an upper-level high via an increase in pressure. In this chapter, using a large domain, we investigate the pathways, if any, through which soil moisture impacts the location and magnitude of the storm track over North American during the summer.

Following the above works, we hypothesize that the distribution of soil moisture, both local and remote, plays an important role not only in determining the strength and location of the LLJ and storm track, but also in determining the strength and location of precipitation peaks over the Great Plains and Midwest.

6.3 Description of Experiments

In this section, we describe the numerical experiments performed in this Chapter. Each simulation set is comprised of six 37 day runs initialized on the 25th of June on each of the following years: 1986, 1987, 1988, 1989, 1990, and 1993. The first six days are ignored for model spin-up considerations. The average of the six years is considered the climatology. The experiments are performed under several moisture configurations and are described below.

Figure 3-1 depicts the domain and associated topography for the simulations presented in this study. Table 6.1 provides a description of the numerical experiments performed. The control simulations (CTL) are initialized using the observed soil moisture for each year (see Figure 6-2). Note that by observed soil moisture, we mean the data derived from the merged HDG/ISWS dataset (see Section 2.2). We realize that these are not the actual observations and can contain significant errors in regions that significantly differ from the Midwest (such as the Southwest). In the climatology simulations (CLM), the soil moisture for each year is initialized using the 25 June HDG/ISWS climatology (the average of the panels in Figure 6-2). The difference between the CTL and CLM simulations provides an indication of the importance of the interannual variability of soil moisture. An additional series of simulations are performed with the soil saturation initialized uniformly in the vertical and horizontal at the following values: 0%, 25%, 50%, 75%, and 100%. Comparing these simulations to each other displays the importance of the spatial distribution of

soil moisture. In addition, comparing these simulations to the CTL simulations indicates the level of importance of initializing soil moisture according the observations. All of the above experiments are performed with both fully interactive soils and fixed soils. In the fixed experiments (FIX), soil moisture is held constant throughout the simulation.

Table 6.1: Description of each simulation performed in this study.

Simulation Start Dates
• 26 May, 1986, 1987, 1988, 1989, 1990, and 1993
• 25 June, 1986, 1987, 1988, 1989, 1990, and 1993
Simulation Duration:
• 37 Days (6 day spin-up)
Soil Saturation:
• CTL: Observed HDG/ISWS for each year
• CLM: Observed HDG/ISWS climatology
• 00%: 0% soil saturation domain-wide
• 25%: 25% soil saturation domain-wide
• 50%: 50% soil saturation domain-wide
• 75%: 75% soil saturation domain-wide
• 100%: 100% soil saturation domain-wide
• 25MWCTL: Fixed at 25% over the Midwest, CTL elsewhere
• 75MWCTL: Fixed at 75% over the Midwest, CTL elsewhere
• 25GCCTL: Fixed at 25% over the Gulf Coast, CTL elsewhere
• 75SWCTL: Fixed at 75% over the Southwest, CTL elsewhere
Soil Moisture Boundary Conditions:
• INT: Free (two-way interaction)
• FIX: Fixed (one-way interaction)
Convective Closure:
• FC80
• AS74

Three additional sets of experiments are performed where the soil moisture is initialized similar to the CTL experiments except over a particular region where it is perturbed and held fixed. Soil moisture over the unperturbed region is fully interactive. In the first set (25MWCTL), the soil saturation is held fixed over the upper Midwest at 25% (see Figure 6-3a). Figure 6-1 indicates that the root zone soil saturation over the upper Midwest is typically 50±20%. The fixed patch spans from 88°W to 103°W in longitude and from 36°N to 44°N in latitude. With this scenario, we can investigate the remote impacts of soil moisture in the upper Midwest under a dry scenario much like we did in Chapter 5 to the local scale. In the second set (25GCCTL), the soil saturation over

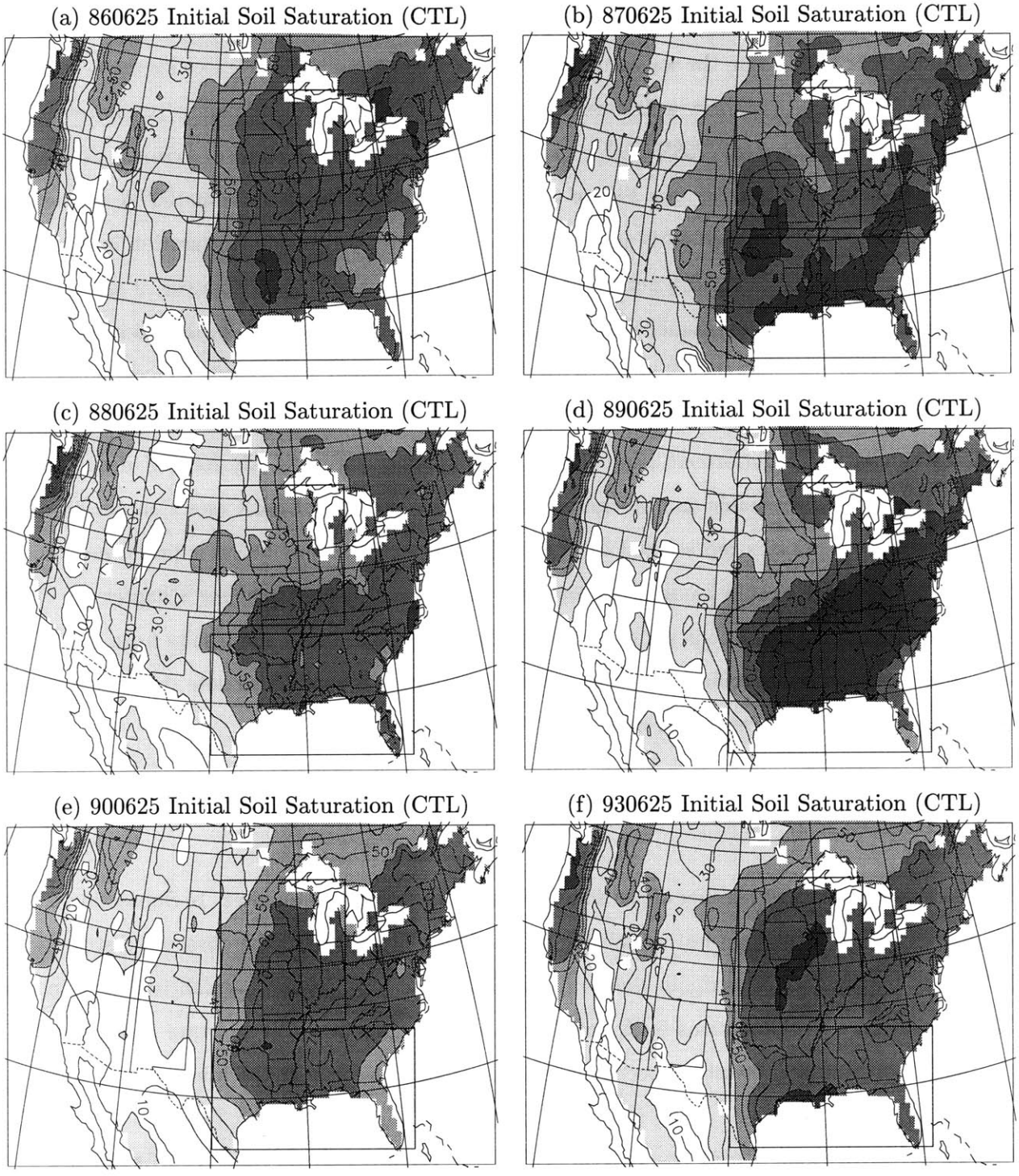

Figure 6-2: Plot of initial root zone soil saturation (%) for the control simulations: (a) 25 June 1986; (b) 25 June 1987; (c) 25 June 1988; (d) 25 June 1989; (e) 25 June 1990; and (f) 25 June 1993. The contour interval is 10% and shading occurs at values above 20% and at intervals of 20%.

the western Gulf Coast and southern Great Plains (entry region to the LLJ) is held fixed at 25% (see Figure 6-3c). The fixed patch spans from 88°W to 103°W in longitude and from 25°N to 37°N in latitude. Over this region, the soil saturation is on average around 60±20% (see Figure 6-1). The purpose of this set is to see how a dry anomaly upstream of the Midwest impacts precipitation in the Midwest. In the third set (75SWCTL), the soil saturation over New Mexico, Arizona, Colorado, and Utah is held fixed at 75% (see Figure 6-3d). The fixed patch spans from 100°W to 115°W in longitude and from 31°N to 42°N in latitude. Over this region, the soil saturation is typically 25±12% (see Figure 6-1). A 50% perturbation is obviously exaggerated. However, it should give an understanding of the importance that soil moisture in the Southwest has in the Midwest. Also, keep in mind that the HDG/ISWS tends to underestimate extremes and is likely to have significant errors in regions away from the Midwest.

Each simulation is performed using the modified version of the NCAR RegCM described in Part I. The large-scale clouds and precipitation are represented by SUBEX (see Chapter 3). The convective precipitation is represented by the Grell scheme. Each simulation is performed twice: once with the FC80 closure assumption and once with the AS74 closure (see Chapter 4). The results for the AS74 simulations are only used to confirm or unconfirm the results from the FC80 simulations. When not specified, the FC80 closure assumption is used. Also note that many of the above experiments are repeated for June (initialized 26 May).

6.4 Results

This section describes the results of the simulations performed in this chapter. In Subsection 6.4.1, we investigate the importance of initializing soil moisture according to the observed distribution. In Subsection 6.4.2, we investigate the local impacts of the soil moisture-rainfall feedback on the Midwest. Finally, in Subsections 6.4.3 and 6.4.4, we investigate how soil moisture anomalies over the Gulf Coast and Southwest, respectively, influence precipitation over the Midwest.

6.4.1 Role of Soil Moisture in Reproducing Observations of Precipitation

s mentioned in Subsection 6.2, many studies using climate models initialize soil moisture uniformly over the entire domain and depth. The main reason for this is because soil moisture observations do not exist on the scale of most climate model domains. By using the merged HDG/ISWS soil moisture dataset described in Subsection 2.2.1, we are able to assess the importance of initializing

(a) Initial Soil Saturation (25MWCTL)

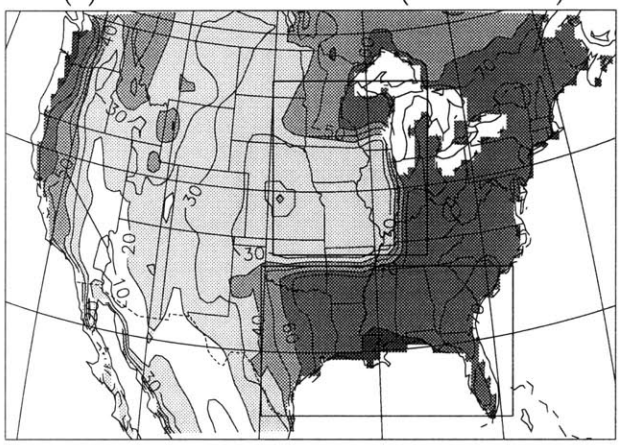

(b) Initial Soil Saturation (25GCCTL)

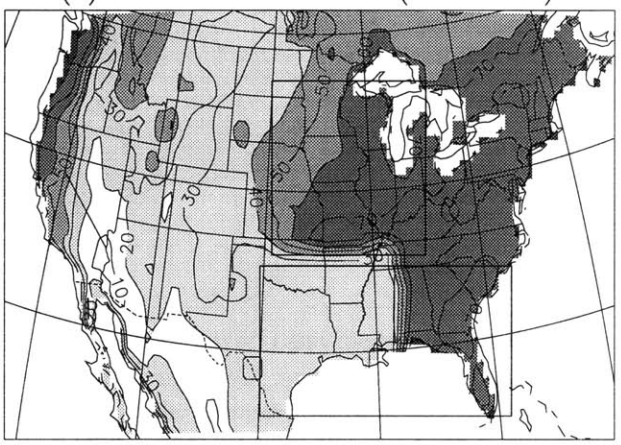

(c) Initial Soil Saturation (75SWCTL)

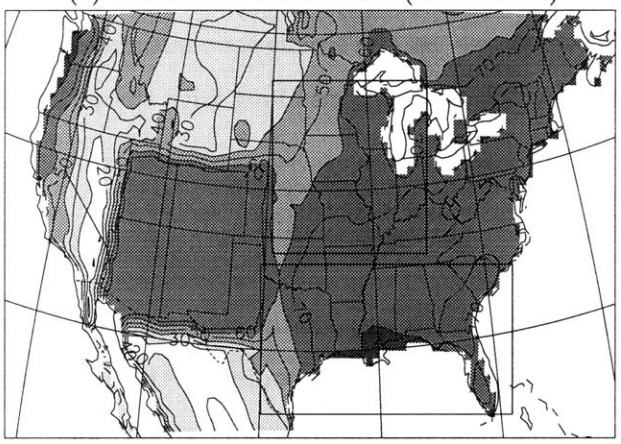

Figure 6-3: Plot of initial 25 June climatology of the root zone soil saturation (%) for the anomalous fixed patch simulations: (a) 25MWCTL; (b) 25GCCTL; and (c) 75SWCTL. The contour interval is 10% and shading occurs at values above 20% and at intervals of 20%.

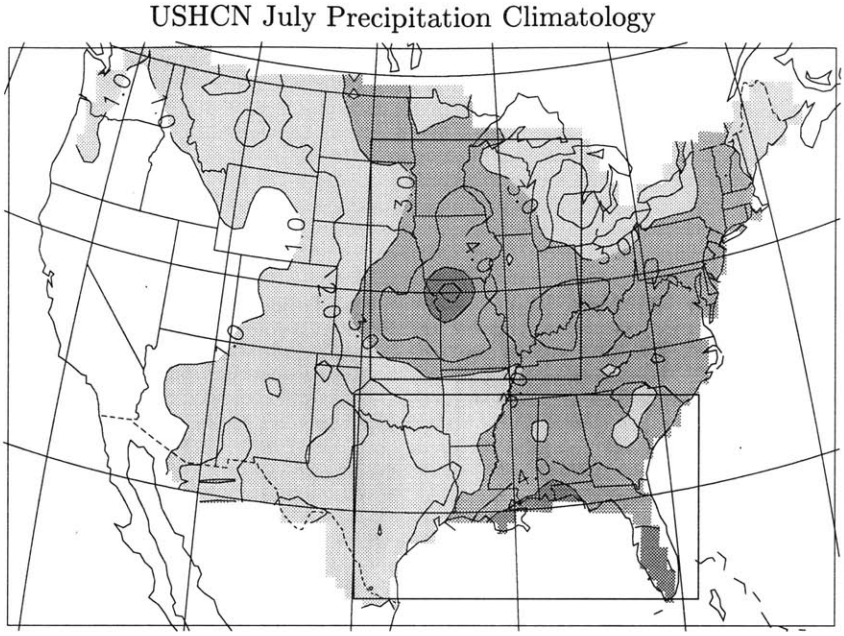

Figure 6-4: July observed USHCN Precipitation Climatology for the years: 1986, 1987, 1988, 1989, 1990, and 1993 (mm/day). Contour interval is specified at 1 (mm/day). Shading occurs at values above 1 mm/day and at intervals of 2 mm/day. Note that the USHCN observations only exist over the United States.

soil moisture according the observed distribution. To do so, we use the simulations initialized with the observed (CTL) and climatological (CLM) soil moisture distributions along with the uniform initializations of 0%, 25%, 50%, 75%, and 100%.

Climatology

Figure 6-4 displays the observed July USHCN precipitation climatology for the six simulated years (1986, 1987, 1988, 1989, 1990, and 1993). Because of the 1993 summer flooding in the Midwest, there is a pronounced peak over that region. Not including 1993 in the climatology tends make the distribution more meridionally symmetric (not shown).

Figure 6-5 displays the simulated precipitation climatology for the CTL simulations using the FC80 closure assumption. Overall, the model tends to underpredict precipitation over most of the domain except the Gulf Coast region where there is an overprediction. Over the Midwest, the model performs well in capturing the region of precipitation above 3 mm/day. However, it is unable to reproduce the region (Iowa, Missouri, and Kansas) where precipitation exceeds 4 mm/day. A considerable portion of the high bias over the Gulf Coast region can be explained by the July 1988 simulation where the predicted convective activity is far too pronounced over this region. In addition, some of the underprediction of precipitation in the Midwest (and the central Atlantic

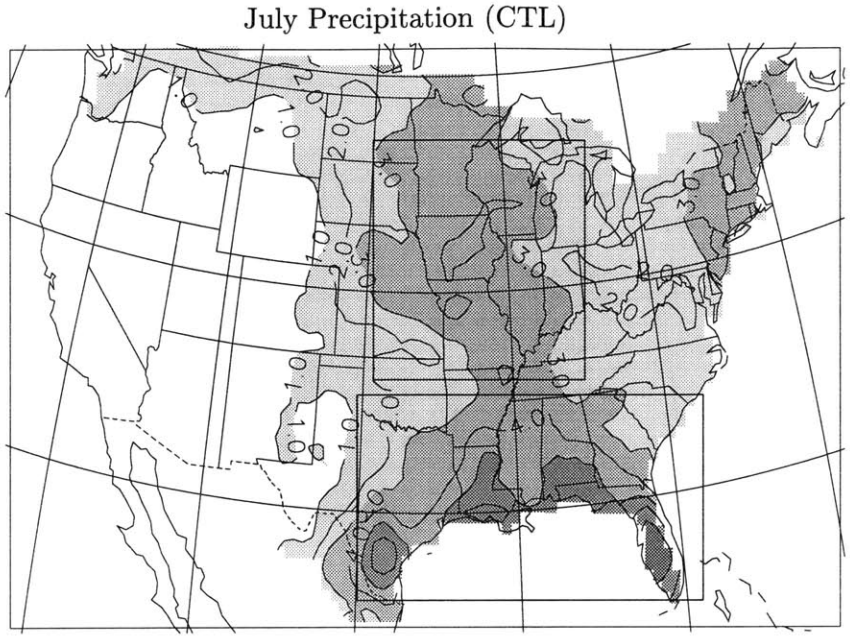

Figure 6-5: July simulated precipitation climatology for the CTL experiments (mm/day). The soil moisture in each simulation is initialized according to the merged HDG/ISWS dataset and is fully interactive. The FC80 closure assumption is used. Note that only values for the United States are displayed.

states) can be attributed to the excessive precipitation forming in the Gulf Coast region which is upstream along the LLJ. Also of particular importance to this study, the precipitation over Colorado, Arizona, and New Mexico is underpredicted. The impacts of this will be discussed in further detail in Subsection 6.4.4. The precipitation underprediction over most of the domain tends to result in an underprediction soil moisture. In addition, there is a also a tendency for soil moisture within BATS to dry more than is observed [primarily due to the lower soil boundary; Yeh and Eltahir (2000) and Yeh and Eltahir (2001)]. For example, even though the model overpredicts precipitation in the Gulf Coast region, soil moisture is underpredicted. Thus, in regions with a pronounced soil moisture-rainfall feedback, this underprediction is self-sustaining and tends to result in a further decrease. Overall the model captures the general observed patterns of precipitation, however, significant differences exist.

To investigate the importance of the interannual variation that soil moisture has on precipitation, we compare the July climatologies of the simulations initialized using the observations of soil moisture for each year (CTL; Figure 6-5) to the simulations initialized with the observed climatology (CLM; Figure 6-6). Comparing the two figures, we see that there is relatively little difference between the simulations including the interannual variability of soil moisture and to

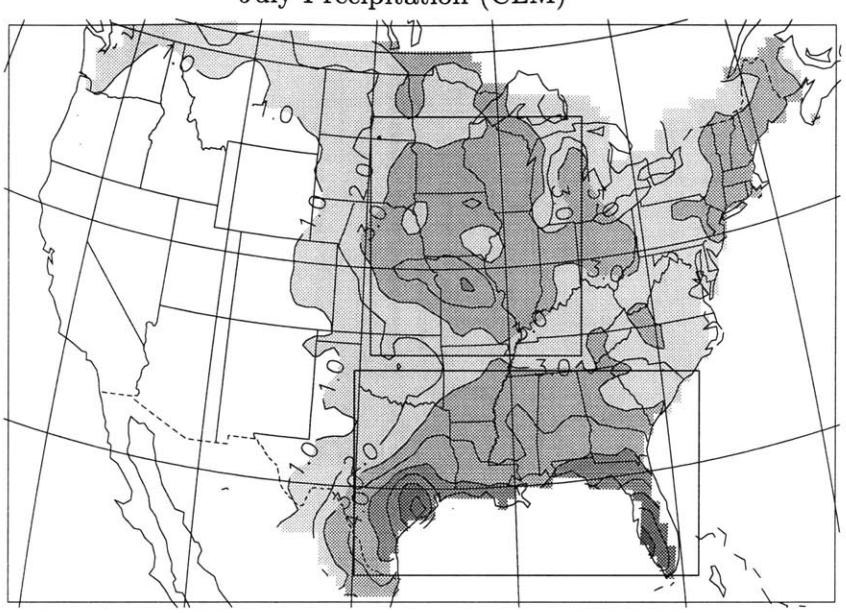

Figure 6-6: July simulated precipitation climatology for the CLM experiments (mm/day). The soil moisture in each simulation is moisture in each simulation is initialized according to the climatology of the merged HDG/ISWS dataset and is fully interactive. The FC80 closure assumption is used. Note that only values for the United States are displayed.

those that do not. Thus, in the context of these simulations, the interannual variability of soil moisture plays little role in the predictability of precipitation. It should be noted, however, that the merged HDG/ISWS data tends to dampen the extremes in soil moisture (at least over Illinois). Thus, it is expected that year-to-year changes in soil moisture are more extreme in nature than the HDG/ISWS data suggest. Therefore, in regions and seasons where the soil moisture feedback is pronounced, the interannual variability of soil moisture is likely to play a more important role than is shown here.

Figure 6-7 displays the simulated climatology for each of the uniform soil moisture initializations. Comparing precipitation in each of these simulations to the observations (Figure 6-4) and the CTL simulations (Figure 6-5), we see the control tends to perform better in reproducing the observations (especially over the Midwest). Exceptions lie over the coastal portions of the Gulf Coast region where the drier simulations (00% and 25%) tend to perform better and over the Southwest region where the wetter simulations (50%, 75% and 100%) tend to perform better. Over the Midwest, contrary to the CTL and CLM simulations, none of the uniform soil moisture initializations are able to predict the precipitation in excess of 3 mm/day over the Midwest. Considering that there is considerably more soil water (and hence more evapotranspiration) in the 75% and 100%

initializations, it is interesting that more precipitation occurs in the control initializations. This suggests that using the observed spatial distribution of soil moisture as initial conditions is necessary to accurately simulate precipitation over the Midwest. This also suggests that remote effects of soil moisture conditions, in addition to the local, are partially responsible for observed climatology of summertime Midwestern precipitation.

Figure 6-8 displays the bias and RMSE averaged over (a) the Midwest region and (b) the Gulf Coast region for the CTL, CLM, 00%, 50% and 100% simulations. Over the Midwest, both the CTL and CLM simulations perform best in reproducing the observations of precipitation. The bias and RMSE are nearly double or greater in all the uniform soil moisture simulations. In addition, the RMSE is nearly equal to the bias in all of the simulations suggesting that the model almost always underestimates precipitation over the Midwest during the summer. Over the Gulf Coast region, none of the simulations perform particularly well in reproducing the observations of precipitation. Between the dry (00% and 25%) and the wetter (50%, 75%, and 100%) simulations, the bias switches directions; When the soil moisture is below the wilting point, the bias tends to be negative and when the soil moisture is above the wilting point, the bias tends to be positive. This suggests that the soil conditions (whether local or remote) play an important role in the triggering of convection in this region. In contrast to the Midwest, the bias in precipitation could have been corrected by carefully selecting a precise configuration of soil moisture. Note that the precipitation underestimation over the Midwest may result from the overestimation of precipitation in the Gulf Coast region which lies upstream.

Figure 6-9a displays the simulated July soil moisture climatology for the CTL simulations, and Figures 6-9c-d display the differences between the 00%, 50%, and 100% uniform initializations and the CTL initializations. In comparing Figures 6-9a and 6-9b, it is evident that the dry soil moisture anomaly sustains itself and is responsible for the low precipitation bias seen in Figure 6-8. The primary difference between the CTL and 00% (and 25%) simulations occurs over the eastern United States since the soils are already dry in the west. However, in comparing Figure 6-9a and d, it can be seen that much of the excess soil water introduced by initializing the model at saturation is removed. This is especially the case in the eastern United States. In BATS, the moisture flux through the lower soil boundary increases exponentially as the soil water increases. For this reason, the soil saturation in the 100% simulations reaches 75% within 5 days of the simulation start (not shown). Because of this, the 75% and 100% integrations result in relatively similar simulations. Due to the climatologically dry conditions in the western United States, much excess soil water remains.

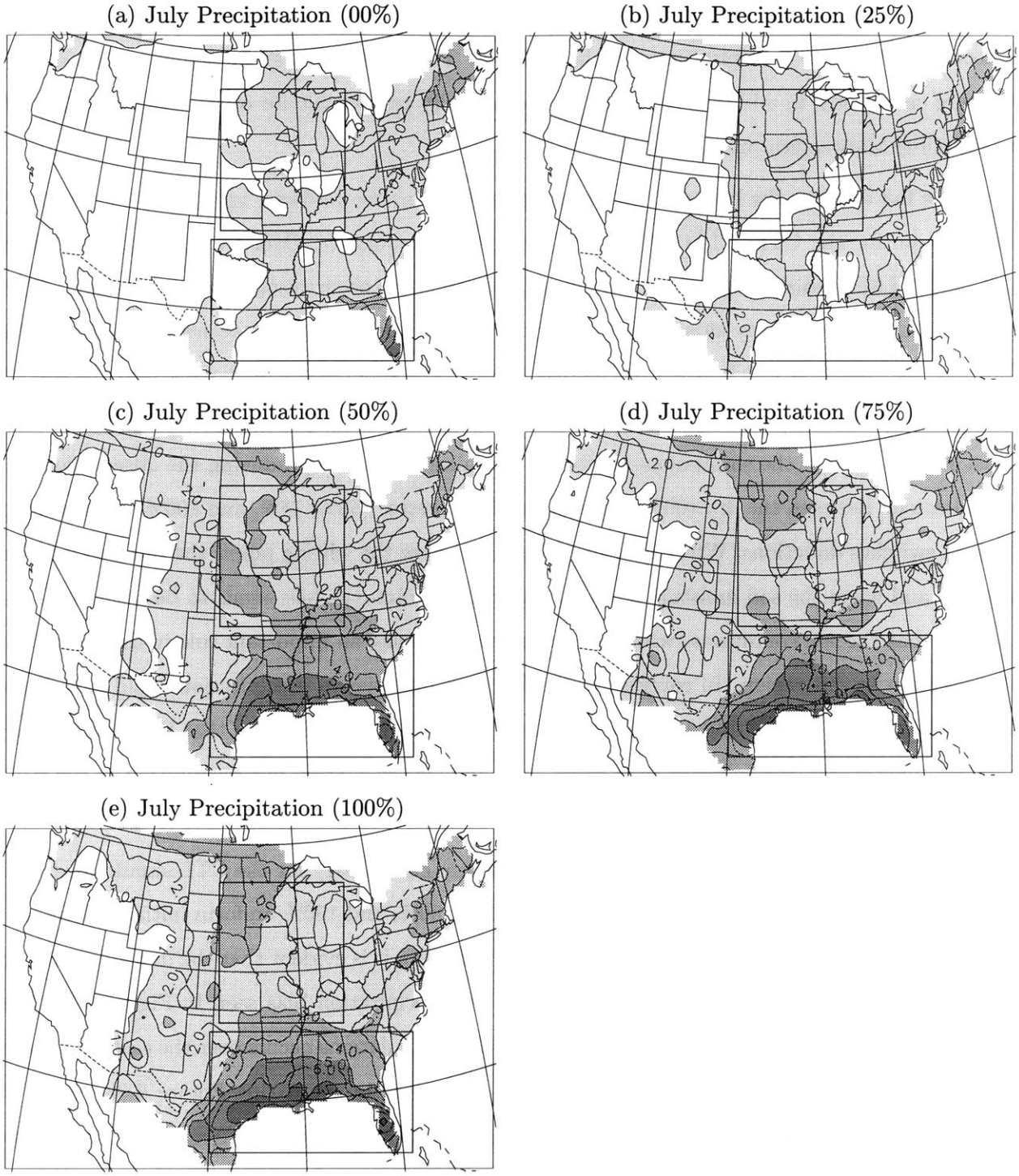

Figure 6-7: July simulated Precipitation Climatology (mm/day) for the years: 1986, 1987, 1988, 1989, 1990, and 1993. The soil moisture in each simulation is fully interactive and the FC80 closure assumption is used. The initial soil moisture fraction is indicated at the top of each plot. The contour interval is specified at 1 mm/day and shading occurs at values above 1 mm/day and at intervals of 2 mm/day. Note that only values for the United States are displayed.

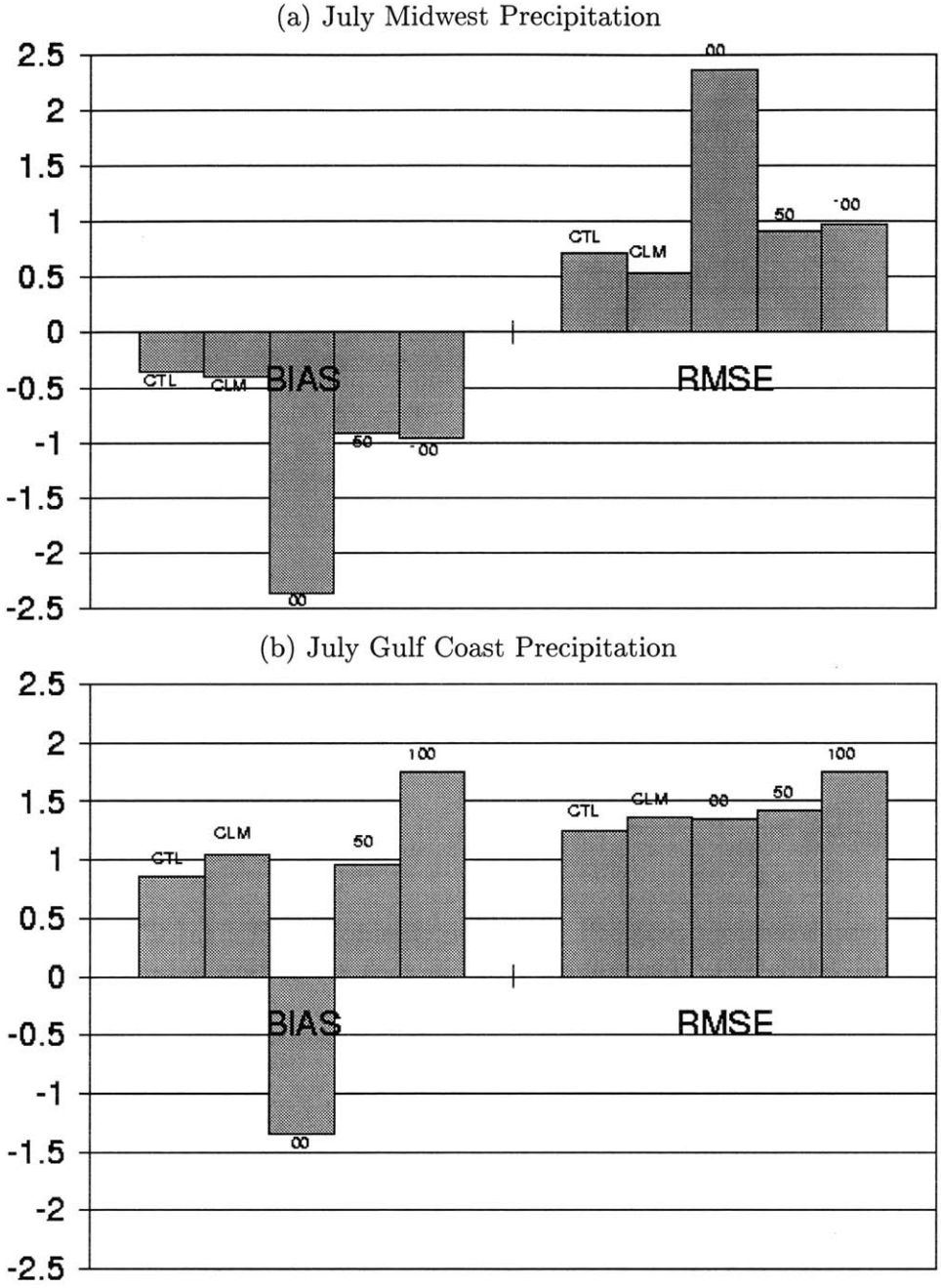

Figure 6-8: July simulated precipitation climatology bias and root mean square error (mm/day) computed over the (a) Midwest and (b) Gulf Coast regions outlined in Figure 3-1. The soil moisture in each simulation is fully interactive and the FC80 closure assumption is used. The initial soil saturation is indicated at the top of each bar. Note that values over water are not included in the computations.

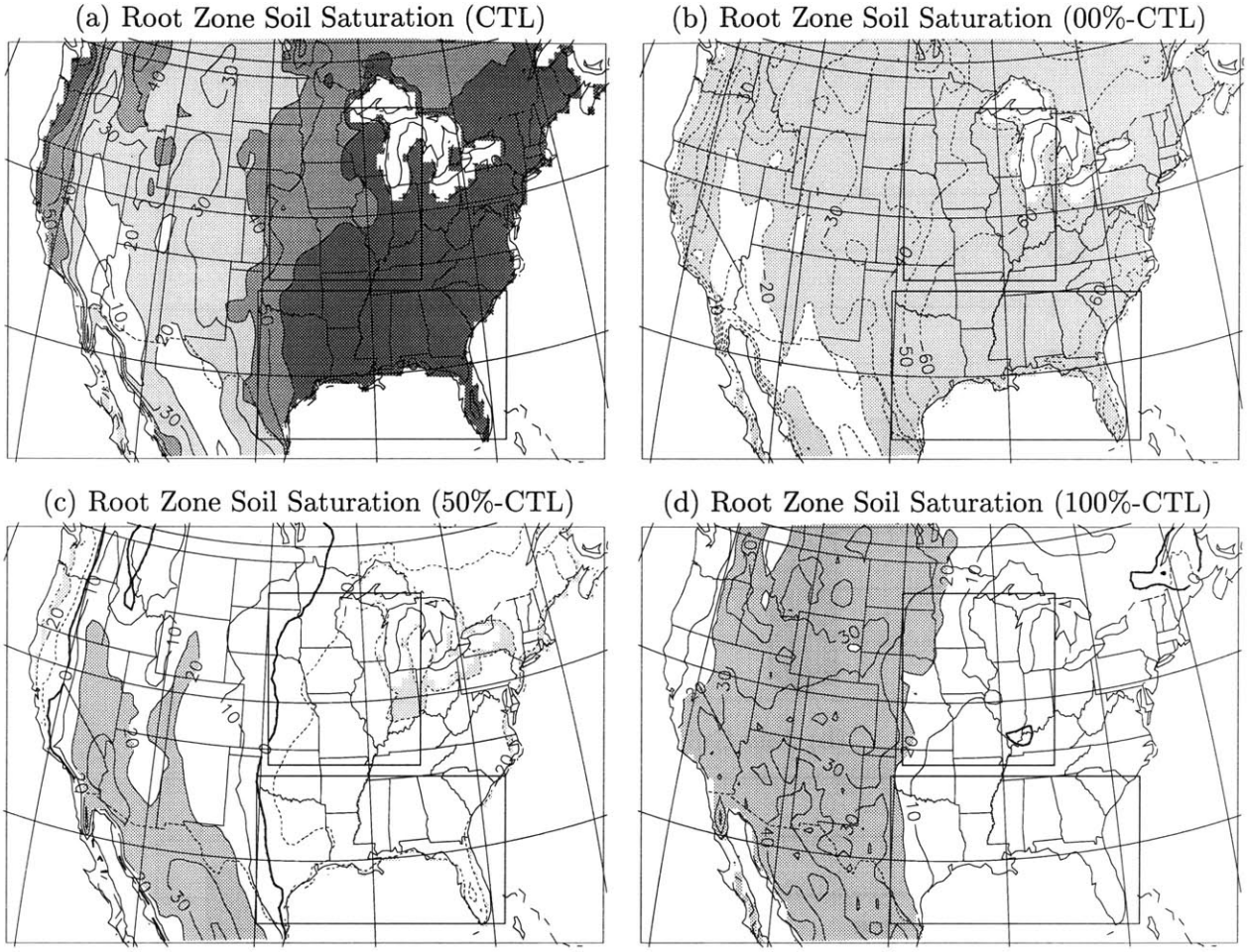

Figure 6-9: July simulated root zone soil saturation climatology (%): (a) CTL; (b) 00%-CTL; (c) 50%-CTL; and (d) 100%-CTL. The soil moisture in each simulation is fully interactive and the FC80 closure assumption is used.

Because of the rapid lower soil boundary drainage, the main soil moisture difference between the control and 100% (and 75%) simulations is the higher soil water content over the western United States. This contrast appears to be responsible for the differences in precipitation distribution observed between Figures 6-5 and 6-7d-e.

To gain an understanding for why these differences in initial soil moisture result in such pronounced differences in the distribution of precipitation, we turn to the large-scale dynamics, in particular the storm track. Here the storm track location is roughly defined as the region where the greatest concentration 500 mb geopotential height contours exist and where the strongest 500 mb winds (particularly zonal) exist. Additional methods for determining the storm track location, such as the variability method proposed by Trenberth (1991), are also used and yield similar results (not

shown).

Figure 6-10a displays the 500 mb height and wind climatology for the control simulations and Figures 6-10b-d display the differences in 500 mb heights and winds between the CTL and the uniform soil moisture initializations (00%, 50%, and 100%). As noted above, in the dry cases (00% and 25%), the most significant portion of the anomaly occurs to the east of the 100°W meridian. The additional dryness results in an anomalous high pressure (dark shading). Given that dry soil moisture conditions result in warmer temperatures, one might expect a low pressure anomaly. However, locally, the dry soil moisture conditions result in a decrease in the MSE per unit depth of PBL and cloud depth (see Section 5.2). This tends to reduce the likelihood and magnitude of convection. Convection is associated with rapid upward motion. An increase in uplift tends to result in a decrease in pressure and hence an increase in low-level convergence. An increase in convergence tends to yield in increase in cyclonic flow. Thus, under dry soil moisture conditions, there is a decrease in convection from the local mechanism described in Section 5.2. The decrease in convection results in an increase in pressure and hence anticyclonic flow. The net result is an anomalous high pressure ridge which causes a northward shift in the storm track over the eastern half of the United States. In the wetter cases, the majority of the soil moisture anomaly occurs in the western half of the United States. The wet anomaly results in an increase in lifting from an increase in convection via the mechanisms described in Section 5.2. The anomalous lifting results in an anomalous low pressure causing anomalous cyclonic flow and a southward shift in the storm track. Note that in both the wet and dry cases, the prevailing westerlies tend to deflect the surface anomaly region downstream (eastward) as it extends upward into the atmosphere.

Figure 6-11 shows the difference in 500 mb zonal winds and sigma 0.895 meridional winds between the CTL and uniform soil moisture integrations. Clearly, there is a storm track shift from north to south when increasing soil moisture from dry to wet. In addition, the dry simulations result an intensification of the storm track due the position of the anomalous cyclonic flow, while the wet simulations result in a weakening of the storm track core. The overall shift is comparable to shift in storm track locations between the 1988 drought and 1993 flood (Trenberth and Guillemot 1996). In addition, the direction of the shift is consistent with what is observed between drought and flood years. That is, spring and summer drought conditions over the Great Plains and Midwest are typically associated with anomalously north storm tracks and vice versa (e.g. Namias (1955)). Thus, when droughts or floods are initiated in the spring, the resulting soil moisture anomaly can maintain, and in fact enhance, the anomalous storm track position and hence the anomalous

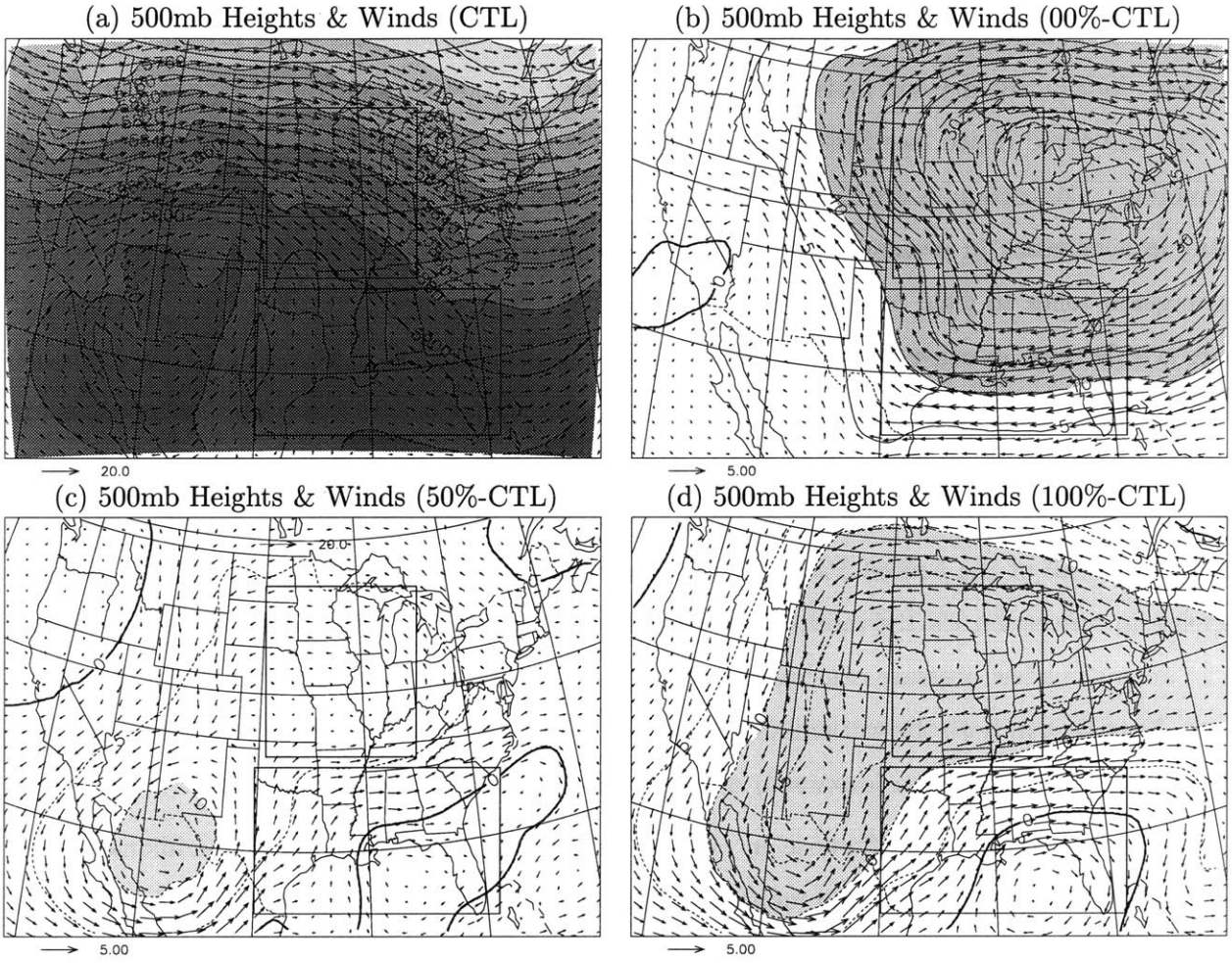

Figure 6-10: July simulated 500 mb wind vectors (m/s) and geopotential heights (m) climatology: (a) CTL; (b) 00%-CTL; (c) 50%-CTL; and (d) 100%-CTL. The soil moisture in each simulation is fully interactive and the FC80 closure assumption is used.

precipitation conditions. Note that the scale and magnitude of the soil moisture anomalies presented here are greater than what are observed in nature. Thus, in nature, it is possible that shifts of this magnitude are be unlikely.

Drier conditions tend to increase the intensity of the LLJ (Figure 6-11b), while wetter conditions result in a decrease in LLJ intensity (Figure 6-11f). Under anomalously wet conditions, there is an increase in lifting due to convection (not shown). This lifting tends to occur further upstream and hence degrades the LLJ flow. In contrast, under anomalously dry conditions, there is a reduction in lifting (convection) and hence a LLJ enhancement. Although, the LLJ is stronger and hence brings additional moisture from the Gulf of Mexico to the Great Plains and Midwest (not shown), the increase in stability over land inhibits most of the advected moisture from precipitating out. These mechanisms are different than those proposed by other such as Fast and McCorcle (1990), Paegle et al. (1996), Beljaars et al. (1996), and Bosilovich and Sun (1999).

In summary, in predicting summer precipitation over the Midwestern United States, it appears crucial to not only initialize soil moisture in the Midwest accurately, but also in the West. The contrasts in soil saturations between the two regions appears to be necessary to properly simulate the large-scale dynamics responsible for the rainfall peak observed over the upper Midwest.

Extreme Precipitation Events

In the summer of 1988, the United States Midwest experienced its warmest and driest summer since the dust-bowl era of the 1930s (Figure 6-12a; Ropelewski (1988)). In contrast, record high rainfall and flooding occurred and persisted over the Midwest throughout much of the summer during 1993 (Figure 6-12b; Kunkel et al. (1994)). This subsection investigates how the distribution of soil moisture impacts extreme precipitation events such as the aforementioned.

1988 Drought Figure 6-13 displays the simulated June 1988 precipitation for the CTL, CLM, 00%, 50%, and 100% simulations. In comparing this figure to the precipitation observations (Figure 6-12a), all of the simulations perform adequately in predicting the lack of precipitation observed over the United States. Each simulation (except for the 00%), predicts the extremely dry conditions south of the Great Lakes and the wetter conditions to the east and west. However, all of the simulations predict too much precipitation along the Gulf Coast. Arguably, the 100% simulation performs best in predicting the observed distribution of the precipitation because it is able to predict the precipitation along the Rocky Mountain States. The higher soil moisture over

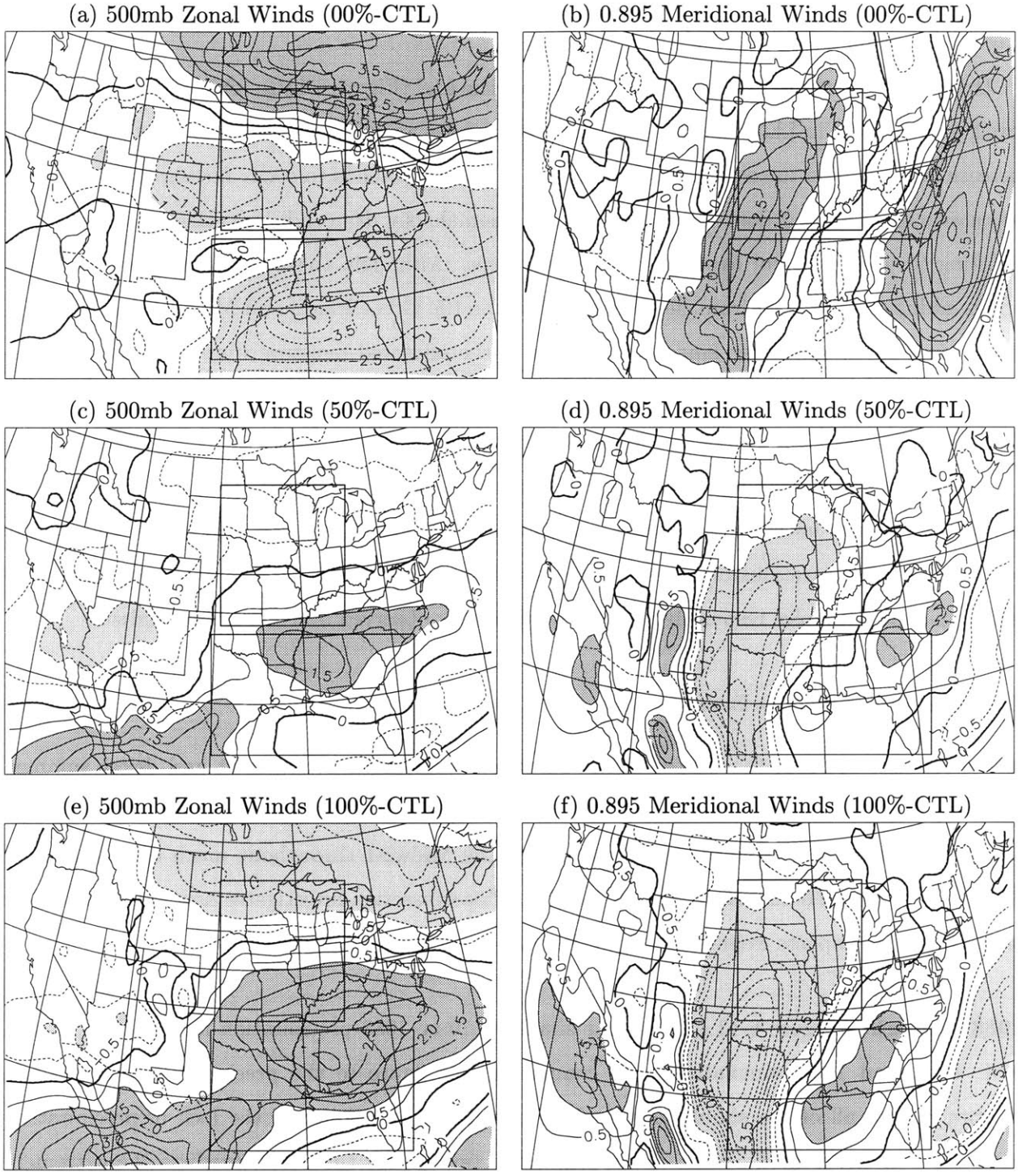

Figure 6-11: July differences between control and uniform simulated 500 mb zonal winds (m/s) and sigma 0.895 meridional winds (m/s). The soil moisture in each simulation is fully interactive and the FC80 closure assumption is used.

(a) June 1988 USHCN Precipitation

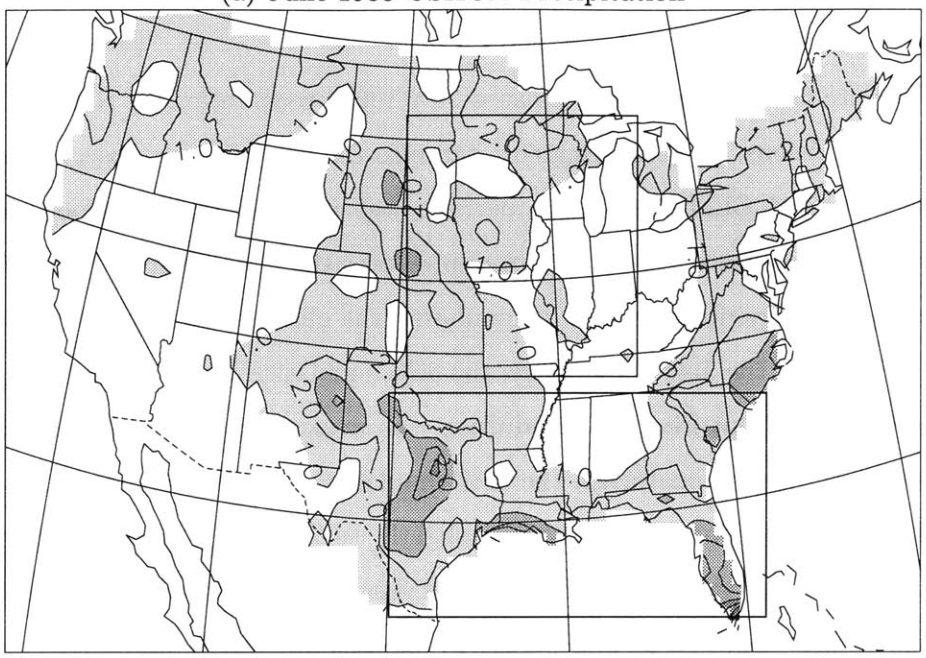

(b) July 1993 USHCN Precipitation

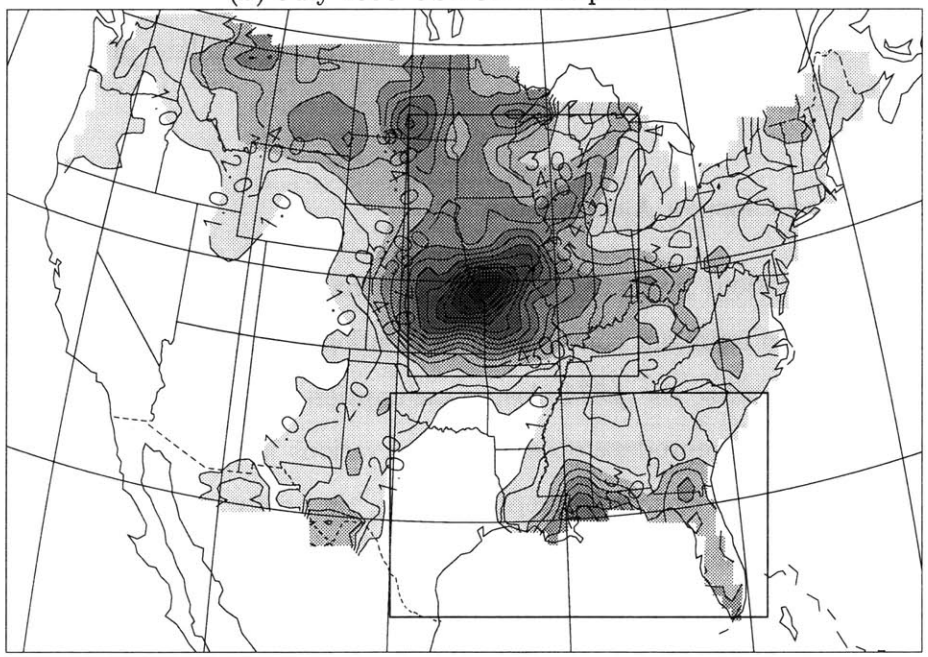

Figure 6-12: USHCN observations of precipitation (mm/day): (a) June 1988 and (b) July 1993. Note the USHCN observations only exist over the United States.

this region appears to be responsible for the higher rainfall. Overall, although the soil moisture-rainfall feedback is strong during June of 1988, it appears that knowledge of the soil moisture distribution does not significantly improve the predicted distribution of rainfall.

1993 Flood Figure 6-14 displays the simulated July 1993 precipitation for the CTL, CLM, 00%, 50%, and 100% simulations. In comparing this figure to the precipitation observations (Figure 6-12b), both the CTL and CLM simulations perform well in predicting the flood peak over the Midwest and in predicting the observed lack of rainfall over the Great Plains. None of the uniform soil moisture simulations perform as well in simulating the observed rainfall distribution over the United States. Similar to the July climatology, the 00% simulation predicts too little precipitation over the entire domain except Florida. In addition, the weak flood peak is shifted too far to the north. Contrary to the July climatology, the 50% simulation adequately predicts the distribution of rainfall. However, the flood peak is shifted slightly to the south of observed and is not as concentrated. Note that in the simulations of other years, the 50% runs do not perform as well. In the 100% simulation, the flood peak is predicted considerably south of observed and dissipated across the Gulf Coast. Overall, contrary to the June 1988 case, knowledge of the observed (or climatological) soil moisture conditions is crucial to accurately simulate precipitation over the Great Plains and Midwest in July of 1993.

Impact of Convective Closure Assumption

Thus far, all of the simulations presented in this chapter have used the FC80 closure assumption within the Grell scheme to represent convection. As mentioned in Chapter 4, most recent studies using the NCAR RegCM utilize the AS74 closure assumption. Also in Chapter 4, we found that the Grell Scheme's ability to reproduce observations of various hydrological fields depended to a certain extent on the choice of closure assumption. Here, we briefly investigate how the choice of convection scheme impacts the above findings.

In Figure 6-15, the predictions of precipitation with RegCM using the AS74 closure assumption are presented. Similar to the FC80 simulations (Figure 6-7), the AS74 CTL and CLM simulations perform better than the uniform soil moisture simulations in predicting the observed distribution of precipitation over the United States. Also similar to the FC80 simulations, there is considerable room for improvement. The CTL and CLM simulations tend to underestimate the peak over the Midwest and shift it too far to the north. This problem, common the AS74 closure assumption,

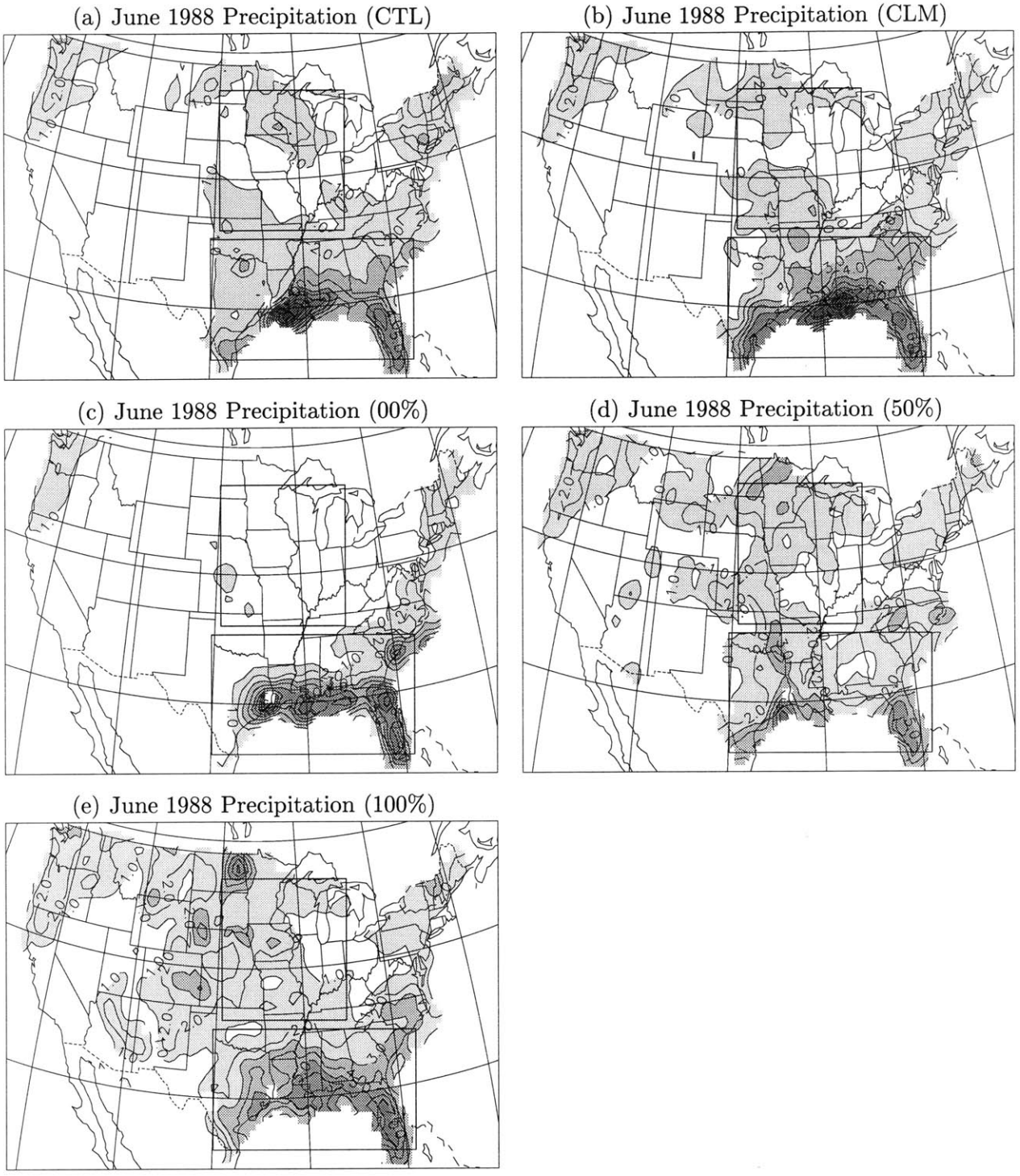

Figure 6-13: June 1988 simulated Precipitation (mm/day) for the following simulations: (a) CTL, (b) CLM (c) 00%, (d) 50%, and (e) 100%. The soil moisture in each simulation is fully interactive and the FC80 closure assumption is used. The initial soil moisture fraction is indicated at the top of each plot. The contour interval is specified at 1 mm/day and shading occurs at values above 1 mm/day and at intervals of 2 mm/day. Note that only values for the United States are displayed.

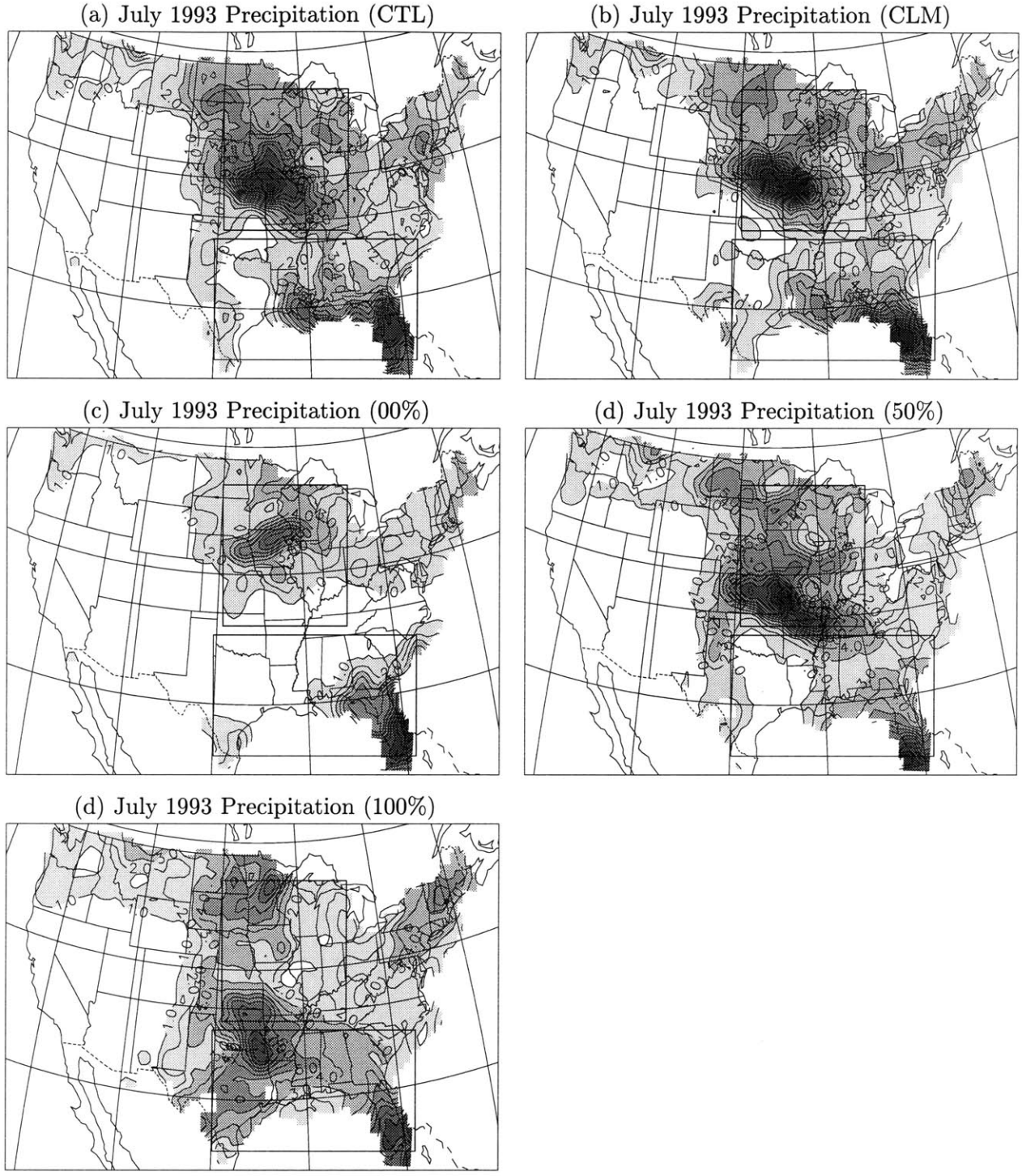

Figure 6-14: July 1993 simulated Precipitation (mm/day) for the following simulations: (a) CTL, (b) CLM (c) 25%, (d) 75%, and (e) 100%. The soil moisture in each simulation is fully interactive and the FC80 closure assumption is used. The initial soil moisture fraction is indicated at the top of each plot. The contour interval is specified at 1 mm/day and shading occurs at values above 1 mm/day and at intervals of 2 mm/day. Note that only values for the United States are displayed.

is discussed in detail in Section 4.3.4. Lastly, the soil moisture-rainfall exhibits similar strength to the FC80 simulations. However, the distribution of rainfall in wetter simulations (50% and 100%) is considerably different in the AS74 simulations.

Figure 6-16 displays the difference in 500 mb zonal winds and sigma 0.895 meridional winds between the AS74 CTL and AS74 uniform soil moisture integrations. Like the FC80 simulations (Figure 6-11), there is a storm track shift from north to south as soil moisture increases from dry to wet. Also similar to the FC80 simulations, soil moisture has a pronounced impact on the strength of the LLJ. Wetter conditions tend to weaken the LLJ. However, the dry simulation (00%) has a relatively minor impact on the strength of the LLJ. This finding is inconsistent with the FC80 simulations where drier soil moisture conditions result in a significant intensification of the LLJ.

Overall, the general findings between the AS74 and FC80 simulations are consistent. However, some differences exist.

6.4.2 Local Effects of Soil Moisture in the Midwest

In Figure 6-7, we saw that over most of North America a significant positive feedback between soil moisture and precipitation exists. However, the soil moisture anomalies that were introduced in these simulations are on a scale that is unlikely to be observed in nature. In this subsection we investigate the local impacts of soil moisture on the Midwest much like we did in Chapter 5 except with a large domain. To do so, we perform an additional set of experiments using the observed distribution of soil moisture over the entire domain except for an isolated region in the Midwest where the soil moisture is held fixed at 25% of saturation (see Section 6.3).

Figure 6-17 indicates that drying the soil saturation over the Upper Midwest region tends to result in a significant reduction (light shading) in precipitation between 105°W and 87°W. Although the dry soil moisture anomaly is limited to the Upper Midwest, lower precipitation occurs in all regions surrounding the anomaly (particularly to the south). Along the eastern Seaboard states (east of 87°W), there is a general increase in precipitation (dark shading).

Chapter 5 provides a detailed description of the soil moisture-rainfall feedback mechanism. Thus, only a brief summary is provided here. It is well documented that anomalously dry soil moisture conditions are associated with anomalously warm temperatures and low humidities at or near the surface via an increase in sensible heat flux and a decrease in latent heat flux. With this in mind, anomalously dry soil moisture conditions suggest a decrease in net surface longwave radiation via an increase in outgoing longwave (Stefan-Boltzmann Law) and a decrease in the

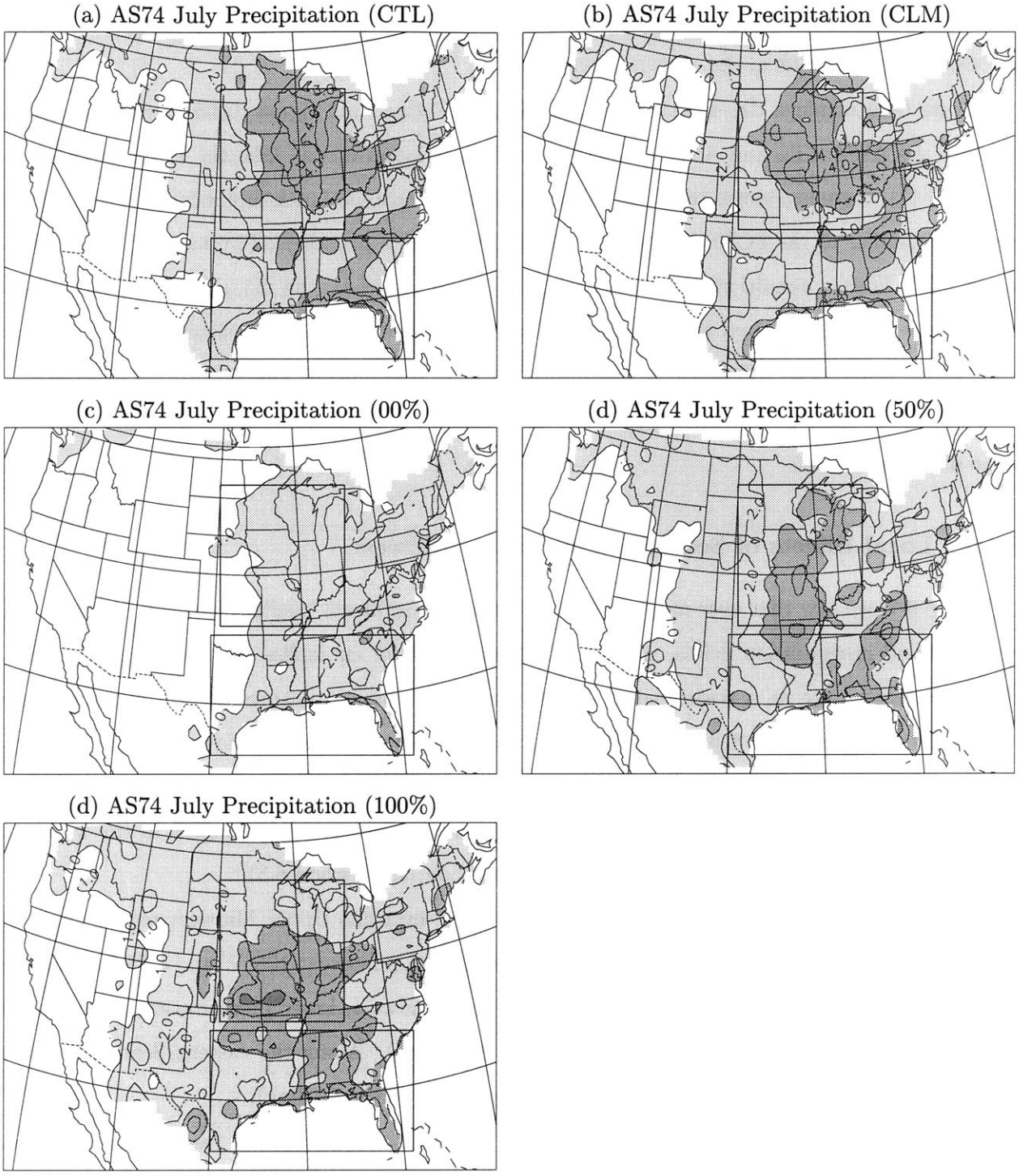

Figure 6-15: July simulated Precipitation (mm/day) for the following simulations: (a) CTL, (b) CLM (c) 25%, (d) 75%, and (e) 100%. The soil moisture in each simulation is fully interactive and the AS74 closure assumption is used. The initial soil moisture fraction is indicated at the top of each plot. The contour interval is specified at 1 mm/day and shading occurs at values above 1 mm/day and at intervals of 2 mm/day. Note that only values for the United States are displayed.

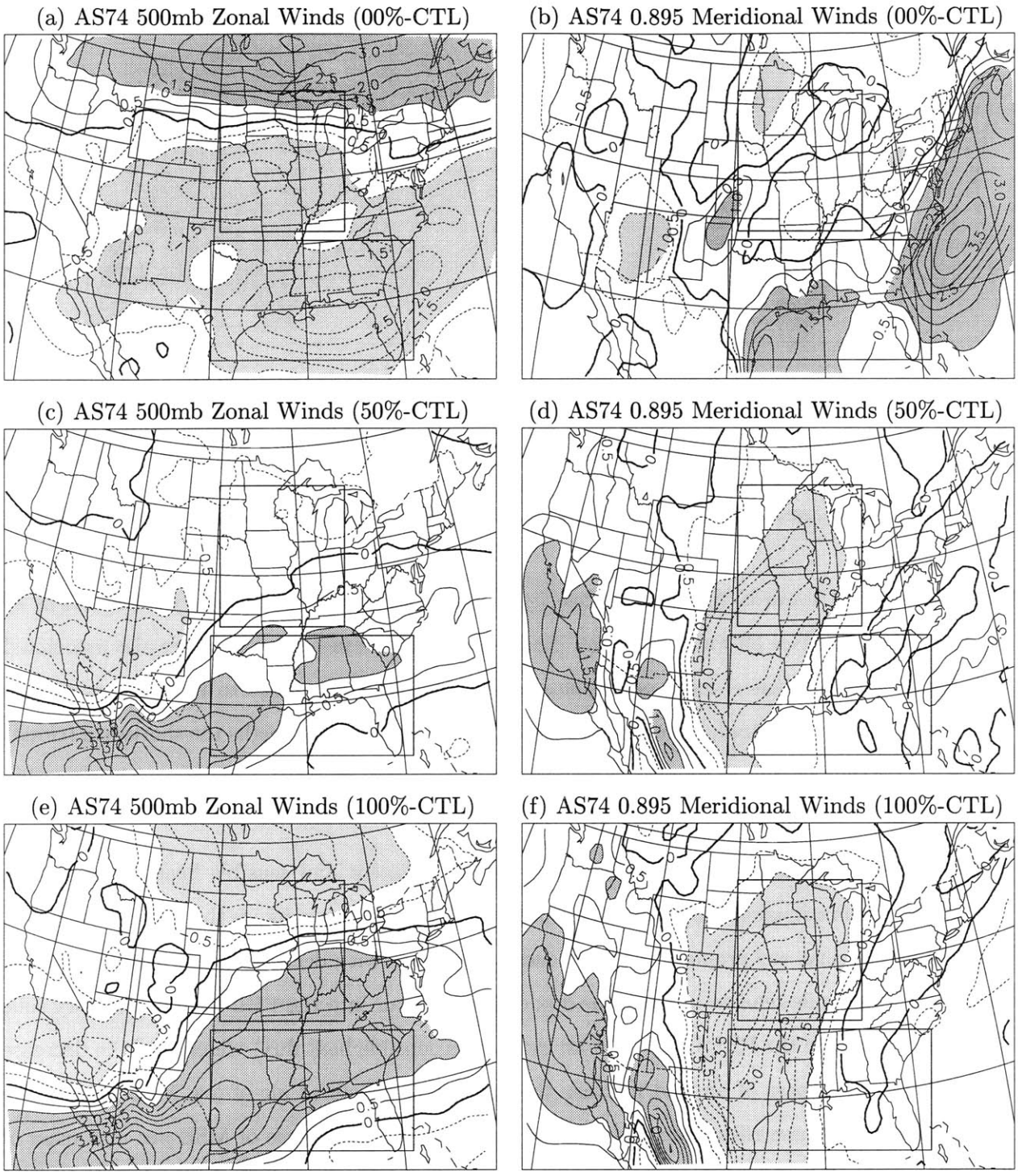

Figure 6-16: July differences between control and uniform simulated 500 mb zonal winds (m/s) and sigma 0.895 meridional winds (m/s). The soil moisture in each simulation is fully interactive and the AS74 closure assumption is used.

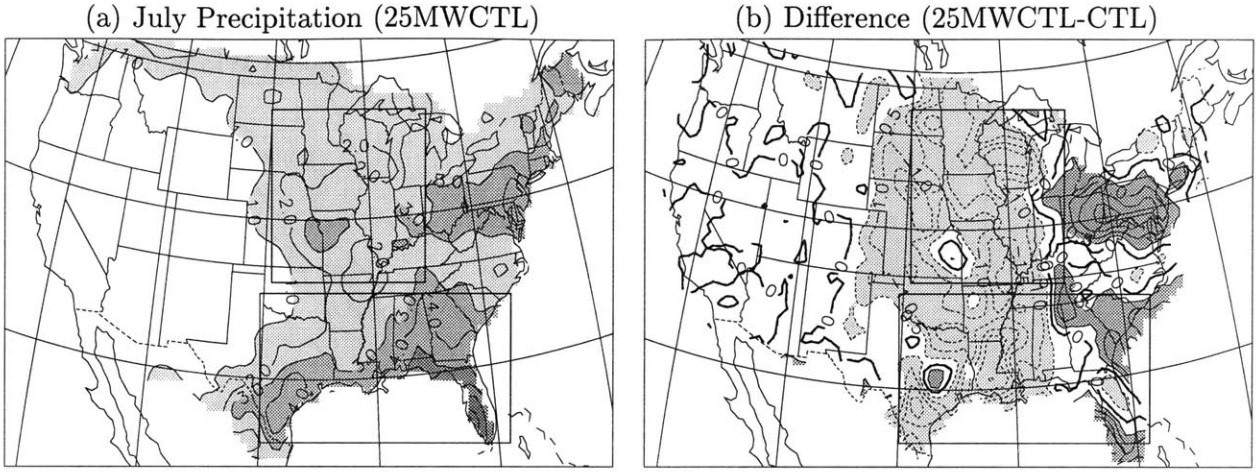

Figure 6-17: July simulated Precipitation Climatology (mm/day) for the (a) 25MWCTL simulations and (b) difference between the 25MWCTL and the CTL simulations. The soil moisture in each is initialized according to the merged HDG/ISWS dataset and is fully interactive except in the 25MWCTL simulations over the Midwest region where the soil saturation is held constant at 25%. The FC80 closure assumption is used. Note that only values for the United States are displayed.

longwave emitted towards the land surface (greenhouse effect for water vapor). This tends to decrease the net surface all-wave radiation. Anomalously dry surface conditions are also associated with less clouds and hence, more net surface solar radiation which tends to increase net surface all-wave radiation. We found, however, that the longwave feedback outweighs the shortwave (cloud) feedback and thus results in an overall decrease in net surface all-wave radiation with increasing soil moisture.

Net surface radiation nearly balances the sum of the latent and sensible heat fluxes at long time scales. The residual of the balance (ground heat flux) tends to enhance the soil moisture-heat flux feedback in that the ground heat flux tends to decrease with decreasing soil moisture. Thus, anomalously dry soils tend to increase the flux of low MSE air into the PBL from below. Dry soils also tend to increase the PBL height (via an increase in sensible heat flux) which tends to decrease the MSE per unit mass of air and increase the amount of entrained air of low MSE from above the PBL. Each of these effects are additive and contribute to a decrease of MSE per unit mass of PBL air when soil moisture decreases. A decrease in the MSE of the PBL tends to decrease the likelihood of occurrence of convective rainfall. All of these factors (except the cloud feedback) work in the same direction and result in a positive feedback between soil moisture and rainfall.

Figure 6-18 compares 25MWCTL simulations to the CTL simulations and attempts to breakdown each of the major links of the soil moisture-rainfall feedback. Strikingly the perturbed

Midwest region stands out in each field displayed. Figure 6-18a shows that longwave feedback dominates the shortwave feedback and results in an overall decrease in net surface all-wave radiation of around 20 W/m^2 by decreasing soil moisture over the upper Midwest. This decrease is translated to the sum of the latent and sensible heat fluxes where a decrease of approximately $25W/m^2$ is observed (Figure 6-18b). The 5 W/m^2 difference between the net radiation and the latent plus sensible heat flux is attributed by a decrease in the ground heat flux by (not shown). Both the increase in heat flux from below the PBL and the deeper more turbulent PBL result in a decrease in the low-level moist static energy (Figure 6-18c). These effects combine to result in a decrease in atmospheric stability and hence a decrease in convective rainfall (Figure 6-18d).

This decrease in convective rainfall, however, is not limited to the perturbed region as it is with the net radiation, total heat flux, and MSE. Thus, the soil moisture conditions influence precipitation on a larger scale than described above (and in Chapter 5). Strikingly, the precipitation significantly decreases from the climatology to the south (upstream along the LLJ) of the perturbed region. To investigate the reasons for this phenomena, we look to the dynamics. Figure 6-19a shows the difference in 500 mb geopotential heights (contours) and winds (vectors) between the CTL and 25MWCTL simulations. The anomalous subsidence resulting from the dry soil moisture anomaly over the upper Midwest results in an anomalous high pressure and hence anomalous anticyclonic flow. It appears from Figure 6-19b that the decrease in latent heat flux outweighs the minimal increase in LLJ flow and results in a decrease in low-level humidity.

Figure 6-20 shows the difference in 500 mb zonal winds and sigma 0.895 meridional winds between the CTL simulations and the 25MWCTL simulations. Similar to the simulations with domain-wide drying, the 25MWCTL simulations result in a northward shift in the storm track resulting from anomalous anticyclonic flow and an increase in the strength of the LLJ. However, both of these features are not as pronounced in the 25MWCTL simulations. It appears the anomalous descending motion over the upper Midwest region from the decrease in convection causes an anomalous high pressure. This in turn results in anomalous anticyclonic flow causing a northward shift in the storm track. Shifting the storm track north tends to reduce the likelihood of occurrence of storm south of the anomaly (which is upstream of the LLJ flow). Note that this shift tends to decrease the non-convective precipitation over the Great Plains and Midwest (not shown) since the storm track is often associated with non-convective precipitation. Lastly, the anomalous flow pattern helps to enhance the dry soil moisture anomaly over the upper Midwest.

In summary, the mechanisms through which soil moisture impacts precipitation over the

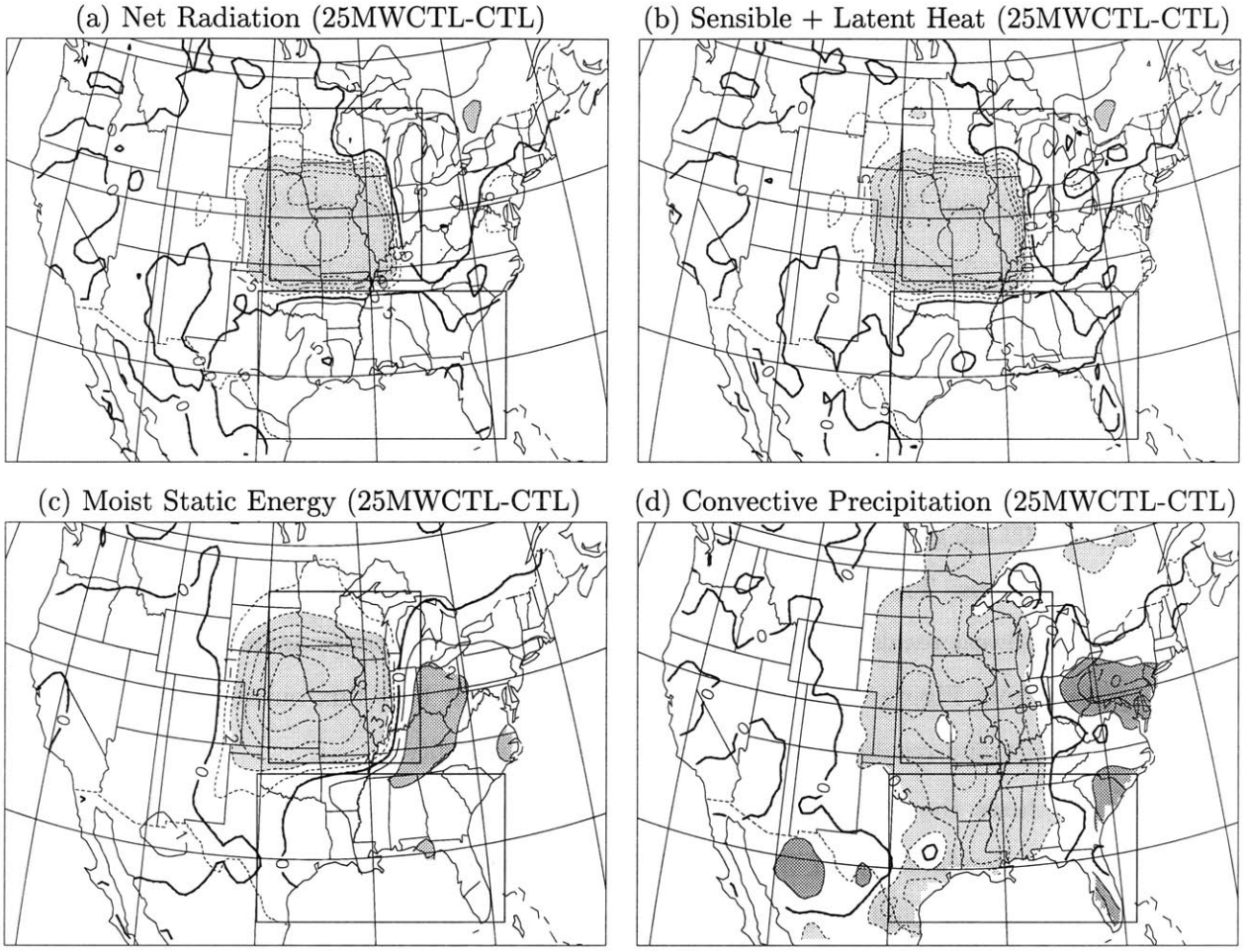

Figure 6-18: July simulated surface climatology difference between the 25MWCTL and CTL simulations: (a) net surface all-wave radiation (W/m^2); (b) surface sensible + latent heat flux longwave (W/m^2); (c) Sigma 0.995 moist static energy (kJ/kg); and (d) convective precipitation (mm/day). The soil moisture in each is initialized according to the merged HDG/ISWS dataset and is fully interactive except in the 25MWCTL simulations over the Midwest region where the soil saturation is held constant at 25%. The FC80 closure assumption is used. Note that only values over land are displayed.

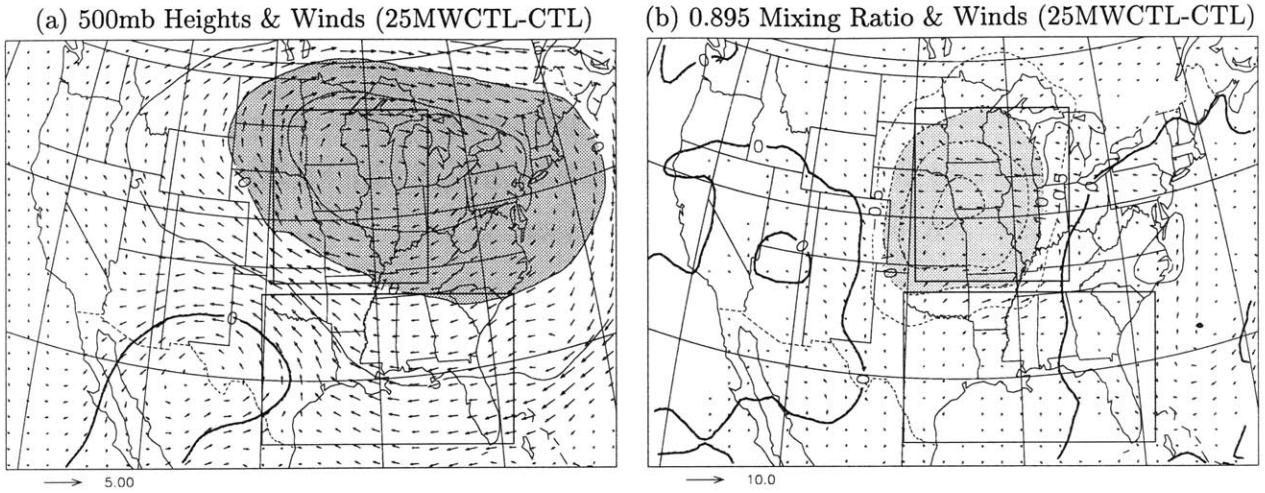

Figure 6-19: July differences between CTL and 25MWCTL simulated (a) 500 mb geopotential heights (m) and winds ($\overrightarrow{5.00}$ m/s) and (b) sigma 0.895 mixing ratio (g/kg) and winds ($\overrightarrow{10.0}$). The soil moisture in each is initialized according to the merged HDG/ISWS dataset and is fully interactive except in the 25MWCTL simulations over the Midwest region where the soil saturation is held constant at 25%. The FC80 closure assumption is used.

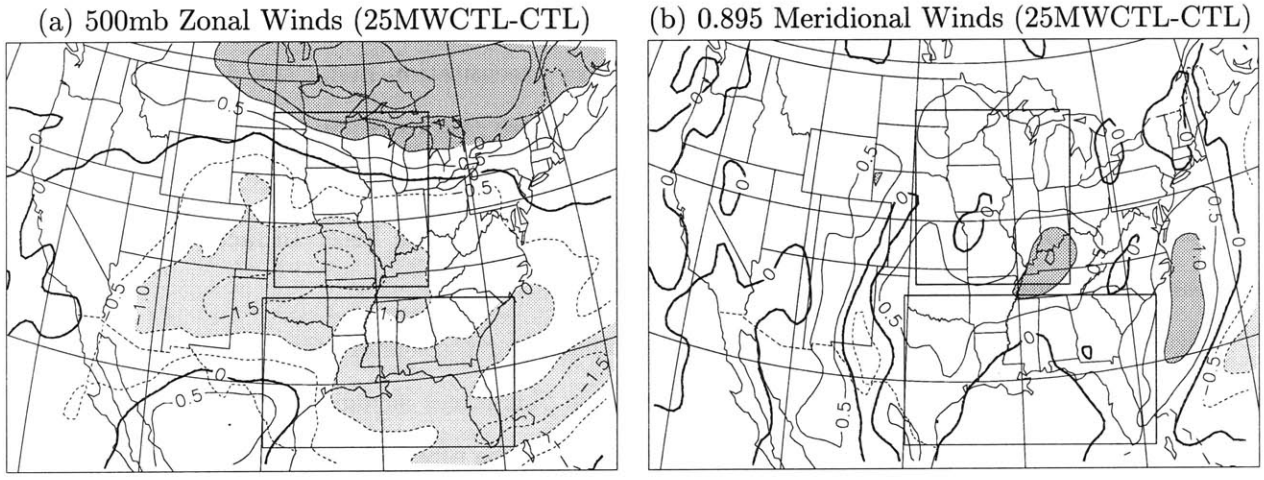

Figure 6-20: July differences between CTL and 25MWCTL simulated (a) 500 mb zonal winds (m/s) and (b) sigma 0.895 meridional winds (m/s). The soil moisture in each is initialized according to the merged HDG/ISWS dataset and is fully interactive except in the 25MWCTL simulations over the Midwest region where the soil saturation is held constant at 25%. The FC80 closure assumption is used.

Midwest are consistent with, but not limited to, the theory presented in Chapter 5. An additional mechanism which is not present in the small domain simulations is introduced in that there is a storm track shift that tends to enhance the soil moisture-rainfall feedback. This mechanism appears to cause the precipitation anomaly to propagate outside of the perturbed region. In the case presented here, a dry perturbation not only leads to drought conditions over the perturbed upper Midwest region, but also to the Great Plains region.

6.4.3 Effects of Soil Moisture in the Western Gulf Coast on the Midwest

Here we investigate how anomalous soil moisture conditions in the western Gulf Coast region impact precipitation in the Midwest. To do so, much like the above experiments, we perform experiments using the observed distribution of soil moisture over the entire domain except for an isolated region in the western Gulf Coast region where the soil moisture is held fixed at 25% of saturation. This region lies to the south of the upper Midwest which is upstream of the LLJ flow. By performing this set of experiments, we can determine the impact that drying upstream of the Midwest has on the precipitation in the Midwest and surrounding regions.

Similar to the upper Midwest experiments seen above, a dry perturbation to the western Gulf Coast region results in a decrease in precipitation not only over the perturbed region, but also over the surrounding regions particularly to the north and east (Figure 6-21). Also similar to the 25MWCTL simulations, there is an increase in precipitation along the Atlantic Seaboard states. Given that a significant amount of moisture in these regions originates from outside of the United States, one might expect that the reduced precipitation over the upstream Gulf Coast might precipitate out downstream over the Midwest. This is not the case here. In fact, the anomalous dry conditions tend to propagate into the Midwest.

Figure 6-22 shows that the dry soil moisture anomaly over the western Gulf Coast region results in a decrease in net surface all-wave radiation, sensible plus latent surface heat fluxes, moist static energy, and convective rainfall over the perturbed region. The physical mechanisms responsible for these changes are similar to 25MWCTL simulations and those presented in Chapter 5.

The increase in subsidence associated with the decrease in convection results in anomalous anticyclonic flow (Figure 6-23). Surprisingly, this widespread anomaly extends northward into Canada where there is cause an intensification of the storm track. Since the storm track does not typically exist in the region of the soil moisture perturbation (see Figure 6-10a), there is little change in the strength of the storm track over the United States. In addition, the anomalously dry

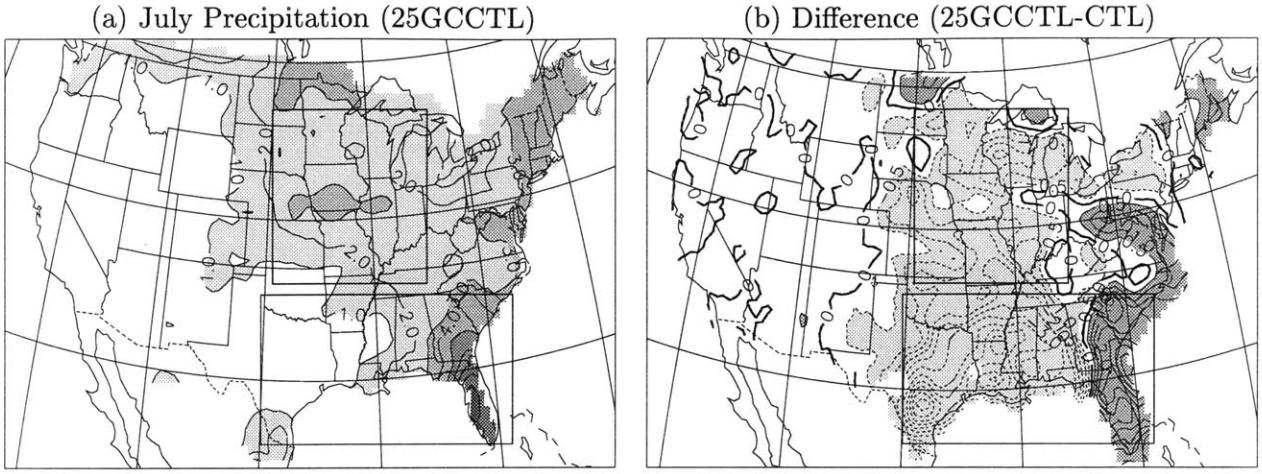

Figure 6-21: July simulated Precipitation Climatology (mm/day) for the (a) 25GCCTL simulations and (b) difference between the 25GCCTL and the CTL simulations. The soil moisture in each is initialized according to the merged HDG/ISWS dataset and is fully interactive except in the 25GCCTL simulations over the western Gulf Coast region where the soil saturation is held constant at 25%. The FC80 closure assumption is used. Note that only values for the United States are displayed.

conditions over the western Gulf Coast are advected into the Midwest region via the LLJ.

In summary, the mechanisms through which soil moisture impacts precipitation over the western Gulf Coast are consistent with, but not limited to, the theory presented in Chapter 5. Like the dry Midwest experiments, the impacts of soil moisture on the large-scale dynamics also prove to be important in determining rainfall in the surrounding regions. The changes to the large-scale circulation appears to cause the precipitation anomaly to propagate outside of the perturbed region. In the case presented here, the dry perturbation not only leads to drought conditions over the perturbed upper western Gulf Coast region, but also to the Midwest region.

6.4.4 Effects of Soil Moisture in the Southwest on the Midwest

As mentioned in Section 6.2, the soil moisture conditions in the Southwest have been hypothesized to have an impact on precipitation in the Great Plains and Midwest. This subsection investigates how anomalously wet conditions in the Four Corners States impact precipitation over the Midwest. To do so, a series of simulations are performed where the soil saturation in Colorado, Utah, New Mexico, and Arizona is held fixed at 75%.

Figure 6-24a displays the precipitation distribution climatology of the 75SWCTL experiments and Figure 6-24b displays its difference with the CTL simulations. As expected, an increase in

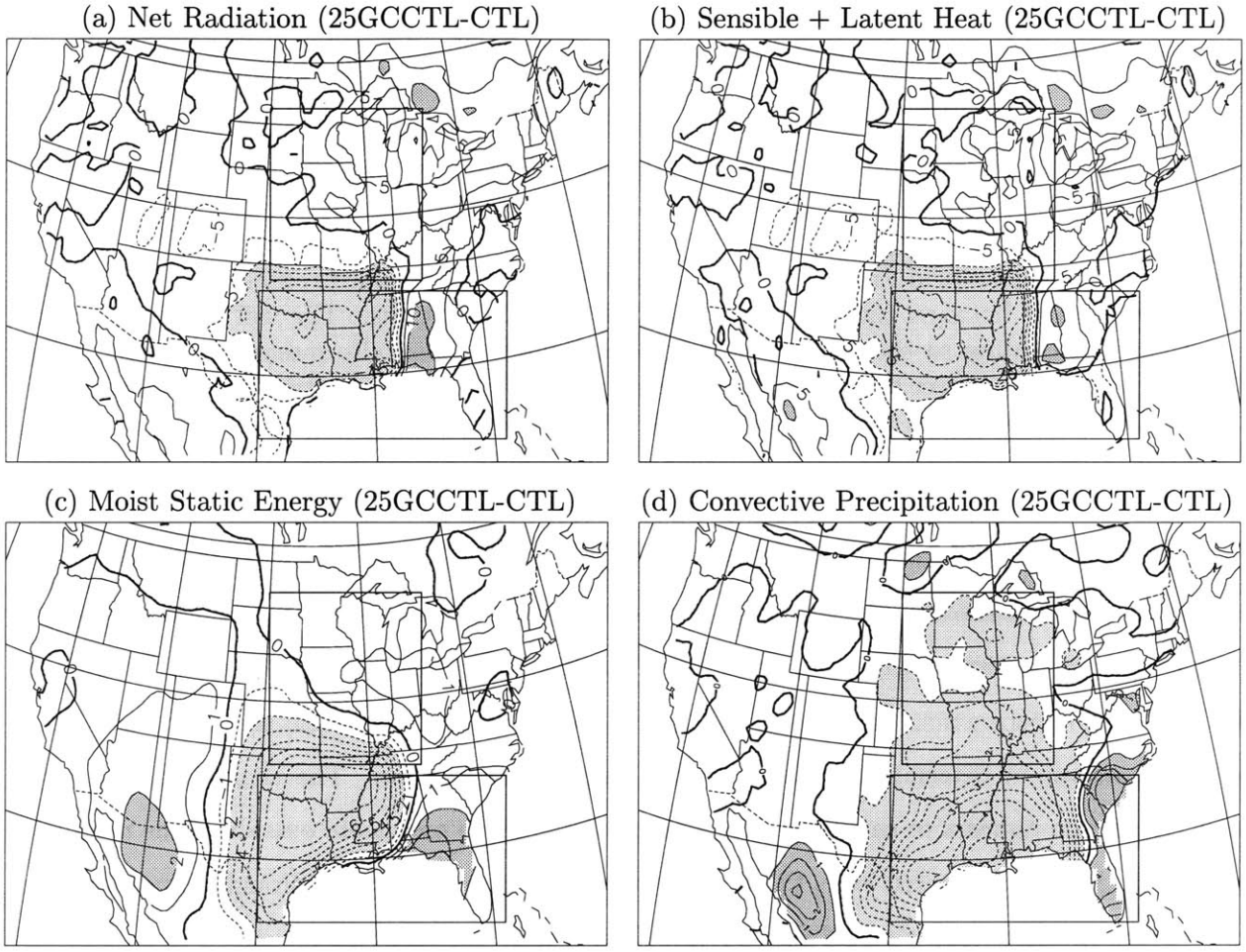

Figure 6-22: July simulated surface climatology difference between the 25GCCTL and CTL simulations: (a) net surface all-wave radiation (W/m^2); (b) surface sensible + latent heat flux longwave (W/m^2); (c) Sigma 0.995 moist static energy (kJ/kg); and (d) convective precipitation (mm/day). The soil moisture in each is initialized according to the merged HDG/ISWS dataset and is fully interactive except in the 25GCCTL simulations over the Midwest region where the soil saturation is held constant at 25%. The FC80 closure assumption is used. Note that only values over land are displayed.

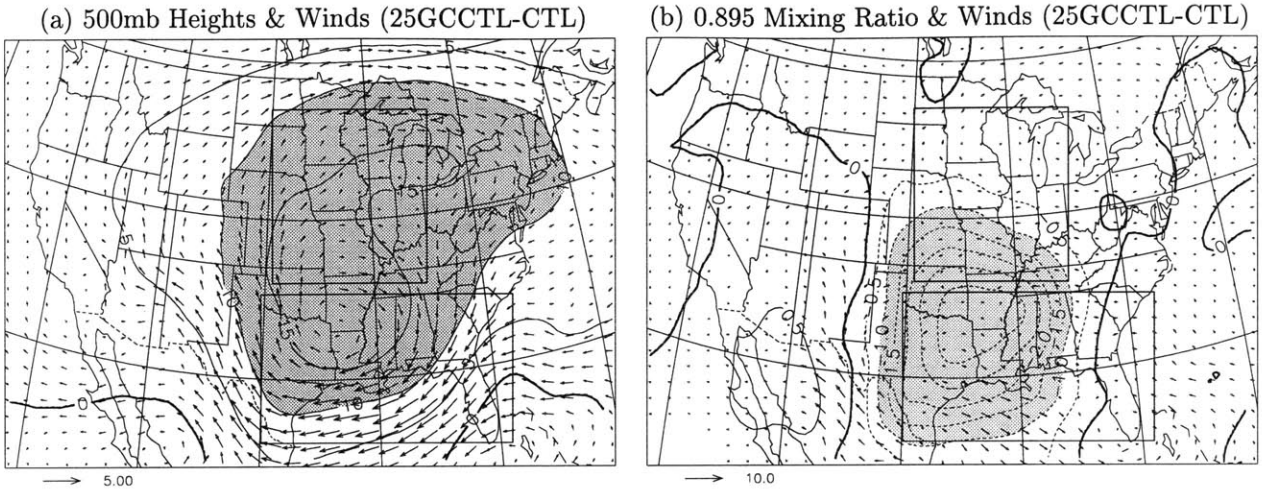

Figure 6-23: July differences between CTL and 25GCCTL simulated (a) 500 mb geopotential heights (m) and winds ($\overrightarrow{5.00}$ m/s) and (b) sigma 0.895 mixing ratio (g/kg) and winds ($\overrightarrow{10.0}$). The soil moisture in each is initialized according to the merged HDG/ISWS dataset and is fully interactive except in the 25GCCTL simulations over the Midwest region where the soil saturation is held constant at 25%. The FC80 closure assumption is used.

soil moisture over the Four Corners States results in a significant increase in precipitation over the same region. However, strikingly, the soil moisture anomaly results in a significant increase in precipitation in the Gulf Coast States (except for southern Florida and southern Texas) and a significant decrease in precipitation in the Midwestern states. From these results, it appears that soil moisture in the Southwest has a pronounced impact on the distribution of precipitation east of the 100°W meridian. The remaining portion of this subsection investigates the mechanisms responsible for these changes in rainfall. The local mechanisms through which soil moisture impacts precipitation over the Four Corners region are similar to those presented in the 25MWCTL and 25GCCTL simulations (Sections 6.4.2 and 6.4.3, respectively). Thus, they are not presented here.

The wet soil moisture anomaly over the Four Corners States impacts the large-scale dynamics by creating an anomalous lifting mechanism induced by an increase in convection. The anomalous lifting generates a low pressure and hence cyclonic flow (see Figure 6-25a). Unexpectedly, the anomalous 500 mb flow associated with the soil moisture perturbation is larger than the observed when initializing the model at 100% of saturation across the entire domain. Part of the reason of the stronger response is because soil saturation is fixed over the perturbed region in the 75SWCTL simulations, while it is not in the 100% runs. This response, however, is only slightly more pronounced when soil moisture is held fixed at 100% of saturation over the entire domain (not shown).

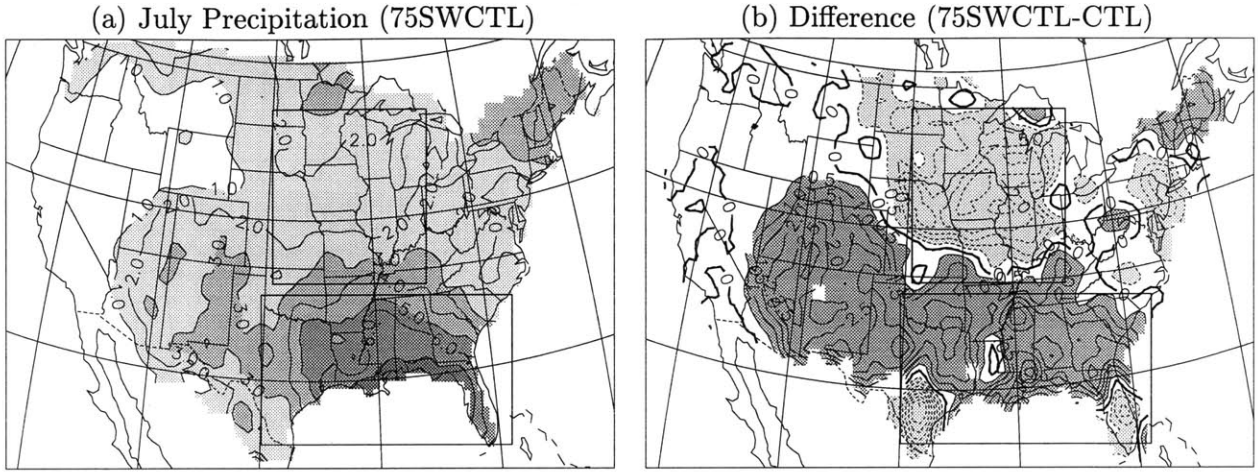

Figure 6-24: July simulated Precipitation Climatology (mm/day) for the (a) 75SWCTL simulations and (b) difference between the 75SWCTL and the CTL simulations. The soil moisture in each is initialized according to the merged HDG/ISWS dataset and is fully interactive except in the 75SWCTL simulations over the western Gulf Coast region where the soil saturation is held constant at 75%. The FC80 closure assumption is used. Note that only values for the United States are displayed.

The anomalous flow, much like the 75% and 100% simulations, causes a weakening of the northern portions of the storm track and an extension of the storm track southward. At lower levels, the westerly air flowing over the Mexican Plateau becomes anomalously moist and cool due to the wet soil moisture anomaly (Figure 6-25b). This tends to result in a significant weakening of the capping inversion over the LLJ. Thus, moist convection is more apt to occur over the Great Plains and Gulf Coast. The resulting anomalous convection extends the low pressure anomaly further to the east across the Gulf Coast. In addition, the anomalous lifting has a tendency to degrade the LLJ. Lastly, the enhanced lifting over the Gulf Coast causes divergence in the Midwest and thus a reduction in precipitation.

In summary, the soil moisture in the Southwest exerts a significant control in determining the location of precipitation in the Great Plains and Midwest. Anomalously wet conditions in the Southwest tend to shift the precipitation from the upper Midwest into the Gulf Coast region. This shift results in drought-like conditions in the upper Midwest and flood-like conditions in the Gulf Coast in addition to the perturbed Southwest region.

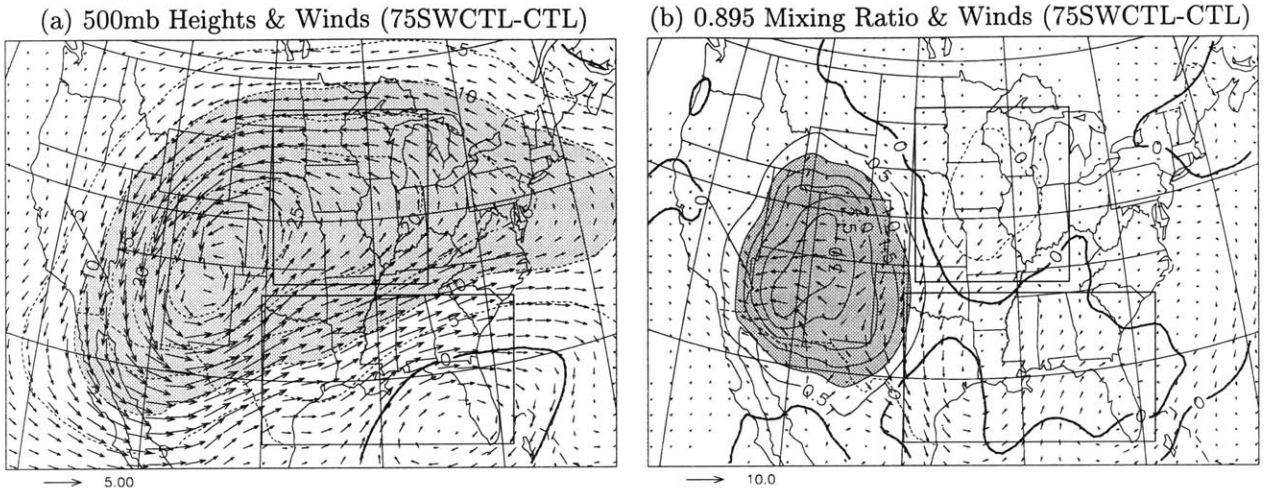

Figure 6-25: July differences between CTL and 75SWCTL simulated (a) 500 mb geopotential heights (m) and winds $\overrightarrow{(m/s)}^{5.00}$ and (b) Sigma 0.895 mixing ratio (g/kg) and $\overrightarrow{\text{winds}}^{10.0}$. The soil moisture in each is initialized according to the merged HDG/ISWS dataset and is fully interactive except in the 75SWCTL simulations over the Midwest region where the soil saturation is held constant at 75%. The FC80 closure assumption is used.

6.5 Discussion of Results

As mentioned in Chapter 1, summer droughts and floods over the United States are typically associated with storm track shifts to the north and south, respectively. However, the exact causes of extreme summertime flood and drought are relatively unknown. On one hand, Trenberth and Guillemot (1996) conclude that the cause of the drought of 1988 and flood of 1993 were related to La Niña and El Niño, respectively. On the other hand, Bell and Janowiak (1995) argue that anomalous SSTs in the tropical Pacific indirectly contributed to overall magnitude and extent of the 1993 flood. However, they state that no single factor alone caused the flooding. Furthermore, Namias (1991) argues that the La Niña observed in 1988 may have contributed to the drought, but was not the primary cause of the drought. Trenberth and Guillemot (1996) and Namias (1991) both agree that soil moisture may play an important role in the increasing persistence of flood and drought. In this thesis, we find that soil moisture does indeed increase the persistence and magnitude of rainfall anomalies. A least some of the increase in the persistence and magnitude of rainfall anomalies results from a shift storm track location. Under anomalously dry conditions, the shift is to the north and under anomalously wet conditions, the shift is to the south. Not only do these shifts enhance the anomalous rainfall conditions, they are also consistent with the above observational studies.

Trenberth et al. (1988) show that the storm track location in April of 1988 was shifted far north of normal. Similarly, Bell and Janowiak (1995) show that the large-scale circulation patterns in the early-spring of 1993 fostered the southward storm track shift in June and July of 1993 and thus the onset of flooding. The anomalous soil moisture conditions in both 1988 and 1993 were in place by April (see Figure 1-3). However, Findell and Eltahir (1997) show that the soil moisture-rainfall feedback over Illinois is insignificant other than during the late-spring and summer. Soil moisture's impact on the initiation of these events is likely to be minimal. However, as these events continue into the late-spring and summer, the soil moisture-rainfall feedback becomes increasingly important. Thus, the anomalous circulations associated with changes in soil moisture act to enhance the large-scale circulation anomalies and increase the persistence. Furthermore, the local impacts of soil moisture also add to the persistence of the events.

As mentioned in Section 6.2, Namias (1982) and Namias (1991) speculate that the anomalously dry soil moisture conditions associated with drought are likely to play a role in the persistence of drought by strengthening and anchoring the anticyclones associated with drought. He argues that the increase in sensible heating encourages the growth of an upper-level high via an increase in surface temperature. The results from this thesis support the observational studies of Namias in that dry soil moisture conditions over the United State results in anomalous anticyclonic flow. However, we disagree with the mechanisms. Here, rather than anomalous high pressure resulting from an increase in surface temperature, we find that the anomalous high pressure results from an increase in subsidence (decrease in convection) due to the mechanisms discussed in Chapter 5. Here we find that anomalously dry soil moisture conditions not only sustain the anticyclonic flow, but they enhance the anticyclonic flow.

Over oceans, precipitation and SST are positively correlated; an increase in SST tends to result in an increase precipitation. Over tropical and summer hemisphere oceans, warm SSTs typically result in an increase in convective activity (rapid lifting). This increase in lifting tends to yield a low pressure anomaly. In this thesis, we found that anomalous wet soil moisture conditions have the same effect as warm SSTs in that they tend to be associated with an increase in convective activity and hence lower pressure.

In an observational study, Higgins et al. (1997a) show that Southwest summer precipitation is characterized by an out-of-phase relationship with the Great Plains-northern tier and in-phase relationship with the East Coast. The findings here are somewhat consistent with the work of Higgins et al. (1997a). Our experiments with a dry perturbation over the Midwest (25MWCTL)

and the western Gulf Coast (25GCCTL) are both consistent although precipitation in the Southwest only slightly increases in these scenarios. However, a wet perturbation over the Southwest (75SWCTL) yields and increase in precipitation over the southern half of the United States and a decrease over the northern half.

6.6 Summary of Results and Conclusions

In this chapter, we investigate the local and remote physical pathways and mechanisms responsible for the soil moisture-rainfall feedback in the Midwest during the summer using a modified version of the NCAR RegCM. In many ways, this chapter is similar to Chapter 5. The primary difference is that a larger domain is used to allow the large-scale dynamics to respond to changes in soil moisture. The following lists the four issues addressed in this chapter and their associated conclusions.

(1) What is the importance of initializing soil moisture according to the observations? Experiments suggest that the domain-wide spatial variations in soil moisture are crucial to accurately reproduce precipitation in the Midwest. The interannual temporal variations of soil moisture prove to be less important.

(2) What are the local impacts of soil moisture in the Upper Midwest? The mechanisms through which soil moisture impacts precipitation over the Midwest are consistent with, but not limited to, the local theory of the soil moisture-rainfall feedback presented in Chapter 5. Soil moisture also has a pronounced impact on the large-scale dynamics which tends to induce a storm track shift that tends to enhance the soil moisture-rainfall feedback. A dry perturbation tends to shift the storm track to the north and result in drought conditions not only over the perturbed upper Midwest region, but also over the Great Plains region.

(3) How does a dry anomaly upstream of the Midwest (western Gulf Coast) impact precipitation in the Midwest? Like the anomalous Midwest experiments, the impacts of soil moisture on the large-scale dynamics also prove to be important in determining rainfall in the surrounding regions. A dry anomaly upstream extends the anomaly downstream into the Midwest causing drought conditions in the Great Plains and Midwest.

(4) How does anomalous wetting in the Southwest impact precipitation in the Midwest? The soil moisture in the Southwest exerts a significant control in determining the location of precipitation in the Great Plains and Midwest. Anomalously wet conditions in the Southwest tend to shift the precipitation peak from the Midwest into the Gulf Coast region. This shift results in drought-like

conditions in the upper Midwest and flood-like conditions in the Gulf Coast.

Chapter 7

Summary of Results and Conclusions and Future Work

In this thesis we investigate the pathways and mechanisms responsible for the soil moisture-rainfall feedback using a regional climate model. This thesis is divided into two parts. In Part I, we focus on the development and verification of the NCAR RegCM. In the second part, we implement the tool developed in Part I to study the soil moisture-rainfall feedback mechanism over North America.

7.1 Model Development

To investigate the pathways and mechanisms of the soil moisture-rainfall, we first identify and improve upon some of the deficiencies within the regional climate model. These improvements include modifications to the model physics in addition to the model forcing.

7.1.1 Modifications to the Model Input

Significant improvements are made to the specification of the initial and boundary conditions of the atmospheric and biospheric variables. The atmospheric initial and boundary conditions are now provided by the NCEP Reanalysis data. The consistent use of the numerical model and high temporal resolution of the NCEP reanalysis product provide significant improvements over the ECMWF non-reanalysis product used in many previous RegCM applications. In addition, improvements to the interpolation procedure of the boundary conditions are made to correct for the Gibbs phenomena. The SSTs are now prescribed using UKMO SST data which are based on in-situ and AVHRR satellite observations. The vegetation is now specified using USGS-GLCC data

which is derived from AVHRR satellite observations. A new soil moisture dataset is presented that merges soil moisture data from the ISWS, HDG, and climatology based on the vegetation type. Lastly, generality has been added to the Mercator map projection so that the deviation of the map-scale factors from unity is minimized. All of these modifications improve the sensitivity of the model.

7.1.2 Modifications to the Large-Scale Clouds and Precipitation

In Chapter 3, a new large-scale cloud and precipitation scheme that accounts for the sub-grid scale variability of clouds is developed and then coupled to the NCAR RegCM. This scheme partitions each grid cell into a cloudy and non-cloudy fraction which are related to the average grid cell relative humidity. Precipitation occurs, according to a specified auto-conversion rate, when a cloud water threshold is exceeded. The specification of this threshold is based on empirical in-cloud observations of cloud liquid water amounts. Included in the scheme are simple formulations for raindrop accretion and evaporation. A series of year long simulations are performed to investigate how the new model compares to the old model and observations.

The results from RegCM using the new scheme, tested over North America, show significant improvements when compared to the old version. The top of the atmosphere outgoing longwave radiation and albedo, cloud water path, incident surface shortwave radiation, net surface radiation, and surface temperature fields display reasonable agreement with the observations from satellite and surface station data. Furthermore, the new model is able to better represent extreme precipitation events such as the Midwest flooding observed in the summer of 1993.

Overall, RegCM with the new scheme provides for a more accurate representation of atmospheric and surface energy and water balances in the mean conditions as well as variability at daily to interannual scales. This suggests that the new scheme improves the model's sensitivity which is critical for both climate change and process studies.

7.1.3 Modifications to the Convection Scheme

In Chapter 4, we investigate how the choice of convective closure assumption impacts the simulation of atmospheric and surface energy and water budgets over North America. Each simulation is performed using the Grell scheme to represent convection. In one set of simulations, the quasi-equilibrium assumption is used as the dynamic control. In the other set, the dynamic control is related to the atmospheric stability. A series of six month (spring and summer) simulations are

performed for six separate years implementing each convective closure assumption.

RegCM regardless of the convective closure assumption performs adequately in reproducing observations of various radiative and hydrologic fields. The top of the atmosphere outgoing longwave radiation and albedo, cloud water path, incident surface shortwave radiation, net surface radiation, and surface temperature fields display reasonable agreement with the observations from satellite and surface station data.

The explosive nature of convective storms in the Great Plains and Midwest is better described by the FC80 closure. In addition, there is a tendency for AS74 simulations to delay onset of convection causing downwind shift compared to the FC80 predictions. However, the FC80 closure tends to be more noisy and can often form unobserved grid point storms.

Both closure assumptions perform relatively well in predicting the drought of 1988 and flood of 1993. They are both able to simulate the overall lack of precipitation observed during the drought and the excessive precipitation observed during the flood. The FC80 simulations, however, perform slightly better in predicting the flood peak location and magnitude.

Overall, this study shows that the FC80 closure assumption implemented within the Grell convective parameterization can be an alternative to the more commonly used AS74 closure.

7.2 Soil Moisture-Rainfall Feedback

The modified NCAR RegCM described in Part I is used to investigate the role that soil moisture plays in the predictability of spring and summer precipitation over North America in particular the Midwest.

7.2.1 Local Feedbacks

In Chapter 5, we investigate the key local pathways and mechanisms through which soil moisture conditions impact future rainfall over the United States Midwest using a regional climate model. A series of numerical experiments are performed to identify these pathways using the drought of 1988 and flood of 1993 as representative events. To isolate the local effects of soil moisture on these events, a small domain is used so that the effects of changes in soil moisture on the large-scale dynamics are constrained.

The results suggest that the soil moisture-rainfall feedback is an important mechanism for the hydrologic persistence during the late spring and summer over the midwestern United States. They

indicate that the feedback between soil moisture and subsequent rainfall played a significant role in enhancing the persistence of the drought of 1988 and the flood of 1993. It is found that there is a pronounced asymmetry in the sensitivity of simulated rainfall to specified initial soil moisture. The asymmetry acts to favor a stronger soil moisture-rainfall feedback during drought conditions as opposed to flood conditions.

Detailed analyses of the simulations indicate that the impact of soil moisture on both the energy and water budgets is crucial in determining the strength of the soil moisture-rainfall feedback. Anomalously high soil moisture tends to: (1) increase the flux of high moist static energy air into the planetary boundary layer from the surface via an increase in net surface radiation; (2) reduce the planetary boundary layer height thus increasing the moist static energy per unit mass of air; and (3) reduce the amount of entrained air of low moist static energy from above the planetary boundary layer. Each of these effects are additive and combine to increase in the moist static energy per unit mass of air in the planetary boundary layer. This results in an increase in the frequency and magnitude of convective rainfall events and a positive feedback between soil moisture and subsequent rainfall.

7.2.2 Remote Feedbacks

In Chapter 6, we investigate the key pathways and mechanisms through which soil moisture conditions, both local and remote, impact future rainfall over the United States Midwest using a regional climate model. A series of numerical experiments are performed to identify these pathways for six summers (July). A larger domain is used to allow the large-scale dynamics to respond to changes in soil moisture.

The experiments suggest that the domain-wide spatial variations in soil moisture are crucial to accurately reproduce precipitation in the Midwest. The interannual variations of soil moisture prove to be less important.

The mechanisms through which soil moisture impacts precipitation over the Midwest are consistent with, but not limited to, the local theory in the Chapter 5 small domain experiments. Soil moisture also has a pronounced impact on the large-scale dynamics which tends to induce a storm track shift that tends to enhance the soil moisture-rainfall feedback. A dry perturbation tends to shift the storm track to the north and results in drought conditions not only over the perturbed upper Midwest region, but also over the Great Plains region.

A dry soil moisture anomaly upstream of the Midwest (western Gulf Coast) extends the anomaly

downstream into the Midwest causing drought conditions in both the Great Plains and Midwest. The anomaly is extended downstream into the Midwest via the LLJ. In addition, similar to the perturbed Midwest simulations, the soil moisture has a pronounced impact on the local and large-scale conditions which tend to sustain each other.

Anomalous wetting in the Southwest exerts a significant control in determining the distribution of precipitation in the Great Plains and Midwest. A wet anomaly results in both a southward storm track shift and the removal of the Great Plains capping inversion from the Mexican Plateau. Both of these factors allow for the anomalous formation of precipitation over the Great plains. The added convergence over this region results in a decrease in precipitation over the Midwest. Overall, a wet soil moisture perturbation in the Southwest results in drought-like conditions in the upper Midwest and flood-like conditions in the Great Plains and Gulf Coast.

The remote and local effects of soil moisture prove to extremely useful for predicting summer rainfall over the Midwest and Great Plains.

7.3 Future Work

Some future efforts should be directed to further improve upon model deficiencies. For example, as mentioned in Chapter 6, the lower boundary of the soil is set to freely drain. This tends to cause wet soils to unrealistically drain even when the model overestimates precipitation. In the future, it would be useful to include a ground water table in the land-surface representation. As another example, there is a tendency for ocean surface evaporation to be excessive. It may be worthwhile to implement a more accurate ocean flux model.

In Chapter 5, we investigated the local pathways and mechanisms through which soil moisture impacts precipitation. We suggested that changes in soil moisture conditions contribute to the overall MSE of the PBL in three ways: (1) surface fluxes from below the PBL; (2) PBL depth; and (3) entrainment from above the PBL. The individual impacts of each of these components remains to be determined. Soil moisture perturbation experiments with the PBL depth fixed according to the control experiments would determine the importance of PBL depth changes in the soil moisture-rainfall feedback. We also argue in Chapter 5 that the radiative effects of the soil moisture-rainfall feedback play a more important role than the water recycling effects. An additional series of experiments could be performed with the net surface radiation and PBL depth held fixed according to the control experiments. This would remove the radiative and PBL effects of

the soil moisture-rainfall feedback and would isolate the water recycling effects. More experiments along these lines could help to further develop a complete understanding of the mechanisms and pathways responsible for the soil moisture rainfall feedback.

In Chapter 6, we determined that relatively small soil moisture perturbations ($\sim$10,000 km^2) had nearly as much impact as continental perturbations ($\sim$100,000 km^2). It would be useful to investigate the smallest scale before which a soil moisture perturbation no longer impacts the large-scale dynamics.

The effects of increasing atmospheric carbon dioxide may have a significant impact on the hydrologic cycle. The impacts of such an increase on the soil moisture-rainfall feedback have yet to be fully determined. A series of experiments similar to those presented in Chapters 5 and 6 could be performed with increased carbon dioxide levels. By performing these experiments we could determine how increases in carbon dioxide impact the strength of the soil moisture-rainfall feedback mechanism and through what pathways. In doing so, we would determine how these increases impact the persistence, magnitude, and likelihood of flood and drought.

References

Anthes, R. A. (1977). A cumulus parameterization scheme utilizing a one-dimensional cloud model, *Mon. Wea. Rev.* **117**: 1423–1438.

Anthes, R. A., Hsie, E. Y. and Kuo, Y. H. (1987). Description of the Penn State/NCAR Mesoscale Model Version 4 (MM4), *Technical Report TN-282+STR*, NCAR, Boulder, Colorado. pp. 66.

Arakawa, A. and Schubert, W. H. (1974). Interaction of a cumulus cloud ensemble with the large-scale environment, Part I, *J. Atmos. Sci.* **31**: 674–701.

Atlas, R., Wolfson, N. and Terry, J. (1993). The effect of SST and soil-moisture anomalies on GLA model simulations of the 1988 U.S. summer drought, *J. Climate* **6**: 2034–2048.

Barkstrom, B. R. (1984). The Earth Radiation Budget Experiment (ERBE), *Bull. Amer. Meteor. Soc.* **67**: 1170–1185.

Beheng, K. D. (1994). A parameterization of warm cloud microphysical conversion processes, *Atmospheric Research* **33**: 193–206.

Beljaars, A. C. M., Viterbo, P., Miller, M. J. and Betts, A. K. (1996). The anomalous rainfall over the United States during July 1993: Sensitivity to land surface parameterization and soil moisture anomalies, *Mon. Wea. Rev.* **124**: 362–383.

Bell, G. D. and Janowiak, J. E. (1995). Atmospheric circulation associated with the Midwest floods of 1993, *Bull. Amer. Meteor. Soc.* **76(5)**: 681–695.

Bengtsson, L., Kanamitsu, M., Kallberg, P. and Uppala, S. (1982). FGGE 4-dimensional data assimilation at ECMWF, *Bull. Amer. Meteor. Soc.* **63**: 29–43.

Betts, A. K. and Ball, J. H. (1994). Budget analysis of FIFE-1987 sonde data, *J. Geophys. Res.* **99**: 3655–3666.

Bosilovich, M. G. and Sun, W.-Y. (1999). Numerical simulation of the 1993 Midwestern Flood: Land-atmosphere interactions, *J. Climate* **12**: 1490–1505.

Brubaker, K. L. and Entekhabi, D. (1996). Asymmetric recovery from wet versus dry soil moisture anomalies, *J. Appl. Meteor.* **35**: 94–109.

Darnell, W. L., Staylor, W. F., Gupta, S. K., Ritchey, N. A. and Wilber, A. C. (1992). Seasonal variation of surface radiation budget derived from ISCCP-C1 data, *J. Geophys. Res.* **97**: 15,741–15,760.

Darnell, W. L., Staylor, W. F., Ritchey, N. A., Gupta, S. K. and Wilber, A. C. (1996). Surface radiation budget: A long-term global dataset of shortwave and longwave fluxes, *Eos, Transactions American Geophysical Union* .

Dickinson, R. E., Errico, R. M., Giorgi, F. and Bates, G. (1989). A regional climate model for the western United States, *Clim. Change* **15**: 383–422.

Dickinson, R. E., Kennedy, P. J., Henderson-Sellers, A. and Wilson, M. (1986). Biosphere-Atmosphere Transfer Scheme (BATS) version 1E as coupled to the NCAR Community Climate Model, *Technical Report TN-275+STR*, NCAR, Boulder, Colorado. pp. 72.

Eltahir, E. A. B. (1998). A soil moisture-rainfall feedback mechanism: 1. theory and observations, *Water Resources Research* **34**: 765–776.

Eltahir, E. A. B. and Bras, R. L. (1994). Sensitivity of regional climate to deforestation in the Amazon basin, *Advances in Water Resources* **17**: 101–115.

Eltahir, E. A. B. and Pal, J. S. (1996). Relationship between surface conditions and subsequent rainfall in convective storms, *Journal Geopyhisical Research* **101**: 26,237–26,245.

Emanuel, K. A. (1991). A scheme for representing cumulus convection in large-scale models, *Quart. J. Roy. Meteor.Soc.* **48**: 2313–2335.

Emanuel, K. A. (1994). *Atmospheric Convection*, Oxford University Press. 56-76.

Entekhabi, D., Rodriguez-Iturbe, I. and Castelli, F. (1996). Mutual interaction of soil moisture state and atmospheric processes, *J. Hydrol.* **184**: 3–17.

Fast, J. D. and McCorcle, M. D. (1990). A two-dimensional numerical sensitivity study of the Great Plains low-level jet, *Mon. Wea. Rev.* **118**: 151–163.

Findell, K. and Eltahir, E. A. B. (1997). An analysis of the relationship between spring soil moisture and summer rainfall, based on direct observations from Illinois, *Water Resour. Res.* **33(4)**: 725–735.

Findell, K. and Eltahir, E. A. B. (1999). Analysis of the pathways relating soil moisture and subsequent rainfall in Illinois, *J. Geophys. Res.* **104 (D24)**: 31565–31574.

Foley, J. A., Prentice, I. C., Ramankutty, N., Levis, S., Pollard, D., Sitch, S. and Haxeltine, A. (1996). An integrated biosphere model of land surface processes, terrestrial carbon balance, and vegetation dynamics, *Global Biogeochemical Cycles* **10(4)**: 603–628.

Fritsch, J. M. and Chappell, C. F. (1980). Numerical prediction of convectively driven mesoscale pressure systems. Part I: Convective paramerization, *J. Atmos. Sci.* **33(4)**: 725–735.

Giorgi, F. (1990). Simulation of regional climate using a limited area model nested in a general circulation model, *J. Climate* **3**: 941–963.

Giorgi, F. (1991). Sensitivity of simulated summertime precipitation over the western United States to physics parameterizations, *Mon. Wea. Rev.* **119**: 2870–2888.

Giorgi, F. and Bates, G. T. (1989). The climatological skill of a regional climate model over complex terrain, *Mon. Wea. Rev.* **117**: 2325–2347.

Giorgi, F., Huang, Y., Nishizawa, K. and Fu, C. (1999). A seasonal cycle simulation over eastern Asia and its sensitivity to radiative transfer and surface processes, *J. Geophys. Res.* **104**: 6403–6423.

Giorgi, F. and Mearns, L. O. (1999). Introduction to special section: Regional climate modeling revisited, *J. Geophys. Res.* **104**: 6335–6352.

Giorgi, F. and Shields, C. (1999). Tests of precipitation parameterizations available in latest version of NCAR regional climate model (RegCM) over continental United States, *J. Geophys. Res.* **104**: 6353–6375.

Grell, G. A. (1993). Prognostic evaluation of assumptions used by cumulus parameterizations, *Mon. Wea. Rev.* **121**: 764–787.

Gultepe, I. and Isaac, G. A. (1997). Liquid water content and temperature relationship from aircraft observations and its applicability to GCMs, *J. Climate* **10**: 446–452.

Gupta, S. K., Darnell, W. L. and Wilber, A. C. (1992). A parameterization for longwave surface radiation from satellite data: Recent improvements, *J. Appl. Meteor.* **31**: 1362–1367.

Gupta, S. K., Ritchey, N. A., Wilber, A. C., Whitlock, C. H., Gibson, G. G. and Stackhouse Jr., P. W. (1999). A climatology of surface radiation budget derived from satellite data, *J. Climate* **12**: 2691–2710.

Haagenson, P. L., Chen, S. and Gill, D. O. (1989). Penn State/NCAR Mesoscale Model users manual - Version 8, *Technical report*, NCAR, Boulder, Colorado. pp. 39.

Higgins, R. W., Yao, Y. and Wang, X. L. (1997a). Influence of the North American monsoon system on the U.S. summer precipitation regime, *J. Climate* **10**: 2600–2622.

Higgins, R. W., Yao, Y., Yarosh, E. S., Janowiak, J. E. and Mo, K. C. (1997b). Influence of the Great Plains low-level jet on summertime precipitation and moisture transport over the Central United States, *J. Climate* **10**: 481–507.

Hollinger, S. E. and Isard, S. A. (1994). A soil moisture climatology of Illinois, *J. Climate* **4**: 822–833.

Holtslag, A. A. M., de Bruijn, E. I. F. and Pan, H. L. (1990). A high resolution air mass transformation model for short-range weather forecasting, *Mon. Wea. Rev.* **118**: 1561–1575.

Hsie, E. Y., Anthes, R. A. and Keyser, D. (1984). Numerical simulation of frontogenesis in a moist atmosphere, *J. Atmos. Sci.* **41**: 2581–2594.

Huang, J., van den Dool, H. M. and Georgakakos, K. (1996). Analysis of model-calculated soil moisture over the U.S. (1931-93) and application in long-range temperature forecasts, *J. Climate* **9**: 1350–1362.

IPCC (1995). *The science of climate change. Contribution of working group I to the second assessment report of the Intergovernmental Panel on Climate Change*, Cambridge University Press, Cambridge, UK.

Kalnay, E., Kanamitsu, M., Kistler, R., Collins, W., Deaven, D., Gandin, L., Iredell, M., Saha, S., White, G., Woollen, J., Zhu, Y., Leetmaa, A., Reynolds, R., Chelliah, M., Ebisuzaki, M., Higgins, W., Janowiak, J., Mo, K. C., Ropelewski, C., Wang, J., Jenne, R. and Joseph, D. (1996). The NCEP/NCAR 40-year reanalysis project, *Bull. Amer. Meteor. Soc.* **77**: 437–471.

Karl, T. R., Williams Jr., T. N., Quinlan, F. T. and Boden, T. A. (1990). United States Historical Climatology Network (HCN) serial temperature and precipitation data, *Technical Report*

Environmental Science Division, Publication No. 3404, Oak Ridge National Laboratory, Oak Ridge, TN. pp. 389.

Kiehl, J. T., Hack, J. J., Bonan, G. B., Boville, B. A., Briegleb, B. P., Williamson, D. L. and Rasch, P. J. (1996). Description of the NCAR Community Climate Model (CCM3), *Technical Report TN-420+STR*, NCAR, Boulder, Colorado. pp. 152.

Kiehl, J. T. and Ramanathan, V. (1990). Comparison of cloud forcing derived from the Earth Radiation Budget Experiment with that simulated by the NCAR Community Climate Model, *J. Geophys. Res.* **95**: 11,679–11,698.

Kunkel, K. E., Changnon, S. A. and Angel, J. R. (1994). Climatic aspects of the 1993 Upper Mississippi River Basin flood, *Bull. Amer. Meteor. Soc.* **75**: 811–822.

Loveland, T. R., Zhu, Z., Ohlen, D. O., Brown, J. F., Reed, B. C. and L., Y. (1999). An analysis of the IGBP global land-cover characterization process, *Photogrammetric Engineering and Remote Sensing* **65(9)**: 1021–1032.

Mayer, T. A. (1988). Generation of CCM format history tape from analyzed data for selected periods RD2CFM Version 1, *Technical Report TN-322+STR*, NCAR, Boulder, Colorado. pp. 68.

McCorcle, M. D. (1988). Simulation of surface-moisture effects on the Great Plains low-level jet, *Mon. Wea. Rev.* **116**: 1705–1720.

Mearns, L. O., Rosenzweig, C. and Goldberg, R. (1997). Mean and variance change in climate scenarios: Methods, agricultural applications, and measures of uncertainty, *Climatic Change* **35**: 367–396.

Mintz, M. (1984). *The sensitivity of numerically simulated climates to land-surface boundary conditions*, Cambridge University Press. 79-105.

Molinari, J. and Dudek, M. (1986). Implicit versus explicit convective heating in numerical weather prediction models, *Mon. Wea. Rev.* **114**: 1822–1831.

Namias, J. (1955). Some meteorlogical aspects of drought with special reference to the summers of 1952-54 over the United States, *Mon. Wea. Rev.* **83**: 199–205.

Namias, J. (1982). Anatomy of Great Plains protracted heat waves (especially the 1980 U.S. summer drought), *Mon. Wea. Rev.* **110**: 824–838.

Namias, J. (1991). Spring and summer 1988 drought over the contiguous United States-causes and prediction, *J. Climate* **4**: 54–65.

NOAA (1993). Weekly weather and crop bulletin, *Technical report*, U.S. Department of Commerce, National Oceanic and Atmospheric Administration, USDA, South Building, Room 5844, Washington D.C. 20250. pp. 24.

NOAA (1998a). Atmospheric conditions affecting the United States during April - June 1998, *Technical report*, U.S. Department of Commerce, National Oceanic and Atmospheric Administration.

NOAA (1998b). Atmospheric conditions and impacts affecting the United States during July and early August 1998, *Technical report*, U.S. Department of Commerce, National Oceanic and Atmospheric Administration.

Oglesby, R. J. (1991). Springtime soil moisture, natural climatic variability, and the North American Drought as simulated by the NCAR Community Climate Model 1, *J. Climate* **4**: 890–897.

Paegle, J., Mo, K. C. and Nogués-Paegle, J. (1996). Dependence of simulated precipitation on surface evaporation during the 1993 United States summer floods, *Mon. Wea. Rev.* **126**: 345–361.

Pal, J. S. and Eltahir, E. A. B. (1997). On the relationship between spring and summer soil moisture and summer precipitation over the Midwest, *Preprints of the 13th Conference on Hydrology* pp. 382–385.

Pal, J. S. and Eltahir, E. A. B. (2001). Pathways relating soil moisture conditions to future summer rainfall within a model of the land-atmosphere system., *In press J. Climate* .

Pal, J. S., Small, E. E. and Eltahir, E. A. B. (2001). Simulation of regional scale water and energy budgets: Influence of a new moist physics scheme in RegCM, *In Press J. Geophys. Res.* .

Pan, Z., Tackle, E., Segal, M. and Turner, R. (1996). Influences of model parameterization schemes on the reponse of rainfall to soil moisture in the Central United States, *Mon. Wea. Rev.* **124**: 1786–1802.

Pinker, R. T. and Laszlo, I. (1992). Modeling surface solar irradiance for satellite applications on a global scale, *J. Appl. Meteor.* **31**: 194–211.

Rayner, N. A., Horton, E. B., Parker, D. E., Folland, C. K. and Hackett, R. B. (1996). Version 2.2 of the global sea-ice and sea surface temperature data set, 1903-1994, *Technical Report Climate Research Tech. Note 74*, Hadley Centre, Bracknell, United Kingdom.

Rind, D. (1982). The influence of ground moisture conditions in North America on summer climate as modeled in the GISS GCM, *Mon. Wea. Rev.* **110**: 1487–1494.

Rogers, R. R. and Yau, M. K. (1989). *A short course in cloud physics*, Pergamon.

Ropelewski, C. F. (1988). The global climate for June-August 1988: A swing to positive phase of the southern oscillation, drought in the United States and abundant rain in monsoon areas, *J. Climate* **1**: 1153–1174.

Rossow, W. B. and Schiffer, R. A. (1999). Advances in understanding clouds from ISCCP, *Bull. Amer. Meteor. Soc.* **11**: 2261–2288.

Rossow, W. B., Walker, A. W., Beuschel, D. E. and Roiter, M. D. (1996). International Satellite Cloud Climatology Project (ISCCP) documentation of new cloud datasets, *Technical Report WMO/TD-No. 737*, World Meteorological Organization.

Rowntree, P. R. and Bolton, J. A. (1983). Simulation of the atmospheric response to soil moisture anomalies over Europe, *Quart. J. Roy. Meteor. Soc.* **109**: 501–526.

Schär, C., Lüthi, D., Beyerle, U. and Heise, E. (1999). The soil-precipitation feedback: A process study with a regional climate model, *J. Climate* **12**: 722–741.

Seth, A. and Giorgi, F. (1998). The effects of domain choice on summer precipitation simulation and sensitivity in a regional climate model, *J. Climate* **11**: 2698–2712.

Showalter, A. K. (1953). A stabilty index for thunderstorm forecasting, *Bull. Amer. Meteor. Soc.* **34**: 250–252.

Small, E. E., Giorgi, F. and Sloan, L. C. (1999a). Regional climate model simulation of precipitation in Central Asia: Mean and interannual variability, *J. Geophys. Res.* **104**: 6563–6582.

Small, E. E., Sloan, L. C., Hostetler, S. and Giorgi, F. (1999b). Simulating the water balance of the Aral Sea with a coupled regional climate-lake model, *J. Geophys. Res.* **104**: 6583–6602.

Sun, L., Semazzi, F. H. M., Giorgi, F. and Ogallo, L. (1999). Application of the NCAR regional climate model to eastern Africa 1. Simulation of the short rains of 1988, *J. Geophys. Res.* **104**: 6529–6548.

Sundqvist, H. (1988). Parameterization of condensation and associated clouds in models for weather prediction and general circulation simulation, *in* M. E. Schlesinger (ed.), *Physically-based modelling and simulations of climate and climate change*, Kluwer Academic Publishers, pp. 433–461.

Sundqvist, H., Berge, E. and Kristjánsson, J. E. (1989). The effects of domain choice on summer precipitation simulation and sensitivity in a regional climate model, *J. Climate* **11**: 2698–2712.

Takle, E. S., Gutowski, W. J., Arritt, R. W., Pan, Z. T., Anderson, C. J. da Silva, R. R., Caya, D., Chen, S. C., Giorgi, F., Christensen, J. H., Hong, S. Y., Juang, H. M. H., Katzfey, J., Lapenta, W. M., Laprise, R., Liston, G. E., Lopez, P., McGregor, J., Pielke, R. A. and Roads, J. O. (1999). Project to Intercompare Regional Climate Simulations (PIRCS): Description and initial results, *J. Geophys. Res.* **104**: 19443–19461.

Trenberth, K. E. (1991). Storm tracks in the Southern Hemisphere, *J. Atmos. Sci.* **48**: 2159–2178.

Trenberth, K. E. and Branstator, G. W. (1992). Issues in establishing causes of the 1988 drought over North America, *J. Climate* **5**: 159–172.

Trenberth, K. E., Branstator, G. W. and Arkin, P. A. (1988). Origins of the 1988 North American Drought, *Science* **242**: 1640–1645.

Trenberth, K. E. and Guillemot, C. J. (1996). Physical processes involved in the 1988 drought and 1993 floods in North America, *J. Climate* **9**: 1288–1298.

Trenberth, K. E. and Olson, J. G. (1992). ECMWF global analyses 1979-1986: Circulation statistics and data evaluation, *Technical Report TN-300+STR*, NCAR, Boulder, Colorado. pp. 94.

Williams, E. and Renno, N. (1993). An analysis of the conditional instability of the tropical atmosphere, *Mon. Wea. Rev.* **121**: 21–36.

Xue, Y. (1996). The impact of desertification in the Mongolian and the inner Mongolian grassland on the regional climate, *J. Climate* **9**: 2173–2189.

Yeh, P. J. F. and Eltahir, E. A. B. (2000). The representation of groundwater dynamics in a land surface scheme, *Eos, Transactions American Geophysical Union* .

Yeh, P. J. F. and Eltahir, E. A. B. (2001). Representation of water table dynamics in a land-surface scheme: 2. Sub-grid heterogeneity, *Submitted to Water Resour. Res.* .

Yeh, T. C., Wetherald, R. T. and Manabe, S. (1984). The effect of soil moisture on the short-term climate and hydrology change - a numerical experiment, *Mon. Wea. Rev.* **112**: 474–490.

Zheng, X. and Eltahir, E. A. B. (1998). A soil moisture-rainfall feedback mechanism: 2. experiments with a simple numerical model, *Water Resour. Res.* **34**: 777–785.

5630-56